Development of artificial hydraulic lime with waste wood biomass ash

Šantek Bajto, Jelena

Download date / Datum preuzimanja: **2025-02-21**

University of Zagreb

Faculty of Civil Engineering

Jelena Šantek Bajto

DEVELOPMENT OF ARTIFICIAL HYDRAULIC LIME WITH WASTE WOOD BIOMASS ASH

DOCTORAL DISSERTATION

Zagreb, 2024.

University of Zagreb

Faculty of Civil Engineering

Jelena Šantek Bajto

DEVELOPMENT OF ARTIFICIAL HYDRAULIC LIME WITH WASTE WOOD BIOMASS ASH

DOCTORAL DISSERTATION

Supervisor: prof. Nina Štirmer, PhD

Zagreb, 2024.

Građevinski fakultet

Jelena Šantek Bajto

RAZVOJ UMJETNOGA HIDRAULIČNOG VAPNA S OTPADNIM PEPELOM DRVNE BIOMASE

DOKTORSKI RAD

Mentor: prof. dr.sc. Nina Štirmer

Zagreb, 2024.

IZJAVA O IZVORNOSTI

Ja, Jelena Šantek Bajto, potvrđujem da je moj Doktorski rad izvorni rezultat mojega rada te da se u njegovoj izradi nisam koristila drugim izvorima osim onih koji su u njemu navedeni.

_____

Jelena Šantek Bajto, mag. ing. aedif.

Zahvale

Bilo je ovo nezaboravno iskustvo, prošarano usponima i padovima. Obogatilo je moj život u svakom pogledu, pruživši mi nevjerojatne trenutke i nova, dragocjena iskustva. Nije samo obogatilo moje radno iskustvo, već sam također imala priliku upoznati i surađivati s iznimnim ljudima. Njihovo znanje, strpljenje, predanost i naposlijetku prijateljstvo bili su poput referentne točke, pružajući mi podršku i nesebično dijeleći samnom svoje vrijeme i znanje.

Kažu da 'sloboda nema cijenu'. Zato posebno zahvaljujem svojoj mentorici, prof.dr.sc. Nini Štirmer, na prilici i povjerenju koje mi je ukazala.

Bez imalo patetike, iskrenu zahvalnost dugujem svim divnim kolegama sa Zavoda za materijale. Njihova podrška bila je više od suradnje. Osjećala sam se kao član te male obitelji unutar Zavoda za materijale, koja me hrabrila i bila ekstenzija moga rada. Posebno zahvaljujem svojim bivšim i sadašnjim cimerima i cimericama, divnim prijateljima s kojima sam dijelila i proživljavala svakodnevne, profesionalne ali i privatne izazove. Svaka njihova riječ utjehe i ohrabrenja utkana je u ovu disertaciju.

Veliko hvala cijelom timu Laboratorija za materijale bez čije pomoći ne bih uspjela!

Neizmjerno cijenim bezgraničnu podršku moje obitelji, Ivana, Lede i mojih roditelja, koji su bili moj oslonac i moja snaga.

Acknowledgments and funding

Short abstract

In the midst of the various environmental challenges and the ever-growing global appetite for energy, renewable sources are boldly stepping up to rival the longstanding dominance of fossil fuels. Europe's dedicated push towards sustainable energy has led to a significant surge in the use of wood biomass as a low-emission alternative fuel. This transition has given rise to the abundant production of wood biomass ash (WBA). This emergent industrial byproduct now calls for strategic and sustainable management, especially when it comes to long-term disposal strategies. Alongside, the repair of historically valuable yet time-worn and energy-inefficient buildings should not only aim to reduce carbon emissions and minimise energy consumption but also embrace innovative repair materials that incorporate supplementary materials such as WBA. This research unveils the potential of WBA as a secondary binder in the formulation of a cement-free, hybrid lime binder. By combining natural hydraulic lime with WBA, an innovative artificial building lime with hydraulic properties (AHL) is introduced, designed for application in repair mortars for historic buildings. The experimentation entailed the preparation of AHL binder blends, followed by their incorporation into mortars, wherein the natural hydraulic lime (NHL) was hybridised by various WBAs at 20, 30 and 40 wt%. The assessment of the viability of WBA in AHL was undertaken, encompassing two core phases: the binder phase and the mortar phase. This approach systematically considered the chemico-mineralogical composition, physical attributes, and reactivity of diverse binder blends, serving as a basis for determining the optimum WBA proportion and refining the design of AHL mortars. The mechanical behaviour, encompassing essential aspects such as compressive and flexural strength, as well as the modulus of elasticity, was examined on mortars of varying ages and subjected to diverse CO_2 and moisture conditions. Durability aspects, including adhesive bond strength, freeze/thaw and salt resistance, were analysed. Microstructural characterization of pore structure accompanied by hygrothermal properties, including capillary water absorption, water vapor permeability, and thermal conductivity, were also examined. In summary, the results indicate that incorporating WBA into the NHL binder matrix at moderately - high hybridisation ratios offers promising opportunities for utilizing WBA as a secondary binder in AHL mortar systems. As a result, fusing WBA with NHL, particularly in higher proportions, has substantial potential to enhance sustainability while preserving the authenticity of repair mortars.

Keywords: wood biomass ash; hybrid lime binders; low-carbon repair material; sustainable conservation, cement-free binder

Prošireni sažetak

Suočeni s različitim ekološkim izazovima i rastućom globalnom potražnjom za energijom, obnovljivi izvori energije silovito konkuriraju dugogodišnjoj dominaciji fosilnih goriva. Tranzicija Europske Unije (EU) usmjerena je prema održivoj energiji što je praćeno znatnim porastom u korištenju drvne biomase kao alternativnog niskougljičnog goriva. Pri tome je drvo sa 70% udjela najrasprostranjenija sirovina za proizvodnju bioenergije. Uz značajni porast broja energana na drvnu biomasu, čije spaljivanje rezultira s približno 3% pepela drvne biomase (PDB) po 1 toni drveta, dolazi do gomilanja ovog industrijskog otpada. Usprkos značajnim količinama otpadnog pepela, postojeća praksa zbrinjavanja zasniva se na izravnom odlaganju na odlagališta otpada ili korištenju u poljoprivredi u manjoj mjeri, često bez ikakve kontrole, rezultirajući zakrčenim i ilegalnim odlagalištima. S naglaskom na minimiziranje stvaranja otpada, ali i povećanje njegove ponovne upotrebe, održivo gospodarenje otpadom istaknuto je kao jedan od ključnih stupova europske strategije za postizanje ugljične neutralnosti do 2050. Istovremeno, obnova povijesno značajnih, ali dotrajalih i energetski neučinkovitih građevina nedvojbeno može doprinijeti smanjenju ugljičnih emisija i potrošnji energije, ali i podržati zelenu perspektivu kroz koju se implementiraju inovativni materijali za popravak, uključujući alternativne materijale poput PDB-a.

Stavljajući sanacije i popravke povijesnih građevina u suvremeni kontekst, kada se suočavamo sa značajnom klimatskom i energetskom krizom, omogućuje se uvođenje kulturne dimenzije u sustav održivih inovacija, što je ključno za stvaranje dijaloga između izgrađenog okoliša i Zemljinih ekosustava. Kao što je su prevencija i recikliranje otpada pri vrhu hijerarhije gospodarenja otpadom EU, popravci i sanacije postojećih zgrada moraju imati prioritet u odnosu na novu gradnju gdje god je to moguće. Zajedničko obilježje povijesnih zgrada je da su građene uglavnom od prirodnih materijala kao što su kamen i opeka, povezanih vapnenim mortom. Prema tome, i danas uz predominaciju cementa kao veziva, postoji potražnja za vapnenim materijalima, odnosno sanacijskim materijalima koji su kompatibilni s onima koji su izvorno ugrađeni. Istovremeno, očuvanje povijesne i kulturne cjelovitosti ostaje nezaobilazno, a kružna ekonomija i održiva gradnja ističu se kao novi standard. Uz poštivanje identiteta građevine i svojstava izvorno ugrađenih materijala bitno je da rješenja budu održiva, ekološki i društveno prihvatljiva. Rješavanjem ovih pitanja, do izražaja dolaze alternativni, lokalno dostupni otpadni materijali poput PDB-a koji se mogu ponovno implementirati pri razvoju bescementnih veziva. Isticanje prednosti recikliranja PDB-a u skladu je i sa sedmim temeljnim zahtjevom za građevine koji se odnosi na održivo korištenje prirodnih resursa. Takvom

afirmacijom zelene obnove podupire se prijelaz na održivo, netoksično, energetski učinkovito i klimatski otporno društvo.

Temeljem rezultata ovog istraživanja evaluiran je potencijal korištenja otpadnog PDB-a kao sastavne komponente bescementnog, hibridnog vapnenog veziva (AHL). Implementacija PDB-a u matricu prirodnog hidrauličkog vapna (NHL) omogućuje umjetnu formulaciju građevnog vapna s hidrauličkim svojstvima, koja je pogodna za primjenu u pri obnovi i popravku povijesnih građevina.

Eksperimentalne faze istraživanja obuhvaćaju pripremu veziva s NHL-om i PDB te njihovu primjenu u mortovima. Pri tome je NHL-PDB vezivni sustav hibridiziran s različitim udjelima pepela drvne biomase. U eksperimentalnoj fazi na razini veziva i pasti uključeno je 11 različitih pepela, primjenjujući umjereni (20%) i umjereno-visoki (30% i 40%) težinski udio PDB-a. PDB proizvedeni su i prikupljeni u bioenerganama diljem Hrvatske, dok je kao primarno vezivo korištena komercijalno dostupna, prirodna hidraulična vapna NHL 3.5 i NHL 5, koja definira umjerena i visoka razina hidrauličnosti.

Karakterizacija sastavnih komponenti AHL-a kroz interakciju na mikrorazini i makrorazini neophodna je za razvoj, prilagodbu i optimizaciju sastava mješavine vapnenog morta, zasnivajući se na funkcionalnoj ulozi samog morta koja se može ostvariti unutar AHL sustava, pri različitim uvjetima izloženosti i podlogama. Kako bi se identificirali i nominirali prikladni PDB za formulaciju AHL-a, provedena je analiza kemijsko-mineraloškog sastava te fizikalnih svojstava NHL-a i PDB-a, prepoznajući njihove uloge unutar formulacije AHL veziva. Da bi se vezivo klasificiralo kao hidraulično vapno, nužno je da zadovoljava sve kriterije definirane normom HRN EN 459-1, kojom su definirani parametri na razini vapnenih veziva i odgovarajućih pasti. Prema tome, određivanje prihvatljivog udjela PDB-a u AHL-u potvrđeno je ispitivanjem standardne konzistencije, vremena vezivanja i volumenske stabilnosti AHL pasti, u skladu s navedenim standardom. Budući da su PDB okarakterizirani visokim udjelima SO_3 te ekspanzivnih komponenti poput slobodnog MgO i CaO, uz smanjeni udio dostupnog vapna ($Ca(OH)_2$), predloženi su postupci pred-obrade kojima bi se anulirali navedeni nedostatci i povećala reaktivnost pepela.

Kako bi se utvrdili dominantni parametri koji utječu na mehanička svojstva i trajnost vapnenih mortova s AHL-om, analiziran je utjecaj PDB-a na mehanička svojstva kao što su tlačna čvrstoća na tlak i čvrstoća na savijanje te elastičnost koja izražena dinamičkim modulom elastičnosti. Analizom kapilarnog upijanja vode, paropropusnosti i toplinske vodljivosti utvrđen

je utjecaj PDB-a na higrotermalna svojstva vapnenih kompozita dok je mikrostrukturna karakterizacija uključivala primjenu živinog porozimetrom (MIP) za karakterizaciju strukture pora na uzorcima očvrsnulog morta pri različitim starostima i različitim uvjetima vlage i CO_2.

Navedene razine procjene prepoznate su kao preduvjet razvoju mortova primjenjivih u povijesnim građevinama. Rezultati upućuju da uvođenje PDB-a u vapnenu matricu NHL-a, pri umjerenim pa čak i visokim omjerima hibridizacije (NHL:WBA 80:20, 70:30 i 60:40), ima obećavajuće izglede za primjenu AHL-a kao hibridnog veziva u mortovima za povijesne građevine. Ovi rezultati potvrđuju primjenjivost materijala poput mortova s AHL-om, ispunjavajući tehničke zahtjeve i uvjete kompatibilnosti s NHL-om, koji se koristi kao referentni materijal za obnovu i popravak povijesnih građevina. Isto tako predstavljaju platformu za usvajanje pozitivnog pristupa nekonvencionalnim materijalima te održivu obnovu povijesnih zgrada.

Ključne riječi: Pepeo drvne biomase, hidraulično vapno, bescementno hibridno vezivo, mort za obnovu povijesnih građevina, održiva obnova

List of figures

Chapter 4

List of tables

Chapter 4

List of abbreviations

ACC	Accelerated Curing Conditions
AHL	Artificial hydraulic lime
CE	Curing environment
CI	Cementation index
CO₂	Carbon dioxide
DC	Semi – Dry Curing Conditions
DTG	Differential Thermogravimetry
EDXRF	Energy-Dispersive X-ray Fluorescence
EU	European Union
FL	Formulated lime
HC	Humid Curing Conditions
HI	Hydraulicity index
HL	Hydraulic lime
LOI	Loss on ignition
MIP	Mercury Intrusion Porosimetry
NF	Nature of failure
NHL	Natural hydraulic lime
OP	Overall performance
RH	Relative humidity
SAI	Strength Activity Index
SDG	Sustainable development goals
SEM	Scanning Electron Microscopy
TG	Thermogravimetry
TGA	Therogravimetric analysis
VAR	Visual Assessment Rating
WBA (*hrv.* PDB)	Wood Biomass Ash (*hrv.* Pepeo Drvne Biomase)
XRD	X-ray Diffraction

Content

1. INTRODUCTION

1.1. Research context

Fostering a harmonious fusion of the cultural dimension and sustainable innovation is essential for forming a constructive dialogue between the built environment and the planet's delicate ecosystem. This synergy aligns with the European waste management hierarchy, which places waste reuse as well as recycling at the forefront and emphasizes the need for preventive measures [1]. Furthermore, there's a compelling argument for prioritizing the maintenance, repair, and restoration of existing structures over new construction [2]. Simultaneously, it's paramount to safeguard the historical and cultural integrity of our built heritage. However, selecting the appropriate materials for repairs presents a unique challenge, as traditional and modern options often collide. This challenge is particularly pronounced when restoring historically significant buildings. As a result, there's a tendency to favor modern materials that adhere to current regulations, sometimes overshadowing the preservation of cultural and historical values. In summary, balancing sustainability with the conservation of cultural and historical heritage is a complex endeavor that necessitates careful consideration and innovative solutions.

In the contemporary landscape marked by the widespread embrace of circular and sustainable architectural principles, a firm emphasis is placed on the adoption of repair materials that effortlessly integrate with the original construction components. These materials, often derived from historical practices, significantly shape the built-in architectural character. In bygone eras, construction elements such as stone and clay bricks were artfully joined with lime mortar, endowing lime-based materials with an indispensable role in upholding compatibility and preserving the historical essence of architectural structures.

Simultaneously, the European Union (EU) is shifting its focus towards renewable energy sources and sustainable solutions to address the increasing energy and material demands dictated by global as well as local conditions. With concerns over rising global temperatures and climate variability, the EU has taken action through initiatives like the European Green Plan [3]. As part of this shift, Europe is compelled to adopt an innovative, resource-efficient economic model and reduce the carbon footprint of energy-intensive industries, including cement and lime production. These manufacturing processes are highly energy-intensive, with

energy costs accounting for a significant portion of the overall production expenses – up to 40% for cement and 50% for lime [4].

Ergo, every industrial sector faces substantial challenges in reducing net greenhouse gas emissions, and the lime industry is no exception. Emissions arising from the downstream processing and hydration of lime contribute to approximately 1.5% of total CO_2 emissions [5]. The competitiveness and sustainability of the lime industry is closely tied to the availability of advanced, multifunctional modern lime-based materials that can be conventionally incorporated into existing processes.

As Europe pursues a greener energy transition, one pivotal step was to elevate the binding target for renewable energy in the EU energy mix from 32% to a more ambitious 40% [6]. Central to achieving this goal is the phased reduction of coal burning in favor of renewable energy sources [7]. The revised Renewable Energy Directive suggests that bioenergy and biomass can play a valuable role in establishing a low-carbon energy system, potentially accounting for 18% of total energy supply by 2050, contingent on sustainable biomass management [8,9]. Industrial utilization of bioenergy is projected to triple by 2060, contributing almost 14% of industrial energy demand [10]. In this context, biomass-derived materials are set to play a crucial role in transitioning to a circular economy, emphasizing sustainable consumption and production practices while promoting the recovery of essential raw materials from waste streams [11]. Currently, biomass stands as a primary source of renewable energy in the EU, constituting more than 58% of energy consumption from renewable sources [12,13]. Wood is the dominant feedstock for bioenergy production, representing 70% of the total [14]. Notably, the combustion of one tonne of wood biomass results in the production of around 3% of WBA [15]. This trend suggests an ongoing increase in both the quantity and disposal costs of this industrial waste. While WBA contains nutrients such as calcium, potassium, and phosphorus with beneficial potential in agricultural uses, it also contains heavy metals that pose environmental risks [16]. Although limited quantities of WBA are employed as a soil amendment or fertilizer, this alone does not significantly address the accumulation of WBA, especially considering a global stock estimated at about 500 million tonnes annually [17]. Given these circumstances, there is a clear imperative for strategic foresight in the management of WBA. Unfortunately, the prevailing practice in Europe involves WBA disposal in landfills, often without adequate control measures, leading to added costs and environmental hazards. This situation has also contributed to the

upturn of illegal landfills, a global issue that underscores the urgency of addressing WBA disposal challenges [12,18,19].

Simultaneously, the EU is resolutely dedicated to mitigating the unregulated dispersion of waste in the environment and fostering its reclamation. The implementation of the new "Circular Economy Package," alongside the enhanced Directive 2018/851 on waste and Directive 2018/850 on waste landfilling [20,21] are expected to overarch these dissonant aspects.

While seeking for practical and sustainable applications of WBA, previous studies have predominantly explored its role as a cement substitute or a replacement for aggregates in cementitious composites. In contrast, research concerning the utilization of WBA as a pozzolanic or hydraulic component in hydraulic lime formulations, the central focus of this dissertation, has been notably limited. Previous investigations have seldomly looked into the effects of WBA on air-lime mortars [22–24], and only a few studies in the literature have explored WBA's integration within the context of hydraulic lime [25,26]. More withstanding harsh atmospheric conditions, hydraulic lime has proven to be favourable. This warrants particular attention when used in historical buildings, as opposed to air-lime, which is often regarded as the closest match to the original materials [27].

1.2. Objectives and hypotheses of research

Underlying this dissertation is an effort to highlight the need for strategic foresight in the management of wood biomass ash, while identifying WBA as a potential constituent of an artificial hydraulic binder for the development of mortars for the rehabilitation and maintenance of historical buildings. To achieve this objective, it is necessary to:

–   Identify and select suitable WBAs, considering their chemico-mineralogical composition and physical properties, that can be used in formulating artificial hydraulic lime binder. A two-fold WBA engagement strategy involves the assesment of predominantly calcareous WBAs and predominantly siliceous WBAs;

–   Define the functional role of mortar as a function of the properties of a particular WBA and the functional requirements of the binder/mortar;

–   Adapt the design of artificial hydraulic lime mortar containing WBA, based on the outlined function.

The focus of this research is on the evaluation of the AHL binder attributes and their impression on mortar properties as a function of different curing conditions. The results of the study will be beneficial in determining favourable curing conditions and practicable WBA contents for hydraulic lime mortars to optimize their formulation for use in mortars for the conservation and maintenance of historical buildings. Since WBA is an industrial by-product that is intended to step in for some of the NHL, it would not only reduce the impact of NHL production on resource depletion and the environment itself, but also solve the problem of industrial waste by cycling resources. Thus, the use of WBA in AHL, especially in higher proportions, could offer an important development perspective by boosting the sustainability of the hydraulic production sector while supporting the authenticity of repair mortars.

In accordance with the above objectives of the proposed research, the following hypotheses were formulated:

H I. Building lime with hydraulic properties, i.e. an artificial hydraulic lime can be prepared with wood biomass ash;

H II. The chemico-mineralogical composition of WBA, in addition to evaluating various WBA with different degrees of pozzolanity and hydraulicity, has a direct impact on its applicability in a hydraulic binder and the possibility of hardening of hydraulic lime mortar systems;

H III. Artificial lime with hydraulic properties containing WBA can be used to produce eco-friendly cement-free mortar for restoration and/or rehabilitation of historical buildings.

1.3. Expected scientific contribution

Showcasing and promoting the health benefits of WBA re-use has been identified as a strategy to promote positive mindset toward the acceptance of unconventional materials. Also, the introduction of the socio-environmental dimension into the historical framework based on circular design has proven to be a breakthrough paradigm shift necessary for long-term, life-cycle thinking in the industrial ecosystem. Stepping up from discarded materials to a level of value through strategic recycling, the fundamental premise behind the proposed research, is expected to bring forth the following scientific contributions:

SC1. Determination of prospects for the use of WBA in artificial hydraulic lime based on the key factors governing the engineering behaviour and durability of a new composite;

SC2. Development of an environmentally friendly lime mortar with WBA suitable for the rehabilitation and maintenance of historical buildings.

This will further align with EU priorities, significantly curbing natural resource consumption and expediting the shift towards a sustainable, non-toxic, energy-efficient, and climate-resilient economy.

1.4. Research strategy and thesis outline

Prior research has significantly advanced the understanding of the utilization of WBA as a substitute raw material in cementitious composites. However, the application of WBA in lime-based materials has not been extensively explored. Consequently, the focus of this research is directed toward locally available WBAs, primarily distinguished by the place of collection, as they emerge as alternative materials with potential pozzolanic and hydraulic properties. These properties make them well-suited for the development of environmentally friendly lime mortars tailored for conservation purposes.

Drawing upon the chemico-mineralogical composition and physical attributes, an evaluation was conducted to determine the prospects of WBAs as constituents of artificial hydraulic lime. The primary objective of this investigation was to formulate a waste-based, cementless binder and validate the synergetic interaction between WBA and other constituents within the AHL binder. In accordance with the criteria set forth in the HRN EN 459 standard for building lime, an evaluation of artificial hydraulic lime incorporating WBA was conducted. Given the favourable attributes of hydraulic lime for structures exposed to significant atmospheric

conditions, its application in historical buildings deserves recognition, as an alternative to air lime. The characterization of the raw components of AHL at both binder and paste levels was the foundation for tailoring the mix design, in relation to the functional role of mortar which can be exerted within the AHL system. This research strived to verify whether this hybrid NHL-WBA bearing mortar could be legitimately regarded as an equivalent material suitable for the conservation of historically significant buildings.

The methodological framework unfolds across five main phases, each detailed upon in the corresponding main chapters:

Chapter 1: INTRODUCTION

The initial chapter explores the research's background and its objectives while introducing the formulated hypotheses. Furthermore, the anticipated contributions to the fields of science and engineering are outlined while promoting sustainable historical framework is underpinned.

Chapter 2: STATE OF THE ART RESEARCH

The second chapter encompasses an extensive examination of existing literature pertaining to the integration of industrial waste streams such as WBA, with a particular emphasis on the modification and substitution of conventional binders. Additionally, the present body of knowledge regarding the application of WBA in lime-based mortars tailored for historical structures was explored. The main focus is on constituent materials, functional requirements, and compatibility concerns.

Chapter 3: EXPERIMENT: FORMULATION AND TAILORED DESIGN OF BINDER BLENDS

This chapter encompassed the first experimental phase which centres around the incorporation of various WBAs within the NHL-WBA binder system, while moderate (20 wt.%) and relatively high (30 and 40 wt.%) hybridisation ratios were employed. The asssessment of the hybrid AHL binder adhered primarily to the criteria stipulated in standard EN 459-1 for building lime. By consolidating the results of this comprehensive assessment of an AHL binder with WBA, specifically focusing on the evaluation of WBA's influence on the specified properties at the AHL binder and paste levels, it was possible to pinpoint suitable types of WBA, and favorable hybridisation ratios. This consideration took into account the chemico-mineralogical composition and physical properties of the WBAs. At this stage, the concept of a tailored design

emerged, aiming to determine the maximum acceptable WBA content that would not significantly compromise the hydraulicity of the primary binder.

Chapter 4: EXPERIMENT: PREPARATION AND EVALUATION OF LABORATORY MORTAR MIXTURES

This chapter centres around the sequential experimental phase where AHL attributes and their impact on mortar properties across diverse curing conditions are evaluated. The findings gained from this research segment served as a guide in identifying the ideal curing environment and feasible WBA share suitable for AHL mortars. Following the completion of phase II, which involved selecting the favourable type and proportion of WBA suitable for AHL binder, this phase of investigation was dedicated to the comprehensive evaluation of both fresh and hardened mortars. This chapter focused solely on the WBAs chosen during the preliminary screening, aiming to unveil their true potential for enhancing AHL mortar performance. A wide range of properties in the fresh state was examined, including fresh mortar consistency, bulk density, air content, temperature, and water-soluble chloride content. Subsequently, a comprehensive evaluation was conducted to investigate the influence of WBA on the mechanical, hygrothermal, and durability properties of AHL mortars.

Chapter 5: CONCLUSIONS, CONTRIBUTIONS, AND OUTLOOKS

In the concluding chapter, the primary discoveries from Chapters 3 and 4 are recapitulated, and the research concludes with a look ahead to future investigations.

2. STATE OF THE ART

2.1. Introduction

This chapter offers an overview of building lime with hydraulic properties. It also presents a review of the literature on incorporating into the building lime framework, which is the central focus of this research. The constraints imposed by modern standards for building lime with hydraulic properties and masonry mortar are discussed. Moreover, within the historic framework, the concept of sustainability is superimposed over the application of building lime with hydraulic properties in conservation purposes, as well as the functional requisites for repair mortars in historic buildings.

2.2. Background on building lime with hydraulic properties

2.2.1. Contemporary classifications

The EN 459-1 standard [28] divides building lime into two families, air lime and lime with hydraulic properties. The lime with hydraulic properties is composed mainly of calcium hydroxide, calcium silicates and calcium aluminates. It is also subdivided into three subfamilies: natural hydraulic lime (NHL), formulated lime (FL) and hydraulic lime (HL). In general, hydraulic lime has a chemical set and hardens when mixed with water. Carbonation, that is the reaction of lime with CO_2 from the air also contributes to the hardening process. Lime with hydraulic properties is defined by the initial set, has a defined range of available lime $(Ca(OH)_2$ content and is classified according to its mechanical properties, i.e., compressive strength. Besides the NHL, which is produced by burning limestone and its hydraulic properties are exclusively a result of the nature of raw materials, FL and HL are subfamilies of let's say artificial hydraulic lime. In this context, FL mainly consists of air lime and/or NHL with added hydraulic and/or pozzolanic materials. According to the specified standard, mixing of the primary binder (calcium air lime and/or NHL) is allowed with other main constituents such as natural pozzolana, including the calcined pozzolana, limestone, granulated blast furnace slag and even cements. Individual minor constituents, such as calcium sulphate or silica fume, are permitted without declaration if their individual share does not exceed 5 wt.%. Organic and mineral additives are also foreseen within the FL composition. In the declaration of the composition of formulated lime, all constituents above 5 % by mass shall be declared, with the exception of cement and/or Portland cement clinker in formulated lime shall be declared by the

producer by using the statement "contains cement". In comparison, the HL is only designated as HL and is classified in accordance with its compressive strength class, while it may consist of lime and other materials such as cement, blast furnace slag, fly ash, limestone filler and other suitable materials, similar as the FL sub-family, but with no mandatory obligation to declare any of its constituents. This implies that a variety of natural and artificial components can be blended to form both FL and HL, while the HL composition is completely non-transparent.

The broad lime spectrum, depending on the raw materials and the firing temperature is depicted in Figure 2.1. Ranging from feebly to eminently hydraulic [29], NHL's hydraulicity is reflected in the current EN 459-1 categories, ascending numerical grades of compressive strength at 28 day, as NHL 2, NHL 3.5 to NHL 5, which are broadly equivalent but not parallel to the old classifications of feebly, moderately and eminently hydraulic limes, respectively. While the EN 459-s standard allows overlapping of various NHL classes, the NHL 5 is most similar to modern date cement, often seen as the 'budget-friendly option'.
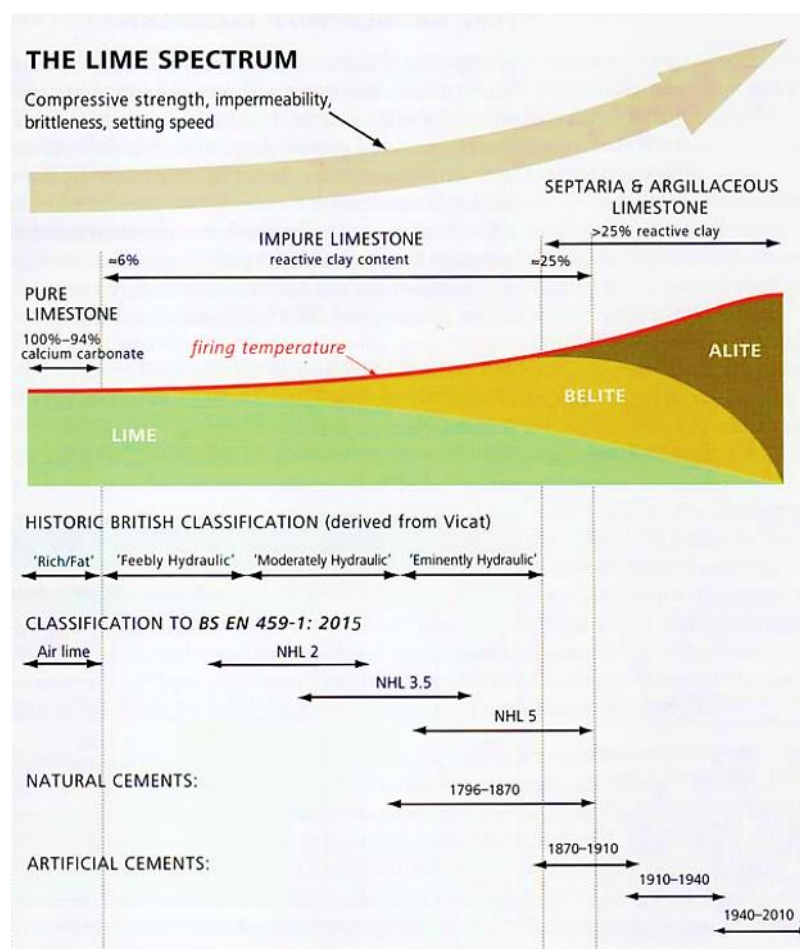
Figure 2.1. Variability in lime characteristics based on raw materials and firing temperature [30]

It can be seen that hydraulic lime binders are produced through the calcination of crushed limestone that includes clay components. These clay minerals, often referred to as impurities, are integral constituents. Within the temperature range of 900°C to 1100°C during the calcination process, there is a promotion of the formation of dicalcium silicates, commonly known as belite. These compounds exhibit a hydraulic set that is comparatively slower and weaker than the tricalcium silicates (alite) commonly found in modern cements, which form at temperatures exceeding 1250 °C [29]. Subsequently, the silica and alumina derived from the clay form reactive silicate and aluminate phases [31]. In instances where these constituent materials naturally coexist, the resulting lime blend is termed natural hydraulic lime (NHL). Alternatively, hydraulic lime can also be synthesized by incorporating pozzolans into pure lime, designating it as artificial hydraulic lime (AHL) [32].

The criteria set out in building limes EN 459-1 standard are founded on the classes of both NHL and AHL and defined by their compressive strength after 28 days in MPa (Table 2.1 and Table 2.2, and Table 2.3). The specified standard is primarily intended to enable manufacturers to produce products (binders) of consistent quality, rather than to directly predict how those products will perform in practical applications [29]. For instance, the strength of lime mortar, whether made with NHL, FL, or HL, is influenced not only by the choice of binder but also by various other factors. These include the type and grading of the sand used, the mixing ratios employed, and the quality of workmanship during the mortar's preparation and application. All of these elements collectively contribute to the final performance of the lime mortar in its intended use. The mortar standards are addressed in EN 998-1 [33], which pertains to mortar for masonry used in rendering and plastering applications, and in EN 998-2 [29], which focuses on mortar for masonry applications, specifically masonry mortar.

The standardised classification from the EN 459 series of standards is primarily determined by the 28-day compressive strength, as assessed in controlled laboratory environments. It's important to note that the strength of mortar in on-site conditions can vary considerably based on the specific microenvironmental factors. In practice, the strength of mortar often continues to increase significantly well beyond the initial 28 days, extending up to and even beyond 90 days [34].

In addition to evaluating the mechanical properties of mortar produced with hydraulic lime, the assessment of hydraulic lime's compliance with the EN 459-1 standard includes considerations of its chemical and physical properties, as well as the soundness and setting time of the lime

paste. Various criteria, such as the maximum SO_3 content, the minimum $Ca(OH)_2$ content, as well as the fineness and moisture levels of the binder, are essential for both NHL, FL, and HL. It is noteworthy that the upper limit for SO_3 content is somewhat more tolerant for HL, allowing for an excess of up to 7% if soundness is maintained. This implies that integrating HL into historical structures may present slightly more challenges compared to FL. However, it also provides greater flexibility for accommodating chemical variations influenced by the potential incorporation of synthetic materials.

Table 2.1. Criteria for NHL as set in EN 459-1 vs. traditional description of hydraulicity [28,29]

Traditional description of hydraulicity		Feebly to moderately	Moderately to eminently	Eminently to natural cement
EN 459-1 classification		**NHL 2**	**NHL 3.5**	**NHL 5**
BINDER	SO_3		≤ 2	
	Minimum available lime as $Ca(OH)_2$ [wt.%]	≥ 35	≥ 25	≥ 15
	Particle size – residue by mass [%] — 0.09 mm		≤ 15	
	Particle size – residue by mass [%] — 0.2 mm		≤ 5	
	Free water content [%]		≤ 2	
PASTE	Soundness [mm] — Alternative method		≤ 20	
	Setting time [h] — initial		> 1	
	Setting time [h] — Final	≤ 40	≤ 30	≤ 15
MORTAR	Air content in fresh mortar [%]		≤ 25	
	Minimum compressive strength (permissible range in brackets) [MPa] — 7 days	–	–	2 (2 – 7)
	Minimum compressive strength (permissible range in brackets) [MPa] — 28 days	2 (2 – 7)	3.5 (3.5 – 10)	5 (5 – 15)

Table 2.2. Criteria for FL as set in EN 459-1 [28]

	EN 459-1 classification		FL 2	FL 3.5	FL 5
BINDER	SO_3 [wt.%]			≤ 2	
	Minimum available lime as $Ca(OH)_2$ [wt.%] (permissible range in brackets)		*FL A*	*FL B*	*FL C*
			15 (15 – 40)	25 (25 – 50)	15 (15 – 40)
	Particle size – residue by mass [wt.%]	0.09 mm		≤ 15	
		0.2 mm		≤ 5	
	Free water content [%]			≤ 2	
PASTE	Soundness [mm]	Alternative method		≤ 20	
	Setting time [h]	initial		> 1	
		Final	≤ 40	≤ 30	≤ 15
MORTAR	Air content in fresh mortar [%]			≤ 25	
	Minimum compressive strength (permissible range in brackets) [MPa]	7 days	–	–	2 (2 – 7)
		28 days	2 (2 – 7)	3.5 (3.5 – 10)	5 (5 – 15)

Table 2.3. Criteria for HL as set in EN 459-1 [28]

	EN 459-1 classification		HL 2	HL 3.5	HL 5
BINDER	SO_3 [wt.%]			≤ 3 [a] (3 – 7)	
	Minimum available lime as $Ca(OH)_2$ [wt.%]		≥ 10	≥ 8	≥ 4
	Particle size – residue by mass [wt.%]	0.09 mm		≤ 15	
		0.2 mm		≤ 5	
	Free water content [%]			≤ 2	
PASTE	Soundness [mm]	Alternative method		≤ 20	
	Setting time [h]	initial		> 1	
		Final		≤ 15	
MORTAR	Air content in fresh mortar [%]		≤ 25	≤ 25	≤ 25
	Minimum compressive strength (permissible range in brackets) [MPa]	7 days	–	–	2 (2 – 7)
		28 days	2 (2 – 7)	3.5 (3.5 – 10)	5 [b] (5 – 15[a])

[a] SO_3 content ranging from 3% to 7% is considered acceptable, provided that soundness is demonstrated after 28 days of water curing, as determined by the test specified in EN 459–2:2021.

[b] HL 5 with a bulk density less than 0.9 kg/dm³ is allowed to have compressive strength up to 20 MPa.

2.2.2. Traditional classifications

Prior to the modern classification system introduced in EN 459-1, natural hydraulic limes (NHLs) were categorized using the Cementation Index (CI), a framework originating from Vicat. It's worth noting that the term hydraulic lime' itself was introduced by Vicat, supplanting previous terms like 'lean lime' and 'water lime' [35]. In this system, limes were grouped into three categories: feebly, moderately, and eminently hydraulic, based on the clay content within the calcareous material. These classifications were initially established through empirical observations involving clay content and setting times. Over time, refinements were made by introducing the 'hydraulicity index' (HI), defined as the ratio of silica and alumina to lime [29]. This method aimed to predict the performance of hydraulic limes by assessing the likely hydraulicity of the raw binder materials. The CI effectively balanced the weight contribution of various components deduced from chemical analyses of the limestone. The most frequently encountered expression in the literature for the CI is represented by Eq. 2.1. Additionally, the HI, as described in Eq. 2.2, serves as another method found in literature for classifying hydraulic lime. It balances only the presence of the most active oxides within the material [36].

$$CI = \frac{(2.8)SiO_2 + (1.1)Al_2O_3 + (0.7)Fe_2O_3}{CaO + (1.4)MgO} \tag{2.1}$$

$$HI = \frac{SiO_2 + Al_2O_3}{CaO} \tag{2.2}$$

Based on the CI values, lime-based binders could be categorized into five distinct classes [36,37], as presented in Table 2.4.

Table 2.4. Cementation index of various types of building lime [36,37]

Lime description	Cementation index (CI)	Active clay in the limestone
Fat lime	Around zero	Very little clay
Slightly hydraulic limes	0.3 – 0.5	Around 8%
Moderately hydraulic limes	0.5 – 0.7	Around 15%
Eminently hydraulic limes	0.7 – 1.1	Around 25%
Natural cement	1.7	Around 45%

While this method is undeniably still practical and simplifies the evaluation process, relying solely on the chemical data of the raw limestone to evaluate the binder assumes that all of the silica is fully activated, a condition that is not always met. It becomes clear that hydraulicity is closely linked to the amount of 'combined' (i.e., soluble) silica, and this aspect should be recognised as a fundamental element in the modern classification of hydraulic limes. Acknowledging the role of 'combined' silica is crucial for a comprehensive and accurate classification of these materials in contemporary contexts [29]. As previously noted, the earlier classifications have been surpassed by EN 459-1:2015 [28].

2.3.   Hardening processes

Hydraulic limes exhibit the ability to set in damp conditions and even underwater. The relatively prompt initial setting is primarily attributed to their hydraulic properties. The presence of calcium silicates and aluminates in hydraulic limes allows them to react with water, forming calcium silicate hydrates and calcium aluminate hydrates. As the process continues, additional strength is gained through the ongoing hydration and the gradual carbonation of remaining available lime ($Ca(OH)_2$). During carbonation, carbon dioxide (CO_2) diffuses through the porous structure and reacts with the $Ca(OH)_2$ and the hydration products, resulting in the formation of calcium carbonates ($CaCO_3$) and amorphous silica and alumina. The effectiveness of the hydration and carbonation processes is influenced by the quantity of hydraulic phases present and the calcination temperature of the original limestone [31]. Hence, in all hydraulic limes (but not in cements), the two setting mechanisms occur concurrently:

−   **Hydraulic reaction:** This refers to the process of setting with water. It can be simplified as a material's ability to solidify in the presence of water. The extent to which this reaction takes place depends on the quantity of hydraulically reactive components within the material, along with the availability of sufficient water. In hydraulic lime mortars, the hydraulic set occurs as a result of the hydration, or reaction with water, of specific compounds present in the fresh mortar;

−   **Carbonation reaction:** This involves the absorption of carbon dioxide and the release of water, which results in a degree of material hardening. Carbonation is a universal process in all lime mortars. In non-hydraulic materials, carbonation and controlled drying are the mechanisms through which the material gains hardness.

In general, there is an inverse relationship between the hydraulicity of the binder and the necessity for carbonation. Put simply, as the hydraulicity of the binder increases, the requirement for carbonation decreases, and vice versa. Table 2.5 provides an estimate of the ratio between hydraulic setting and carbonation setting for various commonly used binders.

In general, in NHL mortars, hydration precedes carbonation, except for pozzolanic materials with low reactivity with lime that favoured the consumption of lime by carbonation reaction [38].

Table 2.5. Approximate hydraulic set versus carbonation set [32]

Binder type	Extent of hydraulic set [%]	Extent of carbonation set [%]
Non-hydraulic lime	0	100
NHL 2	45 – 50	50 – 55
NHL 3.5	75 – 80	20 – 25
NHL 5	80 – 85	15 – 20
Ordinary Portland Cement	100	0

The extent of hydraulic set is ascribed to the presence of particular materials that grant the binder its hydraulic properties. Notably, the content of impurities in the raw limestone, particularly silica (SiO_2) and alumina (Al_2O_3), plays a pivotal role in this process.

Different calcination temperatures and varying quantities of siliceous materials in the raw components lead to differing compositions of hydraulic phases in NHL and cement. These variations exert a significant influence on the ultimate properties of the binder. In cement, sintering gives rise to the formation of calcium silicates (primarily C3S) and calcium aluminates (C3A and C4AF). In contrast, NHL predominantly features larnite (akin to C2S) as the principal hydraulic phase, accompanied by a lesser quantity of gehlenite (C2AS) [39,40]. The presence of gehlenite indicates a lower temperature reached during the burning process of NHL. While C3S, C3A, and C4AF may also be discernible in NHL, they are typically present in minor quantities, possibly due to localized overheating in the kiln. The hydration of C2S (belite) occurs over an extended period, typically around 6 months, whereas C3S and C3A undergo a notably rapid hydration process. Systems containing C3S (alite) demonstrate swift strength gains due to the hydration of this hydraulic component. By the 28th day, belite achieves approximately 10% of the strength of alite. The strength development attributed to C2S hydration extends over the course of a year [38].

Available lime is another significant component of hydraulic limes. Even after the hydration of C2S to form C-S-H, a substantial portion of the binder remains as calcium hydroxide. Consequently, when hydraulicity is lower, the available lime content tends to be higher, leading to a greater extent of the carbonation set.

2.4.   Optimal curing: Balancing hydration and carbonation

The progress of hydration and carbonation reactions, as well as the kinetics of hardening reactions, and consequently, the mechanical properties, are greatly shaped by the curing conditions to which mortars are subjected. Temperature and relative humidity (RH) are key parameters that notably impact the advancement of these mechanisms. Given the substantial variation in the influence of these factors between hydraulic and non-hydraulic mortars, it becomes essential to tailor the adjustment of curing conditions according to the particular type of binder.

Hydration benefits from a higher water content while slowing down the carbonation process. Swift carbonation occurs within the 40% to 80% RH range, coupled with moderate temperatures. In contrast, the hydration of hydraulic binders necessitates a higher RH, typically falling between 95% and 100%, particularly during the initial days after casting [38,41–43]. While average values between 80 and 90% of final carbonation can be achieved near the surface of mortars exposed to the atmosphere, it is widely accepted in scientific literature that 100% carbonation is practically not achievable in an outdoor environment [38,44]. There is no doubt that moisture significantly impacts the extent and sequence of these reactions. Hydration is predominantly facilitated in higher moisture environments, while carbonation tends to occur more prominently under drier conditions. This leads to noteworthy implications for mechanical properties, emphasizing the need to cure mortars with hydraulic lime in moist conditions to promote early hydration.

Many mistakenly believe that strong hydraulic lime, like NHL5, combined with proper care and protection, eliminates the need for carbonation, focusing solely on hydraulic setting. However, skilful contractors understand the relevance of protection in lime work. Therefore, neglecting carbonation during curing can lead to poor results so providing appropriate aftercare and protection to ensure both proper carbonation and hydraulic set is of utmost significance.

Curing hydraulic lime mortars is advisable, irrespective of their classification, as lime materials, like young children, require careful attention during their early stages [32].

Further variables affecting the interaction of these processes encompass the volume of calcium hydroxide, in conjunction with the pore structure and pore water content, which regulate the rate of CO_2 diffusion and, consequently, influence carbonation. Additionally, the levels of calcium silicates and aluminates play a significant role in governing the hydration process [38,43].

Following the guidelines of EN 1015-11 [45], mortars containing hydraulic binders undergo a carefully controlled curing process. For the initial three days after casting, they remain within moulds under specific humid conditions, maintaining a relative humidity (RH) of $90 \pm 5\%$ and a temperature of 20 ± 2 °C. Following demoulding at the end of this 3-day period, the mortar specimens receive an additional 7 days of curing under the same high humidity conditions. Subsequently, they are transferred to an environment with a relative humidity of $65 \pm 5\%$ for up to 28 days.

Simultaneously, according to the provisions of EN 459-1 standard [28], materials like FL 3.5, as well as less hydraulic binders such as NHL 2 and FL 2, adhere to the aforementioned conditions. In contrast, all other types of hydraulic lime are maintained at a relative humidity not less than 90% until the time of compressive strength testing.

Given that the setting and hardening process relies on the cyclic dissolution and precipitation of minerals within the wet mortar, maintaining suitable water supply for an extended period is crucial for sustaining the hydraulic reaction post-placement. Swift water evaporation can result in incomplete hydration. Additionally, due to the gradual nature of hydration reactions, mortars with hydraulic limes benefit from moist conditions to ensure adequate strength development. Consequently, curing under dry conditions does not sufficiently enhance their strength, as the hydration reactions are decelerated or even halted by the full carbonation of lime in lime-pozzolana mortars. Therefore, it is imperative to subject hydraulic lime and lime-pozzolana mortars to moist curing during their early stages to optimize hydration reactions. This highlights the pivotal significance of employing proper curing methods [32,46].

2.5.   Incorporation of pozzolanic materials within NHL binder systems

Pozzolans are materials characterized by a high silica and/or alumina content in an amorphous state, possessing a large specific surface area, and the unique property of reacting with calcium hydroxide when exposed to water. This reaction leads to the formation of hydraulic products. The term 'pozzolan' encompasses a wide array of materials containing reactive silica that can react with lime at ambient temperatures, resulting in the formation of calcium silicates. This definition encompasses both natural and synthetic materials. Artificial pozzolans, a category of synthetic materials, can be produced through thermal treatment. Examples of these include ashes derived from the combustion of plant-based materials (such as rice husk ashes), natural substances like clays (metakaolin, for instance), and industrial byproducts, such as certain ceramics or fly ashes from coal and biomass combustion. The utilization of synthetic pozzolans offers various advantages, both in economic and environmental terms. Indeed, the utilization of pozzolans offers significant advantages, both from economic and environmental perspectives. Notably, interest in their use has been on the rise, driven by the fact that the combination of hydraulic binders and pozzolans yields mortars with enhanced durability characteristics [29,47].

Pozzolanic activity arises from the reaction of lime with the byproducts of alkaline attack on acid silicates. The pozzolanic material interacts with the available lime present in the NHL binder and that which is released during the hydration of cementitious components. This interaction typically exerts a more pronounced effect on weakly hydraulic lime rather than on eminently hydraulic lime, primarily due to the higher quantity of available lime in the former [29]. The strength gained by the hydration reaction of NHL can be improved by using pozzolanic material, as the portlandite produced during the hydration process of NHL can be either carbonated and/or reacted with the pozzolanic material to yield newly-formed C–S(A)–H. The NHL binders enriched with pozzolanic material can yield compact structures formed by C–S(A)–H and calcite, since pozzolanic reaction in the presence of moist conditions and carbonation occurred continuously [38].

It has been found by Cizer et al. [46] that lime-pozzolana compositions, utilizing air lime as primary binder, may lack long-term strength development due to the order of the primary hardening reactions influencing each other. This can cause negative consequences for the long-term durability of such materials. It was concluded that competition between carbonation and hydration can take place in lime-pozzolana mortars under atmospheric conditions if the

pozzolanic material has low reactivity with lime. Highly reactive pozzolanic material like metakaolin may not provide sufficient strength development to the mortar due to phase modifications. It is the hydrated phases and their stability, which are crucial for the achievement of sufficient strength. The degree and the order of hydration and carbonation reactions are strongly influenced by the moisture content. Due to the gradual progress of the hydration reactions, hydraulic lime and lime-pozzolana mortars require moist conditions to ensure sufficient strength development. Curing under dry conditions does not sufficiently increase their strength because the hydration reactions are slowed down or even terminated by the full carbonation of lime in lime-pozzolana mortars. Therefore, hydraulic lime and lime-pozzolana mortars should be treated with moist curing during early stages to improve the hydration reactions.

2.6. Advancing lime framework with WBA integration

In pursuit of identifying enduring, sustainable, economically viable, and pragmatic applications for WBA, the prevailing body of research (in a global and local perspective) predominantly emphasizes its advantageous utilization in cementitious composites [12,48–56], where it serves as a mineral additive in cementitious composites, or aggregate alternative in concrete. In a broad sense, as the proportion of wood ash increases, there tends to be a decline in the mechanical properties and durability of building materials. Conversely, numerous research findings have substantiated that incorporating wood ash at lower to moderate concentrations (less than 30%) has the potential to enhance the microstructure, subsequently mechanical behaviour. However, in stark contrast, the investigation into the potential role of WBA as one of the constituents within the composition of building lime with hydraulic properties, which constitutes the primary focus of this proposed research, has been relatively limited.

For instance, in a study conducted by Baričević et al. [26], a comprehensive analysis was undertaken to explore the development of an eco-friendly lime binder sourced from waste materials. This investigation involved the incorporation of calcareous wood biomass ash in conjunction with coal fly ash within a composite system. The research findings furnished compelling evidence for the categorization of a binder comprising 25 wt.% of wood ash as a hydraulic lime conforming to the HL5 classification as per the EN 459-1 standard. Particular emphasis was placed on monitoring volume deformations observed in pastes and mortars featuring elevated levels of wood ash. It was noted that the presence of expansive elements,

including CaO and MgO, among others, might undergo neutralization through diverse maturation mechanisms while adequate particle fineness could be achieved by grinding.

In the work by Ndahirwa [57], a significant advancement was made in the valorization of various biomass ashes, in conjunction with sunflower particles, to craft eco-friendly lightweight building materials. Biomass ashes took precedence in the formulation of a binder matrix, synergizing with NHL. Through assessment at specified curing intervals, the study loked into the setting time, mechanical attributes, and microstructural features of the resultingly wood ash pastes. The results indicate that all analysed powders are rich in CaO, while the chemical composition of biomass ashes varied from one ash to another. The SiO2 content in biomass ashes was comparable to that in NHL. Moreover, it is noteworthy that wood fly ashes contained higher amounts of K_2O and SO_3. The variability of the chemical composition of biomass ashes can be attributed to feedstock origin, combustion temperatures and technology as well as storage conditions. Moreover, the mechanical tests indicated that using hybridisation ratios of NHL:WBA up to 20:80 may enchance mechanical properties of pastes with fly biomass ashes. The findings illuminated that all examined powders exhibited a notable abundance of CaO, albeit with variations observed in the chemical composition of biomass ashes across samples. Notably, the SiO_2 content in biomass ashes closely mirrored that of NHL. Additionally, it is worth highlighting that wood fly ashes exhibited elevated levels of SO_3 and K_2O. Furthermore, the mechanical assessments underscored that employing hybridization ratios of NHL to WBA of up to 20:80 demonstrated the potential to enhance the mechanical strength of pastes incorporating fly biomass ashes.

Fusade et al. [58] similarly conducted an experimental study aimed at assessing the influence of wood biomass ash on lime mortar properties. A WBA, characterized by a predominance of CaO, was employed as a substitute for aggregates across varying proportions in mortars containing NHL as well as air lime. The research outcomes indicate that incorporating wood ash into lime mortar within moderate ranges (spanning from 20 to 40 wt.%) yields a potentially superior mortar blend for repointing masonry joints, especially in moisture-rich environments. This formulation demonstrates the ability to set effectively in damp conditions, achieve strength gain, exhibit favorable permeability and drying characteristics, all while manifesting minimal shrinkage and cracking. However, in higher proportions (spaning form 70% up to 100 wt.%), certain adverse effects may be noted, including elevated drying shrinkage. However, it's important to note that the findings also emphasize that the presence of fine wood ash particles leads to a higher proportion of pores in the capillary range, ultimately resulting in an

enhancement of compressive strength. These fine particles originating from wood ash are acknowledged for their potential pozzolanic reactivity. Moreover, due to its hygroscopic properties, wood ash enables lime mortars to retain a greater amount of moisture, thereby suppressing capillary absorption.

The findings presented by Fort et al. [24] underscore the potential of wood biomass ash (WBA) as a promising pozzolanic material for enhancing air lime plasters. This assessment is grounded in the results obtained from composite plasters, where WBA was employed as a substitute for up to 50 wt.% of calcium air lime. The study delves into the impact of WBA, characterized by its prominent SiO_2 content, on fundamental material properties, including mechanical and hygric characteristics. The outcomes of this analysis demonstrate that the incorporation of WBA, up to a dosage of 50 wt.%, leads to a significant improvement in both compressive and flexural strength while maintaining capillary absorption at a consistent level. In contrast, there is a notable reduction of approximately 50% in water vapor permeability as the WBA dosage increases. This suggests that the modified lime-pozzolan plasters exhibit substantial potential for application as surface layers in building construction, facilitating the utilization of industrial waste materials in conjunction with conventional binders.

Furthermore, Pavlíková et al. [22] conducted an in-depth investigation into the impact of incorporating wood-based biomass ash into air lime mortars, assessing their structural, mechanical, hygric, and thermal properties. Consequently, it was explored as a potential pozzolanic component in lime-based mortars intended for renovation purposes. The analysis encompassing chemical, physical, and mineralogical aspects of mechanically-activated wood biomass ash, coupled with the evaluation of microstructure, mechanical, hygric, and thermal characteristics of the formulated mortars containing WBA as a constituent of the blended binder, proved that mortars incorporating WBA demonstrate equivalent or improved properties compared to traditional pure lime-based plaster, thereby suggesting their suitability for rendering and walling renovation mortars. Furthermore, WBA was identified as an environmentally efficient and cost-effective alternative pozzolan for integration into lime blend-based construction materials. In a correlated study, Pavlíková et al. [59] investigated an analogous ternary binder blend with the purpose of crafting lightweight mortars specifically tailored for renovation applications. This composite consisted of air lime, wood biomass ash (WBA), and the inclusion of metakaolin. It's worth noting that both metakaolin and WBA exhibited a notable high silica content, showcasing significant pozzolanic activity and the requisite fineness for seamless integration with hydrated lime. The observable increase in

porosity, a pivotal parameter for the effectiveness of repair mortars, in conjunction with a reduction in thermal conductivity, strongly suggests that the engineered mortar featuring WBA holds the potential to elevate the overall hygrothermal performance of renovated masonry structures.

Almeida et al. [60] conducted an assessment of the feasibility of incorporating rice husk ash into air-lime-based mortars for historical buildings. In this study, mortars were formulated with a portion of air lime being substituted with pre-treated siliceous waste ash. The findings derived from mechanical performance tests revealed a notable enhancement in both flexural and compressive strength, along with an increase in the dynamic modulus of elasticity. Of particular note were the significant improvements observed in terms of the resistance to sodium sulfate exposure and a modest reduction in capillary water absorption. Porosity and water vapor permeability remain largely unchanged when compared to pure lime mortar.

Table 2.6. Synthesis of research utilizing WBA in building lime binders

Literature	Type of WBA	Binder system	Function	b/a ratio (by mass)
Baričević et. al. [26]	calclareous WBA	WBA – coal fly ash	binder replacement	1:1.5
Ndahirwa [57]	calclareous WBA	WBA – NHL	binder replacement	-
Fusade et al. [58]	calclareous WBA	WBA – NHL	aggregate replacement	1:3
Fort et al. [24]	siliceous WBA	WBA – air lime	binder replacement	1:3
Pavlíková et al. [22]	siliceous WBA	WBA – air lime	binder replacement	1:3
Pavlíková et al. [59]	siliceous WBA	WBA – air lime & metakaolin	binder replacement	1:1
Almeida et. al. [60]	siliceous rice husk ash	waste ash and air lime	binder replacement	1:2

To date, there is limited research on using WBA in building lime binders, especially in the hydraulic framework, as shown in Table 2.6. Existing research emphasizes the value of hydraulic lime, especially in structures exposed to atmospheric stresses. This highlights the importance of hydraulic lime, particularly in historic buildings, as opposed to air lime, often considered the modern equivalent to the original construction materials.

2.7. Sustainability in the historical framework

Part of this sub-chapter has been published as: Šantek Bajto, J.; Štirmer, N.; Baričević, A. Sustainable Hybrid Lime Mortars for Historic Building Conservation: Incorporating Wood Biomass Ash as a Low-Carbon Secondary Binder. Heritage 2023, 6, 5242–5269. https://doi.org/10.3390/heritage6070278

Following the most devastating earthquakes in the last 140 years, which hit central Croatia in 2020 [61], national plans and strategies narrowed their focus on the comprehensive renovation of buildings, but also on promoting the renovation of buildings with cultural and historical merit, the vulnerability of which was highlighted by the devastation caused by the recent earthquakes. An all-round renovation of these buildings, which are both impaired and energy inefficient, should lead to a reduction in carbon emissions and energy consumption, but also contribute to the development of a circular economy and the application of sustainable solutions. This small niche, which can incorporate other measures to upgrade the basic requirements for construction works already in place, such as using environmentally sound raw and secondary materials in construction [62], can help balance the long-term use of resources while maximizing social benefits and minimizing environmental impacts. In creating a dialogue between the urban environment and ecosystem resources, the link between sustainable innovation and the cultural dimension is all-important. Just as the European waste hierarchy emphasizes that the zero-waste concept [1] means not merely recycling waste, the maintenance, repair, and renovation of existing buildings must be prioritized over new construction [2]. In this context, effective interventions, particularly in heritage buildings, necessitate extensive knowledge and expertise on the chemical, physical, and mechanical properties of both the existing materials and the materials intended for use [63].

2.7.1. Compatibility issues

In order to mitigate the damage to the built heritage and, at the same time, the effects of climate change, the selection of suitable repair materials is crucial. In terms of suitability, traditional and contemporary materials are often at odds with each other, making the selection of a suitable, matching material for historic buildings a particular challenge. It is foreseeable that when modern materials are used and applicable codes are followed, heritage preservation often falls by the wayside. In today's world of circular and sustainable architecture, repair materials that are compatible with the materials originally used are therefore of paramount importance. A renewed interest in natural hydraulic lime (NHL) has emerged as it is a useful, relatively modern

binder for repair mortars, suitable for the conservation of historic buildings that require very flexible, breathable, yet durable building materials [64][65]. Historical records reveal that hydraulic mortar was anciently made by mixing lime and pozzolans and was used in numerous buildings in ancient Rome and Greece [63][66][67]. Not only does it blend well with authentic building materials, it is also considered a more sustainable alternative to cement [34,68]. This ought to be in line with the European Union (EU) mainstreaming renewable energy sources such as biomass, geothermal resources, sunlight, water, and wind.

2.7.2. Sustainable development goals

By following sustainable trends that address complex local conditions and growing energy and material needs, the construction sector is also following the United Nations Sustainable Development Goals (SDGs). The link between the SDGs, focusing on Goals 9, 11, and 12, and the incentive for this research is illustrated by the fact that the use of environmentally friendly technologies, such as biomass, results in additional waste production. Therefore, strategic waste management, i.e., rethinking waste as a resource and preserving built heritage, is essential. This points to the need to include the cultural dimension in a long-term concept of local sustainable development. In order to scale up the manufacturing capacity for the net-zero technologies and products needed to meet ambitious European climate goals [3,69], it is imperative that the EU introduce innovations into mass production that will decarbonize energy-intensive industries such as cement and lime. Currently, lime production is the second largest industrial source of carbon emissions after cement production [70]. Following the European Green Deal, the key EU strategy to address climate change and achieve climate neutrality, the European Commission proposed raising the EU climate target for 2030 to at least a 55 percent reduction in greenhouse gas emissions, which would mean a widespread phase- out of coal by that date [8]. Even more stringent legislation to accelerate the rollout of renewables raises the binding renewable energy target to at least 42.5% by 2030 [71]. Closing the gap left by the decline in coal burning depends largely on the ability of renewables to meet these overall binding targets [7]. According to data of [72], wind, solar, and bioenergy will be the ones providing most of the energy in the EU by 2050. Biomass for energy production is already the most important source of renewable energy in the EU and supports the EU's energy security by holding a share of almost 60% in the total renewable energy mix. Forest biomass is the leading point of biomass supply (logging and wood processing residues, firewood, etc.) [12,13,73], but can only be considered carbon neutral if it comes from a forest system whose carbon stock is balanced [74]. In comparison, bioenergy consumption in the EU in 2017 was almost 120 Mtoe (58%), while

other renewable energy sources such as photovoltaic, wind, and hydropower accounted for about 86 Mtoe (42%) [49]. However, with the increasing number biomass-fired power stations, there is a surplus of waste ash worldwide. It is projected that biomass combustion will generate about 476 million tons of ash annually, assuming that 7 billion tons of biomass are burned with an average ash content of 6.8% [54]. While it may be true that the EU is firmly committed to minimizing the uncontrolled spread of waste in the environment [20,21], the ongoing WBA handling routine in Europe is grounded on basic landfilling [12]. In the interest of finding pragmatic and sustainable yet value-based functions for WBA more broadly, the vast majority of studies address the beneficial use of WBA in cementitious composites, identifying it as a cement replacement, mineral admixture, or aggregate replacement in concrete. In contrast, research on employing WBA as a pozzolanic and/or hydraulic component in the formulation of hydraulic lime, which is the focus of this research, is still limited. Previous studies have focused almost exclusively on the influence of WBA addition on the properties of air-lime mortars [22,23,75], while only a few papers in the literature place WBA within the framework of a hydraulic lime framework [25,26]. As hydraulic lime is a favourable material for use in buildings subjected to considerable atmospheric action [27,76], its value must be highlighted when used in historic buildings, instead of air-lime, which is often considered the material most like the materials originally used. The formulation of hydraulic limes with the addition of WBA complies with the EN 459-1 standard [28], which distinguishes between natural and artificial lime and defines artificial hydraulic lime (AHL) (detailed as hydraulic limes (HL) and formulated limes (FL)) as binders containing air lime and/or natural hydraulic lime (NHL) in combination with hydraulic and/or pozzolanic materials. Hydraulic limes vary in their degree of hydraulicity, extended from feebly to eminently hydraulic, but in all of them, two setting mechanisms take place: a hydraulic reaction, i.e., setting with water, and a carbonation reaction, i.e., uptake of CO_2, which contributes to the hardening of the material [29,32]. The available lime content, limited in EN 459-1 to FL in the form of $Ca(OH)_2$, widely ranges from 15% to 80% by weight, which means that it is possible to produce artificial hydraulic lime with a high content of artificial hydraulic components [27].

2.8.   Functional requirements for repair mortars used in historic buildings

Mortar plays a diverse and vital role in masonry work. It encompasses various types, each serving a unique purpose: bedding mortar for setting masonry units, pointing mortar for sealing joints, grout for filling voids and cracks, exterior render for safeguarding against the elements, interior plaster for both protection and decoration, and surface repair mortar for replacing missing masonry sections.

To determine the characteristics of a repair mortar, a clear understanding of its specific requirements is crucial. The choice of mortar for repair is influenced by its intended function within the structure, which, in turn, is shaped by the type of masonry and the chosen binder.

Functional criteria establish quality standards by assessing the historical and technical aspects of a structure, offering a foundation for selecting raw materials, compositions, and testing methods. The criteria for repair mortars are driven by their function in the structure, exposure levels, and potential environmental challenges [78].

Functional requirements are linked to the unique role that each mortar type plays, aiding in their categorization. For instance, a masonry wall's mortar must withstand vertical and horizontal forces while acting as a weather barrier. On the other hand, technical factors pertain to measurable properties such as strength, modulus of elasticity, and water absorption, directly affecting mortar performance. Together, these functional and technical considerations guide the acceptable compositions for repair mortar. The framework is further influenced by historical and cultural preferences .

The classification of historic masonry is intricate, as it varies by location and reflects local traditions and the availability of construction materials. Each type of mortar is held to specific technical standards tied to measurable physical properties. It's important to note that not all these standards carry the same weight for every mortar type. Table 2.7 illustrates a scale from 0 to 3, signifying the varying importance of these standards, always relative to the specific context.

Table 2.7. Technical requirements vs. classification of mortar [77]

Technical requirement	Mortar type classification				
	Bedding	**Pointing**	**Render**	**Plaster**	**Grout**
Adhesion (bond strength)	3	3	3	3	2
Strength (compressive, flexural, tensile)	2	2	1	1	2
Deformability and elasticity (E modulus)	3	3	2	1	3
Weatherproofing					
Water penetration resistance	2	3	3	1	1
Freeze-thaw resistance	2	3	3	0	1
Thermal dilatation	1	2	3	3	1
Vapour transmission	2	3	3	3	1
Wetting and drying behaviour	2	3	3	2	1
Aesthetics	1	3	3	3	0
Rating scheme: 0: no importance, 1:less important, 2: important, 3:more important					

Compatibility, a key concern in the realm of repair mortars, underscores the need for these materials to seamlessly integrate with the existing masonry. "Compatible" signifies that repair mortars must not inflict harm or adversely affect the existing structure and should strive for optimal durability within these parameters. Compatibility, in this context, should be approached comprehensively, encompassing technical, aesthetic, and historical considerations.

Regarding the substrate, it's vital that the strength and deformability properties of the mortar are less than those of the masonry units and are comparable to or less than those of the existing mortar. This harmony ensures a cohesive and enduring restoration [31,34,78,79].

Recreating the precise composition of historical lime mortars proves challenging due to the effects of weather and the availability of original materials over time. Consequently, mortar formulations derived solely from chemical analysis may not perfectly replicate the original. Nevertheless, many historic mortars included a hydraulic component in the binder, making the addition of hydraulic lime a suitable choice when striving to mirror the chemical composition of historic lime mortars.

2.9. Progress beyond the state of the art

In light of the knowledge gaps concerning the recognition of WBA as a prospective constituent in lime binders and subsequently mortars, this doctoral dissertation presents an extensive analysis of diverse WBA variations, encompassing both calcareous and siliceous compositions as well as fly and mixed ashes. The central aim of this research was to assess the potential for the development of cementless mortar tailored for conservation purposes, achieved through the integration of building lime with hydraulic properties and specially formulated with WBA.

The initial stage, which encompasses the integration of WBA into the composition of hydraulic lime binders, aligns with the criteria outlined in the standard EN 459-1 for building lime [28]. These standards differentiate between natural and artificial lime, further categorizing artificial hydraulic limes into formulated lime (FL) and hydraulic lime (HL). Both of these sub-categories of hydraulic lime combine air lime and/or natural hydraulic lime (NHL) with an array of natural or synthetic materials. According to these contemporary definitions, it is implied that building lime containing WBA, would fall under one of these subsets.

Going back to antiquity, the Romans demonstrated early expertise in the use of formulated limes of that time by using volcanic ash to boost the quality of lime in the construction of iconic structures such as the Colosseum. The skilled combination of pure lime with clay and/or other silicate/aluminate minerals yielded a high-performance artificial hydraulic lime [29,32].

This research aims to create a parallel analogy, yet within a hydraulic binder matrix, utilizing locally sourced WBAs. The chemical composition of these ashes, marked by the prevalent presence of calcium and silicon oxides, supports the hydraulic nature of the primary NHL binder. The outcome would be a cement-free lime binder incorporating WBA, yet still upholding the integrity of restoration mortars. This innovative approach would not only abolish industrial waste but also scale down the depletion of natural resources.

In the wake of the most devastating earthquakes to strike central Croatia in more than a century, an event that unfolded in 2020 [61], national policies and strategies have refocused their efforts on the comprehensive restoration of buildings, with particular attention to those possessing cultural and historical significance. This emphasis has grown in the aftermath of the recent seismic events, which underscored the vulnerability of such structures.

This initiative is aligned with the National Plan for Recovery and Resilience 2021-2026 [80], which, in accordance with the National Energy and Climate Plan 2021-2030, aims to assist in

the recovery of regions affected by the two catastrophic earthquakes. The comprehensive restoration of these culturally prominent yet structurally compromised and energy-inefficient buildings is anticipated to yield a reduction in both carbon emissions and energy consumption. Moreover, it contributes significantly to the advancement of a circular economy and the adoption of sustainable solutions. This niche field, capable of incorporating various measures to upgrade the established basic requirements for construction works [62], including the use of environmentally responsible and resource-efficient materials, such as WBA, provides a means to harmonise the enduring preservation of resources with the maximization of societal advantages, all while minimizing environmental impacts. Establishing a synergy between the urban fabric and natural resources remains high-priority, underscoring the essential connection between sustainable innovation and the historical context.

3. EXPERIMENT: FORMULATION AND TAILORED DESIGN OF BINDER BLENDS

3.1. Investigative objectives

This chapter is dedicated to the thorough assessment of WBA attributes and their impact on NHL-WBA binder system, subsequently extending to the AHL properties under varying WBA proportions, as well as varying hydraulicity of the primary NHL binder. The insights gained from this research segment will serve as a crucial roadmap in pinpointing the most favourable type and feasible percentage of WBA, befitting for AHL binders and ensuing mortars.

The overarching objective is to validate the first and second hypotheses, outlined as follows:

- *'Building lime with hydraulic properties, i.e., an artificial hydraulic lime can be prepared with wood biomass ash';*
- *'The chemico-mineralogical composition of WBA, in addition to evaluating various WBA with different degrees of pozzolanity and hydraulicity, has a direct impact on its applicability in a hydraulic binder and the possibility of hardening of hydraulic lime mortar systems'.*

Hence, in order to identify and nominate suitable WBAs for the formulation of an artificial hydraulic lime (AHL) binder, a thorough investigation of the chemico-mineralogical composition and physical properties of natural hydraulic lime (NHL) and WBAs is carried out, recognising their pivotal roles as major constituents within the binary AHL binder formulations. In addition, the assessment of the prospects for the potential applicability of WBAs as constituents for the development of an artificial hydraulic lime is extended on the basis of the parameters prescribed in the standard HRN EN 459-1 [28], which includes the criteria for hydraulic lime binders and consequently for the corresponding pastes. This means that setting the acceptable share of WBA in the AHL binder is affirmed by achieving standard consistency, setting time and soundness of AHL pastes aligning with the aforementioned standard.

A dual-engagement strategy in relation to WBAs involves the assessment of predominantly calcareous WBAs and predominantly siliceous WBAs. In this context, locally sourced WBAs, characterised by different calcium and silica content and particle size depending on the collection locale (distinguishing between fly and mixed ashes), are investigated as a potential alternative material.

3.2. Materials and methodology

3.2.1. Materials

In this research phase, hybrid artificial hydraulic lime binders were prepared by blending a selection of 11 distinct WBAs with 2 different NHLs (Figure 3.1). Among these WBAs, 4 are characterized as fly ashes, and 7 are classified as mixed ashes, with only two of the mixed ashes being predominantly siliceous. The WBAs were collected from power plants across Croatia, primarily utilizing grate firing systems and fuelling them with untreated wood chips (refer to Table 3.1). Two sources of natural hydraulic lime were incorporated within the AHL binary binder system. The first was NHL 3.5, a commercially available moderately hydraulic natural hydraulic lime, supplied by Baumit Croatia. Additionally, NHL 5, a natural hydraulic lime with enhanced hydraulicity, was utilized, was employed and sourced from Calce Raffinata Italy, provided by Samoborka d.d. in Croatia.

The proposed designations for the WBAs are: WBAi.F and WBAi.M. Here, the subscript "i" represented the assigned ID number of a specific WBA, while the while the "F" or "M" marker designates the type of WBA, indicating whether it is a fly ash or a mixed ash, respectively.

Analogously, the proposed designations for the binder/paste blends are: AHLi-20-B, AHLi-30-B, and AHLi-40-B. Here, the subscript "i" represented the ID number of the respective WBA used, while the percentages denoted the proportion of WBAi in the binder blend. Furthermore, the 'B' designation serves to indicate the binder level, distinguishing it from the mortar level, thus enhancing clarity in the research. For the purpose of establishing reference points, control binder blends were formulated using only natural hydraulic limes as the primary binders. These control blends were designated in accordance with the primary binder label, resulting in NHL 3.5-B and NHL 5-B.

Prior to blending the AHL binders, WBAs were mechanically sieved through a 250 μm sieve to remove impurities such as unburnt wood and pieces of metal or charcoal fragments. This type of selective removal was intended to overcome physical incompatibilities in the AHL binder system that might otherwise lead to higher water requirements or diminished mortar performance. The residue left on the 250 μm sieve demonstrated variations based on the specific type of WBA being examined. After the screening process, the WBAs were mixed with NHL in their dry, powdered state at the specified ratio (20, 30, and 40 wt.%). The mixed ash designated WBA9.M was the only material subjected to grinding in a laboratory mill before the sieving process (Figure 3.2). This was necessary due to the initial state of the material, which was in the form of large, petrified chunks. Grinding was performed using a laboratory mill

designed for processing fine powder samples, specifically Matest A091-02 model. The grinding container has a volume of 1.5 litres, while the abrasive balls employed in the process are composed of a special type of porcelain that has undergone high-temperature thermal treatment. The degree of material grinding is dependent on several factors, including the grinding speed, the properties of the abrasive balls, and, most significantly, the duration of the procedure [81]. Notably, in this particular instance, water was intentionally omitted to preserve the potential hydraulic activity of the ash. Approximately 200 gram samples of ash were placed within the ceramic container, where they were ground for a duration of 2 minutes to achieve the desired level of grinding.

Figure 3.1. Powder samples of AHL raw materials: (a) primary NHL binders; (b) sieved fly WBAs and (c) sieved mixed WBAs, including siliceous variations

<table>
<tr><td>(a)</td><td>(b)</td><td>(c)</td></tr>
</table>
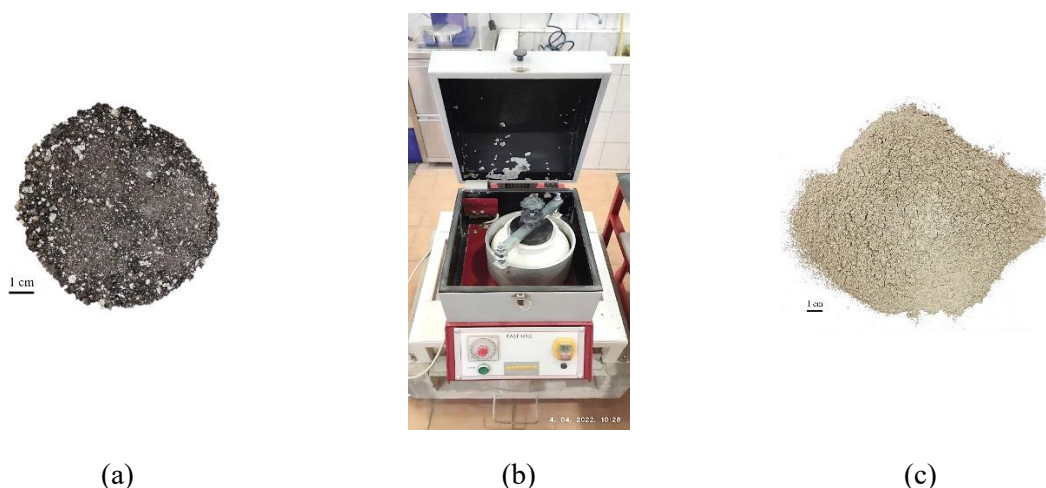
Figure 3.2. Grinding process of WBA9.M: (a) WBA9.M as received; (b) laboratory mill; (c) WBA9.M after grinding and sieving

Table 3.1. NHL/WBA designation and source information

NHL/ WBA ID	Type	Manufacturer/ Origin	Firing technology	Raw material	Firing temp. range [°C]	Filter
NHL 3.5	NHL	Baumit, Austria	lime calcination kiln	limestone	900 - 1100	n/a
NHL 5		Calcinea Calce Raffinata, Italy				
WBA1.F	fly WBA	Karlovac, Croatia	grate	wood chips, residues from wood processing (including bark)	700	electrostatic filter
WBA2.F		Gospić, Croatia	grate	wood chips, wood chips with impurities, residues from wood processing (including bark)	900 - 1050	electrostatic filter
WBA3.M	mixed WBA	Bjelovar, Croatia	grate	pure wood chips	700 - 800	cyclone separator

NHL/ WBA ID	Type	Manufacturer/ Origin	Firing technology	Raw material	Firing temp. range [°C]	Filter
WBA4.M	mixed WBA	Žakanje, Croatia	grate	wood chips with impurities; wood chips from the whole wood, residues from wood processing (including bark)	700 - 800	cyclone separator
WBA5.F	fly WBA	Grubišno Polje, Croatia	bio-grate	pure wood chips, wood chips from whole wood (wood chips containing bark, sapwood, needles/leaves)	680	electrostatic filter
WBA6.F		Glina Drvni Centar, Croatia	grate & pulverised fuel combustors	pure wood chips, wood chips from whole wood (wood chips containing bark, sapwood, needles/leaves)	700 - 800	cyclone separator
WBA7.M						
WBA8.M		Vinkovci, Croatia	grate	wood chips, wood chips from the whole wood, residues from wood processing (including bark)	980	cyclone separator
WBA9.M	mixed WBA	Fužine, Croatia	grate	wood chips with impurities	800 - 900	bottom furnace
WBA10.M		Zagreb, Croatia	grate	wood chips, wood chip with impurities (soil and stones), residues from wood harvesting	700	bottom furnace
WBA11.M		Karlovac, Croatia	grate	wood chips, residues from wood processing (including bark)	700	bottom furnace

3.2.2. Methods

The investigation was conducted at the binder and paste level, preceding the formulation of mortar mixes, as detailed in the following Chapter 4. An in-depth assessment was undertaken to evaluate the distinct WBAs, both independently and within the NHL-WBA binder system. This assessment encompassed an analysis of their physical, chemical, and mineralogical attributes, along with an examination of their reactivity within diverse binder blends. An assortment of double-phase methods pertaining to binder and paste levels were employed as outlined in Table 3.2 and Table 3.3.

Table 3.2. Test methods for NHL and WBA assessment.

Level	Property	Test Period	Unit	Standard
Binder	Density	Prior to mixing of pastes and mortars	g/cm^3	ASTM C-188-17
	Bulk density		kg/dm^3	EN 459-2:2021
	Free water		wt.%	
	Particle size distribution		%	
			μm	ISO 13320:2020
	Chemical composition		wt.%	ISO/TS 16996:2015
	Loss on ignition (LOI)			ASTM D 7348-13
	pH value		-	EN ISO 10523:2005
	Heavy metal concentrations		mg/kg	ISO/TS 16996:2015
	Phase/composition identification		wt.%	Thermogravimetric analysis (TGA)
			-	X-ray diffraction analysis (XRD)

Table 3.3. Test methods for AHL paste assessment.

Level	Property	Test Period	Unit	Standard
Paste	Standard consistency	Immediately upon mixing of pastes	%	EN 459-2:2021
	Setting time		h	
	Soundness		mm	
	Reactivity (Hydration kinetics)		W/g J/g	EN 196-11:2019

The **density** of both WBAs and NHLs was determined using a La Chatelier flask, following the ASTM C 188-17 [82] standard. This process involved measuring the difference between the level of petroleum (V_1) and the level after adding the WBA or NHL (V2). By calculating the volume difference ($V_c = V_2 - V_1$) and considering the known mass of the ash sample, the density was determined.

The **bulk density** of a powder is determined by the ratio of the mass of a powder sample to its volume, accounting for the contribution of interparticle void volume, which includes all pores and voids. To measure this density, a hopper was situated in the rack with its bottom end sealed by the closure flap. Subsequently, the cylindrical cup was weighed, and its weight was documented as "m_{con}." The container was positioned centrally under the hopper. The material was then gently poured into the funnel using a spoon, starting from the lid and progressing downward, with care taken to avoid contact with the material inside the funnel. Following this, the closure flap was removed, enabling the material to flow freely into the container until the cup was filled, resulting in a characteristic sloped mound. Upon the cup being entirely filled, any surplus powder was levelled using a straight-edge blade. Lastly, the mass of the container with the material was measured on the balance and recorded as "$m_{con} + m$." The mass of the material was obtained as the difference in weight between the container with the material and the mass of the container itself.

The bulk density in kilograms per cubic decimetre is calculated using the formula:

$$d_b = (m_{con+m} - m_{con})/V \qquad (3.1)$$

where $m_{con + m}$ represents the mass of the container with the material in grams, m_{con} stands for the mass of the container in kilograms, and V denotes the capacity of the container in decimetres cubed (dm³). The final bulk density result is based on an average derived from three separate measurements, each involving different sub-samples.

The material's **free water**, i.e., moisture content is determined through the following steps: First, the sample is weighed in the as-delivered state, within a range of 5 ± 0.1 g to 10 ± 0.1 g (m_5), using a pre-weighed container. Subsequently, the sample is subjected to drying in a ventilated oven for approximately 2 hours until a consistent mass is achieved, and it is then reweighed (m_6). The moisture content (H_2O) is calculated as a percentage using the formula:

$$w_{H_2O} = \frac{(m_5 - m_6)}{m_5} \cdot 100 \qquad (3.2)$$

with m_5 representing the initial mass of the test portion before heating in grams and m_6 representing the mass of the test portion after drying.

Particle size analysis was conducted using **air-jet sieving**, following EN 459-2:2021, recognized for its effectiveness in evaluating fine particle agglomerates. This process employed test sieves with apertures of 0.2 mm and 0.09 mm. It commenced with weighing the WBA/NHL sample to the nearest 0.01 g (m_{15}). The 0.09 mm sieve was inserted, the sample placed on the sieve mesh, and the apparatus activated, ensuring vacuum and slit nozzle performance. If material adhered to the lid or agglomeration occurred, it was gently addressed. After approximately 5 minutes, the apparatus was turned off, the sieve removed, and the retained material transferred to a container. Cleaning the sieve over the container and determining the residue's mass (including brushed material) followed, rounded to the nearest 10 mg. Finally, the 0.20 mm sieve was used to confirm the end-point mass, recorded to the nearest 10 mg.

The end-point mass was calculated using the formula:

$$R_{0.20 \, or \, 0.09} = \frac{R_i \cdot 100}{m_{15}} \qquad\qquad (3.3)$$

where m_{15} represents the mass of the dry substance in the test portion, and R_i is the residue mass retained on the test sieves, both in grams.

Particle size distribution was further analysed using laser diffraction, employing a SALD-3101 device by Shimadzu. In this method, laser light irradiates the sample, and particle size is derived from the intensity of light refraction and dispersion. The dry measurement unit was employed, with samples dispersed in an air stream at a pressure of 0.4 MPa. The Fraunhofer approximation was utilized to obtain the particle size distribution, and specific parameters such as D10, D50, and D90 were determined in addition to the distribution itself.

The **chemical composition** of the raw materials, WBA and NHL, was analysed at the accredited Central laboratory for chemical analysis operating within HEP-Proizvodnja d.o.o. in Zagreb. This analysis of powdery materials, like WBA, involved the determination of major oxide mass fractions (wt.%). It included measuring pH according to EN ISO 10523:2012 [83], loss of ignition at 950°C (LOI) following ASTM D 7348-13 [84], and major oxide content as per EN ISO 16967:2015 [85]. The total alkali content was determined using the Na_2O_{eq} ratio, following EN 196-2:2013 [86]. In the same laboratory, heavy metal content, such as zinc, cadmium, chromium, nickel, lead, manganese, cobalt, barium, bismuth, strontium, and copper, was

assessed per EN ISO 16968:2015 [87], while mercury content was determined following ASTM D 6722-19 [88].

Furthermore, an analysis of chloride content at the binder level was conducted following the guidelines outlined in EN 196-2 [86] on unsieved WBAs and NHL 3.5.

Thermogravimetric analyses (TGA) of powdered NHL and WBAs were meticulously carried out employing a TA Instruments Discovery TGA 55. These analyses spanned a controlled temperature range from 30°C to 1000°C, featuring a constant heating rate of 10°C/min. Inert nitrogen gas, maintaining a flow rate of 40 mL/min, was employed as the purge gas during the experimentation.

In addition to employing TGA, powdered samples of WBA and NHL underwent analysis using **X-ray diffraction** (XRD). The X-ray diffraction data were collected at room temperature using a Bruker D8 Discover diffractometer equipped with a LYNXEYE XE-T detector, following Bragg–Brentano geometry. The XRD data were collected over a 2θ range of 20–80° using a step size of 0.02°, and each data point was recorded for 25 s. Copper (Cu) radiation (K-Alpha1: 1.54060 Å, K-Alpha2: 1.54443 Å) was employed, while the generator operated at a constant 40 mA and 40 kV configuration. The main focus of the analysis was on qualitative assessment, which involved identifying the presence or absence of specific components, besides quantifying their precise concentrations. The analysis involved a semi-quantitative Rietveld refinement using the Xpert HighScore Plus 3.0, despite the qualitative presentation of the results. The refinement process incorporated the split-type pseudo-Voigt profile function and the polynomial background model. It assumed isotropic vibration modes for all atoms. During the refinement, parameters including zero shift, scale factor, half-width (W), asymmetry (if applicable), and peak shape were simultaneously adjusted. Notably, the analysis did not refine the atomic coordinates.

Standard consistency of AHL pastes was tested complying with EN 459-2:2021 standard for building lime. AHL, that is mix of NHL and WBA in different proportions, in amount of 500 g, was weighed and subsequently combined with 125 g of water, that was added to the mixer bowl. The AHL was carefully incorporated into the water in 5 to 10 seconds, with the starting point marked as zero time. The mixer was initiated and run at a low speed for 90 seconds, followed by a 30-second pause to remove any adhering paste outside the mixing area. The machine was then restarted for an additional 90 seconds, resulting in a total mixer running time of 3 minutes.

The paste was promptly transferred to a mould placed on a lightly greased flat glass base-plate, and it was filled to excess without excessive compaction or vibration. The excess paste was gently removed with a straight-edged tool, leaving a smooth upper surface in the mould. After levelling the paste, the mould and base-plate were transferred to the Vicat apparatus, calibrated with the plunger in advance, and positioned centrally beneath the plunger. The plunger was gently lowered into contact with the paste and paused for 1 to 2 seconds to avoid initial velocity. The plunger was then quickly released, penetrating vertically into the paste. The scale reading was taken when penetration ceased or 30 seconds after plunger release, whichever was earlier. This reading indicated the distance between the plunger's bottom face and the base-plate, along with the water content of the paste as a percentage by mass of the AHL. The test was repeated with pastes of varying water contents until one produced a plunger-base-plate distance of (6 ± 2) mm. The water content of that paste was recorded to the nearest 0.5% as the water for standard consistency.

The determination of **initial and final setting times** was carried out using a ToniSET automatic Vicat needle instrument, following the procedure outlined in EN 459-2:2016 for standard consistency paste. The mould, filled with paste of standard consistency, is transferred to the Vicat apparatus, carefully placed in water, and positioned under the needle. The penetration test was repeatedly conducted on the same specimen, with the machine automatically selecting well-spaced positions, ensuring they were not less than 10 mm from the mould's edge or each other. The timing intervals were determined based on experience and varied according to the type and composition of the WBA. The time measured from zero, which marks the moment when water and AHL are combined, was noted when the distance between the needle and the base-plate reached (6 ± 3) mm, defining the initial setting time of the building lime. To maintain accuracy, the time intervals between penetration tests near the end-point were reduced, with attention given to fluctuations in successive results. The final setting time, signifying when the needle penetrated only 0.5 mm into the specimen, was similarly recorded.

Soundness of AHL pastes was determined in accordance with standard EN 459-2:2016, using the Le Chatelier method as an alternative procedure. Three test specimens were prepared by hand-mixing 75 g of the dry hydrated lime sample with water. The amount of water used was adjusted (around 20 g) to achieve the appropriate paste consistency, which was duly noted. Each Le Chatelier ring mould was immediately filled completely but loosely with the prepared AHL and lightly tamped to prevent air inclusion. This process was repeated until the mix reached the

top of the mould. The distance (A) between the ends of the indicator points, measured to the nearest 1 mm, was recorded. The moulds were then promptly transferred to a vigorously boiling steam cabinet. In the case of NHL class 5, the moulded specimens were precured for (48 ± 0.5) hours at a minimum of 90% relative humidity and (20 ± 1) °C. Following, the moulds were exposed to continuous steam at atmospheric pressure for (180 ± 10) minutes. After this period, the moulds were removed, allowed to cool to room temperature, and the distance (B) between the ends of the indicator points was measured. For each specimen, measurements A and B were recorded, and the differences (B - A) were calculated.

Reactivity of the AHL binder mixtures, i.e., measurement of the heat of hydration of the mixed pastes, was performed using an 8-channel isothermal calorimeter (TAM Air 8-Channel Standard Volume Calorimeter) according to EN 196-11:2019 [89]. The heat of hydration was measured for 3 days at 20 °C, and a w/b ratio of 0.6 was chosen to achieve a paste consistency suitable for filling the ampoules. Approximately 30 g of the paste was mixed manually and/or mechanically for 2 min, and 10 g of the prepared sample was then placed in a sealed ampoule and lowered into the calorimeter conditioned to 20 ± 0.05 °C.

3.3. Results and discussion

3.3.1. Assessment of AHL's physical properties

As part of the fundamental physical characterization of NHLs and WBAs, specific gravity, bulk density, residue on 90 μm and 120 μm sieves, free water content, and an additional particle size distribution obtained by laser diffraction were evaluated. Upon visual inspection, the WBAs subjected to 250 μm sieving exhibited minor differences compared to NHLs, in terms of their varying coloration. While NHLs displayed a lighter, yellowish-beige hue, WBAs ranged from greyish to taupe (as seen in Figure 3.1). None of the sieved fly ashes appeared to contain visible impurities apparent to the naked eye, although some were detected to a limited extent through sieving. Mixed ashes exhibited somewhat coarser particles, which were noticeable without magnification, and a considerable amount of material was discarded during sieving. The screening process effectively reduced the percentage of impurities, such as unburned wood, stones, metal pieces, or charcoal fragments. This reduction was especially evident in WBA3.M and WBA4.M, two of the WBAs used later in the mortar phase, where the impurities averaged around 40 wt% (as shown in Figure 3.3). These elevated values can be attributed not only to impurity levels but also to a distinct distribution of particle sizes within these mixed ashes. Even though the proportion of impurities in fly ashes, such as WBA1.F and WBA2.F, was modest at approximately 4%, they were also subjected to sieving before the preparation of mortar mixtures.

| (a) | (b) |
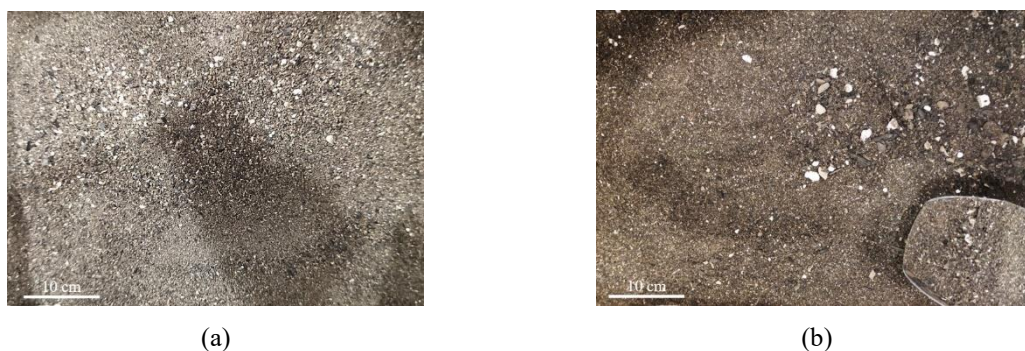
Figure 3.3. Discarded material after sieving mixed WBAs on 250 μm sieve: (a) WBA3.M; (b) WBA4.M.

The specific gravity of both fly and mixed WBAs exhibited a wide range, spanning from the lowest value of 2.44 g/cm^3 (observed in WBA10.M and WBA11.M) to the highest value of 2.86 g/cm^3 (recorded for WBA9.M). It is noteworthy that while the specific gravity values of the fly ashes closely resembled those of the NHLs, the mixed ashes displayed a diverse spectrum of values, encompassing the entire range from the highest to the lowest. The averaged specific gravity values for fly and mixed ashes were 2.66 and 2.67 g/cm^3, respectively. These values closely align with the specific gravity of NHL and are consistent with data available in the literature [90].

The observed trend in bulk density data indicates that fly ashes consistently exhibit significantly lower values compared to NHLs, ranging from 0.29 (observed in WBA2.F) to 0.48 (noted in WBA6.F). Both NHL 3.5 and NHL 5 fall within the characteristic range defined in EN 459-1, with values ranging from 0.4 up to 1 kg/dm^3. Accordingly, AHLs with even higher proportions of WBA would still fall within this acceptable range. Conversely, the mixed WBAs predominantly display higher values compared to both the control NHLs and the fly ashes.

When assessing the particle size of fine particles using air-jet sieving, the fly ashes meet the requirements of EN 459-1 set for all categories of hydraulic lime, which stipulates that the residue on the 90 μm and 200 μm sieves must not exceed 15% and 5% of the binder mass, respectively. However, for the mixed ashes, a higher proportion of the 90 μm residue suggests lower fineness, with some samples significantly exceeding the 15% threshold (WBA9.M, WBA10.M, and WBA11.M with 38%, 28%, and 73% residue on the 90 μm sieve, respectively). The ashes WBA3.M and WBA4.M are at the borderline but still remain below the upper limit. It's noteworthy that even the NHLs exhibit relatively high values, with NHL 3.5 and NHL 5 registering 13% and 10% on the 90 μm sieve, respectively (refer to Table 3.4). The residue material on the 120 μm sieve exhibited a similar trend as the finer 90 μm sieve, consistent with the previously mentioned observations.

Given that materials like WBA, characterized by fine particles prone to cohesion and fragmentation during sieving [91], this method's efficacy is limited. Consequently, laser diffraction analysis was employed to corroborate the findings of air-jet sieving.

Table 3.4. Comparison of physical properties: NHLs and WBAs vs. EN 459-1 limits for NHL and FL/HL

NHL/WBA ID	Specific gravity (g/cm³)	Bulk density (kg/dm³)	Residue on 90 um (%)	Residue on 200 um (%)	Free water (%)
NHL 3.5	2.68	0.79	13%	2%	0.2%
NHL 5	2.62	0.69	10%	1%	0%
WBA1.F	2.66	0.34	1%	0%	0%
WBA2.F	2.66	0.29	1%	0%	0%
WBA3.M	2.51	0.91	15%	1%	0.2%
WBA4.M	2.85	0.87	14%	1%	0.1%
WBA5.F	2.69	0.41	11%	0%	0%
WBA6.F	2.66	0.48	4%	0%	0%
WBA7.M	2.64	0.76	15%	1%	0.2%
WBA8.M	2.84	0.54	8%	0%	0
WBA9.M.g	2.86	1.21	38%	5%	0.1%
WBA10.M	2.44	0.90	28%	2%	0%
WBA11.M	2.44	0.99	73%	10%	0.1%
EN 459-1 [28]	-	0.4 - 1	≤15	≤5	≤2

Laser diffraction unveils that particle size distributions exhibit distinct variations between fly ashes and mixed ashes. Among fly ashes, particle sizes span from 0.1 μm to approximately 60 μm, constituting 90% of the total ash mass. Specifically, WBA1.F and WBA5.F reach a 90% cumulative volume at 45 μm, indicating a finer particle size distribution, followed by WBA2.F at 50 μm and WBA6.F at 64 μm. The median particle size (D50) for fly WBAs ranges from 10.97 μm (WBA 2.F and WBA5.F) to 19.02 μm (WBA6.F). In contrast, WBAs feature a bi-modal particle size distribution, with a prominent range between 10 and 20 μm in diameter, which is absent in the NHL 3.5 sample. Both NHL 3.5 and WBAs share a similar ultrafine range with a diameter of approximately 0.5 μm. Furthermore, NHL 3.5 is characterized by a trimodal particle size distribution, encompassing the smallest ultrafine region at around 0.5 μm, a fine fragmentation range of about 6 μm, and a larger fragmentation region for particles measuring approximately 90 μm (See Figure 3.4, Figure 3.6). In this case, particle sizes in NHL 3.5 extend up to 123 μm, representing 90% of the total volume by weight, with a median particle

size (D50) of 13.67 μm. On the other hand, NHL 5 has particle sizes reaching up to 32.97 μm, accounting for 90% of the total volume by weight, and a D50 of 7.89 μm, signifying a finer particles than the lower hydraulicity NHL 3.5. Unlike the polydisperse distribution in NHL 3.5, NHL 5 exhibits a monomodal distribution, primarily centred around 8 μm. Fly WBAs demonstrate a narrower bi-modal distribution, left-shifted relative to NHL 3.5, indicating a higher concentration of particles in the fine fragmentation region. In contrast, NHL 5 is even finer and exhibits a leftward shift toward smaller particle sizes. The particle size data (D10, D50, and D90) confirm a broader distribution of particles in NHL 3.5, whereas NHL 5 presents a narrower distribution. Mixed ashes exhibit a wide particle size distribution but shifted towards larger particle sizes, mainly over 100 μm. Unlike fly ashes, mixed ashes lack the fine fragmentation region, and D10, D50, and D90 values validate a coarser particle distribution (refer to Table 3.5).

In the general context of particle size analysis, it is well documented that the range of 10 to 45 μm is critical for the observed increase in structural strength, a phenomenon typically noted after a curing time of 28 days and extending for about one year [92]. This critical range comprises about 40% of the particles in the ashes WBA1.F and WBA6.F, with a higher proportion of 50% in WBA2.F and WBA5.F. In contrast, the cumulative volume in NHL 3.5 equivalent to that of the fly samples is achieved only when the particle size reaches 90 μm, indicative of a somewhat coarser granulometric character compared to fly ash-based materials. In addition, NHL 5 shows a discernible tendency towards smaller particle sizes, with about 40% of the particles falling within this defined size range. Looking at the mixed ashes, it is noticeable that WBA4.M, WBA7.M and WBA8.M display an approximation to the particle distribution of fly ash in this size range. In contrast, in WBA9.M, WBA10.M and WBA11.M, only 5.2%, 12.2% and 1.3% of the particles are represented in the crucial 10 to 45 μm. WBA3.M exhibits a particle size falling intermediate to values of fly and mixed ashes, with approximately 24% of particles falling within this specified size range. This notable deviation suggests an incompatibility in particle size distribution, raising concerns about the effectiveness of these materials in the context of an NHL-WBA binder blend.

In the context of fly ash reactivity, it is worth noting that particles with a size below 10 μm are considered to be one of the primary governing factors [92]. This information allows for the categorization of WBAs based on their reactivity, which is significantly influenced by their fineness. Specifically, for WBA1.M, WBA2.M, and WBA5.M, it is observed that approximately 46% of their particles fall within this specified size range, signifying a high level

of reactivity. In contrast, WBA6.M contains a smaller volume of particles below 10 μm, around 30%, indicating a somewhat lower reactivity. The general trend among mixed ashes is that they contain less than 10% of particles below this limit, implying a relatively reduced reactivity. Notably, WBA8.M contains 20% of particles within this range, which, while higher than other mixed ashes, is still significantly less than that of NHL 3.5-B with 45% and NHL 5 with 56% of particles below the 10 μm threshold.

Table 3.5. Particle size data (D10, D50, and D90) for NHL and WBA samples

NHL/WBA ID	D10	D50	D90	Particle size distribution type
		μm		
NHL 3.5	0.98	13.67	123.44	tri-modal
NHL 5	1.89	7.89	32.97	mono-modal
WBA1.F	1.69	12.25	41.08	bi-modal
WBA2.F	1.89	10.97	51.19	bi-modal
WBA3.M	21.23	99.06	238.86	bi-modal
WBA4.M	9.83	41.08	137.80	bi-modal
WBA5.F	1.69	10.97	45.86	bi-modal
WBA6.F	2.11	19.02	63.79	bi-modal
WBA7.M	10.97	45.86	99.06	tri-modal
WBA8.M	4.55	23.70	71.21	bi-modal
WBA9.M.g	51.19	213.98	575.97	mono-modal
WBA10.M	19.02	137.80	462.21	mono-modal
WBA11.M	88.74	238.86	801.20	mono-modal
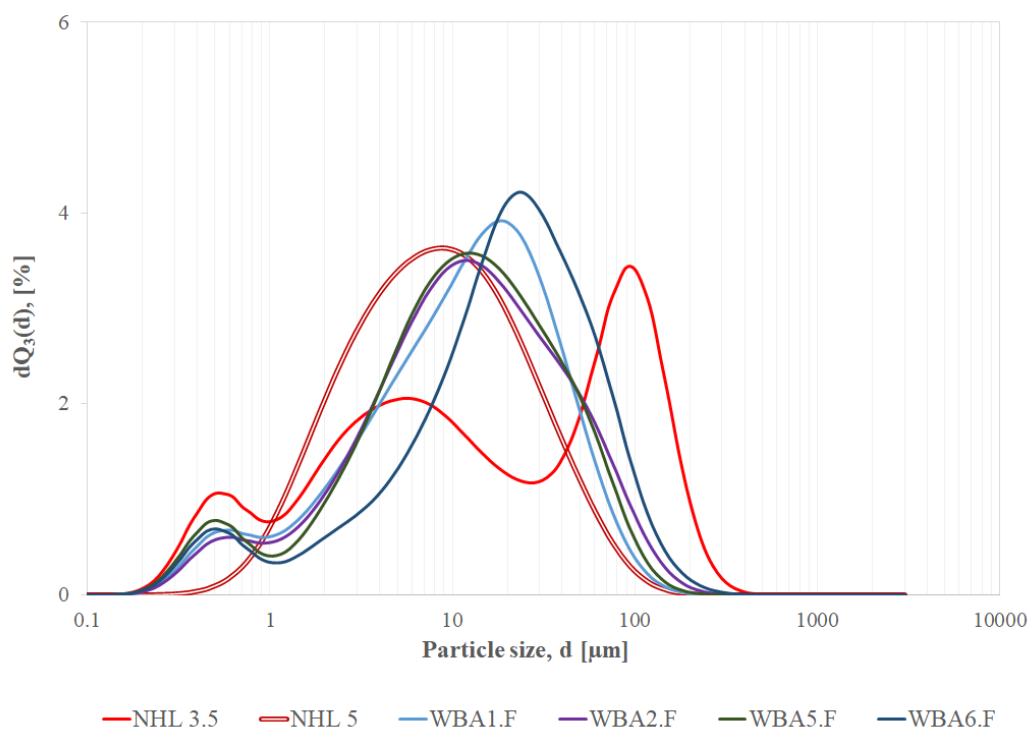
Figure 3.4. Differential volume distribution of particle sizes in NHLs and fly WBAs
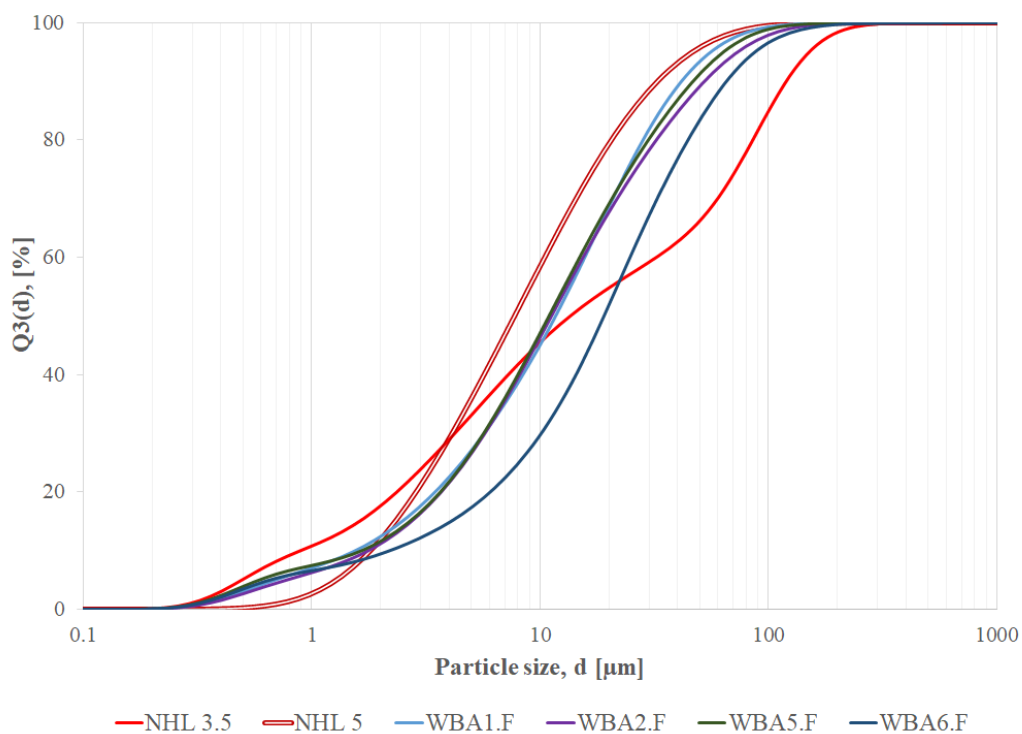
Figure 3.5. Cumulative volume distribution of particle sizes in NHLs and fly WBAs
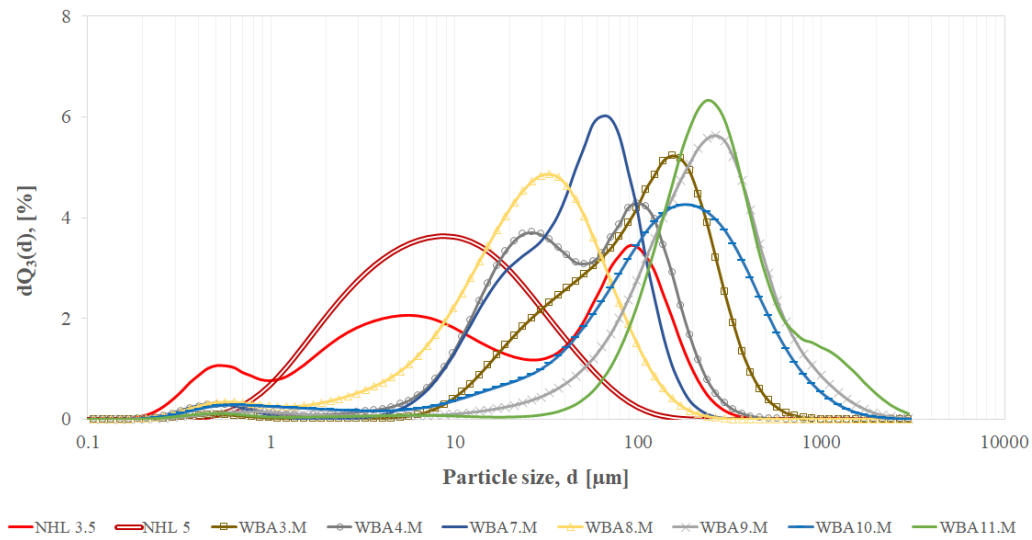
Figure 3.6. Differential volume distribution of particle sizes in NHLs and mixed WBAs
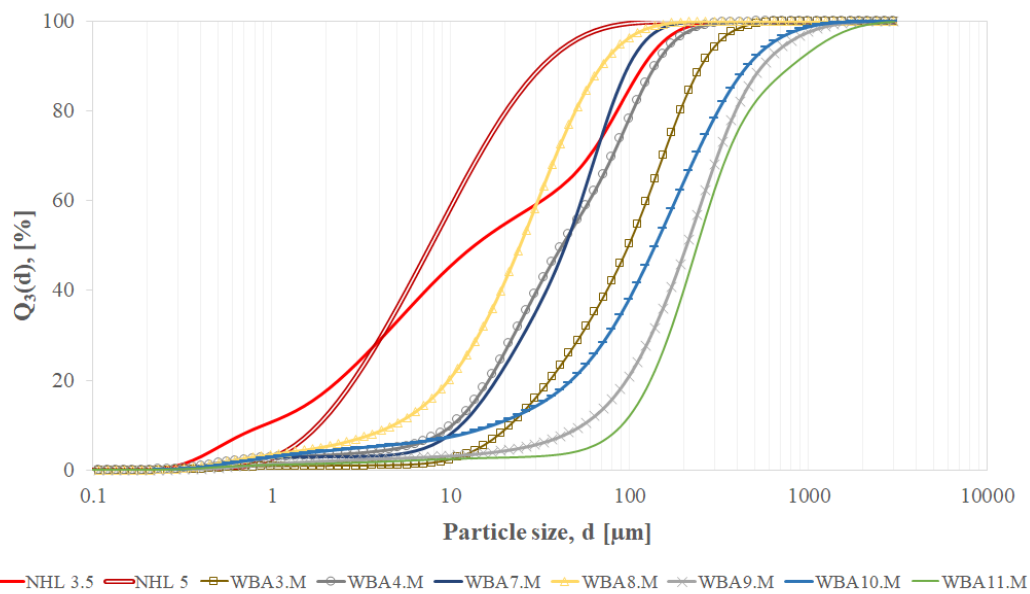
Figure 3.7. Cumulative volume distribution of particle sizes in NHLs and mixed WBAs

3.3.2. Assessment of AHL's chemical and mineralogical properties

3.3.2.1. Overview of chemical properties

The chemical composition of both types of NHL and 11 different WBAs underwent thorough examination via energy dispersive X-ray fluorescence spectrometry (EDXRF). The resulting dataset, comprising the major oxide components, is tabulated in Table 3.6, whereas chemical composition of WBAs was analysed before and after sieving. As the WBAs were introduced into AHL pastes and mortars after the sieving process, the chemical composition of the sieved samples serves as the reference point. Moreover, EDXRF was employed to ascertain the concentrations of heavy metals within the homogenized dry materials, as delineated in Table 3.7.

In both NHL samples, calcium oxide (CaO) predominates, closely followed by SiO_2 content. Similarly, in the WBA samples, CaO also dominates as the primary oxide, with SiO_2 as a close second, aligning with the characteristic composition found in wood ashes [92]. In this context all of the ashes can be characterised as calclareous, except for the two of the mixed ashes (WBA10.M and WBA11.M), which were identified as siliceous ashes, as the SiO_2 share conversely exceeds the CaO share. Both primary binders, NHL 3.5, and NHL 5, consist mainly of four oxides: CaO (52.81% for NHL 3.5 and 56.66% for NHL 5), SiO_2 (35.06% for NHL 3.5 and 27.58% for NHL 5), Al_2O_3 (5.39% for NHL 3.5 and 8.10% for NHL 5), and Fe_2O_3 (2.66% for NHL 3.5 and 1.83% for NHL 5). Although all of the ashes align closely with NHL in terms of these predominant oxides, the SO_3, MgO, P_2O_5, and K_2O values stand out significantly. Looking at the SO_3 content, which is limited by the EN 459-2 standard with a maximum value of 3%, set for artificial hydraulic lime (HL), fly WBAs are characterized as fly ashes with elevated SO_3 levels, as the measured SO_3 content in all fly WBAs exceeds 3%. The threshold set by the same standard for formulated lime (FL) is even more restrictive with a maximum value of 2%. However, this is somewhat mitigated by the weighted average value depending on the NHL to WBA hybridization ratio. Simultaneously, the mixed ashes exhibit significantly lower SO_3 content compared to NHL values, yet still exceed them.

Moreover, WBAs exhibited notably elevated levels of K_2O and MgO, along with free CaO, signifying a substantial enrichment in alkaline-earth and alkaline compounds. This finding aligns with prior investigations conducted by Vassilev et al. [93]. It's imperative to emphasize that the existence of free oxides of alkaline earth metals, including free MgO and free CaO, can lead to their reaction with water, forming respective hydroxides. This chemical process has the

potential to induce expansion and cracking [94–96], thus giving rise to issues of volume instability.

Given the premise that the alkalis within the WBA serve as activators for its pozzolanic reactivity, in synergy with the $Ca(OH)_2$ content found in NHL, facilitating long-term combining with calcium silicate hydrates [97], the exploration of higher ash additions remained a viable option.

In the context of assessing the pozzolanic properties of WBAs as part of an NHL-WBA binder system, the sum of pozzolanic oxides ($SiO_2+Al_2O_3+Fe_2O_3$) was evaluated. According to the EN 450-1 standard [98], this sum should not be less than 70 wt.%, serving as an indicator of potential pozzolanic reactivity and its contribution to increased compressive strength. It's important to note that even if a material doesn't meet the 70 wt.% limit, it can still exhibit pozzolanic properties with a somewhat lower sum of the specified oxides [99].

The sum of pozzolanic oxides in calcareous WBAs averaged at 28.3 wt.% in calcareous fly WBAs and 31.4 wt.% in calcareous mixed WBAs. Notably, these two categories exhibited minimal disparity in pozzolanic oxide content. Conversely, mixed WBAs classified as siliceous, exemplified by WBA10.M and WBA11.M, displayed a substantially higher average of 58.4 wt.% attributable to their siliceous composition.

Given that the majority of the examined WBAs demonstrate a calcareous nature, with CaO as the prevailing oxide, and none of the pozzolanic oxide sums surpass 70%, it strongly indicates that WBAs are more inclined to be hydraulically active materials or possess diminished pozzolanic reactivity.

The loss on ignition measured at 950 °C (LOI 950 °C) has been widely used as a method to estimate the amount of organic matter and carbonate mineral content in materials such as WBA [100,101], serving as a measure of the non-reactive fraction of the WBA. In this view, all investigated WBA exhibit elevated values, exceeding the EN 450-1 limit of 9 wt.% (category C). While fly ashes generally exhibit higher LOI values compared to mixed ashes, on average, these values remain lower than those measured in NHL 3.5. Likewise, the slightly elevated pH values of the fly WBAs, with an average pH of 12.90, align with the control value specified for NHL 3.5, which has a pH of 12.10. In contrast, the average pH values of the calcareous mixed WBAs are somewhat lower at pH 11.20, and the siliceous WBAs exhibit significantly lower pH levels at 4.40.

The evaluation of soluble chloride content at the binder level, with a focus on unsieved WBAs in comparison to the primary NHL binder, reveals notable levels of chlorides (Cl⁻), particularly evident in fly ashes. Distinctively, within the mixed ashes, where chloride levels are less pronounced, WBA9.M stands out with a value of 0.246%. This trend mirrors the observations made in fly ashes.

The examination of heavy metal influence on construction products typically involves the assessment of leaching behaviour. However, it is important to clarify that the focus of this research does not encompass leaching, as it is anticipated that chemical hardening reactions during the formation of the binder matrix will significantly contribute to the stabilization and retention of heavy metals [52].

Nevertheless, elevated levels of heavy metal content were observed, particularly in fly ashes (refer to Table 3.7). Among these, zinc (Zn), lead (Pb), and copper (Cu) are notably prominent in fly WBAs, while chromium (Cr) takes precedence in mixed ashes. Mercury (Hg) and bismuth (Bi) are either negligible or only slightly elevated in comparison to NHLs. As Kostanić Jurić [2] previously noted, the increased levels of heavy metal content in both fly and mixed WBAs exceed the limits favourable for agricultural application. However, when bound in an AHL matrix, they are not expected to pose a threat to the environment.

Subsequently, an analysis of the heavy metal content was conducted within the context of its influence on the setting time of AHL pastes.

Table 3.6. Chemical composition of NHLs and WBAs used

NHL/WBA ID	NHL 3.5	NHL 5	WBA1.F		WBA2.F		WBA3.M		WBA4.M		WBA5.F		WBA6.F		WBA7.M		WBA8.M		WBA9.M		WBA10.M/S		WBA11.M/S	
type	NHL		fly WBA		Fly WBA		mixed WBA		mixed WBA		fly WBA		fly WBA		mixed WBA		mixed WBA		mixed WBA		mixed WBA		mixed WBA	
screening	*n/s*	*n/s*	*n/s*	*s*	*n/s*	*s*	*n/s*	*s*	*n/s*	*s*	*n/s*	*s*	*n/s*	*s*	*n/s*	*s*	*n/s*	*s*	*n/s*	*s*	*n/s*	*s*	*n/s*	*s*
Major oxides											Percentage [wt.%]													
CaO	52.81	56.66	44.05	**43.14**	34.10	**35.42**	37.70	**37.07**	49.33	**50.36**	42.65	**41.90**	45.93	**48.15**	49.96	**52.89**	59.51	**63.39**	40.36	**40.81**	25.83	**26.93**	21.09	**28.73**
SiO₂	35.06	27.58	23.02	**21.73**	24.91	**24.36**	30.44	**31.93**	22.65	**21.95**	14.56	**18.43**	23.48	**23.12**	22.79	**21.4**	20.29	**17.13**	28.57	**29.35**	41.54	**39.08**	46.89	**45.89**
SO₃	0.73	0.37	4.56	**5.34**	6.13	**6.28**	1.16	**1.47**	2.95	**3.23**	13.78	**11.49**	3.63	**3.12**	1.39	**1.77**	1.65	**2.32**	0.7	**0.73**	1.08	**1.85**	0.46	**0.88**
Al₂O₃	5.39	8.10	4.33	**4.06**	5.98	**5.64**	6.56	**6.69**	4.42	**4.2**	4.61	**3.32**	4.24	**4.18**	3.98	**3.69**	3.04	**2.49**	6.43	**6.78**	10.39	**10.03**	10.75	**5.8**
Fe₂O₃	2.66	1.83	2.06	**1.99**	2.64	**2.60**	2.82	**2.85**	2.19	**1.95**	2.09	**1.63**	2.17	**2.16**	3.95	**2.27**	3.26	**1.34**	3.29	**2.91**	4.25	**4.43**	4.68	**2.83**
MgO	1.97	4.67	4.58	**4.53**	4.86	**4.60**	6.90	**4.72**	4.92	**4.21**	4.78	**4.88**	3.48	**3.73**	3.56	**3.81**	3.48	**3.61**	8.8	**9.26**	7.13	**6.62**	3.39	**4**
P₂O₅	0.009	0.009	5.12	**5.08**	4.69	**4.56**	3.11	**3.69**	4.11	**4.37**	4.32	**4.81**	2.56	**2.53**	3.09	**3.41**	1.87	**2**	1.27	**1.26**	2.6	**3.55**	2.58	**4.41**
Na₂O	0.55	0.39	0.65	**0.74**	0.98	**0.89**	1.24	**1.33**	0.59	**0.64**	0.89	**1.03**	0.77	**0.91**	0.64	**0.64**	0.76	**0.94**	5.48	**4.85**	1.48	**1.41**	0.93	**0.6**
K₂O	0.51	0.43	10.87	**12.66**	14.92	**14.87**	9.08	**9.35**	7.62	**8.11**	9.63	**11.90**	12.62	**10.96**	9.19	**8.79**	5.84	**6.69**	3.7	**3.31**	4.9	**5.48**	8.12	**6.16**
TiO₂	0.09	0.01	0.23	**0.22**	0.26	**0.24**	0.52	**0.41**	0.45	**0.23**	0.308	**0.16**	0.32	**0.31**	0.43	**0.25**	0.26	**0.06**	0.99	**0.37**	0.57	**0.46**	0.83	**0.33**
MnO	0.25	0.22	0.54	**0.54**	0.56	**0.58**	0.49	**0.52**	0.79	**0.8**	0.72	**0.46**	0.84	**0.84**	1.06	**1.12**	0.07	**0.06**	0.44	**0.39**	0.17	**0.19**	0.31	**0.38**
SiO₂+Al₂O₃+Fe₂O₃	43.11	37.51	29.41	**27.78**	33.53	**32.60**	39.82	**41.47**	29.26	**28.1**	21.26	**23.38**	29.89	**29.46**	26.59	**20.96**	56.18	**53.54**	62.32	**54.52**	30.72	**27.36**	38.29	**39.05**
Free CaO	n/a	n/a	15.80	n/a	0.33	n/a	6.73	n/a	8.50	n/a	15.34	n/a	0.20	n/a	7.38	n/a	45.75	n/a	n/a	n/a	n/a	n/a	15.80	n/a
LOI 950°C	16.1	n/a	17.9	**18.5**	13.6	**16.5**	15.7	**11.3**	6.2	**13.2**	8.25	**8.3**	16.3	**17.0**	11.7	**15.3**	8	**22.4**	4.8	**7.4**	4.7	**7.0**	1.7	**1.8**
w (Cl⁻)	0.009	n/a	0.246	n/a	0.338	n/a	0.017	n/a	0.058	n/a	0.300	n/a	0.043	n/a	<0.003	n/a	0.063	n/a	0.246	n/a	0.144	n/a	<0.003	n/a
pH	12.1	n/a	12.9	**12.9**	12.8	**13.0**	12.8	**13.1**	13.0	**13.2**	n/a	**12.7**	13.0	**13.0**	13	**13.3**	13	**13.1**	12.8	**13**	12.5	**12.8**	12.7	**12.8**

Legend:
n/s - non-sieved
s - sieved through 250 μm

fly ash/ calclareous	mixed ash/calclareous	mixed ash/siliceous

Table 3.7. Heavy metal content in NHLs and WBAs post sieving

Heavy metal (mg/kg)	Zn (zinc)	Pb (lead)	Cu (copper)	Ba (barium)	Cd (cadmium)	Cr (chromium)	Hg (mercury)	Mn (manganese)	Ni (nickel)	Bi (bismuth)	Sr (strontium)
NHL 3.5	<1.0	1.5	<1.0	84.5	<1.0	12.9	0.038	1755	<1.0	<1.0	344
NHL 5	47.5	3.2	n/a	252.5	n/a	13.1	n/a	1040	9.8	n/a	289
WBA1.F	1065	9.1	113.5	1635	5.3	18.4	0	4415	12.9	<1.0	610
WBA2.F	2590	10.5	95	1000.5	6.9	21.9	0.2	5015	<1.0	<1.0	339
WBA3.M	<1.0	4.5	57.5	1570	<1.0	54.9	0	4805	11.2	<1.0	374
WBA4.M	734.5	6.3	75.2	1420	2.6	43.9	<0.005	6690	9.3	<1.0	500.5
WBA5.F	3517.5	20.4	64.2	1850	23.6	12.2	<0.005	3885	4.3	<1.0	698.5
WBA6.F	150.5	4.7	45.5	3855	<1.0	9.6	<0.005	7325	13.1	<1.0	751
WBA7.M	<1.0	2.7	43.6	2470	1.6	33.3	0	9350	44.8	<1.0	649.5
WBA8.M	183.5	2.5	22.5	821	<1.0	2	0	94.5	<1.0	<1.0	598.5
WBA9.M	891.5	4.2	110	1055	<1.0	79.5	<0.005	3675	10.9	<1.0	239.5
WBA10.M	542.5	13.2	78.3	539.5	<1.0	57.3	0	1790	21.5	<1.0	251
WBA11.M	173.5	5.3	81.9	979.5	<1.0	31.8	<0.005	3065	29.2	<1.0	401.5
min	*<1.0*	*2.5*	*22.5*	*539.5*	*<1.0*	*2*	*0*	*94.5*	*<1.0*	*<1.0*	*239.5*
max	*3517.5*	*20.4*	*113.5*	*3855*	*23.6*	*79.5*	*0.2*	*9350*	*44.8*	*<1.0*	*751*
average	*1094.3*	*7.6*	*71.6*	*1563.2*	*8*	*33.2*	*0*	*4555.4*	*17.5*	*<1.0*	*492.1*

3.3.2.2. Hydraulicity of AHL limes

As evident from the preceding analyses, a point underscored by Gualtieri et al. [102], it becomes apparent that relying solely on chemical data falls short in providing a comprehensive characterization of the hydraulic properties of hydraulic limes. In light of this, the Cementation Index (CI), a well-established method for assessing the hydraulic attributes of lime, has been effectively utilized to anticipate the hydraulic properties of AHL binders [103]. The CI is computed by taking into account the weight contribution of various oxides [104], as outlined in Equation (3.4). An increase in the CI value serves as an indicator of an expected enhancement in the hydraulic properties of the binder. A parallel concept applies to the categorization of lime according to the Hydraulic Index (HI) [35], which incorporates the influence of the most active oxides, as delineated in Equation (3.5).

$$CI = \frac{2.8(SiO_2) + 1.1(Al_2O_3) + 0.7(Fe_2O_3)}{CaO + 1.4(MgO)} \qquad (3.4)$$

$$HI = \frac{SiO_2 + Al_2O_3}{CaO} \qquad (3.5)$$

Since the dominant content of either CaO or SiO_2 influences whether a hydraulic or pozzolanic effect of WBA in the NHL-WBA binder system, it was decided to observe these reactions separately and categorize WBAs them into three distinct classes: calclareous fly WBAs, calclareous mixed WBAs and siliceous mixed WBAs (refer to Table 3.8).

It is apparent that there exists no pronounced disparity in the chemical composition between the two varieties of calcareous ashes, with average values of alumina, magnesium, and iron oxides exhibiting close similarity. On the contrary, WBAs demonstrate a significant shortfall of silica and alumina, approximately 30 wt.% less than the primary NHL binder. These elements are chiefly responsible for granting hydraulic properties upon the binders [31]. This analysis suggests that, in general, WBAs are likely to attain hydraulic reactivity compared to NHL. This is further corroborated by the CI values, which exhibit a reduction of 15% and 17% for fly and mixed ashes, respectively. Nevertheless, both the CI and HI values, surpassing the threshold of 0.7 set as the lower limit for eminently hydraulic limes [105,106], unequivocally affirm the highly hydraulic nature of all examined WBAs.

Table 3.8. Averaged chemical composition of NHLs and WBAs post sieving

	NHLs	fly WBAs/C	mixed WBAs/C	mixed WBAs/S
CaO	54.74	42.15	48.90	24.91
SiO_2	31.32	21.91	24.35	46.39
K_2O	0.47	12.60	7.25	7.14
SO_3	0.55	6.56	1.90	0.67
MgO	3.32	4.44	5.12	3.70
Al_2O_3	6.75	4.30	4.77	8.28
P_2O_5	0.01	4.25	2.95	3.50
Fe_2O_3	2.25	2.10	2.26	3.76
Na_2O	0.47	0.89	1.68	0.77
MnO	0.24	0.61	0.58	0.58
TiO_2	0.09	0.23	0.26	0.35
$SiO_2+Al_2O_3+Fe_2O_3$	40.31	28.3	31.4	58.4
Na_2O_{eq}	0.78	9.18	6.45	5.46
LOI 950°C	16.10	15.08	11.20	4.40
HI	0.69	0.61	0.58	2.04
CI	**1.63**	**1.40**	**1.34**	**4.71**

The siliceous mixed ashes show remarkably high levels, a phenomenon that deserves careful investigation given the almost threefold increase compared to the primary NHL binder — a point that raises questions. This puzzling observation may be due to a factor not considered by Vicat [19], namely that not all SiO_2 is soluble; some of it remains insoluble as quartz and may therefore not be readily available for reaction with calcium oxide and aluminium oxides to form calcium silicates and aluminate phases. Typically, NHL 3.5 contains a range of 6-12% soluble silica, while NHL 5 contains a range of 12-18% soluble silica [29].

In general, raising the calcination temperature typically results in a higher amount of combined (soluble) silica [32,107], which can serve to separate different hydraulic behaviours of lime binders. Nevertheless, once the soluble silica content exceeds 4%, hydraulicity will be generated in a direct correlation with the combined presence of available silica and CaO.

3.3.2.3. Characterization of mineral phases

The presence of different crystalline phases in pure NHL (both NHL 3.5 and NHL 5), along with the distinct, unblended powders of non-hydrated forms of fly and mixed WBAs, was examined through the sophisticated techniques of XRD and TGA analysis.

As it is found that the multi-component, heterogeneous, and non-uniform structure of WBA consists pre-dominantly of inorganic compounds, i.e., amorphous, crystalline to semi-crystalline minerals, and a negligible amount of organic compounds [93,108], complementing the quantitative XRF analysis, Table 3.9 offers a qualitative perspective, presenting XRD results that provide further interpretation on the crystal structure and composition of the AHL's constituents. The spectral representation reveals the presence of mineral constituents, spanning from minor (constituting less than 10%) to extensive (comprising more than 50%). Despite the qualitative nature of the results, a semi-quantitative Rietveld refinement was carried out, as indicated by the complementary ICSD numbers. However, a conscious decision was made to give preference to the qualitative refinement, which establishes the presence or absence of certain components without precise quantification of their concentrations. This decision stemmed from the primary objective of accurately identifying the phases present in WBA in conjunction with the primary binder, NHL.

The findings of XRD unequivocally demonstrate that calcite ($CaCO_3$) is one of the major mineral phases in both NHLs and WBAs. Analogous to the XRF analysis, the mixed ashes additionally characterised as siliceous, exhibit converse crystal phases, whereas quartz, i.e., silicon oxide is identified as the major phase. Notably, the NHLs samples exhibit significant proportions of portlandite and larnite (β-belite) whereas these phases are either present in minor quantities or entirely absent in the WBA samples. Interestingly, the NHL 5 sample had a major presence of portlandite which is contrary to the expectations of a lower presence in relation to NHL 3.5 as the lime of the lower hydraulicity. Larnite was detected solely in the WBA9.M mixed ash sample, and that with a major presence. Calcium silicates, i.e., larnite, is found as the major hydraulic phase in NHL as well as a lower amount of gehlenite (calcium aluminosilicate) [109]. In this context, gehlenite has manifested a presence in vast majority of the examined WBA samples (with WBA8.M as the lone outlier), ranging from minor to even major presence, albeit in NHL only as minor presence. Hatrurite, manifesting as both monoclinic and hexagonal structures (M3-alite and alite, respectively), exhibit a minor presence in NHL while a few WBA samples display a minor presence of alite (WBA2.F, WBA4.M,

WBA7.M., WBA10.M). While it is not anticipated, the presence of small amounts of alite (C3S) in NHL may occur due to localized overheating in the kiln [38].

While the XRF analysis corroborates that calcium oxide is one of the major elements in calclareous WBAs, XRD analysis corroborates two crystalline sources of calcium, $CaCO_3$ as well as CaO. In this sense CaO is found in all of the WBAs examined, prevailingly in major presence. Among the minorly present minerals, periclase, i.e., magnesium oxide, is also detected in majority of ashes, while WBA8.M,WBA9.M and WBA11.M remain free of it. As carbonates can be formed by reaction of these phases with water and carbon dioxide, it is possible to surmise that despite the differences in composition, i.e., scarcity of raw material, WBAs contain useful phases that can potentially be employed to produce AHL.

Calcio olivine (Ca_2SiO_4), one of the belite polymorphs, is minorly or moderately present in WBA samples but is not found to exhibit hydraulic properties [110]. These findings also align with the additional research conducted by Hedayati et al. [111,112], where XRD analysis identified the presence of calcio olivine in biomass ash samples derived from grass and wheat straw at a temperature of 950 °C. Dolomite, calcium magnesium carbonate, is only identified in minor quantities in WBA2.F.

In particular, the XRF analysis shows a significant increase in SO_3 and K_2O levels within the WBAs, especially in the fly ashes. The results of the XRD analysis reveal an interplay between the characteristic peaks originating from calcite and those originating from important minerals such as sulphides, sulphates and potassium-bearing minerals. This revelation could be an explanation for the possible masking of corresponding mineral phases in SO_3-rich WBAs, favoured by the predominance of calcite.

Consequently, this convergence of peaks poses a challenge in accurately distinguishing these minerals during XRD analysis, highlighting the formidable obstacle posed by the prevalence of calcite, which produces peaks in XRD analysis that overlap with those of major minerals such as sulphides or sulphates [113]. It is imperative to acknowledge that certain mineral phases containing potassium may provide favourable conditions for cation substitutions within silicate structures. These substitutions could contribute to the observed fluctuations in chemical and mineralogical composition. Regardless, it is important to emphasise that the absence of conspicuous potassium and sulphate peaks or distinct potassium and sulphate containing mineral phases in the XRD patterns does not diminish the credibility of the results obtained by XRF analysis.

Table 3.9. Mineralogical composition of NHLs and WBAs used

NHL / WBA ID	NHL 3.5	NHL 5	WBA1.F	WBA2.F	WBA3.M	WBA4.M	WBA5.F	WBA6.F	WBA7.M	WBA8.M	WBA9.M	WBA10.M	WBA11.M
Phase	*spectrum-based qualitative representation*												
calcium carbonate *16710-ICSD*	+++	++	+++	+++	+++	+++	+++	++++	+++	+	++	++	++
calcium hydroxide *15471-ICSD*	++	+++	++	+	+	n/d	+	+	+	++	+	+	n/d
silicon oxide *147-ICSD*	+	+	+	+	++	+	n/d	+	n/d	n/d	+	+++	++++
hatrurite monoclinic, M3-alite *9472-ICSD*	+	+	n/d	n/d	n/d	n/d	n/d	n/d	n/d	n/d	n/d	n/d	n/d
larnite, β-belite *39006-ICSD*	++	++	n/d	n/d	n/d	n/d	n/d	n/d	n/d	n/d	+++	n/d	n/d
hatrurite, alite *201469-ICSD*	+	+	n/d	+	n/d	+	n/d	n/d	+	n/d	n/d	+	n/d
Gehlenite *160329-ICSD*	+	+	++	+	+	+	++	+	+	n/d	+	++	+++
calcium oxide *90486-ICSD 82994*	n/d	n/d	++	+++	+++	++++	+++	+++	++++	+++++	+++	++	+
periclase, magnesium oxide *9863-ICSD*	n/d	n/d	+	+	+	+	+	+	+	n/d	n/d	+	n/d
calcio olivine *68754-ICSD*	n/d	n/d	++	+	n/d	++	++	+	+	n/d	n/d	n/d	n/d
dolomite *10404-ICSD*	n/d	n/d	n/d	+	n/d	n/d	n/d	n/d	n/d	n/d	n/d	n/d	n/d

Legend:
n/d - not detected

+	*minor < 10%*
+ +	*10% < moderate < 25%*
+ + +	*25% < major < 45%*
+ + + +	*45% < massive < 55%*
+ + + + +	*extensive > 50%*

Preceding the blending of AHL binders, TGA was conducted on the individual, unmixed powders of un-hydrated NHL 3.5, NHL 5, and the distinct varieties of fly and mixed WBAs (Figure 3.8 and Figure 3.9). It is noteworthy that the thermal attributes of WBA are fundamentally governed by its chemical and mineralogical constitution. These parameters are regulated by the fuel source (raw material) employed, the boiler typology, operational conditions, and the combustion technology implemented. At this juncture, WBA11.M has been excluded from the array of WBAs considered as potential components for AHL. This decision stems from the absence of calcium hydroxide and magnesium hydroxide, as well as the limited presence of calcium oxide, all recognized as phases with potential AHL production value. Additionally, the particle size distribution was deemed unsuitable for AHL binder applications.

No significant mass losses were observed in the interval 50–200 °C, which corresponds to the evaporation of the moisture present, since no free water was present in the samples. Minor mass loss is visible at 110 °C and 131 °C in WBA7.M and WBA1.F, respectively.

Besides this, two predominant phases of weight loss in both NHL and WBA are distinguished. The first predominant range of mass loss from 300 °C to 500 °C can be attributed, at least in part, to the decomposition of portlandite, which is the only one of the aforementioned minerals present in the NHL and WBA that is expected to dehydroxylate in this temperature range [114]. Phases such as brucite, hannebachite or monosulphates, which are noted to decompose at the specified temperature range[115–117], were not identified in the samples through the XRD analysis. Therefore, the available lime in NHLs and WBAs, i.e., the $Ca(OH)_2$ content, was approximated based on mass loss in the 300–500 °C range, while the calcite content present in the samples was determined based on the mass loss in the second dominant range of 550 – 850 °C, which corresponds to CO_2 release from carbonates [68–70]. When comparing the DTG curves of WBAs and NHL, it is noticeable that the endothermic peaks in both regions are shifted to the left, i.e., the decomposition temperature is somewhat lower. Moreover, it is important to underline that, among the samples, WBA2.F, WBA7.M and WBA8.M are notable for exhibiting two distinct peaks within the decarbonation zone. This phenomenon can be attributed to the presence of dolomite [115], which was identified in the WBA2.F sample but was not detected in the case of WBA7.M and WBA8.M.
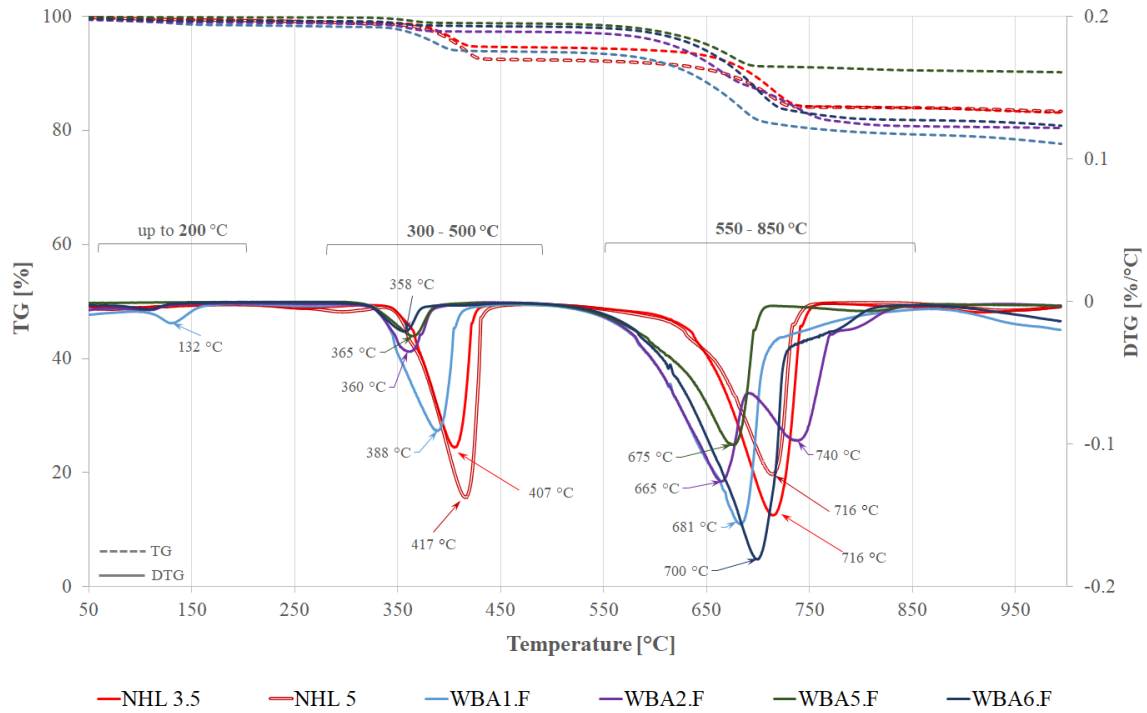
Figure 3.8. TG and DTG curves of un-hydrated NHLs and fly WBAs
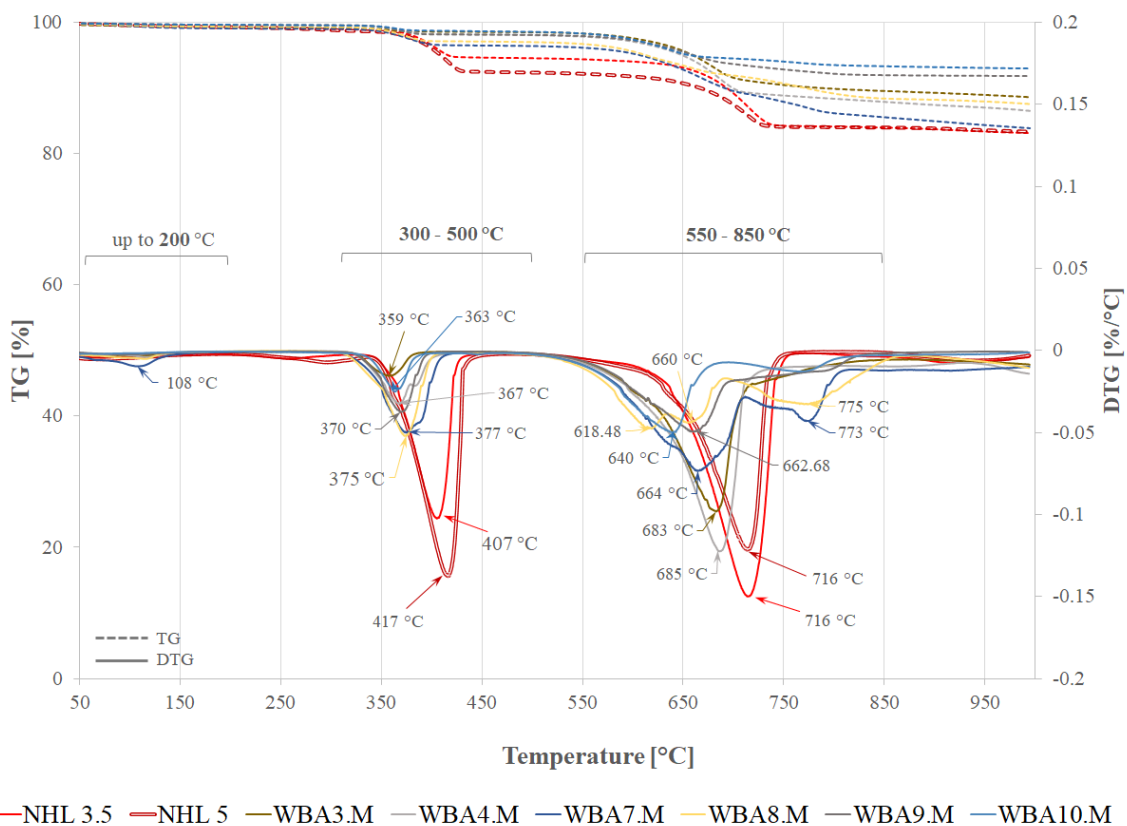
Figure 3.9. TG and DTG curves of un-hydrated NHLs and mixed WBAs

The content of carbonates and portlandite is calculated from the TGA measurements according to the method described in [71] and compared with the qualitative results of the XRD analysis (refer to Table 3.10). Based on the TG data, it seems that NHL 3.5 fails to meet the specifications set forth in EN 459-1 [28], which stipulate a minimum of 25% lime availability in the form of $Ca(OH)_2$. Conversely, NHL 5 demonstrates a notable excess beyond the specified threshold, as the specified standard requires a minimum of 15% available lime. In general, the quantification of carbonates and portlandite content derived from TG measurements aligns with the results obtained through XRD analysis. It's worth noting that while the XRD data for certain ash samples, notably WBA2.F, WBA7.M, and WBA8.M, indicates the coexistence of different carbonates, including magnesium carbonates, the overall correlation between TG measurements and XRD findings remains consistent.

Major and moderate levels of carbonates are verified in all the WBAs, including those categorized as siliceous (WBA10.M). However, the proportion of $Ca(OH)_2$, comparable to NHL 3.5, is found only in WBA 1.F, whereas the other WBAs exhibit a modest presence of portlandite.

Table 3.10. Comparative analysis of carbonate and portlandite phases: TGA vs. XRD measurements

	NHL/WBA ID	Portlandite (%)		Carbonates (%)	
		DTG	XRD	DTG	XRD
NHL	**NHL 3.5**	18.26	moderate	23.65	major
	NHL 5	26.69	major	18.61	moderate
Fly WBAs	**WBA1.F**	18.23	moderate	32.09	major
	WBA2.F	6.09	minor	36.88	major*
	WBA5.F	4.43	minor	17.97	major
	WBA6.F	3.93	minor	36.65	massive
Mixed WBAs	**WBA3.M**	3.68	minor	19.90	major
	WBA4.M	7.19	n/d	22.60	major
	WBA7.M	11.76	minor	24.09	major*
	WBA8.M	10.68	moderate	18.89	minor*
	WBA9.M	6.77	minor	13.55	moderate
	WBA10.M	5.07	minor	11.35	moderate

Refers only to calcium carbonates.

3.4. Assessment of AHL pastes

3.4.1. Standard consistency, setting time, and soundness

The evaluation of standard consistency and setting times for AHL pastes involved a sequential examination. The initial and final setting times were determined by observing the penetration of a needle into standard consistency AHL pastes according to the guidelines in EN 459-2 [118] using a standard plunger. The amount of water required to achieve the desired paste consistency was determined by probing AHL pastes with different water contents. The initial and final setting times were then measured using a ToniSET automatic Vicat needle instrument (see Figure 3.10 (b) and (c)).

(a)   (b)   (c)
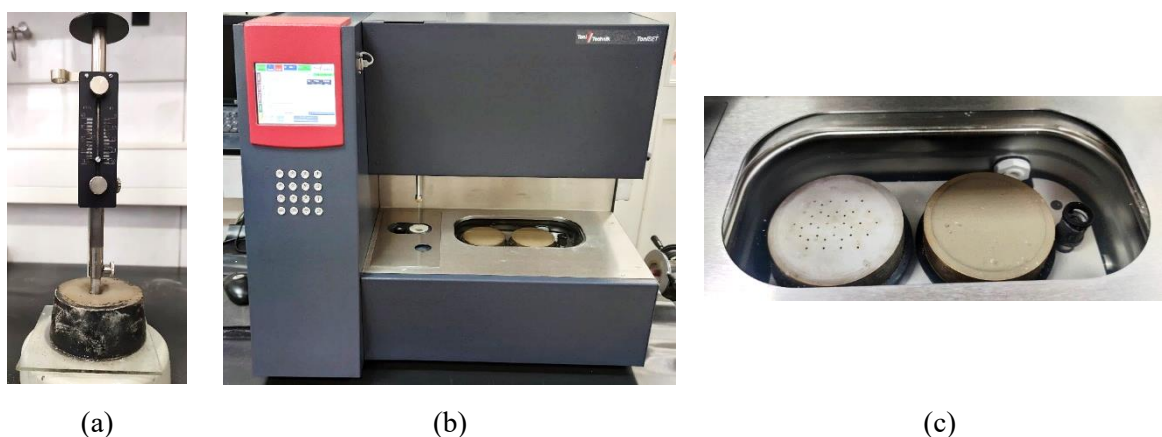
Figure 3.10. Sequential experiment stages: (a) standard consistency test; (b) measurement of setting time; (c) AHL moulded paste emerged in water during the setting time test

In compliance with EN 459-2, an alternative method was used to assess the soundness of AHL pastes. Specifically, 75 grammes of the AHL binder blend was mixed with 35 mL of water in the case of fly ash and 30 mL of water if mixed ash was used. The EN 459-2 standard suggests the use of 20 mL of water for paste preparation, indicating an increased water requirement due to the inclusion of WBA. The appropriate amount of water was determined by testing batches of test pastes. Subsequently, three test specimens were prepared for each AHL binder blend by immediately filling Le Chatelier moulds and subjecting them to a 180-minute treatment in a steam cabinet. After the specified duration and after the Le Chatelier moulds had cooled to room temperature, the distance between the ends of the indicator points was measured.

The effects of WBA on the above properties of AHL pastes are clearly seen. An increase in water requirement to reach standard consistency, prolonged initial and final setting times and volumetric expansion were observed (refer to Table 3.11).

When determining the amount of water required to achieve standard consistency, both NHL and AHL binder mixes were found to have a heightened sensitivity to even marginal alterations in water content. Consequently, all AHL blends with fly ash showed a consistent pattern of elevated water demand that correlated with increasing WBA content. This increased demand can be attributed to the rugged and highly porous morphology of fly ash WBAs, which is characterised by a larger specific surface area, as noted in previous WBA characterisations [7,119,120] while the mixed ash AHL pastes were very similar to the control blends in terms of water requirement, AHL8-30-B was an outlier as it required 50% water, reflecting a 10% increase in water requirement. The maximum observed increase in water requirement for fly ashes was 5% (as seen in AHL2-30-B and AHL5-40-B). Nevertheless, the phenomenon of increased water requirement to achieve standard consistency was more pronounced for AHL pastes containing fly ash than for those with mixed ashes.

Moreover, this increased water requirement was accompanied by prolonged setting times. The contrast between water demand and setting time was notable, as both initial and final setting times were significantly delayed for most AHL pastes, regardless of ash type.

In this context, it is important to note that the final setting time of the AHL8-30-B paste could not be recorded, as it extended beyond the 30-hour threshold specified in EN 459-2. Moreover, the paste continued to set for over 40 hours, which eventually resulted in the disintegration of the moulded sample, thus requiring the test to be prematurely concluded. Therefore, the soundness of the pastes with WBA8.M was not further evaluated.

Besides the AHL8-30-B, the binder blends which did not meet the criteria of EN 459-2 included mainly the higher hybridisation ratios of 30 and 40 wt.%. As such, AHL5-30-B, AHL5-40-B, AHL6-30-B, AHL7-20-B and AHL7-30-B, and AHL10-30-B did not meet the criteria of EN 459-2 as the final setting time occurred after 42, 47, 40, 32, 63 and 43 hours, respectively.

For the remaining binder blends, the final setting was completed before the 30 h limit, although the period was up to three times longer than the final set of the reference mixture. In contrast, the addition of WBA4.M in the highest hybridisation ratio of 40 wt.% in the binder blend where NHL5 is used as the primary binder accelerated initial set from 9 to 5 hours and final set from 16 to 13 hours. It is conceivable that this phenomenon is a result of massive CaO presence in WBA4.M (refer to Table 3.9), which can impact accelerated setting with the rapid formation of the C-S-H phase, as reported in [121,122]. As previously stated, it's worth noting that AHL8-20 and AHL8-30 did not attain a final set. This observation can be reasonably attributed to the

fact that these particular samples exhibited the lowest combined sum of pozzolanic oxides (20.96 wt.%) and an exceptionally high content of free CaO (45.75 wt%). However, it is essential to acknowledge that an excessively high concentration of free CaO can impede the proper hardening of the product when exposed to water, as indicated in [35].

Among the binder blends using NHL 3.5 as the primary binder only WBA9.M affected setting in similar, shortening manner, whereas both 20 and 30 wt.% share equally accelerated final setting, while the higher ratio shortened even the initial set. This phenomenon may be attributed to the fact that WBA9.M is the only ash grinded before blending the pastes, suggesting that grinding contributes to the reactive the behaviour of coarse WBA PDB causing additional activation. Indeed, this observation aligns with prior research findings [81], that have supported the notion that the grinding process yields several effects. These include the enhancement of pozzolanic oxides, the reduction of D50 values, a wider distribution of particle sizes, and the potential for an increase in the proportion of alite. Major presence of β-belite was also noted in the WBA9.M sample, which is found to be the major hydraulic phase in hydraulic limes [38].

The fierce hindering effect of WBA on the setting of hydraulic binders was attributed by [123] [119,124,125] to the high contents of sulphates and heavy metals, especially zinc (Zn), lead (Pb), and copper (Cu), that are usually highlighted in WBAs. The predominance of the SO_3 and Zn content, as well as a very high content of other heavy metals (refer to Table 3.6 and Table 3.7), was also confirmed in the WBAs tested in this study; for example, the Zn content in WBA5.F was 3517.5 mg/kg, while it was absent in the NHL sample. In addition, the highest SO_3 content of 11.49% was found also in WBA5.F, whereas the pastes with 30 and 40 wt.% also exhibited significantly extended setting time of 42 and 47 h. In addition, a high P_2O_5 content could also lead to a delay in setting, as could a high alkali concentration, by preventing Ca^{2+} dissolution [126,127]. Both anomalies, elevated phosphate, and very high alkali content, were also observed in the WBAs used. Thus, the retarded setting of the AHL pastes is strongly influenced by the chemico-mineralogical composition of the ashes.

Although only the total silica content was analysed chemically, it is possible to infer a relationship between soluble silica and setting times. Given the 30% reduction in total silica content in the calcareous WBAs, it may be deduced that the presence of soluble silica is likewise diminished through the incorporation of WBAs, particularly at higher hybridization ratios. As a result, setting times are extended, as longer setting times correlate with lower soluble silica contents.

The relationship between particle fineness and setting time appears to be complex, as fly ashes with a much finer particle size distribution exhibited prolonged setting time. In this context, it is noteworthy that fly ash WBA5.F, which was characterised as highly reactive due to its particle volume of up to 10 micrometres, exhibited one of the longest setting times of all binder blends tested. This observation suggests that factors beyond particle fineness can play a crucial role in determining the setting time of fly ash, underlining the multi-layered nature of the setting process.

Table 3.11. Influence of WBA on the properties of AHL pastes

NHL/WBA ID	Binder blend ID	Hybridisation NHL:WBA ratio (%)		Water requirement for standard consistency (%)	Setting time (h)		Soundness (mm)
		NHL	WBA		Initial set	Final set	
NHL 3.5	NHL 3.5-B	100	0	40%	5	10	5.22
NHL 5	NHL 5-B	100	0	41%	9	16	0.60
WBA1.F	AHL1-20-B	80	20	43%	11	19	6.60
	AHL1-30-B	70	30	44%	11	30	18.45
WBA2.F	AHL2-20-B	80	20	44%	8	20	7.39
	AHL2-30-B	70	30	45%	13	25	9.23
WBA3.M	AHL3-20-B	80	20	40%	7	15	5.02
	AHL3-30-B	70	30	41%	10	22	7.88
WBA4.M	AHL4-20-B	80	20	40%	7	14	13.94
	AHL4-30-B	70	30	40%	9	20	18.60
	AHL4-40-B*	60	40	39%	5	13	22.79
WBA5.F	AHL5-20-B	80	20	41%	15	29	6.64
	AHL5-30-B	70	30	42%	21	42	8.70
	AHL5-40-B*	60	40	45%	30	47	0.60
WBA6.F	AHL6-20-B	80	20	42%	14	27	5.22
	AHL6-30-B	70	30	44%	16	40	8.90
WBA7.M	AHL7-20-B	80	20	40%	13	32	9.58
	AHL7-30-B	70	30	41%	24	63	12.45
WBA8.M	AHL8-20-B	80	20	46%	19	n/d	n/a
	AHL8-30-B	70	30	50%	19	n/d	
WBA9.M	AHL9-20-B	80	20	39%	5	8	9.85
	AHL9-30-B	70	30	37%	3	8	11.25
WBA10.M	AHL10-20-B	80	20	39%	10	27	4.02
	AHL10-30-B	70	30	40%	10	43	2.85
	EN 459-1 criteria			-	>1	<30	≤20

The average soundness values of 7.59 mm and 10.92 mm for all AHL mixtures containing 20 wt.% and 30 wt.% WBA, respectively, as well as the elevated individual values of 18.45 mm for AHL1-30-B and 18.60 mm for AHL4-30-B, all comfortably adhere to the soundness limit of 20 mm prescribed by EN 459-1 [28]. Even though the values are generally elevated in relation to the control values, these findings indicate that the incorporation of WBA, even at a 30% hybridisation level, does not compromise the volume stability within the NHL-WBA system.

However, it is worth noting that certain elevated values, which signify augmented expansibility in the prepared AHL pastes, were observed in scenarios where NHL 5 was employed as the primary binder, along with the highest hybridization ratio of 40%, as evident in AHL4-40-B. Significantly, AHL5-40-B exhibited volume stability comparable to that of the control NHL 5-B.

The observed increase in soundness values, suggestive of heightened expansibility in AHL pastes, may plausibly be attributed to the higher content of periclase (MgO) as well as free CaO [35,128,129]. This interpretation gains support from the chemical and mineralogical analysis of the WBAs, where elevated levels of both MgO and free CaO (CaO overall) were observed. However, a contrasting pattern emerged during testing. The AHL4-40-B binder blend exhibited a notably increased distance between the ends of the indicator points, surpassing the upper threshold of 20 mm (Figure 3.11 (b)). In contrast, AHL5-40-B displayed behaviour consistent with that of the control NHL 5-B (Figure 3.11 (a), (c)). This is particularly intriguing considering the inverse proportionality observed in the free CaO content across the samples and the uniformity of MgO content.

| (a) | (b) | (c) |
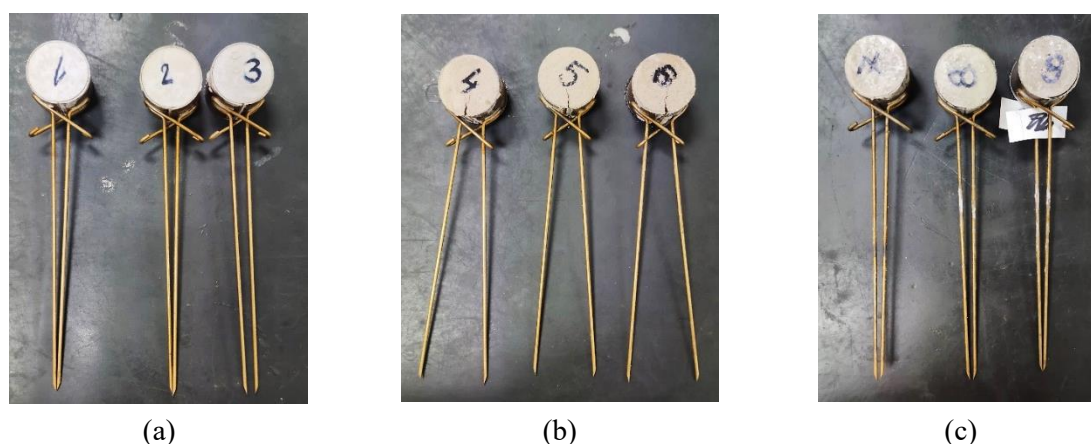
Figure 3.11. Evaluation of soundness after 180 minutes in a steam cabinet: (a) NHL 5-B; (b) AHL4-40-B; (c) AHL5-40-B

3.4.2. Hydration kinetics

Isothermal calorimetry was employed as the method to assess the reactivity of WBAs within NHL binder systems. The NHL:WBA hybridization ratios were varied, along with the hydraulicity of the primary binder. The experimental investigation comprised WBA hybridization ratios of 20, 30, and 40 wt%, conditional upon the hydraulicity of the primary binder, whether NHL 3.5 or NHL 5 was blended with WBA. This research aimed to examine the influence of WBAs on the hydration kinetics of the NHL binder system and to assess its potential contribution to the AHL reactivity.

AHL binder blends are divided into 2 binder groups, distinguished by the hydraulicity of the primary binder, and additionally sub-divided according to the type of WBA utilised (fly or mixed).

The hydration kinetics, i.e., the evolution of the specific hydration power along with the hydration energy in various AHL pastes over 72 h and 168 h, plots the heat evolution in AHL binder blends containing WBA with respect to the reference AHL blend containing solely NHL 3.5 or NHL 5. The flow rate (specific hydration heat power) and the total amount of heat released (specific hydration heat energy) have been normalized to 1 gram of the primary binder (NHL 3.5 or NHL 5) to indicate the prospect reactivity of WBAs. It can be seen that the WBAs did alter the NHL hydration kinetics in the following manner:

Regarding the fly ashes within NHL 3.5 binder group, all specific hydration heat power curves showed relatively high initial values (marker 1 on Figure 3.12), which can be attributed to the heat of wetting and the initial dissolution of the available lime [130]. The marker 1 values are significantly higher for all AHL binder blends, with both employed hybridisation ratios, in relation to the NHL 3.5-B. Moreover, the AHL binder blends with the higher hybridisation ratio have higher hydration heat than the lower, 20 wt.% share, indication increasing reactivity with the increasing WBA share. From the most to the least reactive, WBAs can be placed in the following order: WBA5.F > WBA1.F > WBA2.F > WBA6.F > NHL 3.5. The specified AHL power curves are slightly shifted to the right (marker 2), suggesting a delay in the hydration of calcium silicates [131], consequently accompanied by prolonged setting. In this context, WBA5.F presented the highest reactivity (Figure 3.12, Figure 3.13, Figure 3.14 and Figure 3.15). It is noteworthy that WBA5.F was characterised also as highly reactive due to its particle volume of up to 10 micrometres but also had major extension in final setting time. The initial heightened reactivity decreases around 12 hours (marker 3), when the initially slower WBA2.F

outperforms the WBA5.F, followed by a modest hump around 20 hours of testing (marker 4). The WBA5.F exhibits a thermal peak around 28 hours (marker 5), after which it again surpasses the leading WBA2.F. Similarly, the AHL1-20-B is slightly over the AHL2-20-B in the first 6 hours, with no distinctive thermal peaks. The 30 wt.% counter-lends follow the same behavioural trend, with more elevated values. After about 36 h, all mixtures with WBA show a decreasing trend. The specific hydration energy, where the slope of the curve is related to the reaction rate, shows that all binders continue to exhibit hydraulic reactions until the end of the calorimetric test (72 h). As visible, the control blend made with solely NHL 3.5 exhibited the lowest specific hydration power of all pastes tested and showed a continuous downward trend over the entire test period. The absence of thermal peaks in the NHL 3.5-B binder, but also their secondary presence in the AHL binder blends, is due to differences in hydraulicity. Despite the moderately high total SiO_2 content, which is expected to bring forth the hydraulic capacity of the binders through the formation of belite polymorphs (C2S), the hydraulic substance in the NHL and consequently the AHL binders did not appear to be sufficient to trigger detectable hydration processes in the indicated test time, consistent with the slow reaction of dicalcium silicate (C2S). In view of the absence of noticeable exothermic peaks, the control paste NHL 3.5-B has a relatively low magnitude and approximately the same stance; it can be concluded that the NHL hydration has no direct influence on the heat power from 6 h onwards, which is consistent with the literature data [132].

In general, the reactivity of the material depends on several key factors, including the chemical composition of the material, especially the quantity of soluble silica it contains [29]. Additionally, the fineness of the WBA and the inherent reactivity of the primary NHL binder itself play significant roles in determining the overall reactivity of the AHL binder blend.
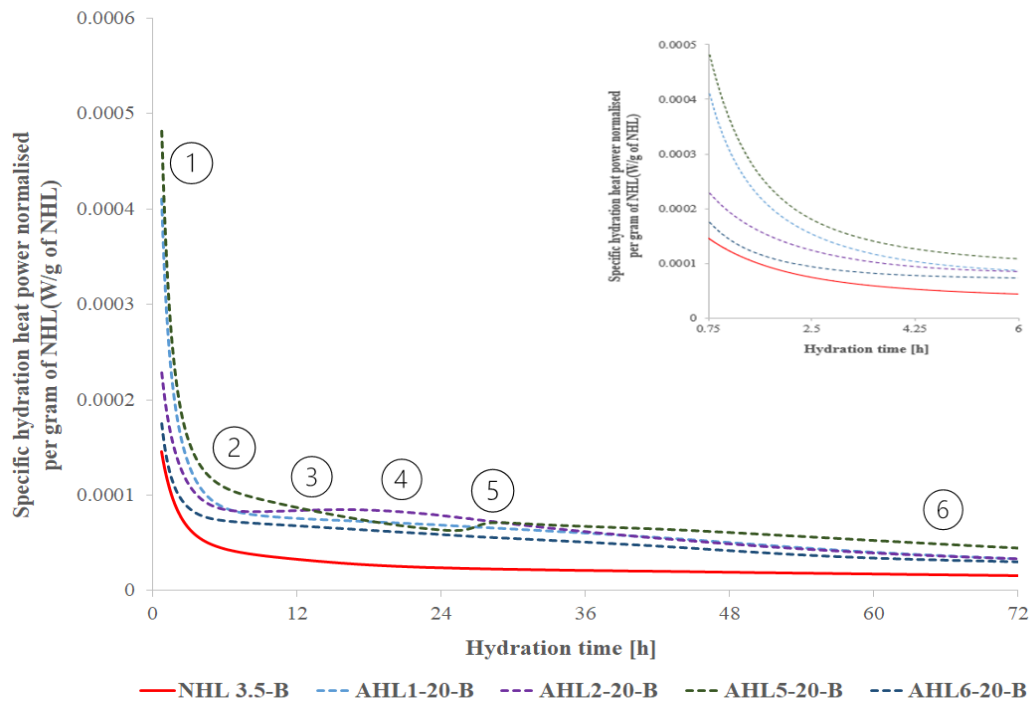
Figure 3.12. Specific hydration heat power in AHL binder blends with 20 wt.% fly WBAs, normalised per 1 g of NHL 3.5
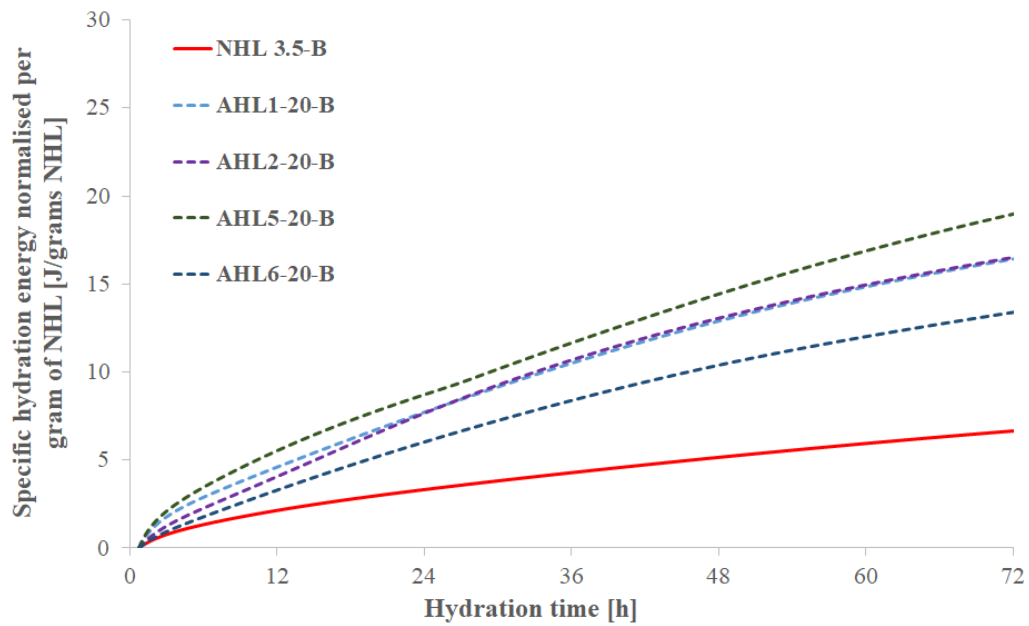
Figure 3.13. Specific hydration energy in AHL binder blends with 20 wt.% fly WBAs, normalised per 1 g of NHL 3.5
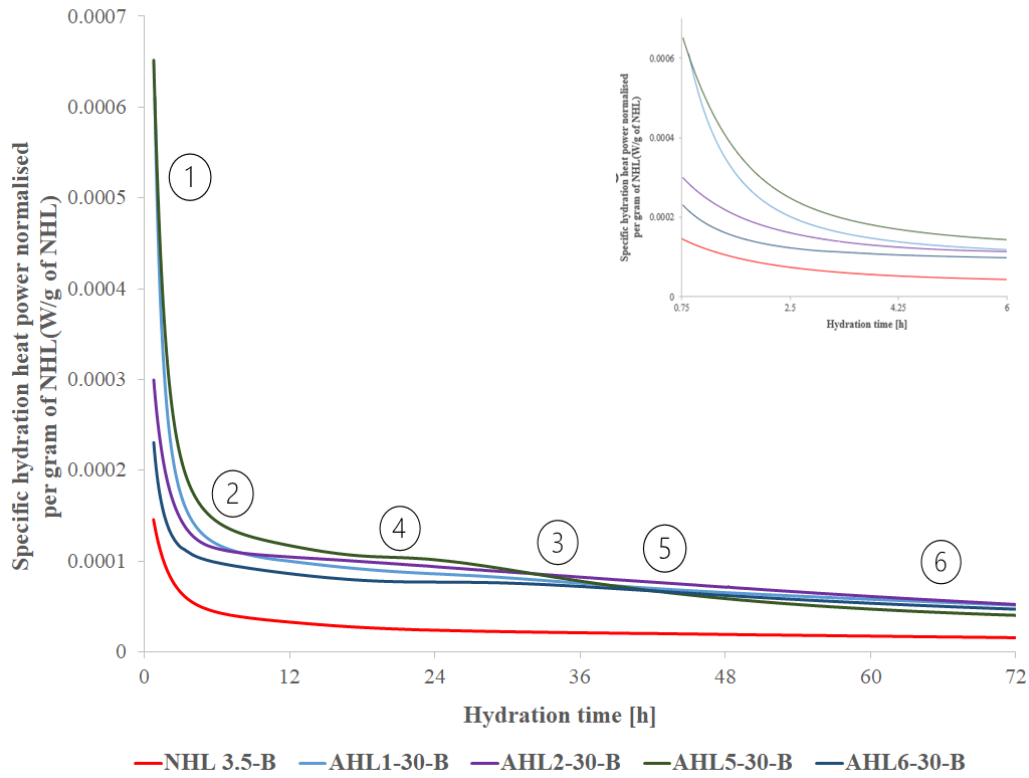
Figure 3.14. Specific hydration heat power in AHL binder blends with 30 wt.% fly WBAs, normalised per 1 g of NHL 3.5
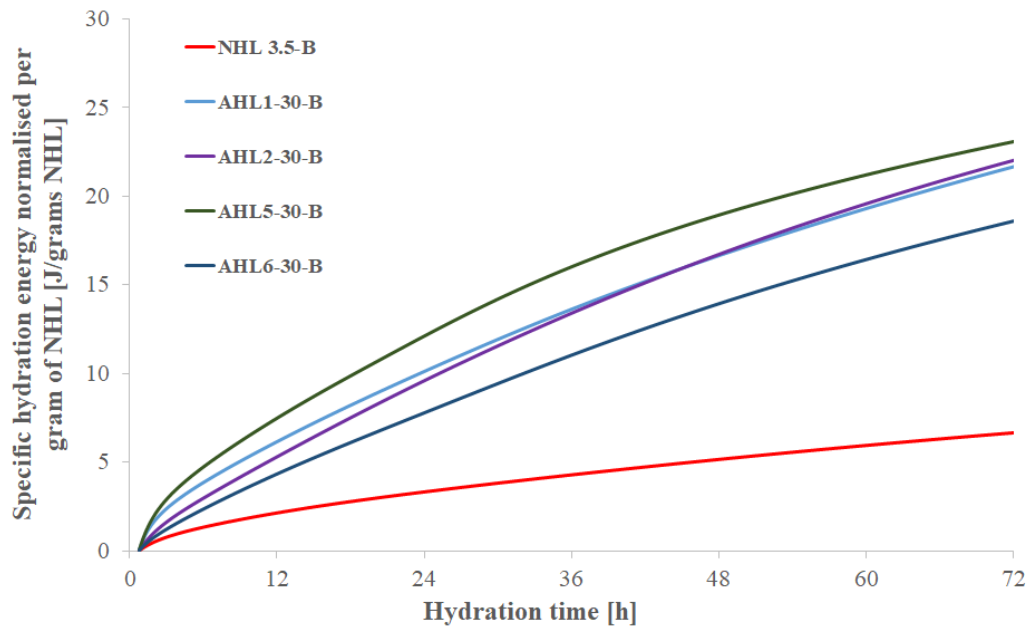
Figure 3.15. Specific hydration energy in AHL binder blends with 30 wt.% fly WBAs, normalised per 1 g of NHL 3.5

Within the same binder group, with a specific focus on the substitution of NHL 3.5 with mixed ashes (depicted in Figure 3.16 and Figure 3.17), notable observations were made regarding the relationship between the reactivity of calcareous mixed ashes and the kinetics of calcareous fly ashes. In this context, the specified WBAs can be categorized in terms of reactivity from the most to the least reactive as follows: WBA8.M > WBA9.M > WBA4.M > WBA7.M > NHL 3.5. Subsequently, ashes with lower reactivity, encompassing both calcareous and siliceous ashes, can be arranged in the following sequence: WBA3.M > WBA10.M > WBA7.M > WBA11.M > NHL 3.5. It's worth noting that the reactivity of these mixed ashes lies somewhat above that of NHL 3.5-B, with AHL11-20-B and AHL11-30-B exhibiting nearly overlapping specific hydration heat power curves compared to the control blend. While AHL8-20-B and AHL8-30-B initially displayed significantly higher reactivity compared to other ash compositions, and AHL7-20-B and AHL7-30-B exhibited relatively lower reactivity levels closer to that of NHL 3.5-B, it is noteworthy that after 17 hours, the reactivity of the former declined, even falling below that of AHL7 binder blends, which then emerged as the more prominent binder blend.

Specific hydration energy of AHL pastes with 20 and 30 wt.% of WBA after 3 days was normalised per gram of NHL 3.5 (Figure 3.13, Figure 3.15, Figure 3.17, Figure 3.19). The data illustrates that the inclusion of a higher hybridization ratio of WBA leads to increased reactivity. It's noteworthy that particle size plays a significant role in this reactivity trend.
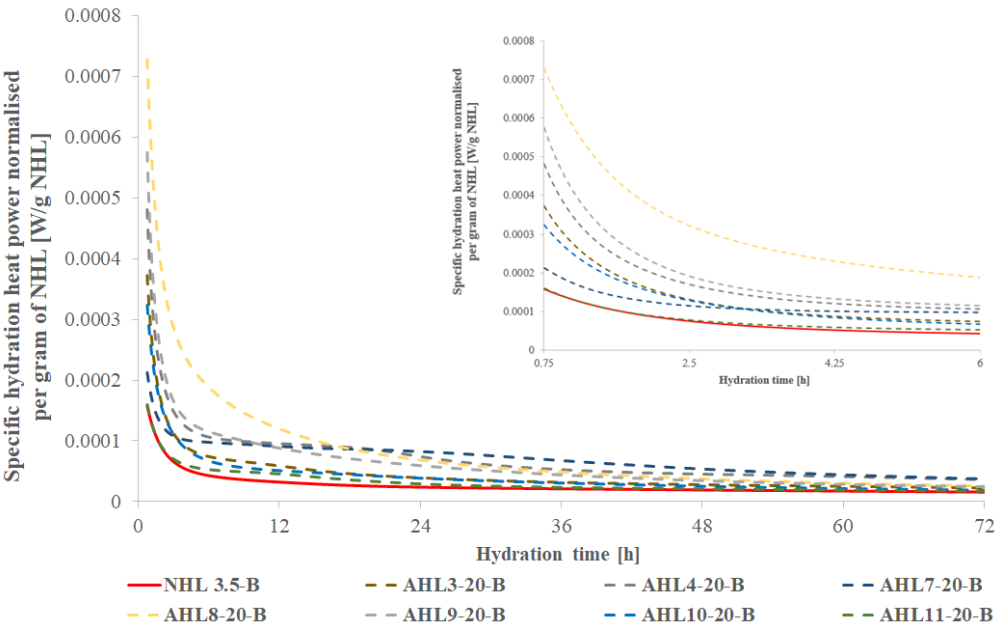
Figure 3.16. Specific hydration heat power in AHL binder blends with 20 wt.% mixed WBAs, normalised per 1 g of NHL 3.5
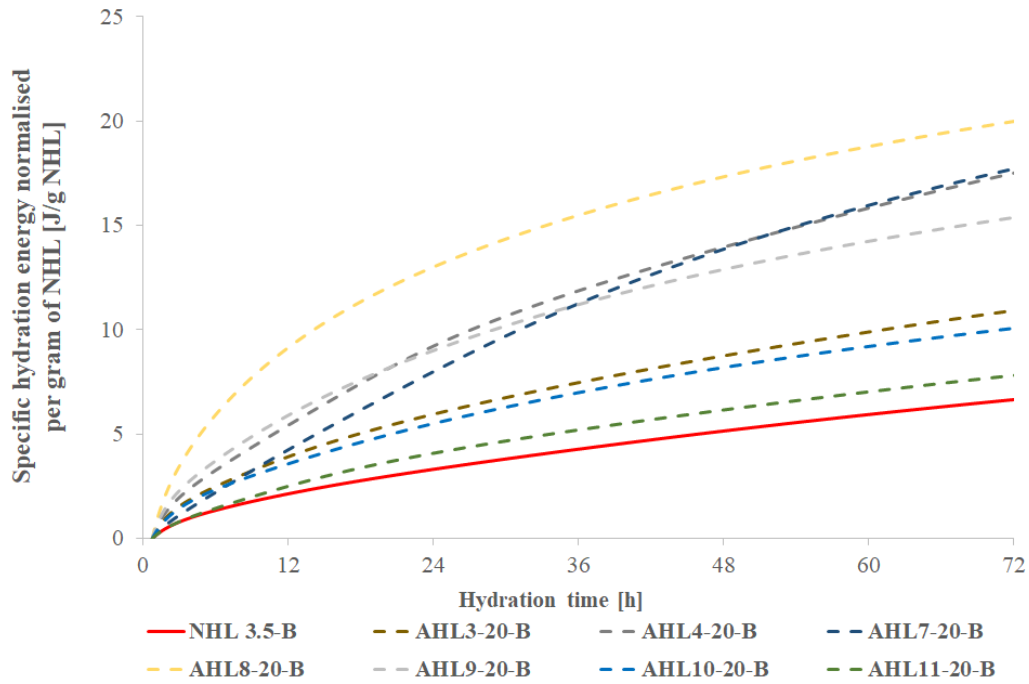
Figure 3.17. Specific hydration energy in AHL binder blends with 20 wt.% mixed WBAs, normalized per 1 g of NHL 3.5
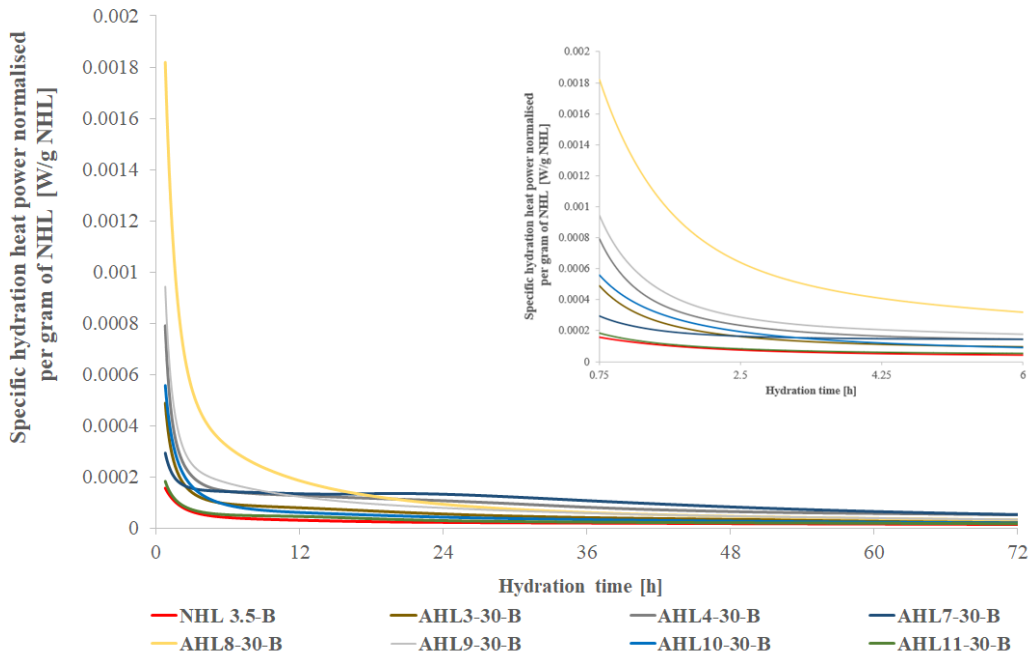
Figure 3.18. Specific hydration heat power in AHL binder blends with 30 wt.% mixed WBAs, normalised per 1 g of NHL 3.5
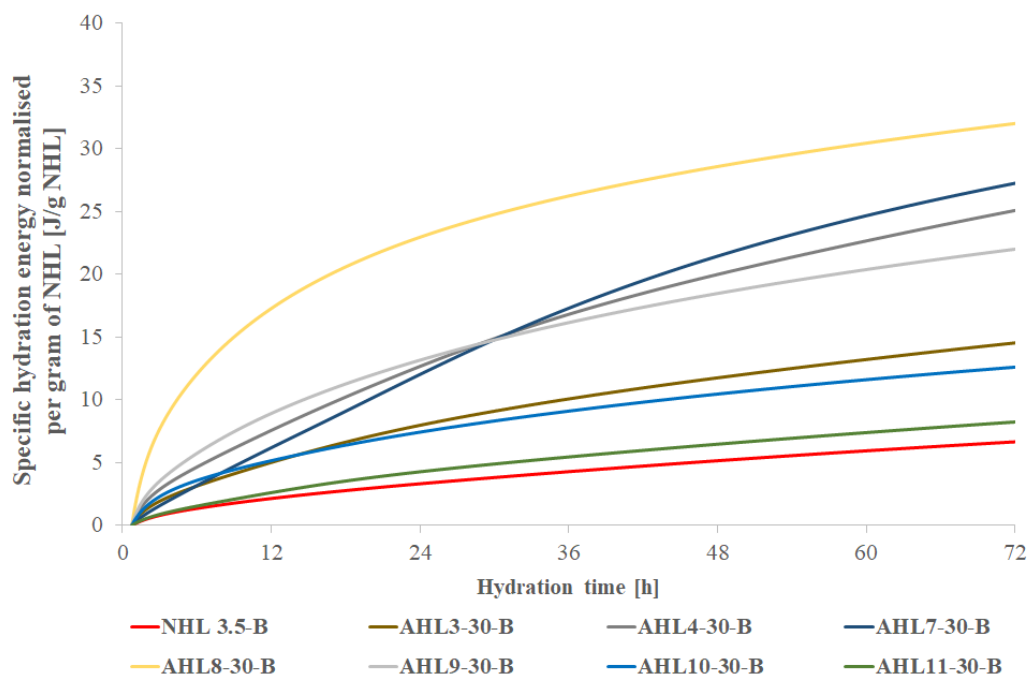
Figure 3.19. Specific hydration energy in AHL binder blends with 30 wt.% mixed WBAs, normalised per 1 g of NHL 3.5

In the context of the fly ashes used within the NHL 5 binder group, findings from the previous set of AHL pastes were validated. Specifically, AHL5-40-B exhibited the highest initial values, although these values experienced a slight reduction after 6 hours. Notably, the energy curve displayed a distinct inflection point around 120 hours, as depicted in Figure 3.20 and Figure 3.21. Subsequently, AHL 4-40-B, which initially demonstrated lower reactivity, surpassed AHL5-40-B in terms of cumulative heat at the conclusion of the 168-hour testing period, as indicated in Table 3.13.
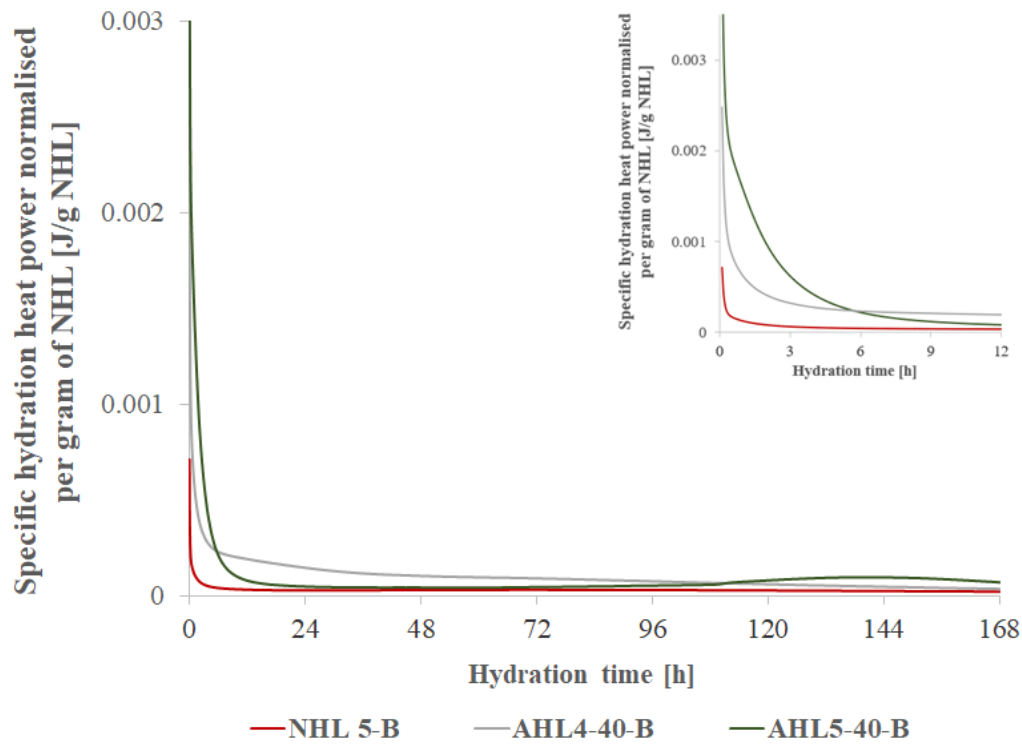
Figure 3.20. Specific hydration heat power in AHL binder blends with 40 wt.% mixed WBAs, normalised per 1 g of NHL 5
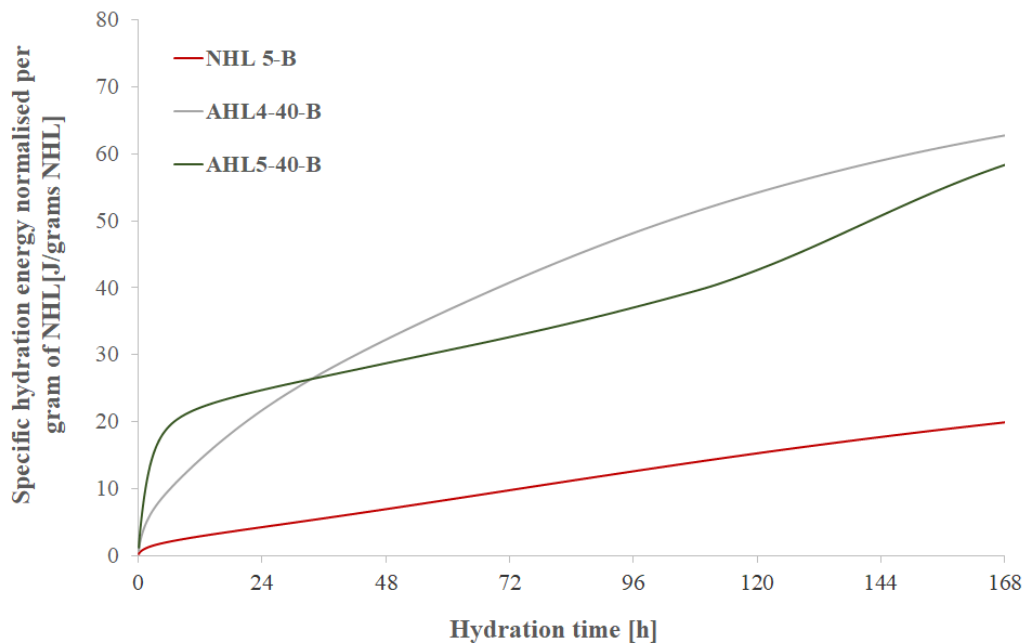
Figure 3.21. Specific hydration energy in AHL binder blends with 40 wt.% mixed WBAs, normalised per 1 g of NHL 5

Table 3.12. Specific hydration energy of AHL pastes with 20 & 30 wt.% WBA after 3 days, normalised per gram of NHL 3.5

NHL/ WBA ID	Specific hydration energy after 3 days [J/g NHL]	
NHL 3.5	7.46	
WBA share	*20 wt.%*	*30 wt.%*
WBA1.F	16.42	21.66
WBA2.F	16.51	22.02
WBA3.M	12.08	16.05
WBA4.M	17.51	25.09
WBA5.F	18.98	23.08
WBA6.F	13.39	18.59
WBA7.M	17.72	27.26
WBA8.M	19.99	32.02
WBA9.M	16.61	23.77
WBA10.M	11.03	13.71
WBA11.M	7.82	8.24

Table 3.13. Specific hydration energy of AHL pastes with 40 wt.% WBA after 7 days, normalised per gram of NHL 5

NHL/ WBA ID	Specific hydration energy after 7 days [J/g NHL]
NHL 5	25.98
WBA share	*40 wt.%*
WBA4.M	71.36
WBA5.F	69.99

The use of an inert reference material, ideally with a particle size distribution closely resembling that of the materials under examination, serves to differentiate between the "filler effect" and the contribution of a reactive mineral addition [115], such as WBA, on the heat of hydration and the heat generated. The term "filler effect" characterizes the impact of introducing a material that does not initially undergo a chemical reaction itself but serves two critical purposes: firstly, it provides additional nucleation sites for the formation of hydrate phases, and secondly it increases the water-to-primary binder (w/b_p) ratio. This, in turn, enhances the long-term hydration degree by creating more space for hydrate precipitation.

As depicted in Figure 3.22 and Figure 3.23, the partial replacement of NHL by quartz results in an increase in cumulative heat due to the filler effect. Within the NHL 3.5 binder group, both WBA2.F and WBA3.M exhibit an additional contribution to the heat of hydration, highlighting the reactivity of the ashes. In the NHL 5 binder group, only the fly ash WBA5.F demonstrates an extra contribution to the heat of hydration, while the mixed ash WBA4.M appears to have no additional contribution on the heat of hydration. This observation contrasts with the findings presented earlier in Table 3.13, where AHL 4-40-B exhibited hydration energy levels comparable to those of AHL5-40-B. This discrepancy may be linked to the heterogeneous nature of the WBA material.
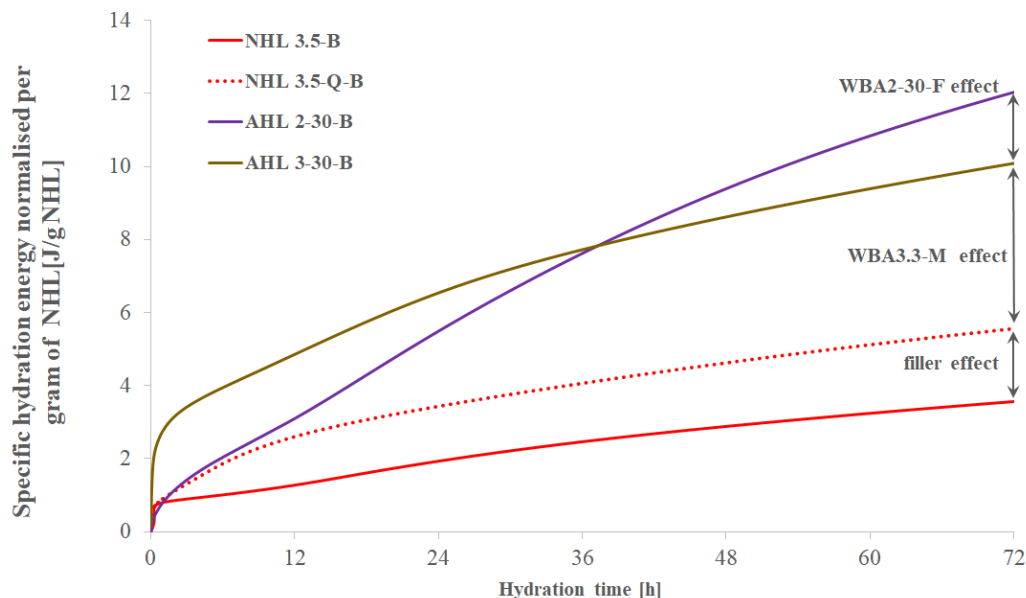
Figure 3.22. Comparing filler and ash effect to specific hydration energy in selected binder blends (AHL2-30-B and AHL3-30-B), normalised to 1 g of NHL 3.5
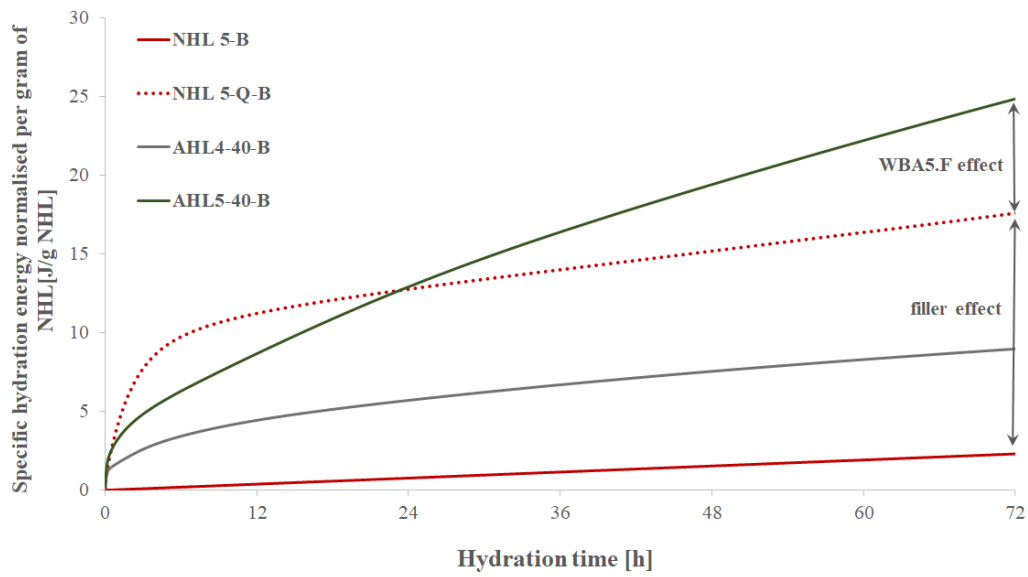
Figure 3.23. Comparing filler and ash effect to specific hydration energy in selected binder blends (AHL4-40-B and AHL5-40-B), normalised to 1 g of NHL 5

3.5. Conclusions and final remarks

In this research segment various 11 WBAs were evaluated within the NHL-WBA binder system, while moderate (20 wt.%) and relatively high (30 and 40 wt.%) hybridisation ratios were employed. Fly and mixed WBAs were used as a substitute for moderately and eminently hydraulic natural natural hydraulic lime.

The validation of the following hypotheses, initially proposed at the beginning of this chapter, was carried out:

H I: 'Building lime with hydraulic properties, i.e. an artificial hydraulic lime can be prepared with wood biomass ash';

H II: 'The chemico-mineralogical composition of WBA, in addition to evaluating various WBA with different degrees of pozzolanity and hydraulicity, has a direct impact on its applicability in a hydraulic binder and the possibility of hardening of hydraulic lime mortar systems'.

These validations adhered primarily to the criteria stipulated in standard EN 459 for building lime. As per the defined standard, lime with hydraulic properties primarily consists of calcium silicates, calcium aluminates, and calcium hydroxide. It is defined by its initial set, has a specified range of available lime in the form of $Ca(OH)_2$ content, and is classified based on its mechanical properties, specifically compressive strength. In addition to natural hydraulic lime (NHL), formulated lime (FL) and hydraulic lime (HL) are two sub-categories of artificial hydraulic lime.

The H1 hypothesis, despite its broad scope, essentially suggests classifying AHL produced with WBA within one of the subcategories of artificial hydraulic lime, as defined by the specified standard. The criteria established for FL and HL are rooted in chemical and physical parameters at the binder level. On the paste level, the emphasis is placed on setting time and soundness, as outlined by EN 459. Consequently, the evaluation of the NHL-WBA system was conducted in accordance with these criteria. In addition, physical properties were further analyzed using laser diffraction to provide detailed insights into particle size distribution and density testing. Furthermore, XRD analysis was employed to investigate the presence of hydraulic phases within the WBAs.

By consolidating the results of this comprehensive assessment of an AHL binder with WBA, specifically focusing on the evaluation of WBA's influence on the specified properties at the AHL binder and paste levels (refer to Table 3.14 and Table 3.15), it was possible to pinpoint suitable types of WBA and favorable hybridisation ratios. At this stage, the concept of a tailored design emerged, aiming to determine the maximum acceptable WBA content that would not significantly compromise the hydraulicity of the primary binder.

Table 3.14. WBA integration effects in NHL binder system at binder level

Property	Major observation
Physical properties	Fineness is acknowledged as a pivotal factor influencing the potential of WBA application in NHL-WBA systems. In this context, sieving emerges as a beneficial pre-treatment method for regulating the particle size distribution. Moreover, milling is observed to enhance the reactivity of WBAs without compromising its potential hydraulicity. Following the sieving process, both fly and mixed ashes meet the EN 459-1 fineness criteria. However, it's worth noting that fly ashes exhibit a narrower, finer particle distribution, whereas mixed ashes demonstrate a broader, larger particle size distribution.
	The bulk density values for both fly ashes and mixed ashes align with the characteristic range outlined in EN 459. However, it's worth noting that fly ashes tend to have lower values, while mixed ashes have higher values compared to NHL. These lower bulk density values are correlated with an increased water requirement, a characteristic that is also distinct in pure NHL systems.
	The average specific gravity of both fly ashes and mixed ashes does not significantly deviate from the control values, with all measurements averaging around 2.7 g/cm³.
	The free water, i.e., moisture present in all WBAs was negligeable, conforming with EN 459 standard.

Property	Major observation
Chemical properties	Majority of WBAs can be categorised as calclareous with CaO as the prevailing oxide, including both fly and mixes ashes.
	Elevated levels of SO_3 were noted, particularly in fly ashes, surpassing the 2% limit set by EN 459-1 for FL. This trend of heightened alkalis (K_2O and Na_2O) and expansive components (MgO and free CaO) is also evident in both fly and mixed ashes.
	Elevated concentration of heavy metals is confirmed in WBAs, which are placed in relation to the extended setting times of AHL pastes.
	Low values of pozzolanic oxides are observed in WBAs by XRF, averaging 28.3% and 31.4% in calclareous fly and mixed ashes, respectively. Given that the pozzolanic activity in WBAs is characterized by a gradual and delayed onset, it is imperative not to underestimate the activity of WBA in a slow-paced NHL system by solely relying on the total sum of pozzolanic oxides.
	While a hydraulicity appraisal based solely on chemical composition may initially suggest that WBAs exhibit high hydraulicity, it is essential to consider a broader context. This should encompass factors like the solubility of silica and be corroborated with an evaluation of the mineralogical composition.
Mineralogical properties	The analysis of crystalline phases in non-hydrated WBA samples has shown the absence of a crucial hydraulic phase typically found in NHL, namely C2S, which is the β-Ca_2SiO_4 polymorph of belite. Instead, calcio olivine, another belite polymorph, is present to a minor or moderate extent in WBA samples, but it is anticipated to have very limited hydraulic properties. Furthermore, gehlenite, a significant hydraulic phase in NHL systems, is also detected in WBAs.
	XRD analysis confirms the presence of two crystalline sources of calcium in WBAs, namely $CaCO_3$ and CaO, representing the predominant phases in the majority of WBAs.
	TG analysis revealed two primary phases of weight loss in both NHL and WBA, attributed to the decomposition of portlandite and calcium carbonates. Additionally, in some of the ashes, the presence of dolomite may be suggested, as indicated by the presence of two distinct peaks within the decarbonation zone, which overlap with the calcite peaks.
	In accordance with EN 459-1 standards, hydraulic lime is specified to contain a minimum of 15 wt.% of available lime ($Ca(OH)_2$) for FL. In the case of both fly and mixed WBAs, the presence of portlandite was observed, albeit in minor to moderate quantities. This decline in portlandite content is anticipated to be compensated for by the weighted averages in the final compositions.

Table 3.15. WBA integration effects in NHL binder system at paste level

Property	Major observation
Consistency	Both pure NHL and AHL binder blends were discovered to be highly responsive to even minor changes in water content. Consequently, all AHL blends with fly ash consistently exhibited a moderate increase in water demand as the WBA content increased. Conversely, pastes with mixed ashes behaved similarly to the control paste, even when using higher hybridization ratios.
Setting time	The delayed setting of AHL pastes is notably influenced by the chemical and mineralogical composition of the ashes, often approaching the upper limit of 30 hours as specified by the EN 459 standard.
	Given the paramount importance of setting time in relation to properties influenced by WBA, the implementation of specific pretreatments emerges as a potential partial remedy for the issue of significantly prolonged setting time. Low-energy-intensive methods, such as sieving and grinding, are preferred options.
Soundness	The notable increase in soundness values, implying greater expansibility of AHL pastes, can be linked to the elevated concentration of expansive components present in WBA.
	While the soundness values are consistently higher compared to the control values, these results suggest that the inclusion of WBA, even at a hybridization level of 30%, does not jeopardize the volume stability within the NHL-WBA system.
Hydration kinetics	It can be seen that the WBAs did alter the NHL hydration kinetics. Elevated flow rates and the total amount of heat released suggest enhancements of reactivity of NHL by the WBA addition.
	The absence of noticeable exothermic peaks was predominantly ascribed to the slow hydration of C2S, while the reactivity enhancement was then related mostly to the fine particle size of WBAs. Furthermore, it was confirmed that WBAs made an additional contribution to the heat of hydration because of their active participation in the hydration reactions. Within this context, the specific hydration energy released in pastes containing fly ashes somewhat exceeded that in pastes with mixed ashes, although not to a significant extent.

The properties under assessment are acknowledged as key factors that govern the NHL-WBA binder system and, consequently, shape the mechanical properties and durability of AHL mortar. This assessment has yielded the following scientific contributions:

'Determination of prospects for the use of WBA in artificial hydraulic lime based on the key factors governing the engineering behaviour and durability of a new composite.'

Based on the presented findings, a selection of WBAs was made to advance into the subsequent research phase, specifically involving mortars. In this context, two fly ashes (WBA1.F and WBA2.F) and two mixed ashes (WBA3.M and WBA4.M) were chosen for incorporation into the NHL 3.5 binder system, with hybridization ratios of 20% and 30% by weight.

Additionally, one fly ash (WBA5.F) and one mixed ash (WBA4.M) were selected to be incorporated into the NHL 5 binder system at the highest hybridization ratio of 40% by weight. Despite the elevated SO_3 values and the notably extended setting time observed in AHL pastes containing WBA5.F, this particular ash was included in the subsequent mortar-level examination. This decision was motivated by the desire to further test the H2 hypothesis, which posits that the chemical and mineralogical composition of WBAs directly impacts their suitability in hydraulic binders and, subsequently, the hardening of mortars using such binders. Within this framework, the relationship between the setting and hardening processes of hydraulic mortar, prepared with an AHL binder containing SO_3-rich WBA, will be evaluated, even if it contradicts the EN 459 criteria.

4. EXPERIMENT: PREPARATION AND EVALUATION OF LABORATORY MORTAR MIXTURES

4.1. Investigative Objectives

This chapter centres around assessment of AHL attributes and their impact on mortar properties across diverse curing conditions. The findings gained from this research segment will serve as a guide in identifying the ideal curing environment and feasible WBA contents suitable for AHL mortars. The ultimate aim is to validate the third hypothesis, which asserts that *'Artificial lime with hydraulic properties containing WBA can be used to produce eco-friendly cement-free mortar for restoration and/or rehabilitation of historical buildings'*.

Following the completion of phase II, which involved selecting the favourable type and proportion of WBA suitable for AHL mortar, the subsequent phase of investigation was dedicated to the comprehensive evaluation of both fresh and hardened mortars. This investigation focused solely on the WBAs chosen during the preliminary screening, aiming to unveil their true potential for enhancing AHL mortar performance.

Initially, immediate mixing allowed for the determination of various critical parameters, including the consistency of fresh mortar, bulk density, air content, temperature and water-soluble chloride content. Subsequently, a comprehensive evaluation was conducted to investigate the influence of WBA on the mechanical, hygrothermal, and durability properties of AHL mortars. The engineering behaviour, encompassing essential aspects such as compressive and flexural strength, as well as the modulus of elasticity, was examined on mortars of varying ages and subjected to diverse CO_2 and moisture conditions. Also, an analysis of durability aspects was undertaken, focusing on adhesive bond strength to substrate and resistance to freeze/thaw action and/or sulphate attack. Furthermore, in-depth microstructural characterization was performed utilizing mercury intrusion porosimetry (MIP) to analyse the pore structure of the hardened mortar samples. This was complemented by scanning electron microscopy (SEM) analysis, offering a detailed insight into the microstructure of the cured mortar specimens. Additionally, the examination of hygrothermal properties, encompassing capillary water absorption, water vapor permeability, and thermal conductivity, was also conducted.

4.2.   Experimental materials and methodology

In this phase of the research, hybrid artificial hydraulic lime binders were prepared by blending the selection of WBAs and NHL, based on the findings from phase II, as described in the preceding chapter. Three fly WBAs (WBA1, WBA2 and WBA5) and two mixed WBAs (WBA3 and WBA4) were collected from power plants that utilize grate firing systems and fuel them with untreated wood chips.

Two sources of hydraulic lime were incorporated within the AHL binary binder system. The first was NHL 3.5, a commercially available moderately hydraulic natural hydraulic lime, thoughtfully supplied by Baumit Croatia. Additionally, NHL 5, a natural hydraulic lime with higher hydraulicity, was utilized, obtained from Calce Raffinata Italy and generously supplied by Samoborka d.d. (Croatia). The previous chapter provided an extensive analysis of the chemical, mineralogical, and physical attributes of these materials.

For mortar preparation, CEN standard sand was employed, a fine quartz sand with a precisely defined particle size distribution ranging between 0.08 and 2.00 mm, serving as the aggregate for all experimental mixtures.

The proposed designations for the mortar mixtures followed the same analogy as the binder/paste blends: AHLi-20-M, AHLi-30-M, and AHLi-40-M. Here, the subscript "i" represented the ID number of the respective WBA used, while the percentages denoted the proportion of WBAi in the mixture. Furthermore, the 'M' designation serves to indicate the mortar level, distinguishing it from the paste level, thus enhancing clarity in the research.

To establish reference points, control mixtures (designated NHL 3.5-M and NHL 5-M) were prepared, utilizing solely NHL as the primary binder.

4.2.1. Mortar mixtures: preparation and curing regime

Prior to blending the AHL binders, WBAs were mechanically sieved through a 250 μm sieve to remove impurities such as unburnt wood and pieces of metal or charcoal fragments. This type of selective removal was intended to overcome physical incompatibilities in the AHL binder system that might otherwise lead to higher water requirements or diminished mortar performance.

The residue left on the 250 μm sieve demonstrated variations based on the specific type of WBA being examined. In the case of fly WBAs like WBA5, the residual content was relatively lower, hovering around 1%. Conversely, WBA1 exhibited a content of roughly 3%, while WBA2

showed a notably higher value at 5%. The mixed ash samples (WBA3 and WBA4) displayed significantly elevated levels, approximately 40% and 45% respectively. These elevated values can be attributed not only to impurity levels but also to a distinct distribution of particle sizes within these mixed ashes.

After the screening process, the WBAs were mixed with NHL in their dry, powdered state at the specified ratio. Prior to introducing potable water and additives, all dry ingredients, including the binder blends and standardized sand, were mixed. This approach corresponds to a prefabricated, ready-to-use mortar that has a high level of uniformity.

The mass ratio of binder to aggregate was consistently maintained at 1:3 across all mortar mixes, while the water–binder ratio remained fixed at 0.60 for all AHL mortar compositions. The content of polycarboxylate superplasticizer was adjusted to achieve a flow diameter of 160 to 170 mm in the mortar, indicating practical workability on the construction site. To maintain a constant water–binder ratio and attain the recommended flow diameter of 162 to 168 mm [28], the dosage of polycarboxylate superplasticizer was adjusted from 0.15% in the control mixes to 0.80% in the mixes with WBA, with the quantity increasing with the amount of WBA used. Furthermore, to optimize the performance of the mortars, an air-entraining agent was included at a dosage of 0.02% of the binder in all mixtures. The additives utilized in the AHL mortar compositions were procured from PINKY-S d.o.o., a Croatian manufacturer specialized in producing concrete and mortar additives. A detailed representation of the experimental mix designs is provided in Table 4.1 and Table 4.2. These designs involve the substitution of NHL 3.5 with 20 and 30 wt.% of WBA, along with the replacement of NHL 5 with a higher concentration of 40 wt.% WBA. While on-site weight batching is infrequently employed, most lime suppliers specify sand volumes per full bag of NHL. It is crucial to recognize that dry hydrates exhibit distinct bulk densities when mixed with sand and WBA. Therefore, the optimal approach involves weighing, not volumetrically measuring, the mixture.

Table 4.1. Formulation of experimental mix designs involving the substitution of NHL 3.5 with 20 and 30 wt.% of WBA

Mix ID	NHL 3.5 - M	AHL1-20 - M	AHL1-30 - M	AHL2-20 - M	AHL2-30 - M	AHL3-20 - M	AHL3-30 - M	AHL4-20 - M	AHL4-30 - M
NHL 3.5 [%]	100	80	70	80	70	80	70	80	70
WBA [wt.% m_b]	0	20	30	20	30	20	30	20	30
NHL 3.5 [kg]	3.93	3.15	2.75	3.15	2.75	3.15	2.75	3.15	2.75
WBA [kg]	-	0.79	1.18	0.79	1.18	0.79	1.18	0.79	1.18
water/binder ratio					0.60				
Additives [wt.% m_b] air entraining agent					0.02				
Additives [wt.% m_b] superplasticiser	0.15	0.40	0.77	0.35	0.43	0.22	0.37	0.20	0.35
Aggregate (CEN Standard sand) [kg]					11.796				
aggregate-to-binder mass ratio					3.00				
aggregate-to-binder volume ratio	3.03	3.03	3.04	2.95	2.90	2.98	2.97	3.08	3.11

Table 4.2. Formulation of experimental mix designs involving the substitution of NHL 5 with 40 wt.% of WBA

Mix ID	NHL 5 - M	AHL4-40 - M	AHL5-40 - M
NHL 5 [%]	100	60	
WBA [wt.% m_b]	0	40	
NHL 5 [kg]	4.81	2.88	2.88
WBA [kg]	-	1.92	1.92
water/binder ratio		0.60	
Additives [wt.% m_b] air entraining agent		0.02	
Additives [wt.% m_b] superplasticiser	0.15	0.33	0.80
Aggregate (CEN Standard sand) [kg]		14.417	
aggregate-to-binder mass ratio		3.00	
aggregate-to-binder volume ratio	2.95	3.06	2.95

Adhering to the guidelines outlined in the EN 459-2:2021 standard [118], which builds upon the principles of EN 196-1:2016, a tailored mortar mixing protocol was enacted. The protocol encompassed the subsequent steps:

1. Primarily, the previously manually homogenized binder and sand mix was placed into the mixer bowl and dry stirred for an additional 60 seconds.
2. The mixing process continued at low speed for 60 seconds, while simultaneously adding water and additives.
3. Subsequently, the mixing speed was increased to high speed for 30 seconds.
4. After 90 seconds of stopping the mixing, any remaining materials from the edges and bottom part of the bowl were scooped out.
5. The mixing resumed for another 90 seconds at high speed, exceeding the standard prescribed time of 60 seconds.

Standard steel moulds measuring $40 \times 40 \times 160$ mm were used to cast the mortar specimens. After casting, the specimens were kept in the moulds under specific humid conditions (relative humidity RH of $90 \pm 5\%$ and a temperature of $20 \pm 2\ °C$) for 3 to 5 days following the mixing and casting process, in accordance with EN 1015-11 [45]. As soon as demoulding was possible, this period being extended by the WBA type and content, the mortar specimens were pre-cured for up to 7 days under humid conditions and then rearranged in different climatic chambers for up to 28 days according to the following curing regimens:

(a) Humid curing (HC) at a controlled temperature of $20 \pm 5\ °C$ and relative humidity RH = $90 \pm 5\%$, with an average CO_2 content between 300 and 400 ppm.
(b) Semi-dry curing (DC) under controlled temperature of $20 \pm 5\ °C$ and relative humidity RH = $60 \pm 10\%$, with an average CO_2 content ranging from 300 to 400 ppm.
(c) Accelerated curing (ACC) at a controlled temperature of $20 \pm 5\ °C$ and relative humidity RH = $60 \pm 5\%$, with a CO_2 content of 30 000 ppm.

The above curing scheme was developed by incorporating insights from previous research [34] and the outcomes of trial batches detailed in [133], as the hydration and carbonation reactions in mortars are influenced by moisture content [46,134]. It was also found that a pozzolan may undergo hydration even under relatively dry curing conditions, depending on its reactivity, suggesting that mortars perform better when initially exposed to moist pre-curing for up to 2 weeks after application, followed by a lower moisture environment.

Therefore, all AHL mortar mixes were initially exposed to HC to improve hydration reactions. DC was used to aid carbonation reactions, while HC promoted hydration reactions. ACC was intended to enhance carbonation reactions in a CO_2 chamber with a CO_2 concentration of 3% by volume and a relative humidity of 60%. The exposure to excessive CO_2 during mortar curing was studied and compared to natural carbonation to simulate the conditions mortars face in historic buildings. Though a higher RH degree allows for increased carbonation and greater hydration of hydraulic compounds in hydraulic mortars [41–43], the AHL mortar samples were fully carbonated after 28 days and exhibited no visible cracks on the surface. While average values between 80 and 90% of final carbonation can be achieved near the surface of mortars exposed to the atmosphere, it is widely accepted in scientific literature that 100% carbonation is practically not achievable in an outdoor environment [38].

4.2.2. Methods

An assortment of double-phase methods was employed to comprehensively evaluate both the properties of fresh and hardened mortars, as outlined in Table 4.3. The influence of wood ash on the properties of fresh mortar was assessed through an examination of temperature sensitivity, consistency (measured by flow diameter), water demand, air content, and density.

Initially, the chloride content was ascertained in fresh mortar samples. Subsequently, the analysis extended to encompass the determination of chloride, fluoride, nitrate, and sulphate levels after the mortar had undergone HC curing for a duration exceeding 3 months.

The investigation of the cured mortar samples took place at both the 28 and 90-day and extended exposure points (beyond the 90-day threshold) within diverse curing environments. This study primarily delved into the mechanical attributes, durability, and hygro-thermal properties of AHL mortars, assessing their correlation with WBA incorporation and the specific curing conditions applied.

Table 4.3. Test methods for assessment of AHL mortars

Level	Property	Test timeframe	Measurement unit	Standard/method
Fresh mortar	Bulk density	Immediately upon mixing of mortars	kg/m^3	EN 1015-6:2000
	Temperature		°C	EN 12350-1:2019
	Air content		%	EN 459-2:2021
	Consistency of fresh mortar (by flow table)		mm	
	Chloride content in fresh mortar		%	EN 1015-17:2000
Hardened mortar	Dynamic modulus of elasticity (ultrasonic pulse velocity)	After 7, 28 and/or 90 days of exposure to various curing environments	m/s	EN 12504-4:2021
	Compressive strength		MPa	EN 1015-11:2019
	Flexural strength			
	Pozzolanic reactivity		%	ASTM C618-22
	Carbonation degree		mm	'Repair Mortars for Historic Masonry' [77]
	Phase/composition identification		-	Scanning electron microscopy (SEM)
	Pore structure		%	Mercury intrusion porosimetry (MIP)
	Capillary water absorption		kg/(m^2·min^{0,5})	EN 1015-18:2003
	Water vapour permeability		kg/m^2·s·Pa	EN 1015-19:2000
	Thermal conductivity		W/m^2·K	EN 12664:2002
	Adhesive bond strength		N/mm^2	EN 1015-12:2016
	Resistance to freeze/thaw action & sulphate attack		visual assessment rating (VAR)	RILEM Recommendation MS-A.4 Determination of the durability of hardened mortar
	Leaching/determination of chloride, fluoride, nitrate, and sulphate		mg/kg	EN 12457-4:2005 EN ISO 10304-1:2009

The procedure for assessing the **bulk density** of fresh mortar (ρ_m) in accordance with the EN 1015-6:2000 [135] standard involves a series of straightforward steps. First, a representative sample of fresh mortar is prepared, taking care to eliminate any air pockets or voids through thorough mixing. Subsequently, the mass (m_1) of an empty measuring vessel with a predetermined volume (V_v) is weighed and documented. The vessel is then filled with the fresh mortar sample, ensuring even distribution, and compacting as necessary. Following this, the mass of the vessel, now containing the compacted mortar, is recorded (m_2). Employing these values, the bulk density (expressed in kg/m³) is accurately computed using the formula:

$$\rho_m = \frac{(m_2 - m_1)}{V_v} \tag{4.1}$$

Following the guidelines of the EN 12350-1:2019 standard [136], the process for **temperature measurement** incorporates the utilization of a dependable and precise temperature measuring instrument, like a digital thermometer. Upon completion of the mortar mixing protocol, the thermometer is introduced into the material at the designated measurement point. Ensuring the proper insertion of the device, it is advisable to permit the temperature measuring equipment to stabilize, furnishing a uniform reading. Once the temperature reading has reached a steady state, the mortar temperature (in °C) is recorded.

The determination of **air content** adheres closely to the EN 459-2:2021 standard [118]. This process employs the pressure method and involves an air entrainment meter equipped with a cylindrical vessel, boasting a 1 dm^3 capacity. Within this apparatus, a one-liter container accommodates mortar, compacted in two layers through simple tamping. A comprehensive cover assembly houses a pressure gauge, air pump, and valves. Ensuring precision, a palette knife achieves a uniform mortar surface. The upper section of the testing apparatus, featuring a gauge cylinder paired with a fitting funnel, is securely affixed. A meticulous water-fill procedure evacuates air from the vessel's remaining space, evident through overflow in the tube. Following valve closure, air is methodically introduced to align with the initial pressure value in the apparatus's upper section. The result is a direct measurement system that precisely indicates the air content in percentage.

Assessing the **consistency of fresh mortar** using the flow table test, as outlined by the standard EN 459-2:2021 [118] starts with a thorough homogenisation of the fresh mortar sample to ensure a uniform composition and employs a special flow table apparatus. This apparatus features a circular table (with dimensions of 300 mm in diameter and 120 mm in height) tailored

to the specific requirements, designed to facilitate unhindered rotational motion along a vertical axis.

Following preparation, a stainless- steel flow mould is positioned to the surface of the table followed by the hopper. This flow assembly, a pivotal element of the test, has certain geometric features, including an upper diameter of 100 mm, a bottom diameter of 70 mm and an overall height of 90 mm. After placing the flow assembly in the centre of the clean, dry surface of the flow table, two layers of mortar are filled. During this process, the mould mounted with the hopper, is held firmly on the plate. Each layer of mortar is spread evenly by tamping it down lightly ten times with the tamper. Subsequent to this, the hopper is promptly removed, and excess mortar is struck off. The flow table is cleaned and any water near the mould is removed. 10 to 15 seconds from striking off the mortar, the mould is gradually lifted vertically from the plate. The mortar is then spread by jolting the plate 15 times, with one jolt per second. The outcome of this procedure is a lateral expansion that leads to a spatial spread that reflects the consistency of the mortar. The subsequent phase entails measurement, wherein the diameter of the resulting spread is measured in two directions perpendicular to each other. This measurement is made with a ruler, whereupon the average of these diametrical observations is calculated. This calculated average represents the flow diameter, a critical metric that holds relevance in evaluating both the workability and the uniformity of the mortar.

The determination of the **water-soluble chloride content** (resistance to soluble salts) in fresh mortar samples begins with the collection of a representative sample that reflects the composition of the entire batch. The sample is then placed in a pre-weighed container, e.g., porcelain, and evenly distributed so that it dries well. The container with the sample is then placed in an oven to dry at a temperature of 105°C to 110°C until a uniform weight is achieved. Upon thorough drying, the sample is grinded to pass a 10 mm sieve, followed by repetition for a 0.125 mm sieve. The fraction finer than 0.125 mm is immersed in distilled water, agitated using a rotary shaker or magnetic stirrer, and left for a minimum of 15 hours for complete dissolution. Afterward, the suspended sample undergoes filtration to isolate dissolved chloride content from the mortar extract. The subsequent addition of excess silver nitrate initiates a chemical reaction, precipitating chloride ions. Titrating the excess silver nitrate determines chloride content, presented as mass percentage in the mortar composition. The described protocol adheres to the description outlined in [137].

Carbonation development was evaluated through visual assessment by applying a phenolphthalein solution to the fractured surface of specimens exposed to the specific curing conditions outlined (HC, DC, ACC) and cured for 28 and 90 days. The extent of carbonation was quantified by measuring carbonation depth on each side of the divided mortar halves, utilizing a precise electronic measuring device and the carbonation depth was then calculated as an average value, as presented in Figure 4.1 [137]. The prismatic specimens, previously tested for flexural strength, were also subjected to compressive strength measurements (a total of three prismatic specimens) within a specified range of 400 ± 40 N/s, following EN 459-2:2021 standards [118], utilizing a manual Form+Test compressive and flexural strength machine.
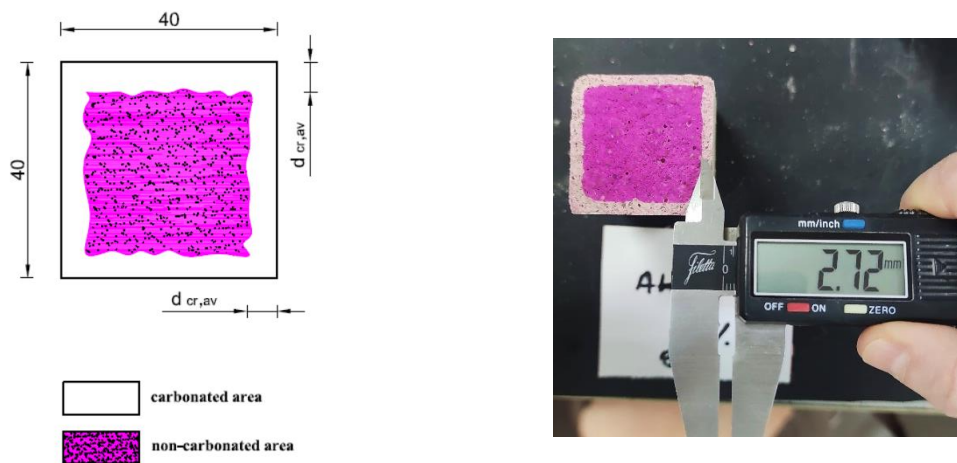
Figure 4.1. Carbonation progress assessment: (a) average carbonation evaluation scheme; (b) measuring carbonation depth on each side of the divided mortar halves

In light of the compressive strength results, the evaluation of the **pozzolanic reactivity** of the WBA followed the ASTM C618 standard [138], employing a strength activity test as the benchmark for performance evaluation. In accordance with the criteria established by ASTM C618, the pozzolanic reactivity is deemed successful if the activity index (SAI) surpasses 75% following a 28-day testing period. In specific terms, when coal fly ash or natural pozzolans substitute 20 wt.% of the binder, the achievement of an SAI exceeding 75% signifies the attainment of the desired pozzolanic reactivity. The strength activity index is expressed as the ratio between the compressive strength of mortar incorporating partial WBA substitution and the compressive strength of the reference mortar, where only NHL functions as the primary binder.

The **dynamic modulus of elasticity** was evaluated both after 28 days and after 3-month marks of mortar age. For this evaluation, three distinct prismatic specimens were used for each mortar mix design, within a specific curing environment. These specimens will subsequently serve a dual purpose: to evaluate the carbonation degree and to perform tests to determine flexural and compressive strength. In particular, the ultrasonic pulse velocity (UPV) measurements were carried out using the direct method along the prisms featuring a path length of 160 mm. The procedure followed the guidelines outlined in EN 12504-4:2021 [139]. Through this approach, the dynamic Young's modulus of elasticity was calculated. In the realm of experimentation, the non-destructive UPV measurements were performed using the Proceq TICO ultrasonic testing instrument along with transducers operating at a frequency of 150 kHz and a transducer diameter of 25 mm. Ensuring optimal contact between the mortar surface and the transducers was primary, for which a specialized coupling paste (grease with a medium soft consistency) was employed. This helped to minimise air gaps or uneven surfaces that could interfere with the transmission of the ultrasonic waves. Prior to each measurement, a careful calibration was performed using a reference calibration rod with a predetermined ultrasonic pulse velocity.

The pulse velocity of the longitudinal stress waves was taken into account to estimate the dynamic modulus of elasticity using the following equation:

$$E_d = \rho \cdot V_{us}^2 \cdot \frac{(1+v)\cdot(1-2v)}{(1-v)} \tag{4.2}$$

Here, E_d represents the dynamic modulus of elasticity, expressed in GPa. V_{us} stands for ultrasonic pulse velocity of longitudinal stress waves, while ρ signifies density. The dynamic Poisson's ratio, v, has been derived from the literature for lime mortar and is set at 0.25 [78].

After 90 days of curing, **scanning electron microscopy (SEM) analysis** was executed on the mortar samples subjected to both HC and DC environments, utilizing the JSM-IT200 microscope manufactured by JEOL. To enhance image contrast, a preliminary gold coating procedure was applied to the samples prior to analysis. The SEM analysis was carried out under a consistent acceleration voltage of 15 kV, while maintaining a steady probe current of 50 nA across all samples. This methodology is particularly advantageous for untreated samples, as it amplifies the visibility of slopes, pores, and other morphological characteristics. Employing a secondary electron detector (SED), renowned for its capacity to yield high-resolution surface images, facilitated the examination of the intricate sample morphology.

Mercury intrusion porosimetry (MIP) was utilized to evaluate the pore structure parameters of fully carbonated and non-carbonated mortar samples at both the 28-day and 90-day marks of exposure to specific curing environments. Following the curing process, hydration was stopped using a solvent exchange method, involving immersion in isopropanol for 7 days. Subsequently, the samples underwent a 48-hour vacuum drying period. The pore entry diameter was determined by integrating the data obtained from Micromeritics' AutoPore IV 9500, considering an assumed contact angle of 130° and a maximum pressure of 420 MPa.

Following the guidelines stipulated in EN 1015-18:2003 [140], the water absorption coefficient due to **capillary action of hardened mortar** was evaluated. This investigation covered mortar samples exposed to HC and DC curing environments, both at the 28-day and 90-day marks. The analysis involved the selection of three mortar samples, each measuring 160x40x40 mm, derived from various mortar mixes. To commence the procedure, epoxy sealing material was utilized to seal the long faces of the samples. Subsequently, the samples were split into two halves and subjected to a meticulous drying process within a well-ventilated oven set at a temperature of 60±5 °C, ensuring a consistent mass was achieved. Upon achieving this stable mass, the specimens were immersed in water, positioned with their fractured faces facing downward and bolstered by supporting pads resting on the tray base. The immersion depth was maintained within the range of 5 to 10 mm. The specimen were removed from the water, wiped of and weighed after 1, 5, 10, 15,30,60 and 90 minutes. The coefficient for water absorption is determined by the slope of the straight line that connects the representative points at 10 and 90 minutes, as defined in the standard, calculated by the following formula:

$$C = 0{,}1 \cdot (M_2 - M_1) \tag{4.3}$$

In this context, the water absorption coefficient of hardened mortar (C) is denoted in units of kg/(m²·min$^{0.5}$). The values M1 and M2 represent the sample mass after 10 minutes and 90 minutes respectively. Additionally, following the 90-minute immersion period, the depth of water penetration is measured and expressed in millimetres (mm).

The analysis of **water vapor permeability** in hardened mortars was carried out in the higher hygroscopic range, following the guidelines set forth in EN 1015-19:2000 [141]. Circular samples were carefully cut from cylindrical mortar specimens. Mortars using NHL 3.5 as the main binder were exposed to a DC environment, while mortars utilizing NHL 5 as the primary binder underwent curing HC environment, as outlined in EN 459-2:2021.

These circular samples, resembling plates with a thickness of 20 mm and a diameter of 100 mm, were subjected to diverse curing conditions spanning more than 90 days. Following this interval, three circular plates from each mortar mix were positioned atop shallow Petri dishes, measuring 80 mm in diameter, repurposed as makeshift test cups. The edges of the plates themselves were securely sealed through a layer of epoxy, followed by silicone sealant, extending across the interlock with the test cups. This sealing procedure was implemented to facilitate unobstructed and direct vapor transmission through the sample.

To establish the targeted water vapor milieu within the test cups (93%), positioned in the higher hygroscopic range, a potassium nitrate (KNO_3) saturated solution was employed to induce water vapor pressure. In each instance, a controlled gap of 10 ± 5 mm was maintained between the specimen and the solution surface. The samples, positioned atop the test cups, were stored within a controlled environment maintained at a consistent temperature of 20 ± 2 °C and a relative humidity of $60 \pm 5\%$. In order to regulate the environmental conditions within the climatic chamber, encompassing both temperature and humidity levels, as well as the relative humidity within the test cups, temperature and humidity sensors were strategically positioned within the chamber and inside an experimental test cup. Subsequently, data logs verified the consistent maintenance of the specified temperature and humidity parameters throughout the entire 7-day testing period (Figure 4.2). Following this, the samples, along with the test cups, were weighed at 24-hour intervals continuously for a duration of 7 days.

Figure 4.2. Water vapour permeability examination set: (a) makeshift test cups; (b) specimen prepared for testing; (c) thermohygrometer tracking T & RH conditions

The water vapor permeance ((Λ)) is determined using the following equation:

$$\Lambda = \frac{1}{(A \cdot \Delta_p)/(\frac{\Delta G}{\Delta t}) - R_a} \tag{4.4}$$

In this context, the water vapour permeance (Λ) is quantified in units of $kg/(m^2 \cdot s \cdot Pa)$. The value of A signifies the open area of the test cup's aperture (m^2), Δ_p represents the difference in water

vapor pressure between the surrounding air and the salt solution, expressed in Pascals (Pa). The water vapor flux ($\Delta G/\Delta t$) is denoted in units of kg/s. R_a stands for the water vapor resistance of the air gap located between the sample, with a value of $0{,}048 \cdot 10^9$ Pa·m²·s/kg for every 10 mm of the air gap's thickness. Subsequently, the water vapor resistance factor (μ) was calculated by taking the reciprocal of the product of the water vapor permeance and the resistance of an air layer with an equivalent thickness.

Thermal conductivity was assessed in accordance with the directives set forth in EN 12664:2002 [142], a standardized procedure designed to determine the thermal resistance and thermal conductivity of building materials featuring medium and low thermal resistance. This methodology involved employing the FOX 200 HT heat flow meter, an apparatus engineered by TA Instruments. The mortar specimens were obtained from cube mortar samples with dimensions of 150 x 150 mm by slicing them into 20 mm thick flat plates. These samples underwent a curing period of 90 days within both DC and HC curing environments. The primary aim was to establish a uniform square specimen, with parallel flat surfaces, guaranteeing a consistent, unvarying density of heat flow rate in a singular direction.

The FOX 200 HT apparatus facilitated the maintenance of a controlled temperature disparity across the specimen, a process complemented by the utilization of external thermocouples positioned at the specimen's point of contact. To ensure precise thermal contact and insulation of the thermocouples, thin sheets of silicone rubber with an approximate thickness of 3 mm were inserted, serving as intermediaries between the thermal sensor and the heating plates.

In particular, moisture-laden specimens underwent examination, involving two specimens derived from various mortar mixtures. Preceding the testing phase, the specimens underwent drying within a well-ventilated oven at 105°C until a constant mass was achieved. Subsequent to drying, a period of 5 days was allocated for the specimens to attain equilibrium with the laboratory atmospheric conditions denoted as 23/50, reflecting a temperature of 23±2 °C and a relative humidity of 50±10%. Moisture distribution is considered uniform due to the test's conduction under a temperature differential of 10K and a moisture concentration that remained below the equilibrium point of 80% relative humidity. Furthermore, the consideration of edge heat losses was omitted, while the mean temperature applied, at 25°C, aligns with standard laboratory conditions. The process of calculating thermal conductivity involves measuring heat flux and monitoring temperature variances.

The assessment of **adhesive bond strength** of hardened mortars adheres to the protocol defined by EN 1015-12:2016 [143]. The adhesive strength is determined as the maximal tensile stress applied by a direct load perpendicular to the surface of the mortar, seated atop a substrate. Practical considerations led to the utilization of alumina silicate bricks, possessing dimensions of 300 x 300 x 30 mm, as the substrate of choice. Derived from the same batch as other specimens destined for stipulated tests, the mortar was applied onto the horizontally oriented substrate. Precursory to mortar application, the substrate slabs underwent a 24-hour immersion in water to mitigate undue moisture absorption from the ensuing mortar. The mortar was then uniformly applied to attain a total thickness of (10±1) mm, subjected to light compaction, and its upper surface levelled and smoothed. At a maturity age of 28 days and subsequent exposure to a controlled environment, the mortar slabs are subjected to examination via the MATEST E142 digital pull-off strength tester. At the outset of the test, circular test regions, approximating 50 mm in diameter, are incised using a core drilling machine throughout the set mortar layer, reaching depths approximating 2 mm. Subsequently, pull-head fixtures are glued on these sites, facilitating the subsequent application of a uniform tensile load oriented perpendicularly to the test site, transmittable through the pull-head apparatus. The imposition of the loading rate is determined in correspondence with the projected adhesive strength, ensuring that the point of failure manifests between intervals of 20 to 60 seconds. The quantification of adhesive strength involves dividing the maximum applied load (F_u) by the area (A) of the test site. It's worth noting that the determination of adhesive strength relies on data collected from five distinct specimens within each slab, expressed in N/mm^2. This calculation is expressed using the formula:

$$f_u = \frac{F_u}{A} \tag{4.5}$$

These values are complemented by an analysis of the failure mode, distinguishing between adhesive fractures (occurring at the interface between mortar and substrate designated as mode A) and cohesion fractures (within the mortar or substrate material itself designated as mode B and C respectively). In instances where no failure arises at the mortar/substrate interface, the recorded values are deemed as lower bound figures, signifying that the adhesive strength is greater than the indicated test value.

Determination of the durability of hardened mortar in the realm of the **resistance to freeze/thaw action and sulphate attack** was conducted following the RILEMs Technical Committee 127 recommendations [144]. These recommendations outline a laboratory testing method to assess the durability of masonry mortars containing mineral binders and both normal and lightweight aggregates, subjecting them to freeze/thaw action, sulphate attack, or a combination of both. This method covers preparation of two mortar beds which were prepared and placed between two sets of moistened brick units (standard substrates). The latter were readied by immersing them in water for a span of 16 hours, followed by a 5-minute drainage period at a temperature of 20°C + 5°C. To execute this, two layers of surgical gauze, each measuring 50 mm larger than a single unit, were cut. The first layer was placed on the surface of the lower unit in the pair that was in direct contact with the applied mortar. This positioning allowed for an overhang of roughly 25 mm on each side of the unit. The gauze was pressed down firmly onto the damp surface to ensure a smooth adherence. This strategic application was designed to aid in the later removal of the mortar bed. Concurrently, the second layer of gauze was attached to the sides of the upper unit. The mortar was applied onto the bottom unit, allowing it to slightly protrude above the height of the spacers, used to gauge mortar bed thickness 10 mm high. Subsequently, the other unit was placed, also equipped with gauze, onto the unit covered with mortar. A gentle tapping motion was employed until contact with the spacers was established. Any excess mortar was eliminated by careful scraping, followed by refining the finish of both struck surfaces.

The couplets underwent curing in HC curing environment, maintained at 20°C ± 2°C, and a relative humidity of 90% ± 5%. This curing phase lasted for a duration of 2 to 5 days before proceeding to the separation of the mortar beds from the units. Following this initial period, the mortar beds were detached from the brick units and subjected to an additional 90 days of curing in the same controlled environment. Around the 21-day mark, the beds were meticulously cut to yield 9 distinct small mortar joint sized specimens (35 x 55 x 10 mm), which were subsequently placed back into the curing cabinet for further conditioning. Given the categorization into three distinct groups representing various deterioration mechanisms, the total number of specimens required for the durability test is 9.

This distribution entails three specimens allocated to each group:

- − Group 1: Exposed to potassium sulphate attack only;
- − Group 2: Subjected to the combined influence of sulphate and frost attack;
- − Group 3: Exposed solely to frost attack.

The specimens were positioned with their tooled faces facing upward on horizontal plastic trays. Specimens 1 and 2 were placed on a tray drip fed with a sulphate solution (2% K_2SO_4), while specimen 3 was positioned on a tray drip fed with distilled water. The use of a potassium sulphate solution was chosen to create an environment with varying degrees of aggressiveness, ranging from moderate to highly aggressive. This is facilitated by the internal sulphate attack due to the elevated levels of K_2O found exclusively in the WBA samples themselves. Surface tension forces interacted to maintain a solution depth of around 1 mm. After approximately 20 minutes of solution uptake, the specimens were removed. Each specimen was packed tightly, surrounded by insulation material, leaving only the tooled face exposed. Specimen 1 was individually placed within a plastic case, while specimens 2 and 3 were packed into a shared plastic case with separate compartments to prevent contamination. Before sealing, 5 ml of distilled water were introduced to each case to ensure saturation of the specimen to a level that would trigger failure in frost-vulnerable materials. Corresponding plastic lids were placed on top of the boxed specimens to safeguard against moisture loss.

The enclosed cases were stored within the laboratory for a period of 2 to 3 days. During the final 5 hours of this interval, the cases containing specimens 2 and 3 were transferred to a deep freeze cabinet operating below −15 °C. After this 5-hour period, the trays were retrieved, and the specimens were allowed to thaw at room temperature. It's important to note that the tray housing specimen 1 remained at room temperature throughout this process. Subsequently, all specimens were removed from their cases, re-packed (also with insulation) into a second set of dry boxes and placed in a ventilated drying oven for a duration of 24 hours at a temperature of 50 °C. Continual observation of the mortar specimens' condition after each cycle of sulphate addition and freezing was carried out. The evaluation outcomes are quantified through a visual assessment rating (VAR), encompassing an assessment of the sample's overall performance (ranging from good to marginal or poor) and identifying the nature of failure. Frequently encountered failure patterns include corner loss or a gradual disintegration of the exposed faces of the specimens. Upon the completion of 16 cycles, each specimen was assigned a VAR on a scale of 1 (representing a 50% loss in area) to 10 (indicating an unaffected state).

To complement the assessment of **salt content extent** in fresh mortar, conducted in accordance with EN 1015-17 [145], a procedure in alignment with RILEM Technical Committee 203-RHM recommendations [146] was implemented. This approach entails the extraction of granules from mortar cube samples that have undergone a controlled three-month curing within specific environments. The process involves the straightforward crushing and sieving of the mortar

samples to yield granules ranging from 4 to 10 mm. These granules are then enclosed in a gauze bag and submerged in distilled water within a beaker. Over a span of 24 hours, the mixture undergoes agitation, potentially facilitated by a magnetic stirrer, to ensure thorough interaction. Maintaining a mass ratio of granules to water at 1:10, a subsequent chemical analysis of ion composition within the water is executed, employing ion chromatography, in tandem with pH measurement. This protocol provides insights into efflorescence and leaching attributes of mortar components by delivering chloride, fluoride, sulphate, and nitrate content in the mortar eluates.

4.3. Results and discussion

4.3.1. Assessment of fresh-state properties in AHL mortars

Evaluating the consistency of fresh AHL mortars is crucial for optimizing their workability in a range of interior and exterior applications, such as plastering, coating, bricklaying, repointing, and the overall regularization of facades [147]. In this study, the consistency of the tested mortars was determined using a flow table, following the guidelines outlined in standard EN 459-2 [118]. The key parameters obtained from the flow tests, primarily the flow diameters, were emphasized, with additional support from visual observations of segregation or bleeding. These flow diameters were subsequently analysed in relation to the disposition and the proportion of WBA to ensure consistent consistency across different mortar mixes. The results, including flow values for both the control and AHL mortars, as well as data on mortar density, air content, and post-mixing temperature, are summarized in Table 4.4. (mortar mixes with NHL 3.5 as the primary binder) and Table 4.5. (mortar mixes with NHL 5 as the primary binder).

Table 4.4. Fresh-state properties of NHL 3.5 and AHL mortars with 20 & 30 wt.% WBA

Mix ID	NHL 3.5-M	NHL 3.5-1-M	NHL 3.5-2-M	NHL 3.5-3-M	AHL1-20-M	AHL1-30-M	AHL2-20-M	AHL2-30-M	AHL3-20-M	AHL3-30-M	AHL4-20-M	AHL4-30-M
	control mortar mixes				AHL mortar mixes							
primary binder	NHL 3.5											
WBA share [wt.%]	0				20	30	20	30	20	30	20	30
WBA variety	-				fly				mixed			
w/b ratio	0.60		0.70	0.60	0.60							
air-entraining agent [wt.%]	0.02		-	-	0.02							
polycarboxylate superp. [wt.%]	0.15	0.15			0.16	0.40	0.77	0.35	0.43	0.22	0.37	0.20	0.35
bulk density [kg/m^3]	2051	2053	2029	2016	2011	1983	1953	1990	2056	1971	1967	1942
air content [%]	6.9	7.2	5.6	7	8.3	9.4	9.6	10.2	8	10.1	9.6	13
flow diameter [mm]	164	170	188	170	161	161	169	160	166	174	161	162
temperature [°C]	23.3	20	20	21.1	25	25.2	20.4	19.4	22.1	20.5	24	21.5

Table 4.5. Fresh-state properties of NHL 5 and AHL mortars with 40 wt.% WBA

Mix ID	NHL 5 - M	NHL 5 - 1 - M	NHL 5 - 4 – M	AHL 4-40 - M	AHL 5-40 - M
	control mortar mixes			AHL mortar mixes	
primary binder	NHL 5				
WBA share [wt.%]	0			40	
WBA variety	-			mixed	fly
w/b ratio	0.60	0.70	0.60	0.60	
air-entraining agent (wt.%)	0.02	-	-	0.02	
polycarboxylate superp. (wt.%)	0.15		0.46	0.33	0.80
bulk density [kg/m^3]	2060	2057	2066	1938	1898
air content [%]	6.5	3.2	6.9	11.5	14.5
flow diameter [mm]	165	180	180	165	164
temperature [°C]	19.7	20.1	20.3	22.2	23.7

A constant water-to-binder ratio (w/b) was maintained while achieving the flow diameter of 162 to 168 mm, ideal for NHL 3.5 and FL 3.5, as recommended in EN 459-2 [118]. The dosage of polycarboxylate superplasticizer (SP) ranged from 0.15% in both control mixes (NHL 3.5-M and NHL 5-M) to the highest levels observed in AHL1-30-M (0.77%) and AHL5-40-M (0.80%), respectively. The mixed ashes (WBA 3 and WBA 4) required a lower amount of SP than the fly ashes (WBA 1 and WBA 2), while the SP requirement increased with the WBA content in mortars containing both fly and mixed WBA dispositions. This indicates a consistent trend where water requirements increase with the amount of WBA. Nevertheless, all AHL mortar mixes, regardless of composition, exhibited similar workability, with no significant segregation or bleeding observed after testing (Figure 4.3). The flow values measured for all AHL mixes were within the desired range of 160 to 170 mm, which is considered a guarantee of good workability on site [148]. The only exception was the AHL 3-30-M, where the measured flow value of 174 mm slightly oversteps the preferred flow range.

(a)

(b)

(c)
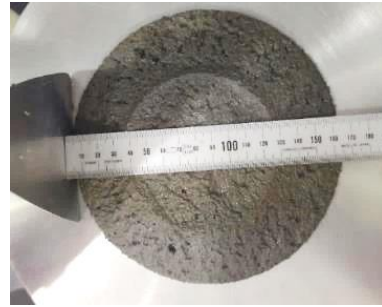
(d)

(e)
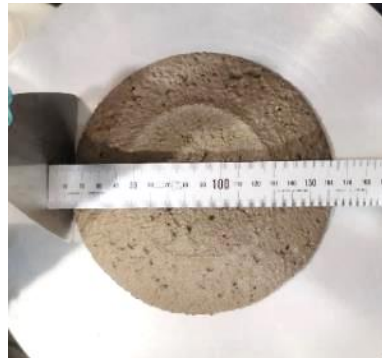
(f)

(g)

(h)

Figure 4.3. Consistency of fresh mortar mixes determined by flow table: (a) NHL 3.5 – M; (b) NHL 5-M; (c) AHL1-30 – M; (d) AHL2-30 – M; (e) AHL3-30 – M; (f) AHL4-30 – M; (g) AHL4-40 – M; (h) AHL5-40 – M

Previous studies and test batches [120][149] led to the assumption that the addition of WBA might destabilize the air content, necessitating an increased amount of air-entraining agent. As a result, a proportion of 0.02% was consistently applied to all mortar mixes., aligning with the recommended guidelines of the additives manufacturer. However, despite equal additions of the air-entraining agent to all mixes, the observed air content contradicted the initial assumptions. In AHL mortar mixes where NHL 3.5 served as the primary binder, the air content varied, ranging from a minimum of 8% in AHL3-20-M to a maximum of 13% in AHL4-30-M, differing by as much as 6% from the control mix NHL 3.5-M.

In light of these findings, additional test batches were prepared, each containing solely NHL 3.5 as the core binder, to address specific issues:

    i.   NHL 3.5-1-M: This batch aimed to verify the repeatability of the initial NHL 3.5-M mortar mix;

    ii.   NHL 3.5-2-M: In this batch, no additives were used, and additional water was added to address low flow values, even when the superplasticiser was incorporated;

    iii.   NHL 3.5-3-M: This batch was prepared without the air-entraining agent to assess its impact on properties in both fresh and hardened states.

Similar procedures were followed for additional test batches containing NHL 5:

    i.   NHL 5-1-M: No additives were used, and extra water was added according to the flow value guidelines set in the EN 459-2 standard for NHL/FL 5;

    ii.   NHL 5-2-M: This batch was prepared without the air-entraining agent.

With respect to repeatability, validation was endorsed using the NHL 3.5-1-M, wherein discernible changes were limited to temperature measurements. In the case of the NHL 3.5-2-M mix, an increase of water content (w/b=0.70) implemented without the inclusion of any additives resulted in an observed increase in flow value (188 mm) alongside a decrease in air content (5.6%). Interestingly, the NHL 3.5-3-M mixture, devoid of any air-entraining agent, exhibited nearly identical air content as the NHL 3.5-1-M mixture, which contained 0.02% of the air-entraining agent. Consequently, the lowest air content recorded in the additive-free mix (NHL 3.5-2-M) suggests a causal relationship between the superplasticizer and elevated air content in the mortar compositions.

Despite observing consistently elevated air content levels in all AHL mixes, these values exhibited variation across different WBAs while remaining independent of the superplasticizer (SP) percentage. For instance, AHL1-30-M, which necessitated the highest SP dosage to

achieve the desired workability (0.77 wt.%), displayed an air content of 9.4%. This air content was comparable to that of AHL4-20-M, in which the lowest SP dosage among all AHL mixes was employed (0.20 wt.%).

Similar trends emerged in the mortar mixes using NHL 5 as the sole binder. Notably, NHL 5-4-M exhibited a slightly higher air content when compared to the NHL 5 – M mix, even in the absence of an air-entraining agent, in conjunction with the application of a higher quantity of SP to align with the increased flow value observed in the NHL 5-1-M mixture. Continuing with these patterns, the AHL 5-40-M mixture, utilizing the highest SP dosage (0.80 wt.%) among all AHL mixes in both binder groups and maintaining a consistent air-entraining agent dosage, exhibited the highest air content among all AHL mixes in both groups. These findings adhere to the outcomes of previous research, as indicated by [150], reveal that the newer generation of polycarboxylate superplasticizers can be associated with side effects, specifically an elevation in the air content. Hence, there are indications that suitability of the applied additives may need further examination.

Slightly elevated temperatures were observed for all mortars containing WBA compared to the reference mix. A maximum temperature rise of approximately 4 °C was detected in the AHL1-30 and AHL5-40 mixes when compared to the average temperature of their respective control mixtures. Nonetheless, the discernment of specific trends beyond a general increase in relation to the influence of WBA on the temperature of fresh mortar mixes remains elusive.

The measured values for salt content in fresh mortar mixes according to the protocol described in EN 1015-17 [145] are given in Table 4.6. The percentages of water-soluble chloride content in fresh mortar are compared with the concentrations of chloride, sulphate, fluoride and nitrate ions found in the eluate extracted from the mortar granules, as shown in Table 4.7. The quantification of the salt content was carried out in the control mortar mixes as well as in the AHL mixes with 30 and 40 wt.% WBA. At the same time, the evaluation of the chloride, sulphate, fluoride, and nitrate ions concentration in the eluates extracted from granulated mortar was carried out exclusively in specific mixtures involving fly ash and mixed ash, alongside their corresponding control mixes (Figure 4.4 and Figure 4.5). This approach allowed for the evaluation of the highest binder substitutions, representing a worst-case scenario.

| (a) NHL 3.5 - M | (b) AHL2-30 - M | (c) AHL3-30 - M |

Figure 4.4. Granulated mortar, with NHL 3.5 serving as the primary binder, prepared for the purpose of eluate extraction

| (a) NHL 5 - M | (b) AHL4-40 - M | (c) AHL5-40 - M |

Figure 4.5. Granulated mortar, with NHL 5 serving as the primary binder, prepared for the purpose of eluate extraction

Table 4.6. Water soluble chloride content in fresh mortar [%] complying to EN 1015-17:2000+A1:2005

Mix ID	1st cycle	2nd cycle	Average value of both cycles
	chloride content [%]		
NHL 3.5 - M	0	0	**0**
NHL 5 - M	0	0	**0**
AHL 1-30 - M	0.02	0.02	**0.02**
AHL 2-30 - M	0.02	0.02	**0.02**
AHL 3-30 - M	0	0.01	**0.01**
AHL 4-30 - M	0.01	0.01	**0.01**
AHL 4-40 - M	0.01	0.01	**0.01**
AHL 5-40 - M	0.03	0.03	**0.03**

Table 4.7. The concentration of chloride, sulphate, fluoride, and nitrate ions in the eluate extracted from mortar granules

Mix ID		NHL 3.5-M	AHL 2-30-M	AHL 3-30-M	NHL 5-M	AHL 4-40-M	AH5 4-40-M
chloride content Cl^-	[mg/kg]	26.5	121	24	6.1	73	379
	[%]	0.00	0.01	0.00	0.00	0.01	0.04
sulphate content SO_4^-	[mg/kg]	14.7	22	17	23	37	74
	[%]	0.001	0.002	0.002	0.002	0.004	0.007
fluoride content F^- [mg/kg]		<5	1.8	1.5	1.9	1.8	3.6
nitrate content NO_3^- [mg/kg]		<5	<5	<5	<5	27	<5

According to the standard EN 998-2:2016 [151], the chloride content should not exceed 0.1% of the dry mass of the mortar. When analysed according to the cited standard EN 998-2:2016, specifically referencing EN 1015-17:2000 [145], it becomes evident that this prescribed limit has not been exceeded (refer to Table 4.6). However, the data reveals a pronounced upward trend in chloride content, particularly evident in mortar mixes with fly ashes, while mixes containing mixed ashes exhibit values similar to those in the control mixes. In the case of AHL mortar mixes incorporating fly ashes, specifically AHL 1-30 – M and AHL 2-30 – M, as well as AHL 5-40 – M, there has been a respective increase of 0.02 and 0.03 from the initial baseline value of 0. Concerning AHL mortar mixes incorporating mixed ashes, that is AHL 3-30 – M and AHL 4-30 – M and AHL 4-40 – M, there was a marginal increase of 0.02 noted, up from 0.

Yet, when the chloride ion content was determined via the water eluate, somewhat more favourable results were obtained, when expressed in percentages. In this context, AHL 2-30-M and AHL 3-30-M were found to be within the range with a chloride content of no more than 0.01%, while AHL 5-40- M further exceeded this threshold, reaching 0.04% (refer to Table 4.7).

Analogously, a notable trend emerges in the concentration of sulphates, which are known to be a prevalent salt type found in historic buildings [152]. These concentrations are elevated in mixtures containing both fly ash and mixed WBAs, whereas mixed ash dispositions exhibit comparatively lower sulphate content. In this context, the AHL3-30-M mixture exhibits chloride and sulphate levels similar to the control mix. However, these disparities become more pronounced within the second binder group: AHL4-40-M demonstrates higher chloride and

sulphate levels, though still lower than those observed in AHL5-40-M, which registers the highest values among all mortar mixtures.

The ion content analysis reveals minimal fluoride and nitrate levels in all AHL mixes in comparison to their respective control mixes, except for AHL4-40, which exhibits the highest nitrate concentration at 27 mg/kg. Chlorides are the dominant ionic species in the majority of the samples investigated, except in NHL 5, where sulphate levels surpass chloride content.

In the context of the provided data, the initial salt load is amplified by introducing WBA into the binder system, especially in higher WBA levels and in fly ash dispositions. These alkali-chloride-sulphates bearing binder systems therefore pose a potential threat to compromising the compatibility requirement for restoration mortars. Under specific conditions, the presence of such expansive and soluble salts, as well as frost, can potentially result in damage to lime-based mortars. While sulphates are commonly known to be responsible for extensive salt damage due to their crystallization and dissolution cycles, it's important to highlight that chlorides can also be particularly detrimental, as they have the potential to significantly impact the hygroscopic shrinkage behaviour of substrates loaded with salt [39]. Therefore, it is advisable to conduct a thorough investigation of the moisture and salt content in the substrate prior to application, allowing for necessary adaptations to the mortar mix [34].

4.3.2. Assessment of mechanical properties of AHL mortars

The effect of the WBAs on the mechanical properties of the AHL mortar was initially evaluated using compressive and flexural strength tests conducted after 7 days, 28 days and 90 days of curing in the designated curing environments, as summarised in Table 4.8 to Table 4.12. These tables present the collected data on the average compressive and flexural strengths during the specified curing periods, taking into account the diverse curing conditions, namely HC, DC and ACC. In addition, the values for the specific activity index (SAI) are given, while the results are categorised according to the content of the primary binder (NHL 3.5 and NHL 5) in the respective binder blends. The dynamic modulus of elasticity was assessed at three specific time points during the mortar's aging process: at the 7-day, 28-day, and 3-month marks. These findings are detailed in Table 4.13 and Table 14. Additionally, the ratio of compressive to flexural strength (f_C/f_F) was considered, providing supplementary insight into the potential ductility of the AHL mortars [153].

In addition to the aforementioned properties, it's important to highlight that compressive strength serves as a principal benchmark for assessing the performance of the cured AHL mortars. To provide a comprehensive analysis, the findings are sectioned into two groups based on the hydraulicity of the primary NHL binder: one group featuring NHL 3.5 as the primary binder and another with NHL 5 as the primary binder. Furthermore, the second group extends its scope to encompass variations where the proportion of WBA reaches 40 wt.%.

From the absolute compressive strength values of mortars within the NHL 3.5 group at the 28-day mark (as depicted in Figure 4.6), it becomes apparent that the incorporation of all four WBAs into the NHL-WBA binder system contributes to the enhancement of compressive strength of AHL mortars. Notably, this upturn becomes more prominent when employing the higher hybridization ratio of 30 wt.% WBA across all of the established curing environments, barring AHL 1-30 - M, wherein no increase of compressive strength was observed at the 30 wt.% hybridization ratio; instead, the values remained at a level comparable to the control mix. Furthermore, it is worth noting that the mortar mix with a lower hybridisation level of 20 wt.% of the same WBA 1 showed higher compressive strength in specimens exposed to both HC and DC, not only compared to the control mix NHL 3.5, but also to the counterpart mix with 30 wt.% WBA 1. It also recorded as the highest value among all AHL mortars with 20 wt.% of WBA. However, the AHL20-20 and AHL 3-20 mortars exposed to the DC environment exhibited a decline in strength, with the AHL3-20–M, cured in DC, demonstrating the lowest

compressive strength of 1.18 MPa. Therefore, a positive contribution is evident in all three curing regimes, except for the previously mentioned mixes that underwent DC curing. Moreover, the highest compressive strength values were achieved under the conditions of accelerated carbonation. In the comparison between natural and enhanced carbonation, the control mortar mix NHL 3.5 exhibited a significant increase in compressive strength of approximately 120% when exposed to a high CO_2 concentration. Conversely, the NHL 3.5-1-M mix demonstrated an even more substantial growth rate, reaching approximately 230%. Regardless of the staggered contribution from the simulated aging in the NHL 3.5-M mix, the HC values were equalised after 90 days (as depicted in Figure 4.7). The compressive strengths of the mortars with WBA exposed to a high CO_2 concentration for 28 days were comparable to or exceeded those of the control mix NHL 3.5-M. Notably, after 90 days in the DC environment, the strengths increased by approximately 20% (AHL1-20-M, AHL2-20-M, and AHL3-20-M) up to nearly 100% (AHL 2-30-M and AHL3-30-M) compared to the 28-day values. However, these values remained lower than those achieved after 28 days of ACC curing. It can be hypothesized that the relatively higher values obtained after 28 days of ACC were a result of simulated aging. The synergistic reaction between lime and WBA, in addition to natural carbonation, was enhanced after the 28-day curing period in the AHL2-30-M, AHL3-30-M, and AHL4-30-M mixes, where the measured values were comparable to or even exceeded those obtained through enhanced carbonation. On the other hand, mortar mixes AHL4-20-M and AHL1-30-M, cured in the DC environment, showed no significant strength gain beyond the 28-day mark.

When choosing the favourable curing environment for AHL mortars, the HC curing environment seems to be advantageous in the case of the mortars with the hybridisation ratio of 20 wt.%, while the mortars with a higher WBA content yield corresponding values in both curing environments with natural carbonation, leaning slightly in favour of HC. Nevertheless, all AHL mortar samples cured in HC more than doubled their compressive strength after 90 days, following the same trend as the control mixes, with the AHL4-20-M sample showing the most modest increase of 44%.

It is also noted that beyond the 90-day mark, the compressive strength values of the control mixes slightly surpasses those of the AHL mortars, except for the AHL2-30-M mix, which exhibits the highest recorded values across all mixes at 9.45 MPa, representing a 54% increase compared to the NHL 3.5-M mix. Following closely, AHL3-30-M shows a minimal downturn of 4%. When distinguishing between the behaviour of fly ash and mixed ash, it is evident that

fly ashes yield favourable results at both WBA shares, with the maximum compressive strength reduction being 22% in the case of AHL1-30-M. In contrast, mortars containing mixed ashes show a preference for a higher hybridization ratio of 30 wt.%, where the most significant reduction in compressive strength, amounting to 17%, is observed in the AHL4-30-M case.

In the case of mortars with NHL 5 as the primary binder, the inclusion of WBA at the highest hybridisation ratio in the NHL-WBA binder system leads to a notable increase in the compressive strength of AHL 5-40-M mortar, as illustrated in Figure 4.8 at the 28-day mark. This enhancement is consistently observed across all established curing environments, except for simulated aging. Here, the control NHL 5-M mix exhibits the highest value, surpassing 15 MPa. For the AHL 4-40-M mix, there is no significant decline in compressive strength noted in the DC environment. Instead, the values remain comparable to those of the control mix. However, a significant 35% decrease in compressive strength is evident when compared to the values noted in HC regime. After the 90-day curing period, the DC environment, conversely, shows higher values in both NHL 5-M and AHL 5-40-M mixes. Otherwise, the trend in compressive strength closely resembles what was observed at the 28-day mark (as shown in Figure 4.9), although the difference between the AHL4-40-M mix and the control mix is less pronounced, decreasing by approximately 14%. Once again, mortars with a higher WBA content yielded similar values in both curing environments with natural carbonation, slightly favouring DC after 90 days, particularly for mixes exhibiting higher compressive strength.

Otherwise, the compressive strength trend mirrors that observed at the 28-day mark (Figure 4.9), even though the discrepancy between the AHL4-40-M and the control mix is less prominent, dropping around 14%.

Again, the mortars with a higher WBA content yielded corresponding values in both curing environments with natural carbonation, while leaning slightly in favour of DC after 90 days when it comes to the mixes with higher compressive strength.

On average, NHL repair mortars achieve about 50% of their final strength within the first 28 days of curing [67], with full stabilisation of compressive strength expected after 90 days [34]. It can be deduced that the values reached in both natural carbonation environments (HC and DC) after 90 days are very close to the expected final values after a relatively rapid increase between the 28 and 90 day marks. Analysing the compressive strength results of mortars subjected to HC curing, which are recognised as favourable for this type of material [134][38] [68][154], it is clear that the WBAs have attenuated the hydraulic properties of the primary

NHL binder. This effect is particularly pronounced for mixed ashes. Looking at the compressive strength in the DC environment, with the exception of the AHL1-30-M mortar, which performed better under HC curing, it is reasonable to conclude that WBAs exhibit (low) pozzolanic reactivity when employed in higher hybridisation ratios. This implies that WBAs can undergo pozzolanic reactions even under semi-dry curing conditions. Consequently, maintaining a moderate moisture levels, as applied during the DC regime following the first 7 days of HC curing, may also promote enhanced mechanical properties of AHL mortars, which is consistent with the results in [38]. In addition, the fine particles of the WBAs may have contributed to their potential pozzolanic activity, a phenomenon also investigated in previous studies [25]. It can also be inferred that, despite the known slow pace of the pozzolanic reaction, when blended in specific proportions, WBAs can markedly increase the ultimate strength of AHL based mortars.

In NHL-pozzolan mortars, multiple simultaneous processes contribute to both the setting and strength development. Early hydration of the NHL clinkers begins concurrently with the pozzolanic reaction, in which the pozzolan, in this case WBA potentially react with the available lime ($Ca(OH)_2$) present in the NHL binder. Notably, the hydration process advances more rapidly than the pozzolanic reaction. The NHL 3.5 binder is anticipated to initially contain a minimum of 25 wt.% of $Ca(OH)_2$, whereas NHL 5 is expected to start with at least 15 wt.%. The pozzolanic reaction, utilizing the $Ca(OH)_2$ generated during NHL hydration, results in the formation of additional cementing hydrates. Meanwhile, the pozzolanic reaction that employs the pre-existing lime within the NHL begins very early, typically within the first 24 hours, but proceeds at a slower rate compared to hydration [155].

Another possible reaction for the calcium hydroxide is carbonation, which occurs with lower needs of water, and is hindered in saturation conditions. This means that pozzolanic reaction and carbonation are competitive reactions [95] and that the existent calcium hydroxide will be preferentially consumed by the reaction that has better conditions to develop faster. In fact, if the material is saturated with water for enough time, the pozzolanic reaction occurs and the free lime is consumed in forming hydraulic compounds. On the other hand, if the relative humidity allows for carbonation to occur, making the pozzolanic reaction more difficult, calcium carbonate is formed instead of hydraulic compounds, and the pozzolan, without possibility to react, acts as a filler.

In this context, the following conclusions are drawn: After 28 days of exposure to HC environment, the phenolphthalein test revealed no consumption of portlandite (refer to Table 16), indicating the absence of both carbonation and a significant pozzolanic reaction. Consequently, the observed increase in compressive strength of AHL mortars during this period can be attributed primarily to the hydration of the primary NHL binder. The hydrates formed during this hydration process play a pivotal role in determining the final compressive strength, with WBAs acting as fillers, a role less pronounced in the mixed ashes. After 90 days, the observed changes in compressive strength are accompanied by portlandite consumption, with carbonation accounting for much of this effect. The pozzolanic reaction becomes more noticeable, especially in the case of the higher 30 wt.% hybridization ratio. Notably, the compressive strength values after 28 days of curing in DC are generally quite low, indicating the unsuitability of this curing environment for hydraulic mortars in the early stages. However, after 90 days of curing with the incorporation of 20 wt.% WBA, a slight increase is observed. In contrast, when 30 wt.% WBA is added, the increase in compressive strength values is significantly higher. Consequently, the strengths achieved in both curing environments become nearly equal, suggesting a pozzolanic reactivity of the WBAs. This reactivity, in addition to the hydration products and filler effect, contributes to the observed enhancement in strength, alongside the impact of natural carbonation.

In accordance with ASTM C618 [138], a strength activity index (SAI) exceeding 75% after 28 days indicates pozzolanic reactivity when 20% of the cementitious binder is replaced with coal fly ash. Similarly, as per EN 450-1 [89], achieving a result of over 75% with a 25% substitution confirms pozzolanic reactivity after 28 days. However, it's important to note that the SAI values calculated in this study were derived from wood ash substitution of NHL at an even higher degree. As previously stated in Chapter 3, WBA does not appear to qualify chemically as a pozzolanic material (refer to Table 3.6). However, the observed increase in strength could suggest pozzolanic activity. Consequently, these SAI values were utilized solely for the purpose of comparison in this research and not for acceptance in accordance with these standards. Additionally, given the relatively slow rate of strength development in the early stages, SAI values after 90 days were also examined. The following observations were made:

The calculated SAI was consistently higher for all AHL mortars containing 20 and 30 wt.% WBA compared to the control mix based on their compressive strength at 28 days. This trend was particularly pronounced in AHL mortars incorporating ashes in a higher hybridisation ratio. Notably, the AHL1-20-M mortar exhibited a higher SAI when using a lower WBA

proportion, while the AHL2-30-M mortar demonstrated the highest SAI, when employing the higher hybridization ratio, with 239% in HC and 262% in DC environment. However, after 90 days, there was a minor reduction in the SAI values. At this stage, only the fly ashes in both WBA proportions, when cured in HC environment, maintained SAI values exceeding 75%, thus affirming the pozzolanic characteristics of these WBAs. When subjected to HC curing for 90 days, the mixed ashes displayed satisfactory results, especially in the case of the higher 30 wt.% WBA proportion. The DC curing environment exhibited favourable results, particularly with the 30 wt.% mixes. However, the mortar mixes containing AHL2, AHL3, and AHL4 at 20 wt.% failed to meet the 75% SAI criterion. An interesting observation was that the mortar with WBA1 demonstrated superior results when a lower WBA proportion was incorporated into the mix.

In the second binder group, where NHL 5 served as the primary binder, the samples exhibited noteworthy behaviour after 7 days in a HC environment. AHL mixes with a 40 wt.% substitution of NHL with both WBA4 and WBA5 showed comparable or even higher compressive strength when compared to the control NHL5-M mix. The trend in SAI values after 28 days in the same curing environment remained consistent. However, AHL4-40 demonstrated a somewhat slower compressive strength growth, approaching SAI value with a borderline 74%. Interestingly, while the DC dry curing environment proved more favourable after 28 days, with both mixes showing a higher rate of increase, the situation reversed after 90 days of curing. This suggests a preference for humid curing in the long term. Notably, AHL5-40 displayed a consistent SAI growth trend throughout the entire curing period. The faster initial hydraulic activity observed can be attributed to the availability of CaO and the higher concentration of finer particles in the mix.

Table 4.8. Compressive and flexural strength of NHL 3.5 and AHL mortars with 20&30 wt.% WBA after 28 days in different curing environments

NHL share [%]	Mix ID	Compressive strength $f_{C,28}$ [MPa]		Flexural strength $f_{F,28}$ [MPa]		SAI$_{28}$ [%]
-HC	**HC Environment**					
100%	**NHL 3.5 - M**	2.24	(±0.34)	1.03	(±0.05)	-
	NHL 3.5-1 - M	2.98	(±0.04)	1.41	(±0.23)	
	NHL 3.5-2 - M	2.48	(±0.17)	0.98	(±0.20)	
	NHL 3.5-3 - M	3.98	(±0.23)	1.85	(±0.13)	
80%	**AHL1-20 - M**	3.64	(±0.14)	1.03	(±0.10)	163%
	AHL2-20 - M	2.75	(±0.12)	0.91	(±0.09)	123%
	AHL3-20 - M	2.48	(±0.11)	0.97	(±0.11)	111%
	AHL4-20 - M	2.38	(±0.36)	1.34	(±0.24)	106%
70%	**AHL1-30 - M**	2.39	(±0.02)	0.99	(±0.23)	107%
	AHL2-30 - M	5.35	(±0.14)	1.88	(±0.21)	239%
	AHL3-30 - M	2.94	(±0.14)	0.96	(±0.13)	131%
	AHL4-30 - M	3.46	(±0.19)	1.44	(±0.38)	155%
-DC	**DC Environment**					
100%	**NHL 3.5 - M**	1.94	(±0,27)	0.76	(±0.15)	-
	NHL 3.5-1 - M	2.87	(±0,51)	1.24	(±0.06)	
	NHL 3.5-2 - M	1.91	(±0,16)	0.77	(±0.19)	
80%	**AHL1-20 - M**	2.66	(±0.13)	0.98	(±0.10)	137%
	AHL2-20 - M	1.60	(±0.07)	0.75	(±0.09)	83%
	AHL3-20 - M	1.18	(±0.33)	0.66	(±0.08)	61%
	AHL4-20 - M	2.08	(±0.02)	0.83	(±0.04)	107%
70%	**AHL1-30 - M**	2.10	(±0.21)	0.84	(±0.24)	108%
	AHL2-30 - M	5.10	(±0.08)	0.97	(±0.36)	262%
	AHL3-30 - M	2.73	(±0.20)	1.23	(±0.13)	140%
	AHL4-30 - M	3.64	(±0.33)	1.22	(±0.24)	187%
-ACC	**ACC Environment**					
100%	**NHL 3.5 - M**	4.28	(±0.18)	1.27	(±0.17)	-
	NHL 3.5-1 - M	9.39	(±0.45)	3.09	(±0.36)	
	NHL 3.5-2 - M	5.48	(±0.22)	2.11	(±0.23)	
80%	**AHL1-20 - M**	6.33	(±0.15)	2,00	(±0.10)	148%
	AHL2-20 - M	5.07	(±0.22)	2.00	(±0.11)	119%
	AHL3-20 - M	4.78	(±0.20)	1.79	(±0.03)	112%
	AHL4-20 - M	4.87	(±0.30)	1.54	(±0.13)	114%
70%	**AHL1-30 - M**	5.39	(±0.11)	1.64	(±0.08)	126%
	AHL2-30 - M	10.15	(±0.27)	3.43	(±0.24)	237%
	AHL3-30 - M	4.55	(±0.21)	2.03	(±0.18)	106%
	AHL4-30 - M	4.62	(±0.44)	2.69	(±0.15)	108%

Table 4.9. Compressive and flexural strength of NHL 3.5 and AHL mortars with 20&30 wt.% WBA after 90 days in different curing environments

| NHL share [%]	Mix ID	Compressive strength $f_{C,90}$ ($\pm\sigma$) [MPa]		Flexural strength $f_{F,90}$ ($\pm\sigma$) [MPa]		SAI$_{90}$ [%]
		HC Environment				
100%	NHL 3.5 - M	6.15	($\pm$0.25)	2.03	($\pm$0.15)	
	NHL 3.5-1 - M	5.93	($\pm$0.32)	3.46	($\pm$0.09)	-
	NHL 3.5-2 - M	4.68	($\pm$0.21)	1.45	($\pm$0.39)	
80%	AHL1-20 - M	5.52	($\pm$0.01)	2.37	($\pm$0.30)	90%
	AHL2-20 - M	5.30	($\pm$0.10)	2.17	($\pm$0.14)	86%
	AHL3-20 - M	3.79	($\pm$0.00)	0.94	($\pm$0.12)	62%
	AHL4-20 - M	3.42	($\pm$0.11)	1.92	($\pm$0.13)	56%
70%	AHL1-30 - M	4.81	($\pm$0.11)	1.72	($\pm$0.07)	154%
	AHL2-30 - M	9.45	($\pm$0.10)	3.23	($\pm$0.21)	78%
	AHL3-30 - M	5.88	($\pm$0.29)	3.35	($\pm$0.01)	96%
	AHL4-30 - M	5.12	($\pm$0.30)	1.67	($\pm$0.15)	83%
		DC Environment				
100%	NHL 3.5 - M	2.03	($\pm$0.24)	0.99	($\pm$0.23)	
	NHL 3.5-1 - M	3.62	($\pm$0.14)	1.61	($\pm$0.13)	-
	NHL 3.5-2 - M	2.60	($\pm$0.06)	1.45	($\pm$0.11)	
80%	AHL1-20 - M	3.20	($\pm$0.10)	1.01	($\pm$0.18)	88%
	AHL2-20 - M	1.96	($\pm$0.11)	0.99	($\pm$0.13)	54%
	AHL3-20 - M	1.52	($\pm$0.11)	1.72	($\pm$0.13)	42%
	AHL4-20 - M	2.03	($\pm$0.16)	0.81	($\pm$0.09)	56%
70%	AHL1-30 - M	2.00	($\pm$0.18)	1.01	($\pm$0.10)	55%
	AHL2-30 - M	9.71	($\pm$0.11)	2.46	($\pm$0.49)	269%
	AHL3-30 - M	5.41	($\pm$0.19)	1.65	($\pm$0.27)	149%
	AHL4-30 - M	4.52	($\pm$0.32)	1.67	($\pm$0.14)	125%
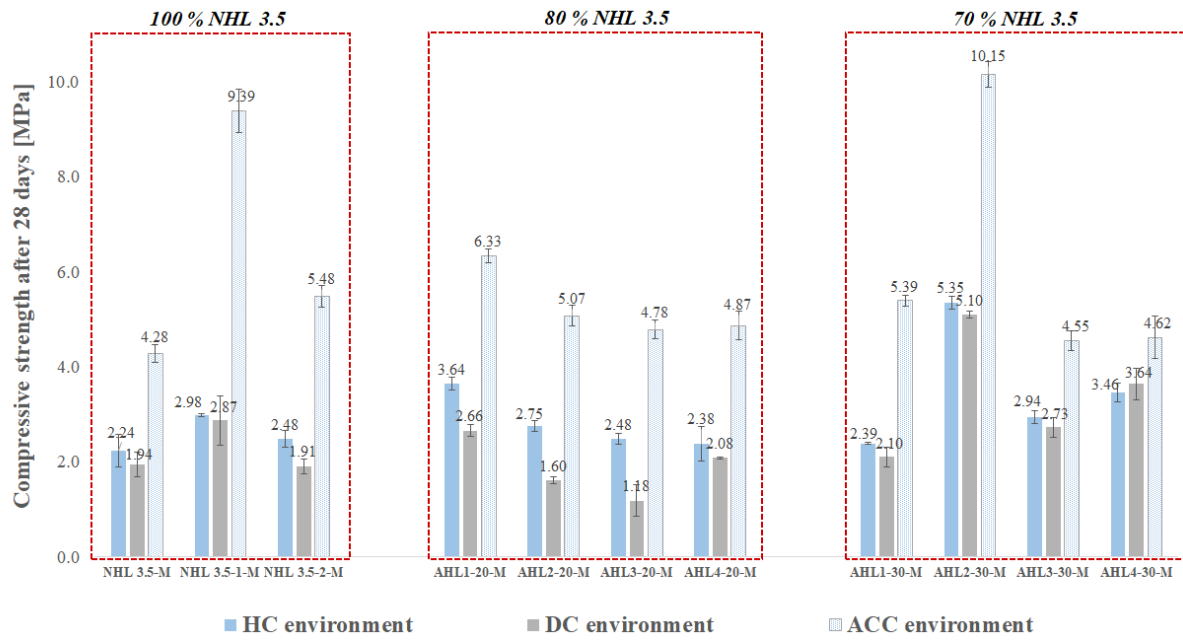
Figure 4.6. Compressive strength of NHL 3.5 and AHL mortars with 20&30 wt.% WBA after 28 days in different curing environments
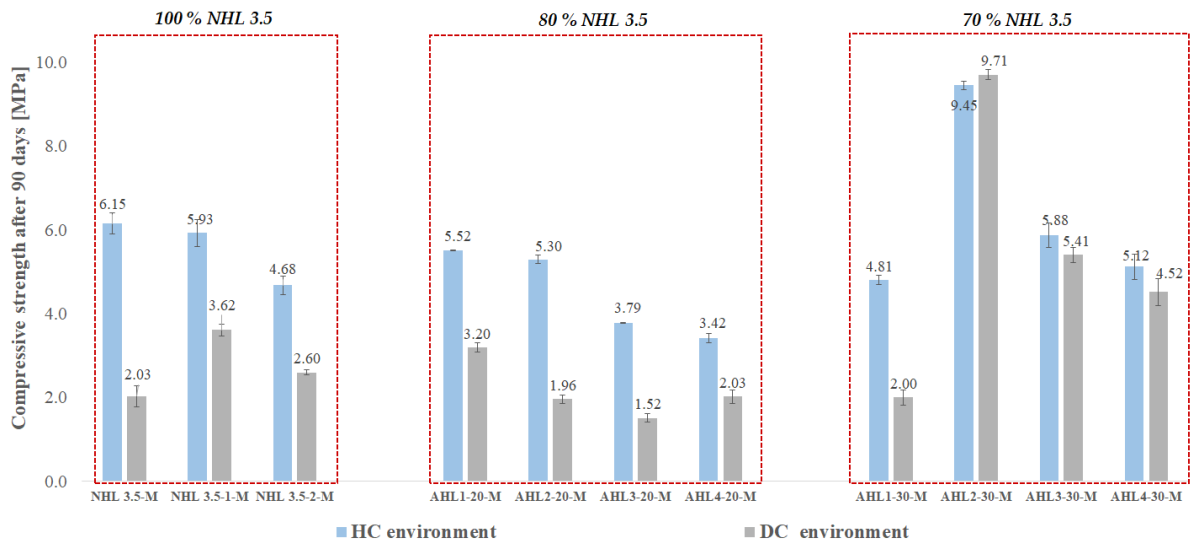

Figure 4.7. Compressive strength of NHL 3.5 and AHL mortars with 20&30 wt.% WBA after 90 days in different curing environments

Table 4.10. Compressive and flexural strength of NHL 5 and AHL mortars with 40 wt.% WBA after 7 days in HC curing environments

NHL share [%]	Mix ID	Compressive strength $f_{C,28}$ [MPa]		Flexural strength $f_{F,28}$ [MPa]		SAI$_7$ [%]
		HC Environment				
100%	**NHL 5 - M**	2.88	(±0.19)	0.77	(±0.09)	-
	NHL5-1 - M	1.58	(±0.07)	0.88	(±0.01)	
60%	**AHL4-40 - M**	2.80	(±0.14)	1.15	(±0.08)	97%
	AHL5-40 - M	3.58	(±0.48)	1.42	(±0.05)	125%

Table 4.11. Compressive and flexural strength of NHL 5 and AHL mortars with 40 wt.% WBA after 28 days in different curing environments

NHL share [%]	Mix ID	Compressive strength $f_{C,28}$ (±σ) [MPa]		Flexural strength $f_{F,28}$ (±σ) [MPa]		SAI$_{28}$ [%]
		HC Environment				
100%	**NHL 5 - M**	7.13	(±0.31)	2.72	(±0.16)	-
	NHL5-1 - M	4.50	(±0.35)	2.01	(±0.20)	
	NHL5-4 - M	8.39	(±0.34)	2.17	(±0.23)	
60%	**AHL4-40 - M**	5.26	(±0.39)	1.82	(±0.07)	74%
	AHL5-40 - M	9.56	(±0.29)	3.15	(±0.16)	134%
		DC Environment				
100%	**NHL 5 - M**	5.52	(±0.08)	1.53	(±0.07)	-
	NHL5-1 - M	4.35	(±0.21)	1.47	(±0.10)	
60%	**AHL4-40 - M**	4.92	(±0.17)	1.49	(±0.13)	89%
	AHL5-40 - M	9.99	(±0.24)	3.41	(±0.03)	181%
		ACC Environment				
100%	**NHL 5 - M**	15.81	(±0.28)	3.74	(±0.18)	-
	NHL5-1 - M	12.99	(±0.02)	4.09	(±0.02)	
60%	**AHL4-40 - M**	7.52	(±0.11)	1.91	(±0.01)	48%
	AHL5-40 - M	12.76	(±0.03)	3.85	(±0.27)	81%

Table 4.12. Compressive and flexural strength of NHL 5 and AHL mortars with 40 wt.% WBA after 90 days in different curing environments

NHL share [%]	Mix ID	Compressive strength $f_{C,90}$ ($\pm\sigma$) [MPa]		Flexural strength $f_{F,90}$ ($\pm\sigma$) [MPa]		SAI$_{90}$ [%]
		HC Environment				
100%	**NHL 5 - M**	8.32	($\pm$0.31)	2.72	($\pm$0.02)	-
60%	**AHL4-40 - M**	7.28	($\pm$0.26)	2.14	($\pm$0.05)	87%
	AHL5-40 - M	11.16	($\pm$0.09	3.41	($\pm$0.21)	134%
		DC Environment				
100%	**NHL 5 - M**	9.46	($\pm$0.14)	2.56	($\pm$0.34)	-
60%	**AHL4-40 - M**	6.00	($\pm$0.17)	1.18	($\pm$0.13)	63%
	AHL5-40 - M	14.15	($\pm$0.05)	4.23	($\pm$0.43)	150%
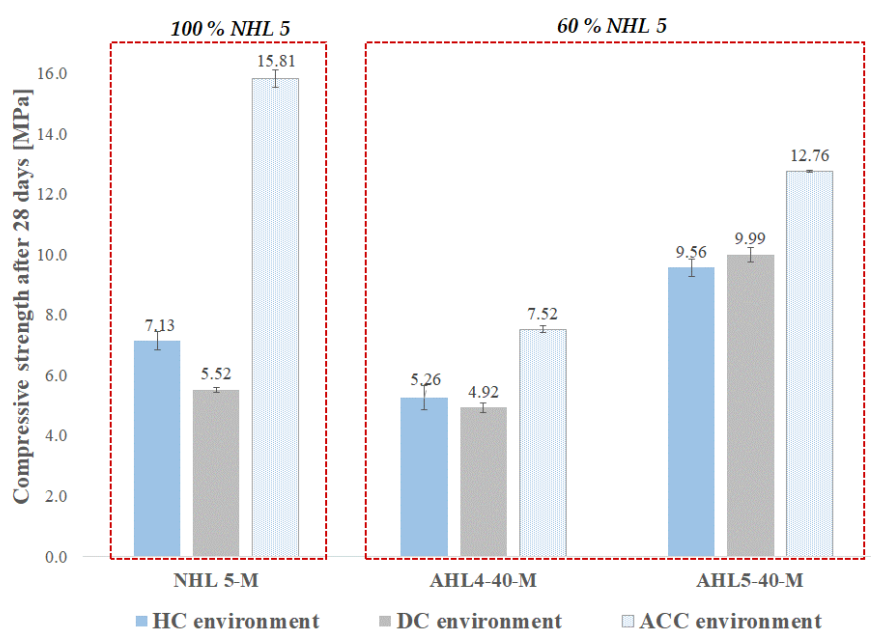
Figure 4.8. Compressive strength of NHL 5 and AHL mortars after 28 days in different curing environments
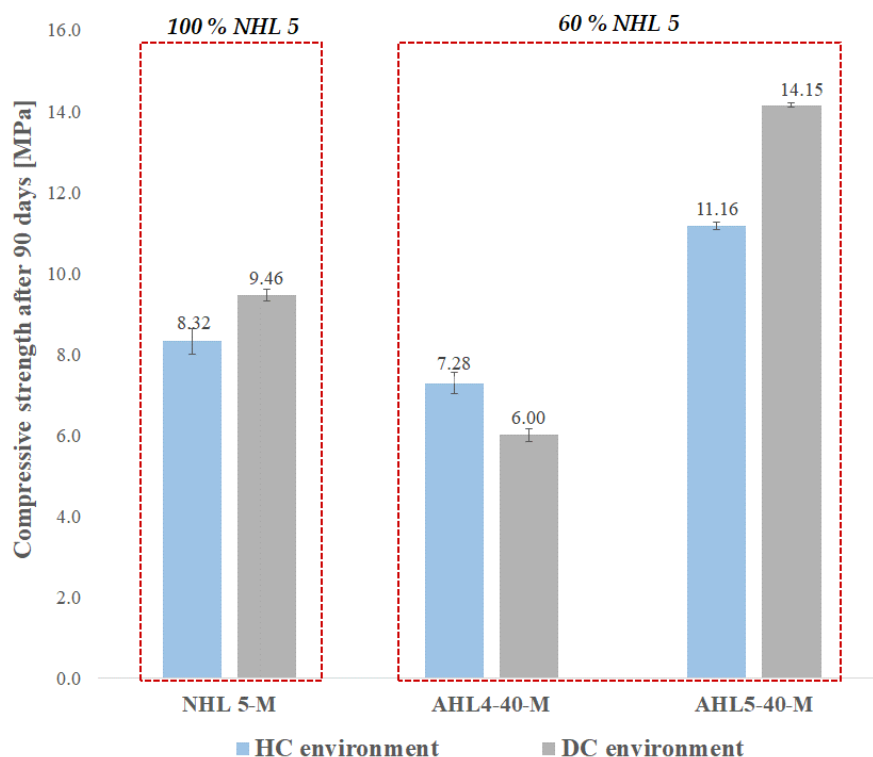
Figure 4.9. Compressive strength of NHL 5 and AHL mortars after 90 days in different curing environments

When placing the AHL mortars to the framework outlined in the EN 459-1 standard [28], which sets a minimum compressive strength requirement of 3.5 MPa after 28 days, it became evident that none of the control mixes achieved this threshold within the 28-day curing period under either of the curing regimes (Figure 4.10 and Figure 4.11). Among the AHL mixes with 20 wt.% WBA content, those subjected to DC failed to meet the 3.5 MPa requirement even after 90 days of curing. In contrast, the HC regimen proved to be beneficial, with all mixes exceeding the 3.5 MPa threshold but only after the 90-days mark. Conversely, AHL1-20-M reached the minimum value after 28 days, achieving a compressive strength of 3.64 MPa. In the case of higher hybridization ratios, AHL2-30-M and AHL4-30-M also met the prescribed criterion. Notably, AHL2-30-M demonstrated an approximately 50% increase in compressive strength compared to the required strength for its class (FL 3.5, with a (A/B/C) prefix depending on the $Ca(OH)_2$ content). In this context, AHL2-30-M emerged as the superior mix, having achieved the 90-day control value (5.35 MPa) within a mere 28 days of the curing process. Following the 90-day curing period, it nearly doubled its 28-day value, attaining compressive strengths of 9.45 MPa and 9.71 MPa in HC and DC, respectively. These values closely approach the maximum limit stipulated in the standard, which is set at 10 MPa. It is worth noting that the prescribed

compressive strength range for repair mortars typically falls between 6 and 10 MPa, especially for application in older, historic masonry structures [77]. Consequently, there is a need for caution to ensure that the compressive strength does not become disproportionately high.

When AHL mortars were evaluated according to the EN 998-1 [33] standard framework, all mortars, including those with 20 and 30 wt.% WBA substitution, after the 90-days mark, fell into either the CII or CIII category, indicating compressive strength ranging up to 5 and 7.5 MPa, respectively. In this sense, AHL mortars could be labelled as 'renovation' mortars (R). The exception was AHL2-30-M, which exceeded 6 MPa in compressive strength and, therefore, belonged to the CIV category, classifying it as a general-purpose mortar. Simultaneously, when following the EN 998-2 standard [151], these mortars could be categorized as general-purpose masonry mortars (G) within the M5 mortar classification and a minimum compressive strength of 5 MPa.
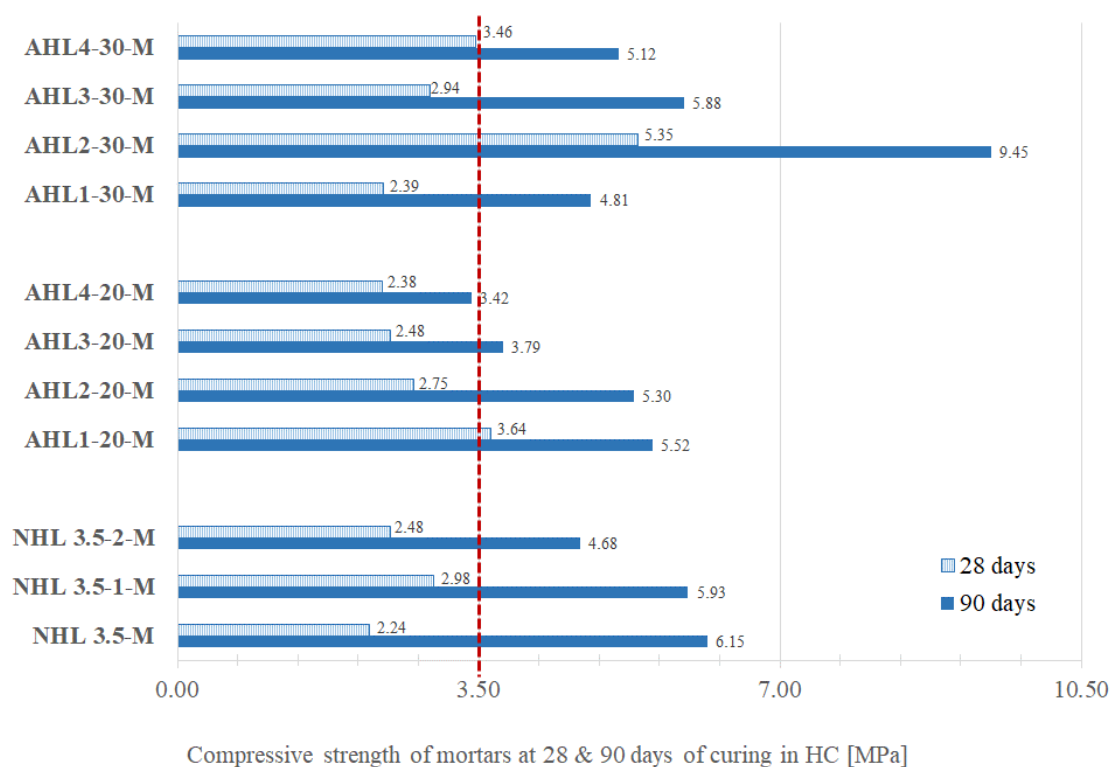

Figure 4.10. Compressive strength of NHL 3.5 and AHL mortars with 20&30 wt.% WBA after 28 & 90 days in HC curing environment
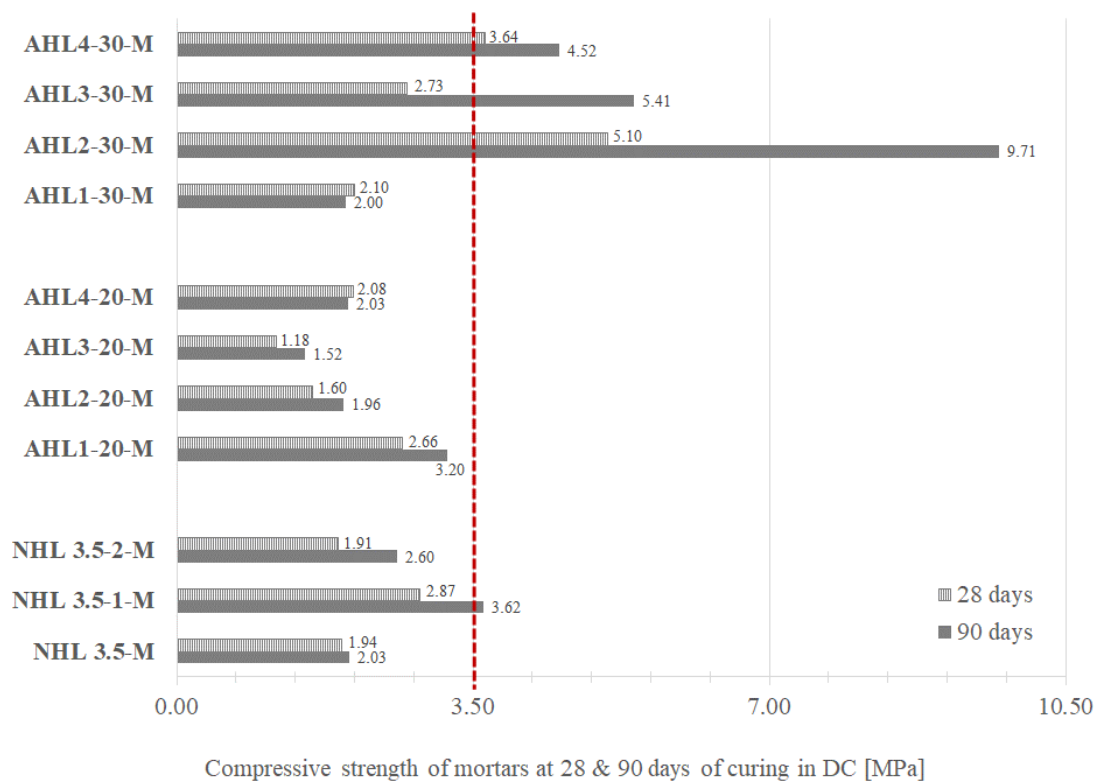
Figure 4.11. Compressive strength of NHL 3.5 and AHL mortars with 20&30 wt.% WBA after 28 & 90 days in DC curing environment

In the AHL mortars, where the primary NHL 5 binder was replaced with 40 wt.% of WBA 4 and WBA 5, the compressive strengths met the minimum requirements outlined in EN 459 standards. These standards specify a minimum of 2 MPa at 7 days and 5 MPa at 28 days. Furthermore, the fly ash mix consistently demonstrated more favourable results compared to the mixed AHL4-40-M mortar, surpassing the control mix values starting from the 7-day mark. For instance, the AHL5-40-M exhibited 90-day compressive strengths of 11.16 MPa and 14.15 MPa for HC and DC curing, respectively, signifying a remarkable increase of +34% and +50% compared to the control NHL5-M mix. Conversely, the AHL4-40-M experienced a modest decrease of -13% in HC, while the decline was more pronounced in DC, amounting to -37%.

It's noteworthy that both mixes with a relatively high 40 wt.% WBA substitution remain well within the thresholds established by the EN 459-1 standard. These values not only meet the standard criterion but also incorporating several aspects of high quality.

When evaluating NHL 5 and AHL mortars with a 40 wt.% WBA content according to the EN 998-1 [33] standard, all mortars exhibited compressive strength exceeding 6 MPa after both 28 and 90 days. This classification places them in the CS IV category, designating them as general-purpose mortars, as they surpass the maximum values specified for 'renovation' mortars (CS II). Furthermore, following the EN 998-2 standard [151], these mortars can be classified as

general-purpose masonry mortars (G) within the M5 or M10 mortar category, meeting the minimum compressive strength threshold of 5 MPa and 10 MPa, respectively.
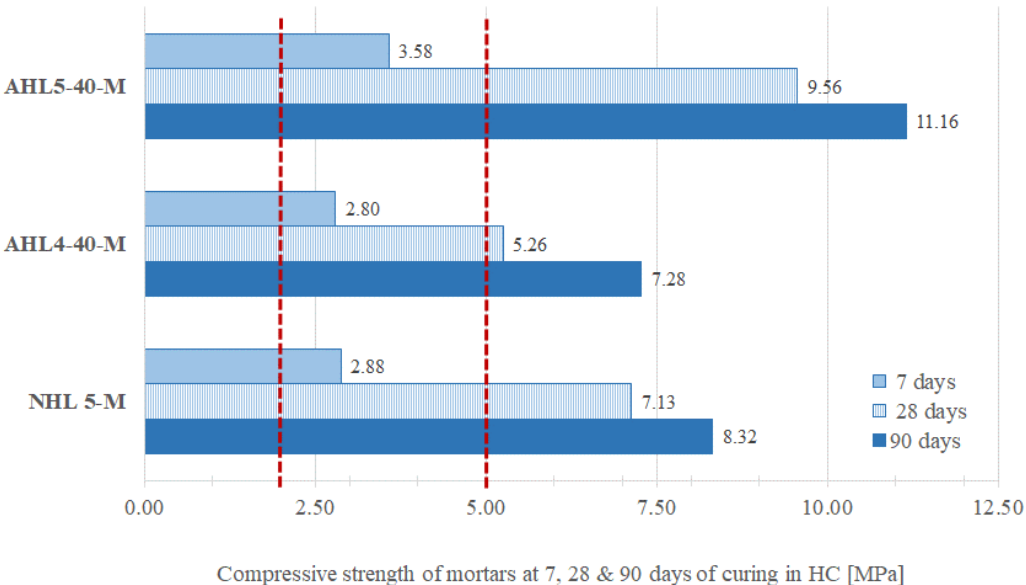

Figure 4.12. Compressive strength of NHL 5 and AHL mortars after 7,28 & 90 days in HC curing environment
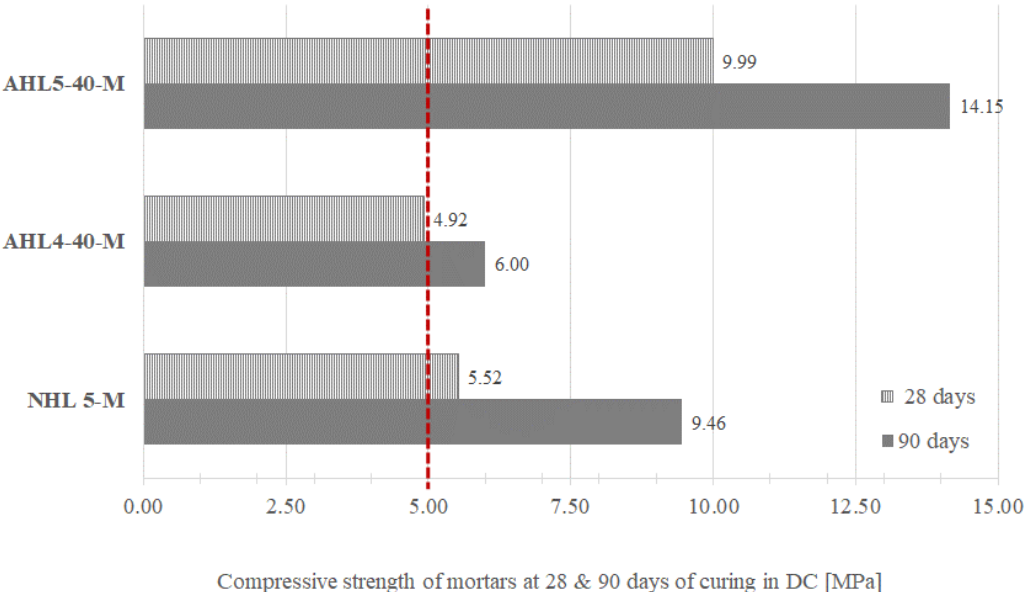

Figure 4.13. Compressive strength of NHL 5 and AHL mortars after 28 & 90 days in DC curing environment

In this research, the section pertaining to the ductility assessment of NHL and AHL mortars was conducted throughout the determination of the dynamic modulus of elasticity, using ultrasonic pulse velocity measurements (refer to Table 4.13 and Table 14) on NHL and AHL mortars. The

findings indicated a close alignment of dynamic modulus values and velocity measurements with those previously reported in the literature for NHL mortars [78, 154].

In this context, two AHL mortar compositions, namely AHL 2-30-M from the first NHL 3.5 binder group and AHL5-40-M from the second group, stand out by achieving maximum modulus values after a 90-day curing period, extending from their high compressive strength values. Both AHL2-30-M and AHL5-40-M modestly surpassed the dynamic modulus values of NHL 3.5-M and NHL 5-M, respectively, by approximately 8% after 90 days of curing in HC environment. In the same curing regime, the AHL1-30-M mortar exhibits a modulus of 10.30 GPa, being the closest to the control mix (10.64 GPa), while the AHL 3-30-m demonstrated 8.55 GPa value, as the lowest threshold in this group. The AHL4-40-M, as the mixed ash representative in the second binder group, demonstrated lower values compared to the NHL 5 values, with around 15% decline.

Table 4.13. Ductility assessment of NHL 3.5 and AHL mortars with 20&30 wt.% WBA after 28 & 90 days in different curing environments

Curing environment	Curing duration	Ductility parameters	NHL 3.5-M	AHL1-20-M	AHL2-20-M	AHL3-20-M	AHL4-20-M	AHL1-30-M	AHL2-30-M	AHL3-30-M	AHL4-30-M
HC environment	28 days	$f_{c,28}/f_{F,28}$	2.16	2.72	3.03	2.56	1.77	2.40	2.85	3.08	2.41
		E_d [GPa]	8.17	12.10	8.25	6.69	7.60	10.50	16.41	6.79	8.99
		V_{us} (km/s)	2.23	2.68	2.28	2.04	2.18	2.49	3.13	2.05	2.37
	90 days	$f_{c,90/fF,90}$	3.04	2.34	2.44	4.02	1.78	2.80	2.93	1.76	3.07
		E_d [GPa]	10.64	11.74	9.60	7.97	7.76	10.30	11.45	8.55	8.65
		V_{us} (km/s)	2.58	2.69	2.46	2.26	2.25	2.56	2.68	2.32	2.34
DC environment	28 days	$f_{c,28}/f_{F,28}$	2.55	2.72	2.13	1.79	2.49	2.49	5.25	2.22	2.99
		E_d [GPa]	5.13	5.66	4.65	4.94	5.56	5.08	13.41	6.00	8.25
		V_{us} (km/s)	1.83	1.91	1.76	1.78	1.90	1.81	2.87	1.94	2.29
	90 days	$f_{c,90}/f_{F,90}$	2.05	3.17	1.98	0.88	2.51	1.98	3.95	3.27	2.70
		E_d [GPa]	6.14	6.27	5.73	4.55	5.40	5.83	10.98	8.38	8.90
		V_{us} (km/s)	1.97	2.00	1.93	1.71	1.87	1.95	2.63	2.32	2.40
ACC environment	28 days	$f_{c,28}/f_{F,28}$	3.36	3.17	2.53	2.68	3.15	3.28	2.96	2.24	1.72
		E_d [GPa]	6.98	7.88	6.81	7.06	6.94	7.58	10.77	7.17	9.18
		V_{us} (km/s)	2.10	2.24	2.10	2.10	2.11	2.18	2.57	2.10	2.44

Table 4.14. Ductility assessment of NHL 5 and AHL mortars with 40 wt.% WBA after 7, 28 % 90 days in different curing environments

Curing environment	Curing duration	Ductility parameters	NHL 5 - M	AHL4-40 - M	AHL5-40 - M
HC environment	7 days	$f_{c,7}/f_{F,7}$	3.76	2.44	2.52
		E_d [GPa]	8.65	5.21	9.57
		V_{us} (km/s)	2.31	2.33	2.40
	28 days	$f_{c,28}/f_{F,28}$	2.62	2.89	3.03
		E_d [GPa]	13.34	10.54	14.49
		V_{us} (km/s)	2.88	2.62	3.02
	90 days	$f_{c,90}/f_{F,90}$	3.06	3.40	3.28
		E_d [GPa]	13.85	11.64	14.94
		V_{us} (km/s)	2.90	2.74	3.08
DC environment	28 days	$f_{c,28}/f_{F,28}$	3.62	3.30	2.93
		E_d [GPa]	9.64	10.28	13.80
		V_{us} (km/s)	2.46	2.60	2.96
	90 days	$f_{c,90}/f_{F,90}$	3.69	5.08	3.35
		E_d [GPa]	12.23	10.46	16.30
		V_{us} (km/s)	2.77	2.63	3.20
ACC environment	28 days	$f_{c,28}/f_{F,28}$	4.22	3.93	3.32
		E_d [GPa]	14.34	7.90	12.46
		V_{us} (km/s)	2.93	2.26	2.79

While a wide distribution of E_d values was observed, mortars exhibiting higher compressive strength also showcased elevated dynamic modulus of elasticity. A relatively strong linear correlation between the compressive strength and the dynamic modulus of elasticity was noted upon samples from both NHL 3.5-WBA and NHL 5-WBA binary systems (Figure 4.14 and Figure 4.15). Notably, a better fit was found in samples corresponding to the NHL 3.5 group in the early ages (28 days) and DC environment. Meanwhile, the NHL 5 binder group exhibited a strong correlation across all testing ages and curing regimes. This relationship underscores the critical influence of the pore network structure within the mortars. A more compact pore structure contributes to higher compressive strength but simultaneously results in a material with lower ductility.
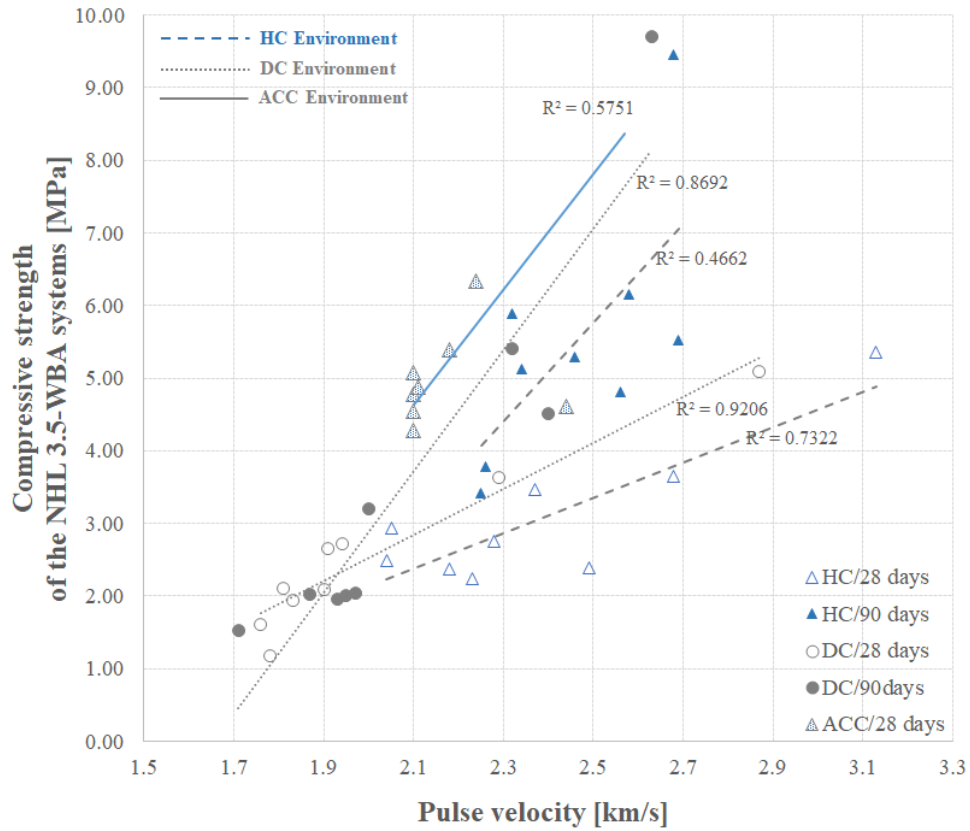
Figure 4.14. Correlation between compressive strength and pulse velocity in NHL 3.5-WBA systems
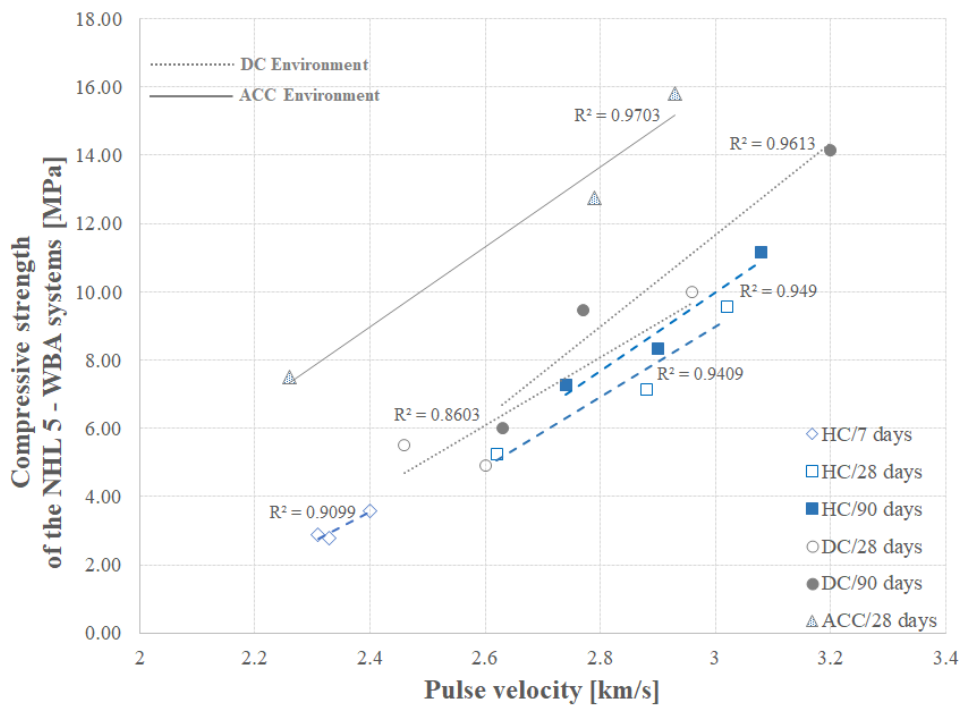

Figure 4.15. Correlation between compressive strength and pulse velocity in NHL 5-WBA systems

Several prior investigations [153,156,157] have proposed a direct proportional relationship between the ratio of compressive to flexural strength (f_C/f_F) and the modulus of elasticity during tests conducted at various ages ranging from 1 to 6 months. A lower f_C/f_F ratio is hypothesized to correlate with a lower modulus of elasticity. Additionally, lower modulus of elasticity values and a reduced f_C/f_F ratio are indicative of enhanced flexibility in the mortar. Consequently, mortars with a low f_C/f_F ratio exhibit elastic behaviour, potentially making them equivalent to authentic materials and ensuring heightened durability.

However, the f_C/f_F ratio was employed as a simplified method to evaluate mortar ductility, in addition to the ultrasound measurements. It's worth noting that it doesn't demonstrate a seamless alignment with the dynamic modulus of elasticity acquired through ultrasonic pulse velocity measurements (refer to Figure 4.16). This discrepancy can partly be attributed to the assumption of a Poisson's coefficient of 0.25, which may vary from one mortar composition to another. A moderate linear correlation between the f_C/f_F ratio and the dynamic modulus of elasticity was noted only upon samples cured in DC environment for both NHL 3.5-WBA and NHL 5-WBA binary systems (Figure 4.16), whereas better fitting is noted in the early ages (28 days).
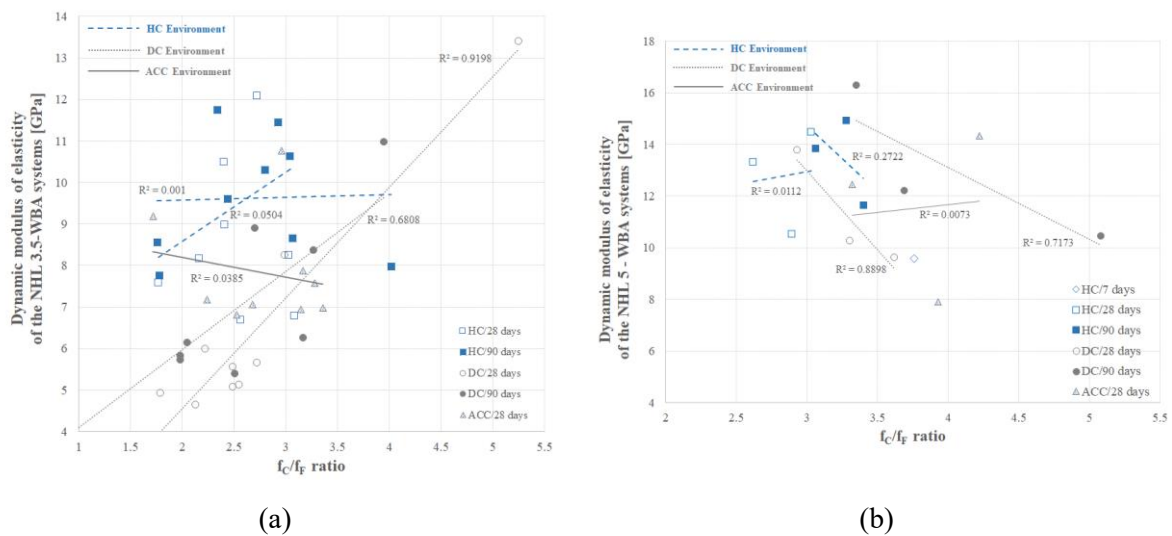

(a)   (b)

Figure 4.16. Correlation between the dynamic modulus of elasticity and the fc/ff ratio in NHL-WBA systems

While flexural strength exhibited a similar behavioural trend to compressive strength (shaped more by the curing regime than on the WBA share), albeit slightly in favour of the HC curing environment, the f_C/f_F values were observed to be higher than those of control mixes during the initial 28 days. Subsequently, the 90-day values were either lower or remained comparable to those of the control mixes, with a few exceptions, such as AHL2-30-M and AHL5-40-M in both natural carbonation environments.

Nevertheless, the f_C/f_F ratio values, as well as the calculated values of dynamic modulus of elasticity for AHL mortars containing 20, 30, and 40 wt.% of WBA (as presented in Table 4.13 and Table 4.14) fall within the documented ranges from previously mentioned literature. Within these established ranges, the tested mortars consistently displayed elastic behaviour, aligning with the characteristics of historic mortars.

4.3.3. Assessment of carbonation progress in various curing environments

Based on an analysis of carbonation depth in NHL-WBA mortar systems, spanning a 90-day period under various curing conditions several significant findings have come to light. An analysis was conducted to discern the interplay between the pozzolanic reaction and carbonation reaction, with the aim of understanding the factors influencing compressive strength across various WBA proportions and different curing environments. Plausible pozzolanic reaction, taking place in AHL-based system, is inevitably accompanied by carbonation, both of them being portlandite consuming reactions. Hence, when assessing the 'carbonation' progress through phenolphthalein staining, it can also indirectly suggest the presence of a pozzolanic reaction in mortars.

On that account, it is evident that carbonation in mortars containing WBA undergoes accelerated advancement (refer to Table 4.15 and Table 4.16), i.e., the phenolphthalein staining (Figure 4.17, Figure 4.18 and Figure 4.19), showed higher reduction of alkalinity, particularly within the initial 28 days of curing in a DC environment. This phenomenon is most pronounced in the AHL mixes that incorporate fly ash (WBA1 and WBA2). Specifically, the highest rate of carbonation was observed in the AHL1 mixes containing both proportions of WBA. In contrast, the carbonation pattern of the AHL 3-30-M and AHL4-30-M mortar mixes closely resembled that of the NHL 3.5-M control mix. Nevertheless, it is worth noting that higher WBA proportions in the AHL mixes tend to decelerate the carbonation process in the first 28 days of DC environment. An additional cause for this observed behaviour may stem from the lower porosity (filler effect) and higher superplasticiser content in the AHL mortar mixes containing WBA at a 30 wt.% hybridization ratio, which could hinder the process of carbonation. In this regard, the additives may have exhibited an inhibitory effect on the precipitation of $CaCO_3$, as suggested by previous research [158].

After the 90-day curing period, carbonation progress reached approximately 60% in the DC environment for the AHL1-20-M, AHL2-20-M and AHL3-20- M mixes. At the same time, it

was observed that maintaining a high relative humidity of up to 95% (HC curing regime) effectively inhibited carbonation for the initial 28 days. In contrast, carbonation and/or portlandite consumption continued unhindered throughout the 90-day curing period in HC environment, culminating in a maximum of 55% for the AHL4-30 - M mix.

When investigating carbonation progress in AHL mortar mixes with NHL 5 as the primary binder, similar trends were observed, though with some noteworthy distinctions (refer to Figure 4.19 and Table 4.16). In this context, carbonation was facilitated in both DC and HC environments from an early stage and persisted throughout the 90-day curing period. The AHL4-40-M and AHL 5-40-M mixes exhibited carbonation depths after 28 days that were comparable to those of the control NHL 5-M mix, with carbonation depth evolving over time. With around 30% carbonation progress, this evolution was most clearly demonstrated in AHL4-40-M when cured in both curing environments. The observed carbonation progress in AHL5-40 and the slightly higher progression in AHL4-40-M can be attributed to changes in permeability, with the former indicating a decrease and the latter an increase, detailed in sub-chapter on *4.3.5 Pore structure*.

In the DC environment, the carbonation development of the control mix was slower, exhibiting decelerated carbonation from 28 to 90 days of curing. In this sense, AHL5-40 – M showed a carbonation progress of +22% after 90 days, which was akin to that of NHL 5 – M, while AHL 4-40 – M reached a maximum carbonation level of 52% after 90 days, all within the HC environment, which was not expected to foster carbonation in this setup.

The variation in relative humidity within the HC curing chamber during the winter months, fluctuating between 85% and 95%, could potentially have played a role in equalizing the effects of these two curing environments, further amplifying the influence of WBA on the portlandite consumption.

The greater reduction in alkalinity observed in mortars containing WBA, in both binder groups of different primary hydraulicity, especially noted after 90 days of curing in HC environment, in comparison to the control mixes may be attributed to the reduced presence of portlandite in the AHL mortars. This reduction stems from the partial replacement of the primary NHL3.5 and NHL 5 binder with WBA and the potential pozzolanic reaction associated with these mortars.
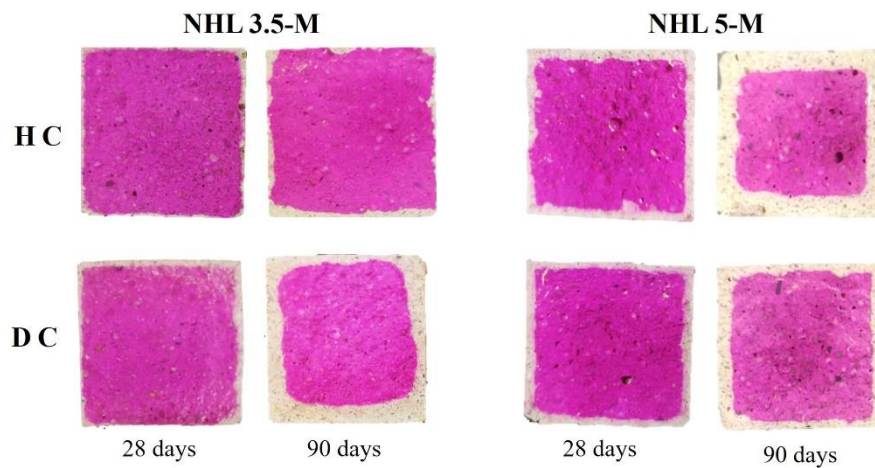
Figure 4.17. Carbonation progression in control NHL mortars: phenolphthalein staining evaluation over time in different curing environments (HC: Humid Conditions, DC: Semi-Dry Conditions)
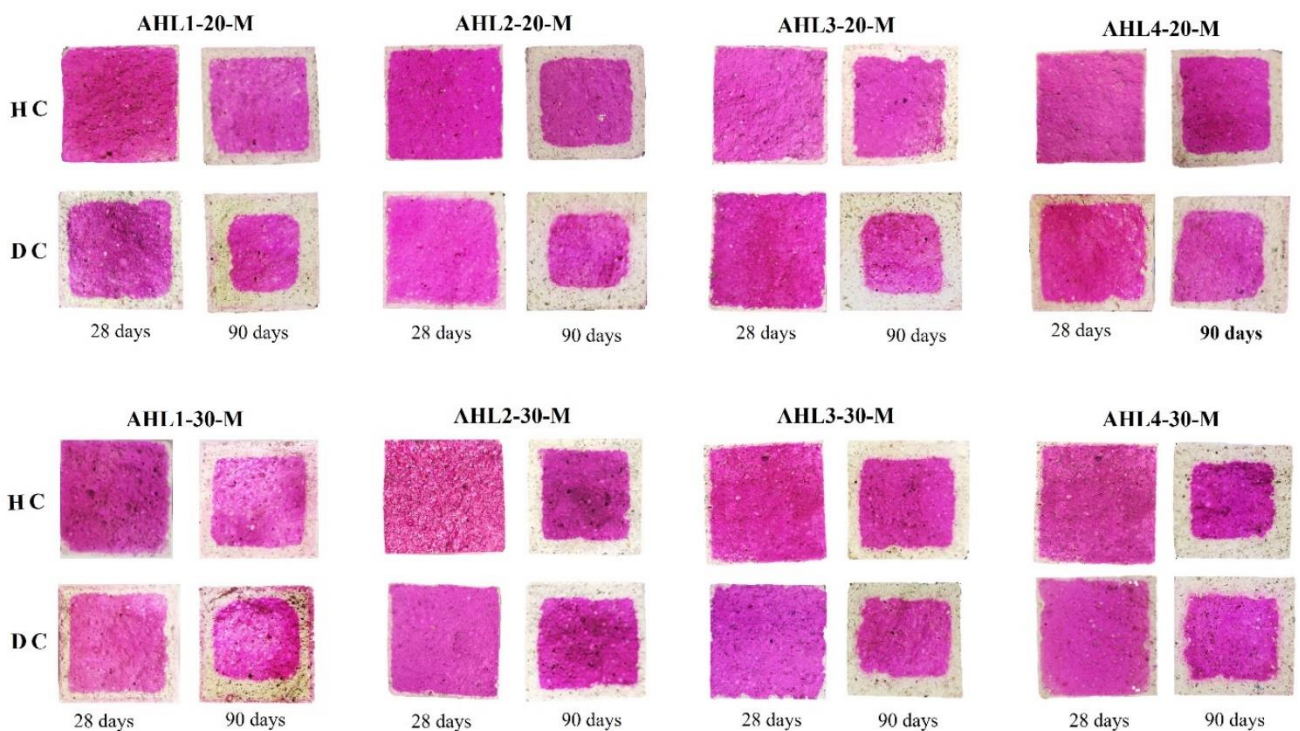

Figure 4.18. Carbonation progression in AHL mortars with 20% and 30% WBA: phenolphthalein staining evaluation over time in different curing environments (HC: Humid Conditions, DC: Semi-Dry Conditions)
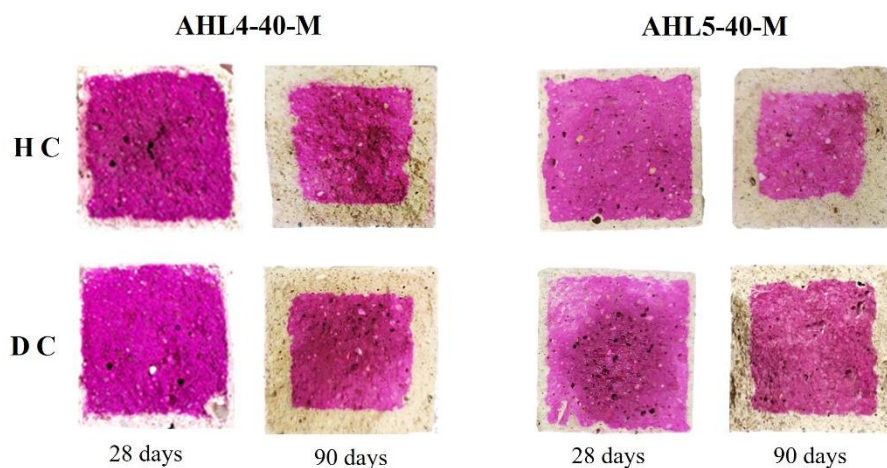
Figure 4.19. Carbonation progression in AHL mortars with 40 wt.% WBA: phenolphthalein staining evaluation over time in different curing environments (HC: Humid Conditions, DC: Semi-Dry Conditions)

Table 4.15. Carbonation progress (percentage) on AHL mortar halves with NHL 3.5 as the primary binder through time and in different curing environments

Curing environment	DC		HC	
Curing duration	28 days	90 days	28 days	90 days
NHL 3.5 – M	12%	42%	0%	7%
AHL1-20 - M	40%	60%	0%	34%
AHL1-30 - M	38%	51%	0%	37%
AHL2-20 - M	27%	59%	0%	40%
AHL2-30 - M	17%	39%	0%	40%
AHL3-20 - M	17%	64%	0%	39%
AHL3-30 - M	12%	46%	6%	51%
AHL4-20 - M	27%	42%	0%	34%
AHL4-30 - M	13%	49%	8%	55%

Table 4.16. Carbonation progress (percentage) on AHL mortar halves with NHL 5 as the primary binder through time and in different curing environments

Curing environment	DC		HC	
Curing duration	28 days	90 days	28 days	90 days
NHL 5 - M	18%	26%	20%	42%
AHL4-40 - M	23%	54%	19%	52%
AHL5-40 - M	20%	33%	24%	46%

The effect of accelerated carbonation curing on the compressive strength of the NHL mortar is shown in Figure 4.20, whereas the complete carbonation of prismatic samples was confirmed after 28 days of ACC.
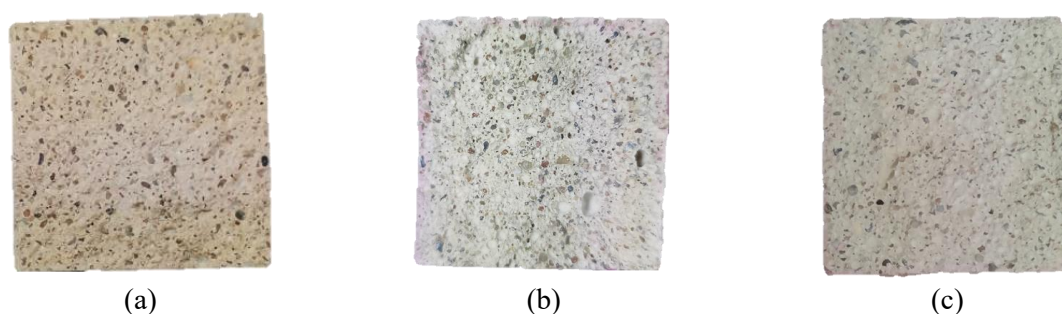

| (a) | (b) | (c) |

Figure 4.20. Complete carbonation of prismatic samples after 28 days of ACC: (a) NHL 3.5-M; (b) AHL1-20-M; (c) AHL 3-20-M

4.3.4. Assessment of the morphology of AHL mortars cured in various environments

The morphology of both the control mixes and the AHL mortars, which were cured in various environments for a duration of 90 days, was investigated using SEM on fresh mortar fractures. This investigation is supported by the 1000x and 2000x magnified micrographs displayed in Figure 4.21 and Figure 4.22. However, it's important to note that the microscopic analysis was exclusively conducted on the non-carbonated section of the mortar specimen.

In Figure 4.21, the micrographs present the mortar compositions containing NHL 3.5 that were unaffected by carbonation. Correspondingly, Figure 4.22 illustrates the mortar structures incorporating NHL 5. These microscopic images were acquired after a 90-day exposure of the mortars to a HC environment, as depicted in Figure 18a, c, and e, and Figure 19a, c, and e, respectively. Conversely, sections b, d, and f of both figures exhibit the mortar structures that remained non-carbonated and were cured within an DC environment.
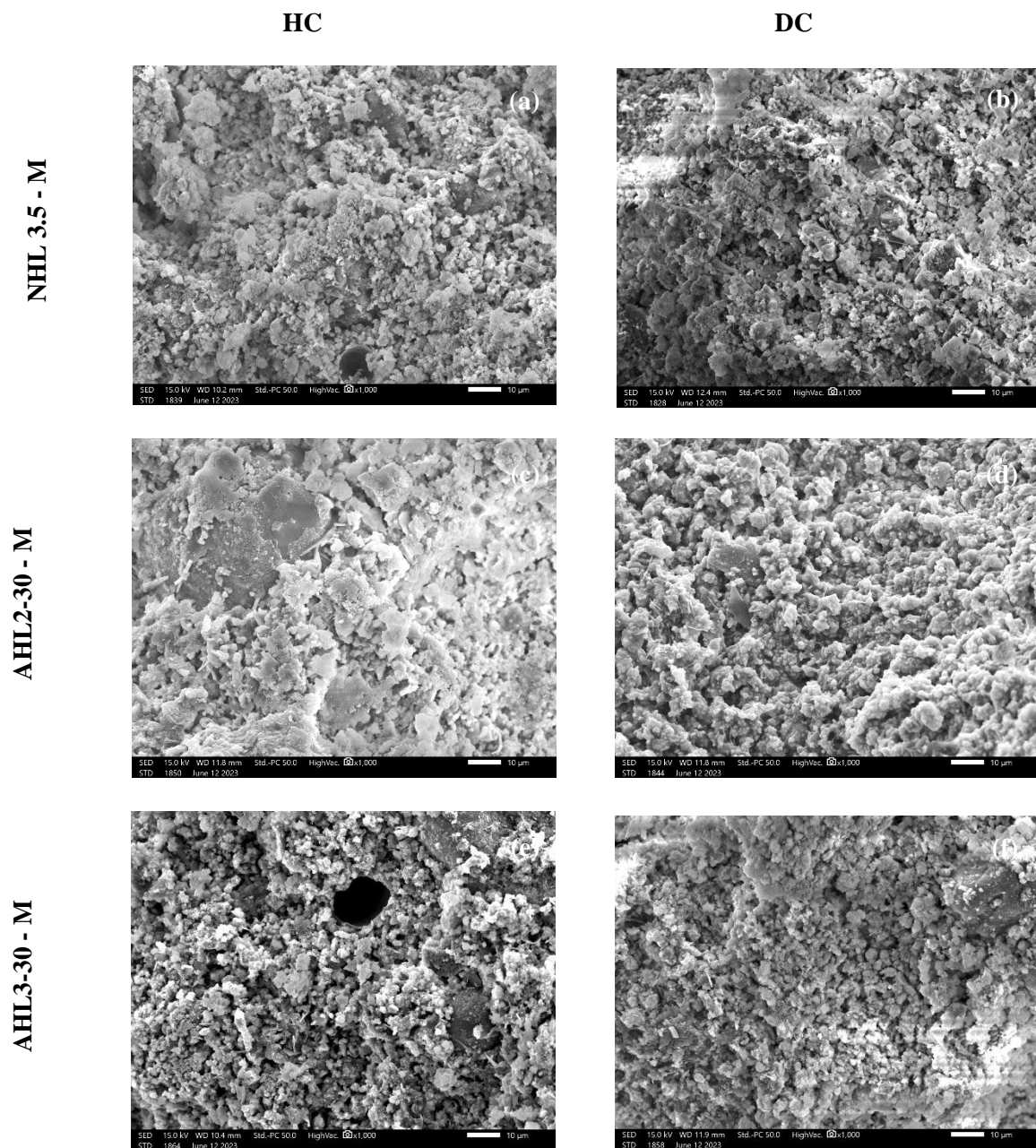
Figure 4.21. SEM micrographs of NHL 3.5 and AHL mortars with 30 wt.% WBA at HC (a, c, e) and DC (b, d, f) at 1000× magnification
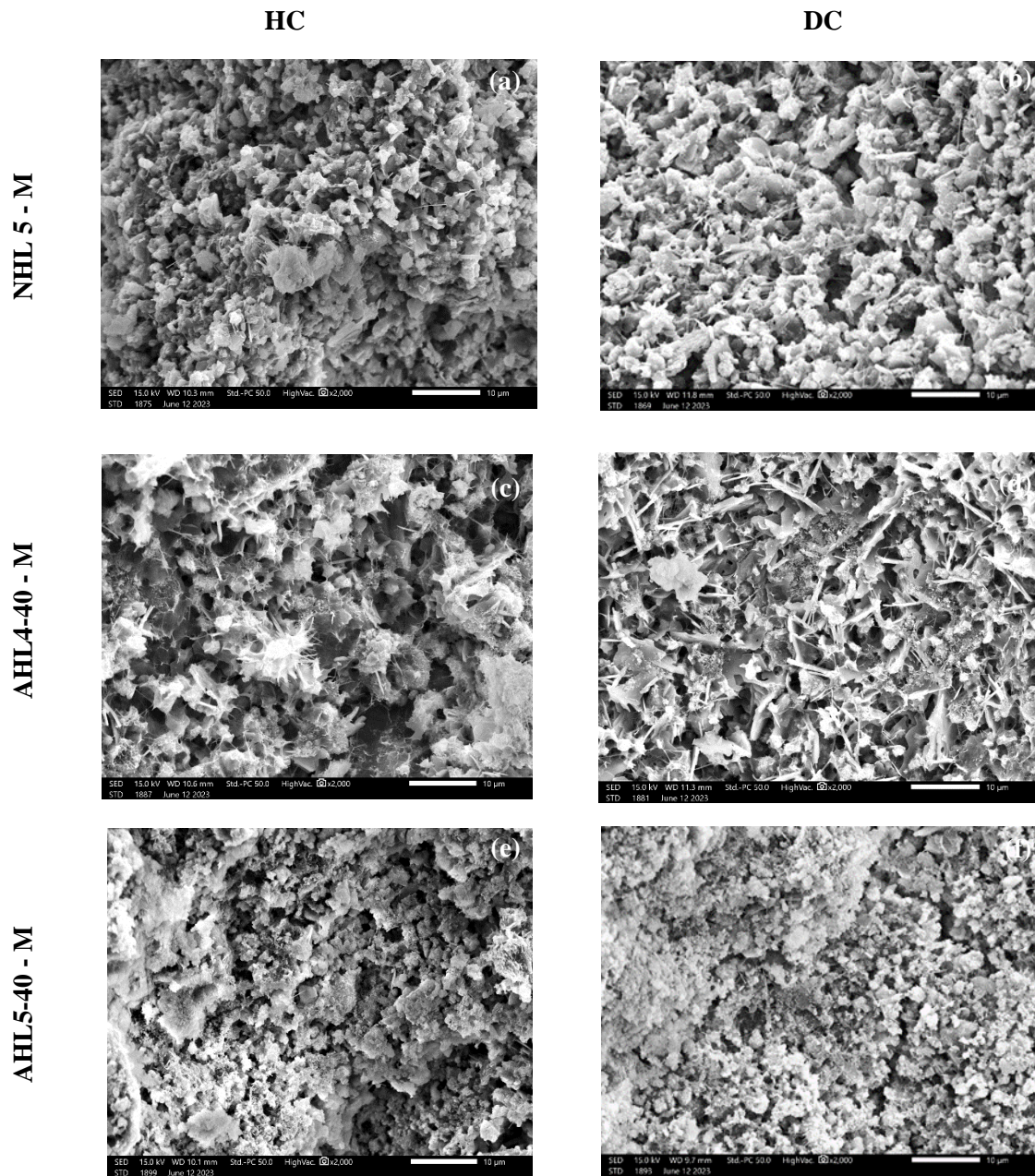
Figure 4.22. SEM micrographs of NHL 5 and AHL mortars with 40 wt.% WBA at HC (a,c,e) and DC (b,d,f) at 2000× magnification

When the NHL 3.5-M samples were examined after 90 days of exposure to both DC and HC environments (Figure 4.21 (a), (b)) recognisable portlandite crystals were observed scattered in the needle-like hydration products (possibly ettringite) alongside pores with a rounded morphology. Given the presumed secondary C-S-H formation resulting from the pozzolanic reaction between WBA and $Ca(OH)_2$, SEM micrographs of AHL2-30M-M reveal a microstructure characterised by enhanced homogeneity, compaction and density (Figure 4.21 (c), (d). The sand grains are well integrated into the hydrated matrix, which is rich in low-crystallinity hydrates. There are no visible cracks, indicating strong cohesion between the phases.

In contrast to AHL2-30-M, the micrographs of AHL3-30-M reveal a comparatively more porous structure, showcasing the presence of substantial rounded pores amid flocculent C-S-H phases characterised by amorphous hydrated phases (Figure 4.21 (e), (f)).

Similarly, micrographs of NHL 5-M (Figure 4.22 (a), (b)) show the presence of needle-shaped hydrates and numerous hexagonal portlandite plates in both curing regimes. For AHL4-40-M, micrographs show a notably porous microstructure, especially at HC, with floc-like C-S-H amorphous hydrated phases clearly visible (Figure 4.22 (c), (d)). AHL5-40-M shows a dense and compact structure composed mainly of amorphous C-S-H hydrated phases, with no portlandite presence (Figure 4.22 (e), (f)).

Generally, the degree of C-S-H and other hydraulically reactive components associated with the hydraulic materials increased from being rather slightly and sporadically distributed in the moderately hydraulic mortars containing NHL 3.5 through to more evenly distributed in the mortars containing eminently hydraulic lime NHL 5. The acicular C-S-H and C-A-S-(H) crystals were expected to bridge the pore structure in those materials with higher levels of hydraulicity [159].

Although these observations were made without the benefit of EDS analysis, it is important to recognise their preliminary nature. Nevertheless, the value of these observations should not be underestimated, especially in view of the clearly discernible features of the microstructure. The EDS analysis, when carried out, can provide valuable and confirmatory insights. Therefore, the results presented here should be considered as initial assessments, with further EDS analysis potentially providing a more comprehensive understanding of the issues.

4.3.5. Pore structure assessment

Categorizing the tested mortar specimens into two distinct groups, non-carbonated and completely carbonated, porosity parameters, including permeable porosity and critical pore radius, were obtained by using mercury intrusion porosimetry (MIP) technique. These distinct groups underwent curing processes in HC, DC and ACC environments. While the first two environments provided the non-carbonated structural sections of the specimens following 90 days of curing, the latter environment prompted full carbonation within a shorter period of 28 days. The primary focus in this section was on mortars with the higher level of hybridization, specifically those containing higher hybridisation ratios, i.e., 30 and 40 wt.% WBA. This choice was based on reported enhancements in mechanical properties and the significant sustainability benefits it offers.

The total porosity accessible to mercury, as indicated by the permeable porosity, is influenced significantly by both the curing regimen and the addition of WBA, as detailed in Table 4.17 and Table 4.18. In particular, the HC environment yields lower permeable porosity values compared to both natural and accelerated carbonation environments. This distinction is even more pronounced when analysing the results from the ACC environment. Notably, the compressive strength of NHL and AHL mortars improves after exposure to ACC environment curing. In fact, the 28-day compressive strengths of carbonated specimens are comparable to the 90-day compressive strengths of mortars cured under HC and DC regimens. Despite accelerated carbonation curing resulting in reduced permeable porosity for NHL and AHL mortars, a phenomenon supported by [133], and the formation of numerous $CaCO_3$ crystals that refine the pores and promote a denser matrix, thereby enhancing the mechanical properties of AHL mortars, it is observed that the carbonated structures remain more porous after 28 days compared to their non-carbonated counterparts after 90 days. At the same time, it's noticeable that the mortar with mixed ash (AHL3-30-M) has higher porosity than both the control mix and the fly ash mortar (AHL2-30-M), which has the lowest permeable porosity values. This pattern remains consistent across all curing methods. This difference can be attributed to the lower presence of hydraulic compounds present in the primary NHL binder, which subsequently lead to a slower hydration reaction as well as the granulometric distribution favouring porosity. On the other hand, in the mixture incorporating fly ash WBA2, a reduction in porosity values indicates that changes in the microstructure are initiated due to the pozzolanic reaction and a more uniform granulometric distribution which enables better filling of the voids.

In the mixes falling within the higher hydraulicity range, where NHL 5 served as the primary binder, the HC environment, conversely, did not result in lower permeable porosity values in the binary AHL systems; instead, it produced the highest values. The only exception to this trend was the control mix, which exhibited the lowest value of 23.79%. The AHL5-40-M mix followed with a permeable porosity of 27.32%, and finally, the AHL4-4-M mix exhibited the highest value, surpassing 30%. Importantly, this trend persisted consistently across all curing regimes. Previous researchers [39,159] suggest that as the formation of C-S-H progresses and as $Ca(OH)_2$ develops, the material's porosity diminishes. These findings may imply that the introduction of mixed ashes into the NHL matrix hinders the densification of C-S-H within the pore structure, resulting in increased porosity values. Conversely, fly ashes seem to enhance densification, leading to lower porosity values across different hydraulicity ranges and curing regimes.

The critical pore entry radius, a parameter indicating the predominant grouping of the largest interconnected pores within the binder system [39], aligns with the peak in the differential pore volume curve, representing the pore size associated with maximum volume intrusion. Under accelerated carbonation conditions (ACC), NHL 3.5-M exhibited the highest critical pore entry radius at 1.30 μm. In comparison, the critical pore entry radii of AHL2-30-M and AHL3-30-M either decreased or remained constant (measuring 1.04 and 1.30 μm, respectively). Therefore, the porosity of the carbonated structure exhibited notable trends; AHL3-30-M displayed peak values similar to the control mortar, while the lower peak value of AHL2-30-M, both values aligning with the HC environment, suggesting a refinement of pore size typically associated with the reactivity of pozzolanic materials.

With the integration of WBA into the NHL 3.5 system, AHL mortars demonstrate enhanced mechanical performance under high-curing (HC) conditions compared to the DC curing regime, especially during the initial 28-day period. This enhancement can be attributed to the higher levels of relative humidity, which facilitate both hydration and pozzolanic reactions, as investigated in [114]. These two reactions significantly influence the evolution of the microstructure, resulting in a reduction of the primary pore size. Consequently, this leads to a denser mortar and, ultimately, higher compressive strength values.

A parallel pattern emerges within the second mortar group, with NHL 5 as the primary binder characterized by higher hydraulicity. Here, the control mix NHL 5-M exhibited the lowest critical pore entry radius under HC curing conditions. Among the natural carbonation

environments, the AHL mortars displayed consistent behavior. Notably, the mixed ash variant (AHL4-40-M) exhibited peak values surpassing those of the control mortar (1.04 µm), while AHL5-40-M had a lower peak value (0.43 µm), in contrast of the inverse permeable porosity values. Furthermore, the implementation of the ACC regime resulted in a significant refinement of porosity for AHL4-40-M, to the extent that the critical pore entry radius equaled that of the control value (0.67 µm).

Table 4.17. Porosity parameters of NHL 3.5 & AHL mortars with 30 wt.% cured in HC, DC and ACC environment, obtained via MIP

Curing conditions	Mix ID	Critical pore entry radius (µm)	Median Pore Diameter (Volume) (µm)	Median Pore Diameter (Area) (µm)	Average Pore Diameter (µm)	Permeable Porosity (%)
HC	NHL 3.5 - M	0.83	0.19	0.02	0.05	26.09%
	AHL 2-30 - M	1.04	0.68	0.02	0.05	22.71%
	AHL 3-30 - M	1.31	0.99	0.01	0.07	28.24%
DC	NHL 3.5 - M	0.83	0.78	0.04	0.20	26.44%
	AHL 2-30 - M	1.59	6.28	0.03	0.07	26.71%
	AHL 3-30 - M	1.31	0.85	0.04	0.12	28.15%
ACC	NHL 3.5 - M	1.30	0.90	0.04	0.24	28.30%
	AHL 2-30 - M	1.04	0.17	0.02	0.06	24.12%
	AHL 3-30 - M	1.30	1.00	0.03	0.20	29.11%

Table 4.18. Porosity parameters of NHL 5 & AHL mortars with 40 wt.% cured in HC, DC and ACC environment, obtained via MIP

Curing conditions	Mix ID	Critical pore entry radius	Median Pore Diameter (Volume)	Median Pore Diameter (Area)	Average Pore Diameter	Permeable Porosity
		(µm)	(µm)	(µm)	(µm)	(%)
HC	NHL 5 - M	0.55	0.29	0.02	0.05	23.79%
	AHL 4-40 - M	1.04	0.51	0.05	0.13	31.52%
	AHL 5-40 - M	0.43	0.16	0.05	0.09	27.32%
DC	NHL 5 - M	0.83	0.29	0.02	0.05	25.59%
	AHL 4-40 - M	1.04	0.51	0.05	0.13	30.06%
	AHL 5-40 - M	0.43	0.16	0.05	0.09	25.94%
ACC	NHL 5 - M	0.67	0.44	0.02	0.07	24.23%
	AHL 4-40 - M	0.67	0.46	0.05	0.13	29.21%
	AHL 5-40 - M	0.55	0.26	0.05	0.12	25.34%

Figure 4.23 illustrates the pore size distribution of non-carbonated structures for the control mix NHL 3.5-M and AHL mortars with 30 wt.% WBA, subjected to both HC and DC environments for 90 days. Figure 4.24 showcases the pore size distribution for the non-carbonated structures of the same materials, including control mix NHL 3.5-M and AHL mortars with 30 wt.% WBA exposed to DC environments, alongside structures that underwent full carbonation in ACC for 28 days. It is noted that the non-carbonated specimens cured in the HC environment exhibit a multi-modal distribution characterized by several sharp peaks representing the main intruded volume. However, the non-carbonated specimen cured in DC display a bimodal distribution with two prominent peaks. Only the control mix NHL 3.5-M from the DC environment displays a unimodal curve, featuring a sharp peak around 1 µm. In contrast, the counterpart mix cured in HC shows a maximum intruded volume for pores also around 1 µm, albeit slightly reduced, and accompanied by a few secondary peaks in the region up to 0.1 µm. These secondary peaks are associated with the hydration process, particularly the formation of C-S-H [78].

On the other hand, the AHL mortars cured in DC exhibit peaks in the region of small capillary pores (0.01-0.1 um), with AHL2-30-M demonstrating a primary peak around 0.04 µm and AHL3-30-M showing a secondary peak around 0.06 µm. Notably, the mixed ash mix AHL3-30-M displays a primary peak around 1 µm, mirroring the secondary peak for the fly ash mix AHL2-30-M. This suggests a higher percentage of smaller capillary pores within the range of

0.1–1 μm for NHL systems with fly ash. A similar trend is observed in the HC environment, where there is a shift of the peaks related to small capillary pores towards gel pores, typically around 0.01 μm in diameter. Notably, curing of AHL mortars in an HC environment resulted in curves with a slightly wider pore range and reduced intrusion peaks, aligning with the observation of lowered porosity achieved in the HC environment.

An observable change in the peaks related to small and medium-sized pores toward larger pore diameters is apparent in the carbonated specimens of NHL and AHL mortars. A unimodal distribution pattern is observed in both NHL 3.5-M and AHL3-30-M mixes, where the distributions feature peaks representing the highest intruded volume, surpassing a pore diameter of 1 μm. Meanwhile, the intrusion peak around 0.06 μm, which was visible in the non-carbonated AHL3-30-M mix, diminished. In contrast, the AHL2-30-M mix exhibits a bimodal distribution, featuring an intrusion peak within the range of smaller capillary pores, approximately around 0.1 μm, and a second peak around 1 μm. However, both of these observed peaks, particularly the prominent one at 1 μm found in the control mix and the mortar mix with mixed ash, show reduced intensity in the AHL2-30-M mix after carbonation.
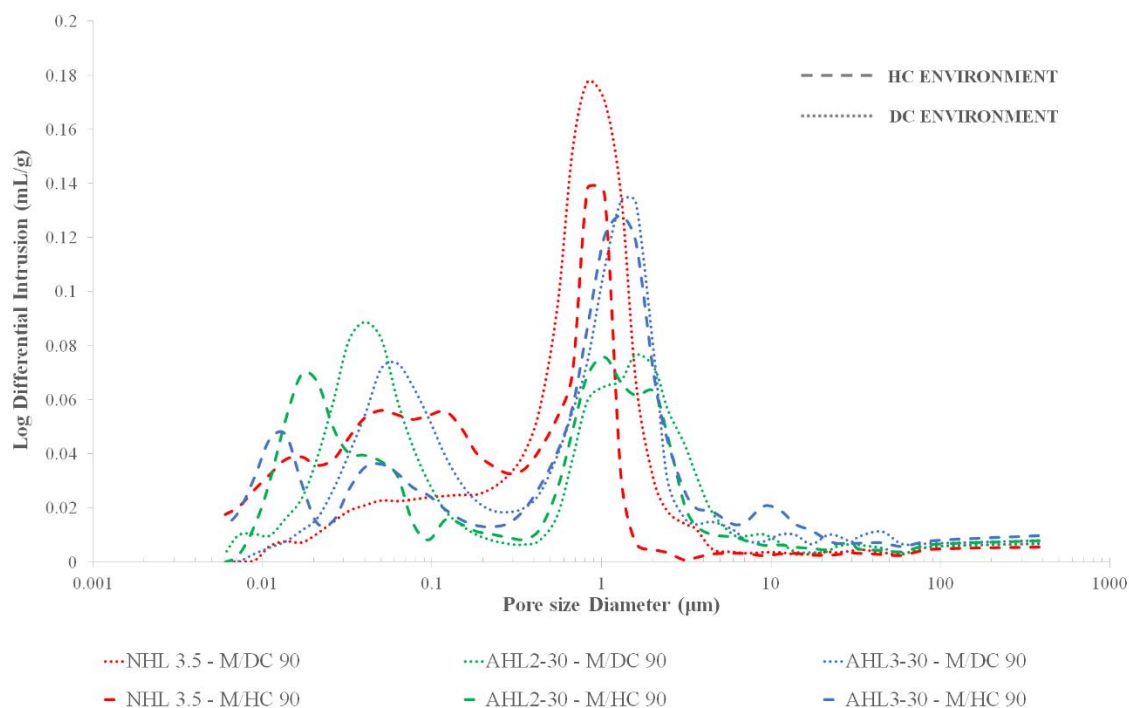

Figure 4.23. Pore size distribution in NHL 3.5 & AHL mortars with 30 wt.% WBA cured in HC and DC environments
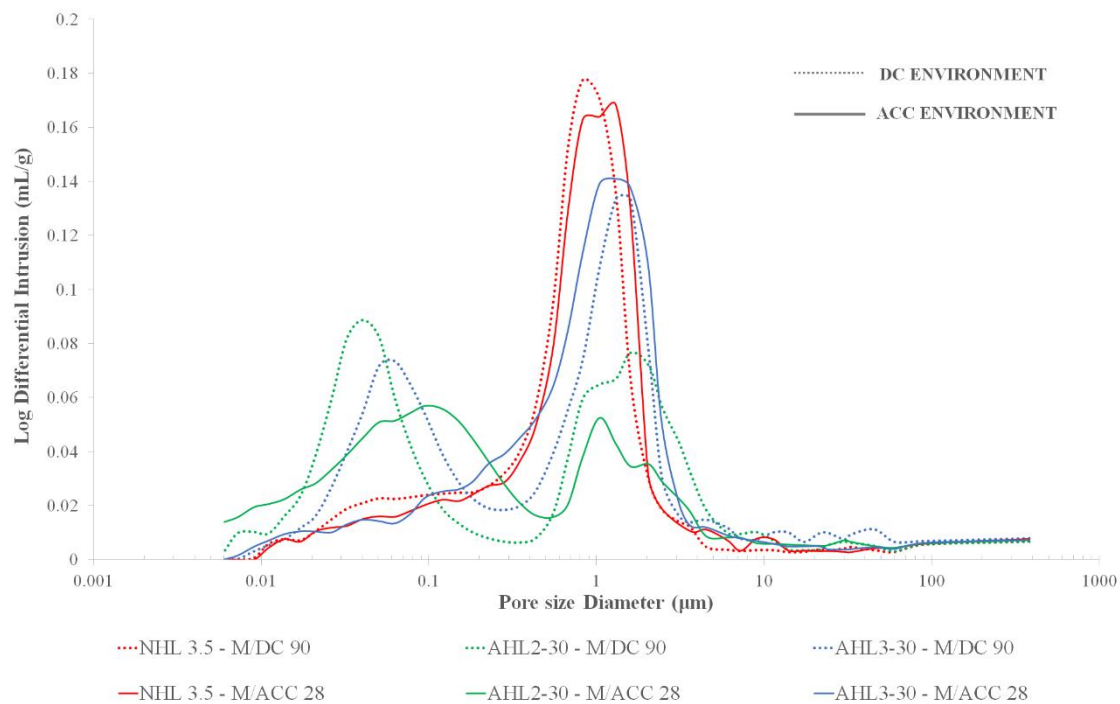
Figure 4.24. Pore size distribution in NHL 3.5 & AHL mortars with 30 wt.% WBA cured in DC and ACC environments

Mercury intrusion curves, illustrating the cumulative pore volume occupied by mercury as pressure increases, are displayed in Figure 4.25 through Figure 4.27 for samples of NHL 3.5-M and AHL mortars with 30 wt.% WBA subjected to various curing environments. The total specific pore volume represents the cumulative intrusion volume of mercury in a 1-gram sample. A higher cumulative intrusion volume indicates a material with an increased level of porosity. The variation in intruded mercury volume also mirrors the differences in pore size distribution between NHL and AHL mortars.

It is of significance to highlight that AHL2-30-M consistently exhibits a finer pore structure, as evidenced by consistently registering the lowest cumulative intruded mercury volume values across all curing environments. This distinction becomes notably pronounced, particularly in the ACC regime. Furthermore, in comparison to the control mix's higher cumulative intrusion curve, it is observed that when AHL2-30-M is subjected to HC curing conditions, a greater proportion of pores falls within the 0.1–1 μm range, while DC curing results in a greater proportion of pores exceeding 1 μm. Conversely, the pore structure of the AHL3-30-M mortar appears notably porous, emulating the behaviour exhibited by the mortar containing fly ash.
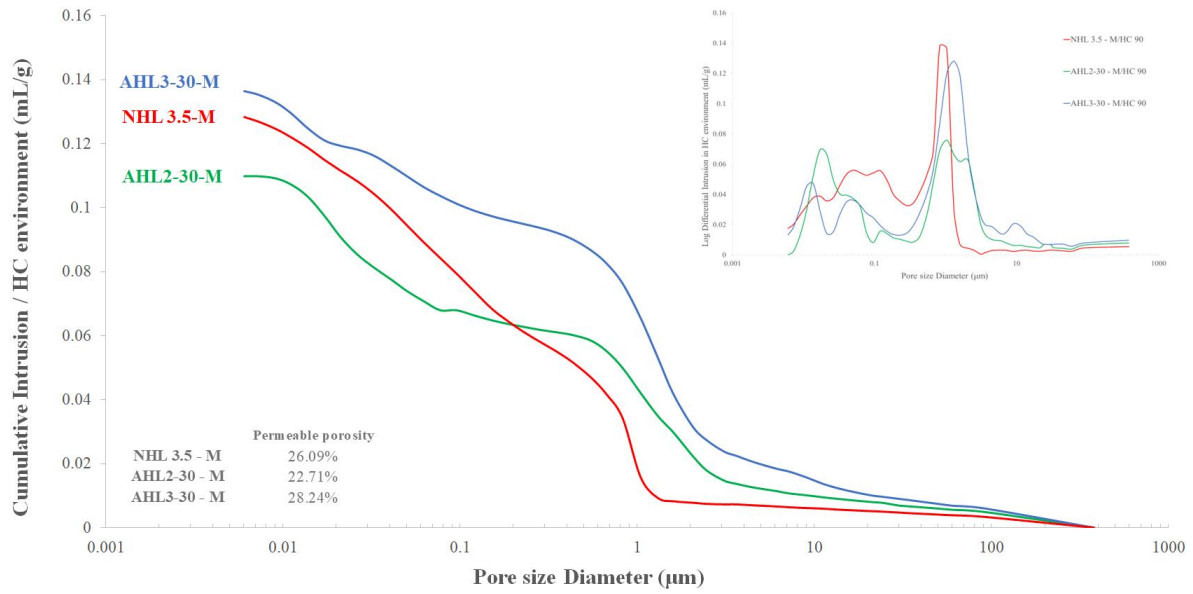
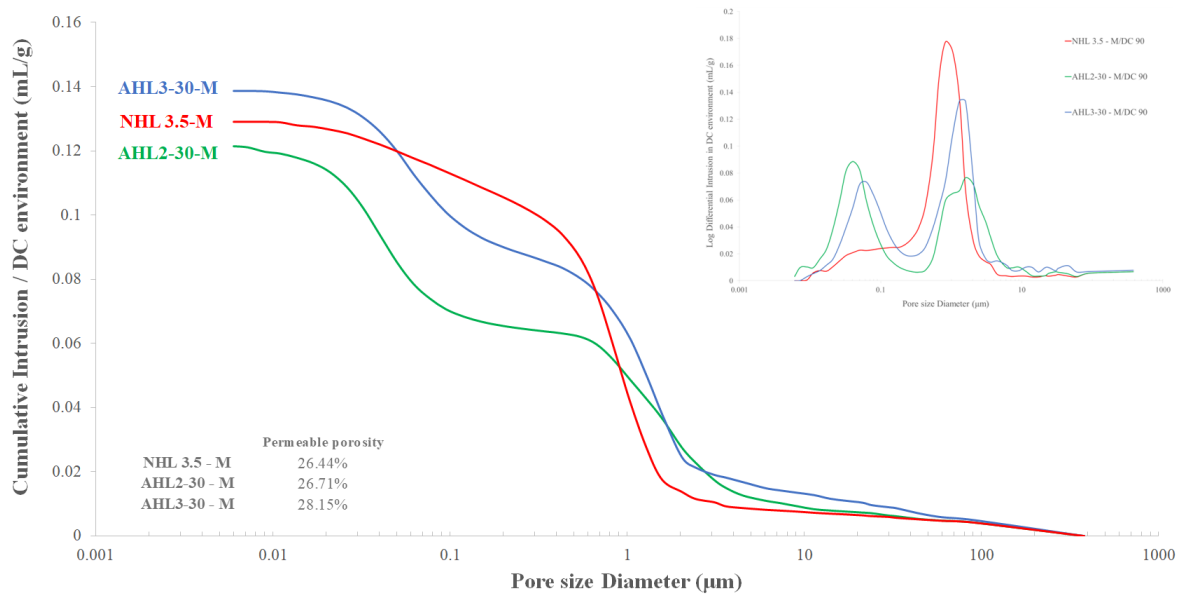**Figure 4.25.** Cumulative intrusion curves of NHL 3.5 & AHL mortars with 30 wt.% WBA cured in HC environment

Figure 4.26. Cumulative intrusion curves of NHL 3.5 & AHL mortars with 30 wt.% WBA cured in DC environment
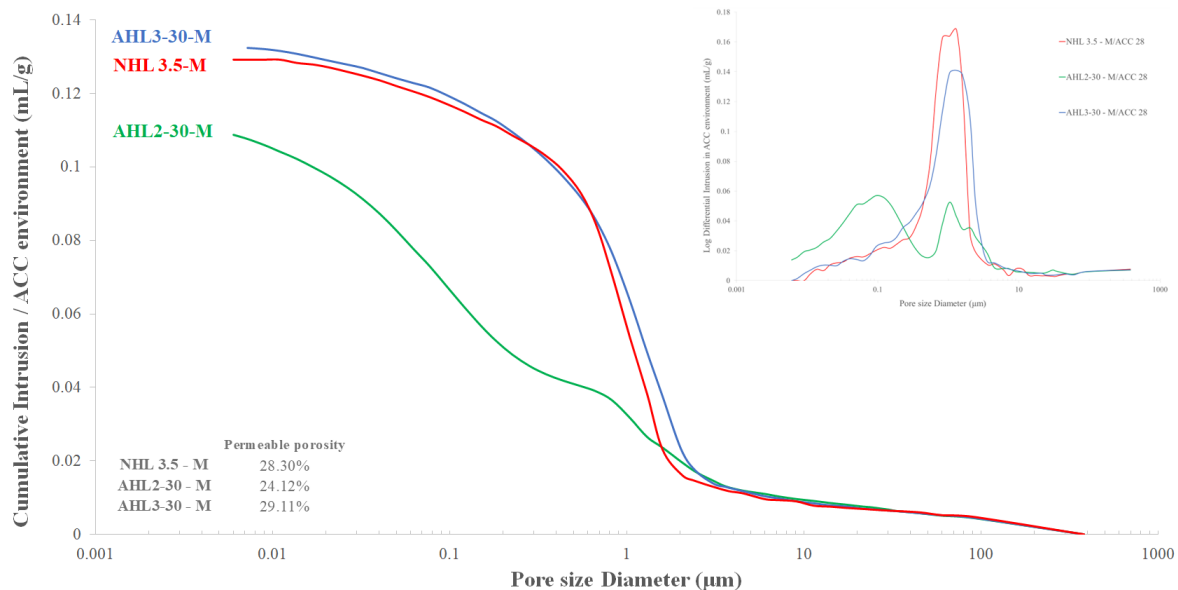
Figure 4.27. Cumulative intrusion curves of NHL 3.5 & AHL mortars with 30 wt.% WBA cured in ACC environment

Figure 4.28 depicts the pore size distribution of non-carbonated structures for the control mix NHL 5 and AHL mortars containing 40 wt.% WBA. These structures were subjected to both HC and DC environments for a duration of 90 days. Meanwhile, Figure 4.29 showcases the pore size distribution for non-carbonated structures of the same materials exposed to DC environments alongside the structures that underwent full carbonation in ACC for 28 days.

It's worth noting that the non-carbonated specimens cured in HC and DC environments exhibit a multi-modal distribution, characterized by the presence of multiple minor peaks alongside a few sharp peaks representing the primary intruded volume. Despite similarities in pore distribution between non-carbonated structures subjected to HC and DC curing, HC counter mixes show a slight shift towards smaller pore diameters. In the HC regime, the AHL 5-40-M mortar features a prominent peak around 0.4 µm, accompanied by a few secondary peaks at 0.05 up to 0.1 µm, while AHL 4-40-M displays a similar profile with a sharper peak at 0.05 µm and a secondary peak at 1 µm. The minor peaks within the range up to 0.01 µm, observed in all three mortars cured in HC, are attributed to the hydration process.

It's also noteworthy that the DC environment leads to refinement in AHL5-40-M and NHL 5-M mortars, particularly in terms of an increase in finer pores within the range up to 0.05 µm. In contrast, AHL 4-40-M exhibits a minor rightward shift of small capillary pores (up to 0.1 µm) towards medium-sized pores and a decrease in pore diameters around 1 µm, compared to the HC regime. Similarly, a noticeable shift in peak distribution from small pores toward medium-

sized pore diameters (0.01-0.1 μm) is evident in the carbonated specimens of NHL and AHL mortars. After carbonation, the major peaks become less prominent.

The cumulative intruded volume in both AHL mortar mixes surpasses that of the control mortar (Figure 4.30, Figure 4.31, Figure 4.32). AHL4-40-M consistently reveals a more porous structure, consistently recording the highest cumulative intruded mercury volume values across all curing environments. Following closely, AHL5-40-M exhibits slightly higher intruded mercury values than the control mix, while maintaining similar total porosity results. Notably, in the HC environment, AHL 5-40-M demonstrates permeable porosity exceeding that of the control mix, whereas the DC and ACC environments yield comparable results, albeit with fewer pores in the 0.1–1 μm range and an increased number of pores exceeding 2 μm.
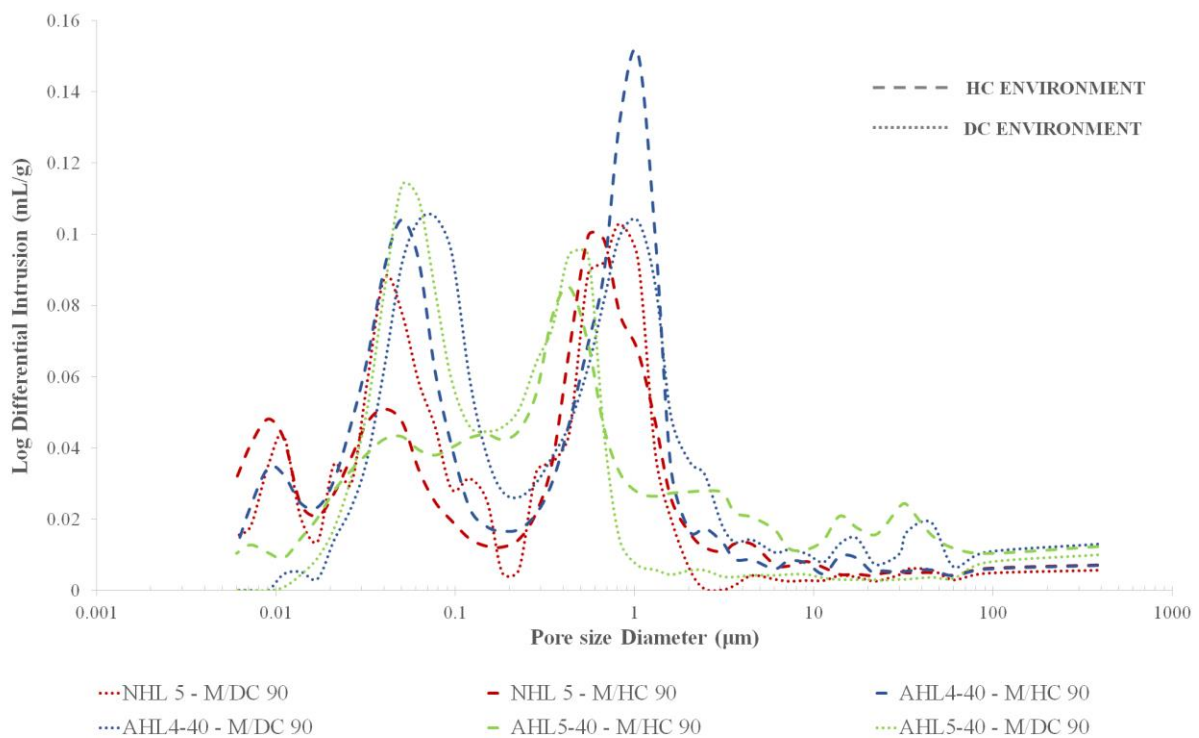

Figure 4.28. Pore size distribution in NHL 5 & AHL mortars with 40 wt.% WBA cured in HC and DC environments
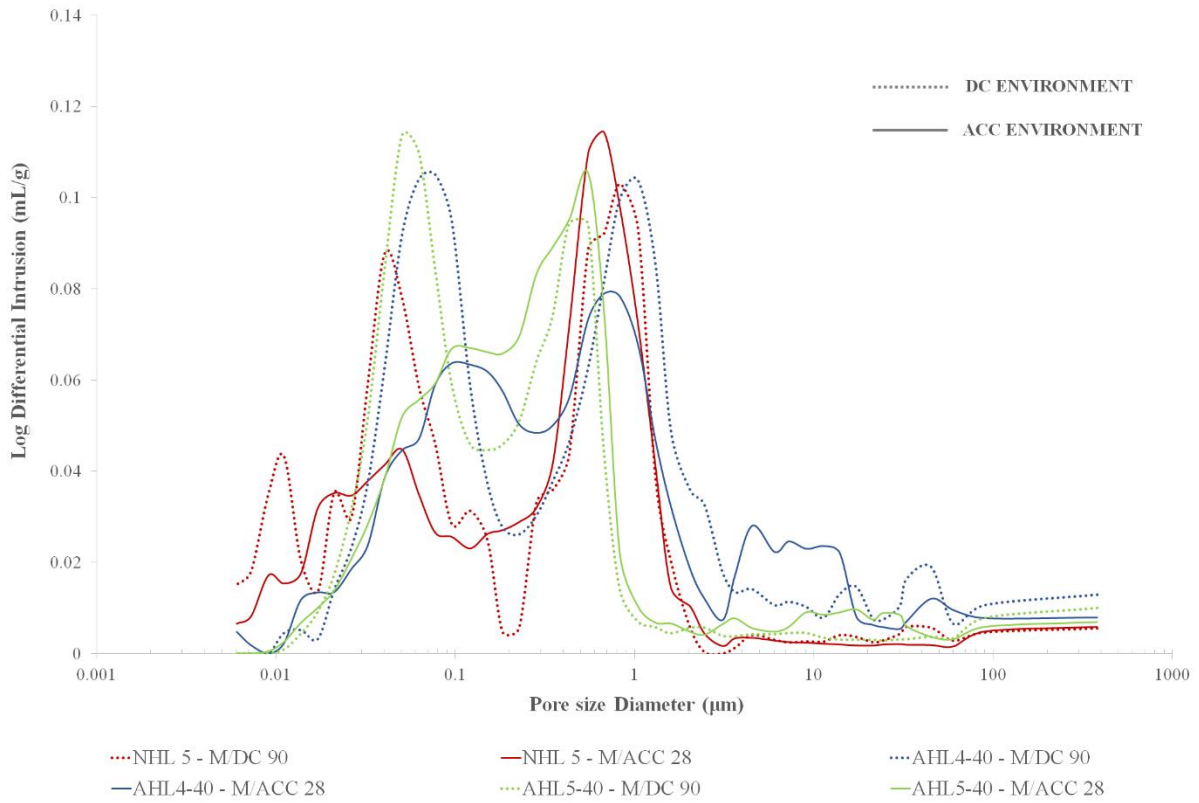
Figure 4.29. Pore size distribution in NHL 5 & AHL mortars with 40 wt.% WBA cured in DC and ACC environments
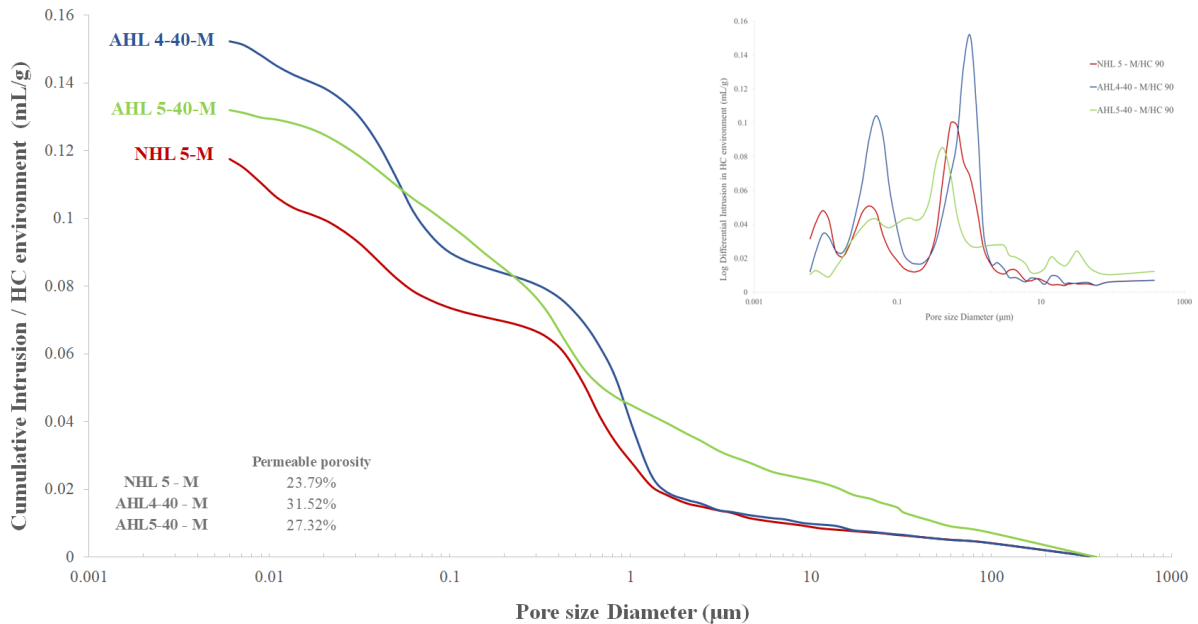

Figure 4.30. Cumulative intrusion curves of NHL 5 & AHL mortars with 40 wt.% WBA cured in HC environment
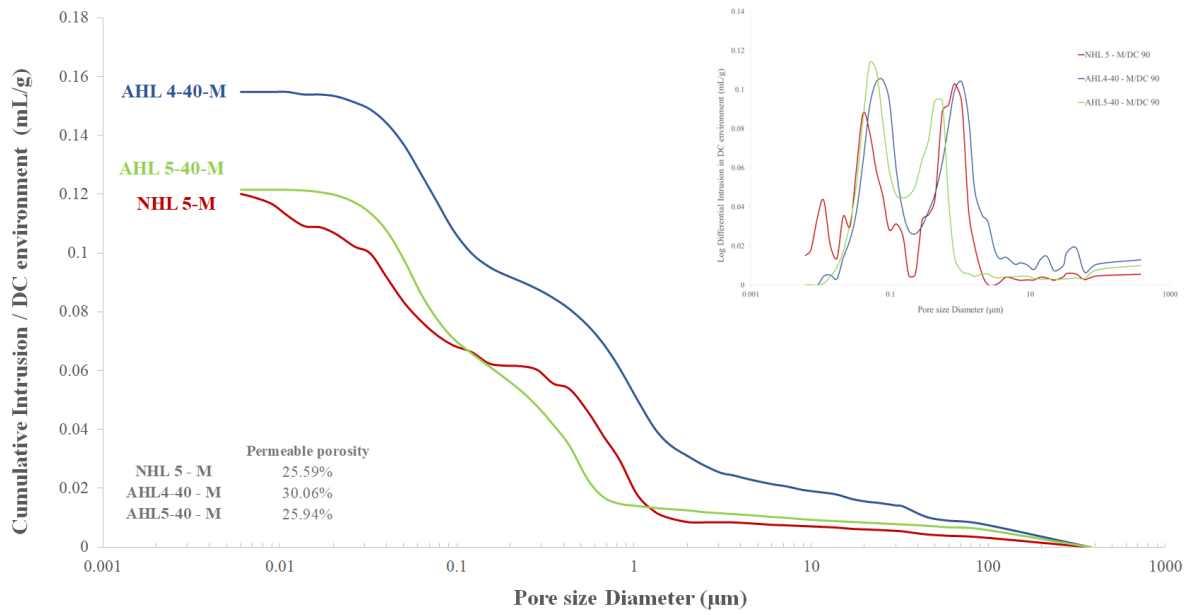
Figure 4.31. Cumulative intrusion curves of NHL 5 & AHL mortars with 40 wt.% WBA cured in DC environment

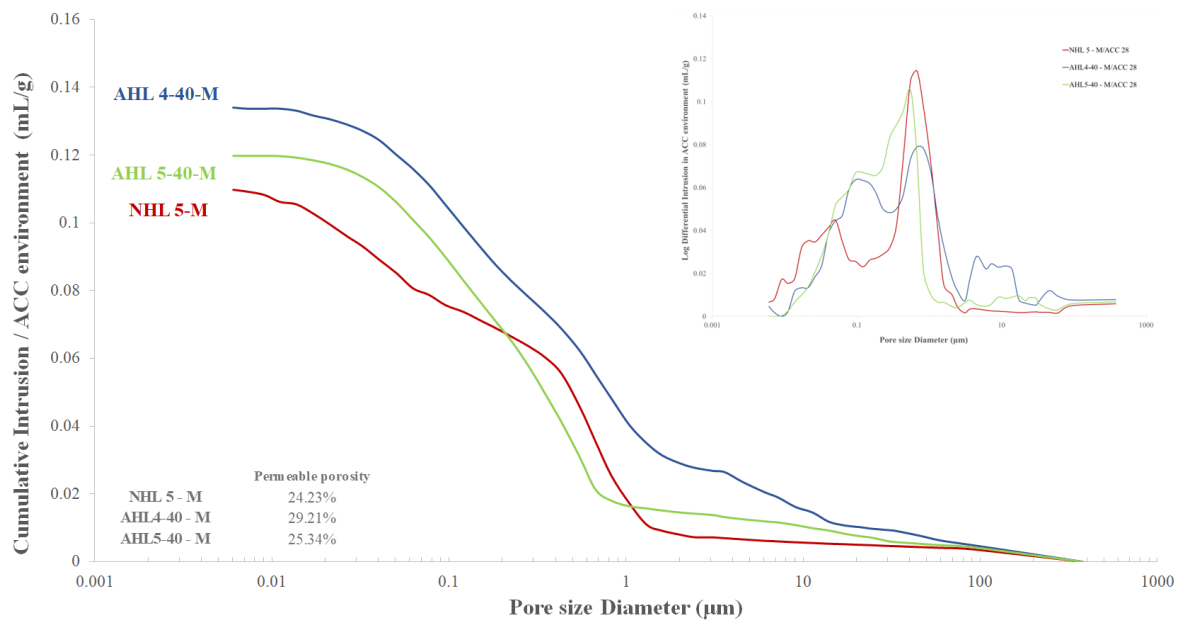**Figure 4.32.** Cumulative intrusion curves of NHL 5 & AHL mortars with 40 wt.% WBA cured in ACC environment

The relative distribution of pore volumes (%) in the studied NHL and AHL mortars is analysed within specific pore radius categories (as outlined in Table 4.19 & Table 4.20). To establish these pore radius categories, the ranges suggested by previous researchers in the context of lime mortars [78,79,160–162] were considered.

Pores with a radius measuring less than 2 μm are commonly ascribed to the binder phase. In the pore size range of 2 to 100 μm, pores within the interfacial transition zone (ITZ) are typically identified. Pores exceeding the 100 μm threshold are predominantly associated with entrapped air voids [78,162]. In all the AHL mortars examined, binder pores were found to be the prevailing type, constituting over 80% of the total, with variations depending on the specific curing regime. Pores outside this range, i.e., ITZ corresponding pores, also described as large capillary pores in the range 2-10 μm are found mainly in AHL mortars: AHL2-30-M with 11.7%, 15.7% and 9.6% share and AHL3-30-M with 13.2%, 8.4% and 11.1% share when cured in HC, DC and ACC environment. In contrast, these pores are less prevalent in the control mix NHL 3.5-M with 1.5%, 5.0% and 6.6% in HC, DC, and ACC respectively.

When examining the second binder group (as detailed in Table 4.20), with NHL 5 as the primary binder, it becomes evident that non-binder pores larger than 2 μm and up to 10 μm are more prevalent in the mortar mix containing mixed ash WBA 4, constituting 7.8% and 10.8% in samples from the DC and ACC curing regimen. In contrast, the control mixes NHL 5 and AHL 5-40 demonstrate relatively similar values in the afore mentioned DC and ACC environments, with around 2% and 3% shares. When comparing these findings to those obtained under the HC curing regime, AHL 4-40 exhibits a pore size distribution more akin to that of the control mix, with a representation of around 5%. Interestingly, AHL 5-40 displays an increase compared to the control mix within the same curing regime, as well as in comparison to its counterpart in the DC regimen.

In the context of the studied AHL mortars, a clear pattern emerges regarding the ITZ pore volume. Specifically, all AHL mortars consistently display a higher ITZ pore volume. This porosity in the ITZ is influenced by the volumetric relationship between the binder, the aggregate, and the aggregate's gradation [162]. Notably, despite the consistent binder-to-aggregate ratio and uniform grain size distribution among all investigated mortars, the elevated values observed in this pore range suggest that the ITZ undergoes a more complex transformation. This encompasses changes in the development of the pore structure and the distribution of the primary binder.

A previous study [78] identified an inverse relationship between compressive strength and the prevalence of pores within a specific pore radius range. As the pore structure shifts towards narrower pore radii, an increase in compressive strength is observed. Conversely, larger pores tend to have a detrimental impact on mechanical performance. It's important to highlight that

when the ITZ region exhibits weaker characteristics compared to the binder, it can serve as a point of weakness from which potential crack propagation may initiate. Therefore, it's worth noting that the compressive strength of AHL mortars doesn't appear to show a strong, inverse linear correlation with the relative pore volume within the pore radius range exceeding 2 μm. The nature of this relationship varies based on the type of binder, with mortars using NHL 3.5 as the primary binder displaying a more pronounced effect, particularly in harsh chemical (HC) environments. This observation could be partially attributed to the reduced hydraulicity of this binder. Despite the increased porosity of the ITZ in AHL mortars, there is no apparent correlation to the impairment in their mechanical behaviour, and no discernible presence of cracks has been detected.

The gel pores (pore radii < 0.01 μm), which are strongly associated with the formation of hydration products [78], are most prominent in the samples subjected to HC. In this view, the control NHL 3.5 – M and AHL3-30-M appear to have almost identical proportion of gel pores (4.9% and 5%) while AHL2-30-M has half the amount present in the other two samples (2.3%). This indicates that replacing 30 wt.% of NHL 3.5 with WBA2 as a secondary binder component, substantially affected the hydraulics of the binder blend. Likewise, the proportion of gel pores decreases from around 5% in the non-carbonated NHL 3.5-M and AHL3-30-M samples to totally absent in the carbonated structures, where hydration reactions are put off or even terminated by the complete carbonation of lime. When it comes to the AHL2-30-M mortar mix, it exhibited a converse behaviour with a highest 4.2% share in the sample from the ACC regime.

In the context of the second binder subgroup utilizing NHL 5, a similar pattern was observed. Gel pores were predominantly present in the samples subjected to HC curing conditions, and there was also a modest representation in the control mix cured in DC and ACC environment, accounting for approximately 6% and 3%, respectively. Upon comparing NHL5-M with NHL 3.5-M, a noticeable rise in gel pores was observed. This outcome aligns with expectations, given that gel pores are closely linked to the formation of hydration products, and NHL 5 is recognized for its heightened hydraulicity. Furthermore, as observed in the NHL 3.5 binder subgroup, the mortar incorporating fly ash exhibited a lower proportion of these pores (around 2%) in contrast to the mixture containing mixed ash (approximately 5%).

A relatively high volume of pores in the range of 0.1–1 μm is commonly associated with lime-based mortars [25]. Numerous studies have correlated pores of this size with carbonation and hydration reactions, while pores with a radius of approximately 0.5 μm are linked to the

conversion of portlandite to calcite [25,78] From this standpoint, transitioning from the control NHL 3.5 formulations to AHL mortars impacted a reduction in pore volume within the lime-characteristic 0.1–1 μm radius range, accompanied by an increase in medium capillary pores ranging from 0.01 to 0.05 μm. All AHL mortars investigated exhibited notable porosity within the lower specified pore range, particularly AHL 2-30-M. The proportion of the binder-related pores within this range (pores with radii > 0.1 μm and < 2 μm) is more pronounced in the mortar incorporating mixed ash, AHL 3-30-M, with values of 49.4%, 51.7%, and 71.0% in HC, DC, and ACC conditions, respectively, aligning closely with the control values. Conversely, the fly ash mix, AHL 2-30-M, experiences a decrease in this pore range, which subsequently impacts its hygric properties. This observation suggests a more favourable compatibility of mixed ash mortars with historic mortars, which typically exhibit the highest pore volume in the pore range of > 0.1 μm [78]. Nevertheless, pores with a radius smaller than 0.05 μm, associated with the hydration of hydraulic compounds and typically unobserved in pure aerial lime mortars, are present in both AHL2-30-M and AHL3-30-M mortars, constituting 32.8% and 19.6%, respectively, when cured in an HC environment. Pores of such dimensions are also present in the other two curing regimes with lower humidity conditions, suggesting that moderate humidity conditions facilitate hydraulic reactions and that porosity in this range in the fly ash mortar is also influenced by its inherent reactivity.

In a similar vein, Arizzi et al. [154] asserted that the existence of smaller pores, measuring up to 0.05 μm, can be attributed, on one hand, to the presence of a more permeable matrix within NHL mortar systems, and on the other hand, to the generation of a larger quantity of C-S-H. This, in turn, results in the formation of a greater volume of minuscule micro-pores.

In addition, the pore volume associated with the above-mentioned pore radius of 0.5 um, i.e., the pore range of 0.1–0.5 μm, averaged around 20% in the non-carbonated NHL 3.5 samples, while the AHL mixes reached these values only at ACC environment, by increasing in regard to HC for 13% and 10%, respectively, for the carbonated specimen from the AHL2-30, and AHL3-30 mixes, which is consistent with the fully carbonated structure. The presence of a substantial 20% portion within this pore range, associated with the conversion of portlandite to calcite, in the non-carbonated NHL 3.5-M structures appears contradictory to its association with the portlandite-to-calcite conversion. While this is the predominant pore range in all carbonated specimens and reveals larger pores in the carbonated structure of the AHL mortars, the range of 0.01–0.05 μm is the prevailing one in the non-carbonated structure fly ash mix.

Conversely, the mixed ash mortar AHL 3-30-M, exhibits a coarser pores structure with the 1-2 μm pore range prevailing.

In the context of the second binder subgroup utilizing NHL 5, transitioning from the control NHL 5 formulations to AHL mortars slightly impacted a reduction in pore volume within the lime-characteristic 0.1–1 μm radius range, in average 7% regarding the AHL4-40-M mixed ash mix, accompanied by an increase in large capillary pores ranging from 0.05 – 0.1 μm. The fly ash AHL mortar designated AHL5-40-M showcases results almost identical as the control NHL 5-M values across all curing regimes. The latter mortar also shows an increase in the 0.1-0.5 um pore range, whereas it double folds the NHL5 and AHL 4-40-M values. Pores with a radius smaller than 0.05 μm, associated with the hydration of hydraulic, are present in both AHL4-40-M and AHL5-40-M mortars, constituting 26.4% and 16.8%, respectively, when cured in an HC environment, showcasing inverse results when compared to the mortars from the lower hydraulicity grade, whereas the mixed ash favours the mentioned pore range.

Table 4.19. Distribution of relative pore volume (%) in different ranges of pore radius for NHL 3.5 & AHL mortars with 30 wt.% WBA cured in HC, DC and ACC env.

Pore classification	Pore size	HC curing			DC curing			ACC curing		
	μm	NHL 3.5 - M	AHL2-30 - M	AHL3-30 - M	NHL 3.5 - M	AHL2-30 - M	AHL3-30 - M	NHL 3.5 - M	AHL2-30 - M	AHL3-30 -M
Gel capillaries	< 0.01	4.9%	2.3%	5.0%	0.1%	1.9%	0.4%	0.0%	4.2%	0.6%
Medium c.	0.01-0.05	21.7%	30.5%	14.6%	7.0%	27.9%	13.2%	5.6%	19.8%	5.6%
Large capillary pores	0.05-0.1	16.0%	6.9%	7.8%	6.8%	13.9%	17.1%	5.4%	19.0%	5.2%
	0.1-0.5	21.0%	7.2%	9.1%	19.2%	5.2%	11.6%	17.2%	19.9%	19.3%
	0.5-1	24.2%	14.8%	15.5%	34.3%	11.0%	13.5%	30.4%	8.0%	21.1%
	1-2	6.1%	18.0%	24.9%	21.9%	17.5%	26.6%	28.8%	11.1%	30.7%
	2-10	1.5%	11.7%	13.2%	5.0%	15.7%	8.4%	6.6%	9.6%	11.1%
Non-capillaries	> 10	4.6%	8.6%	10.0%	5.6%	6.9%	9.2%	6.1%	8.4%	6.4%
	Total	*100%*	*100%*	*100%*	*100%*	*100%*	*100%*	*100%*	*100%*	*100%*

Table 4.20. Distribution of relative pore volume (%) in different ranges of pore radius for NHL 5 & AHL mortars with 40 wt.% WBA cured in HC, DC and ACC env.

Pore classification	Pore size	HC curing			DC curing			ACC curing		
	μm	NHL 5 - M	AHL4-40 - M	AHL5-40 - M	NHL 5 - M	AHL4-40 - M	AHL5-40 - M	NHL 5 - M	AHL4-40 - M	AHL5-40 - M
Gel capillaries	< 0.01	9.7%	4.8%	2.1%	6.1%	0.0%	0.0%	3.2%	0.2%	0.1%
Medium c.	0.01-0.05	20.2%	21.5%	14.7%	24.6%	11.7%	19.7%	19.2%	10.2%	11.4%
Large capillaries	0.05-0.1	8.6%	16.1%	11.5%	13.9%	23.7%	26.1%	10.4%	15.9%	19.3%
	0.1-0.5	18.0%	12.1%	29.5%	17.0%	15.9%	35.4%	25.8%	27.4%	43.7%
	0.5-1	20.4%	20.8%	8.5%	23.3%	16.1%	7.3%	25.5%	16.2%	11.9%
	1-2	9.6%	13.6%	6.1%	7.9%	12.7%	1.3%	8.6%	8.5%	1.5%
	2-10	6.3%	4.8%	11.0%	1.3%	7.8%	2.8%	2.2%	10.8%	3.9%
Non-capillaries	> 10	7.2%	6.3%	16.7%	5.8%	12.1%	7.6%	5.0%	10.8%	8.3%
	Total	*100.0%*	*100.0%*	*100.0%*	*100%*	*100%*	*100%*	*100%*	*0%*	*0%*

4.3.6. Assessment of hygrothermal properties

This investigation was aimed to assess the influence of WBAs on hygrothermal performance of NHL mortars under diverse humidity conditions. Hygrothermal behaviour of AHL mortars was evaluated with regard to the curing regimen. Specimens of AHL mortars, containing NHL 3.5 as the primary binder at levels of 20 wt.% and 30 wt.% WBA, underwent testing following exposure to a controlled DC environment for either 28 or 90 days. Similarly, NHL 5-M and AHL mortars with 40 wt.% WBA, were evaluated after curing in a HC environment. Alongside the designated primary curing environments for specific binder groups, capillary uptake was examined across various humidity levels (both HC and DC curing regimes) and at different ages (28 and 90 days).

In addition to the evaluation of capillary water absorption, other hygrothermal properties underwent testing, including assessments of water vapor permeability and thermal conductivity. In conjunction with the collected numerical data, a discernible trend emerged in the hygrothermal characteristics of AHL mortars when compared with the corresponding control mixes, all of which are presented in Table 4.21 and Table 4.22.

While assessing the capillary water absorption for NHL 3.5-M and AHL mortars with NHL 3.5 as the primary binder over time, a modest increase in the values of capillary water absorption coefficient is observed. In this context, the mortars with a 20 wt.% WBA demonstrated values that closely resembled the control values. Specifically, AHL1-20-M, as the 20 wt.% AHL mortar mix displaying the lowest capillary uptake, demonstrated absorption coefficients of 0.91 kg/m²√min and 0.98 kg/m²√min after 28 and 90 days of curing, respectively. These values denote a reduction of 14% and 13% over the respective time periods. Furthermore, the 30 wt.% counter mix AHL 1-30-M displayed modestly increased yet comparable values, measuring 1.04 kg/m²√min after the 90-day curing period. A consistent trend is observed in the capillary water absorption coefficient concerning the control NHL 3.5-M mix: mortars with a lower 20 wt.% hybridization ratio exhibit marginally reduced, closely aligned to the control values, while those with the higher 30 wt.% hybridization ratio display a more notable cut. The trend of decreased values is particularly evident in the mortars with mixed ashes (AHL3-30-M and AHL4-30-M), where the capillary water absorption coefficient after 90 days amounts to 0.85 kg/m²√min and 0.79 kg/m²√min, respectively. Fusade et al. [163] reported similar findings, highlighting that WBA exhibits hygroscopic properties, enhancing lime mortars' water retention capacity and consequently delaying capillary absorption. The AHL2-3-M mortar mix stands out as an outlier,

displaying exceptionally low values of 0.20 and 0.17 kg/m²√min after 28 and 90 days, respectively. Such lowered values correspond to cement mortars, rather than lime mortars. The visual disparity in capillary water uptake between mortar halves observed after 90 minutes, following a 90-day curing period in a DC environment, is presented in Figure 4.33. Complete saturation is evident in the control NHL 3.5-M sample, while a noticeable contrast is observed between the fly and mixed mortars. In AHL 2-30-M, water uptake reached approximately 1 cm, whereas in AHL 3-30-M, it extended to about 2/3 of the mortar half's height, approximately 6 cm.

Table 4.21. Hygro-thermal properties of NHL 3.5 & AHL mortars with 30 wt.% WBA cured in DC environment

Mix ID	capillary water absorption coefficient, C kg/m²√min			water vapor permeance, Λ (kg/m²·s·Pa) · 10⁻¹⁰		water vapor diffusion resistance factor, μ -	thermal conductivity, λ W/m·K	
	28 days	90 days	Trend	90 days	Trend	90 days	90 days	Trend
NHL 3.5-M	1.06	1.13	-	13.88		7.52	0.72	
AHL1-20-M	0.91	0.98	▼	27.53	▲	3.94		
AHL2-20-M	1.01	1.07	▼	19.60	▲	5.47	n/a	-
AHL3-20-M	1.00	1.03	▼	12.66	►	8.23		
AHL4-20-M	0.74	1.03	▼	29.00	▲	3.84		
AHL1-30-M	0.88	1.04	▼	24.91	▲	4.33	0.80	▲
AHL2-30-M	0.20	0.17	▼ ▼	22.50	▲	4.96	0.76	▲
AHL3-30-M	0.71	0.85	▼	15.17	▲	6.81	0.69	►
AHL4-30-M	0.82	0.79	▼	24.53	▲	4.30	0.71	►

Trend legend: ► constant; ▲ increase; ▼ decrease

Cured in DC
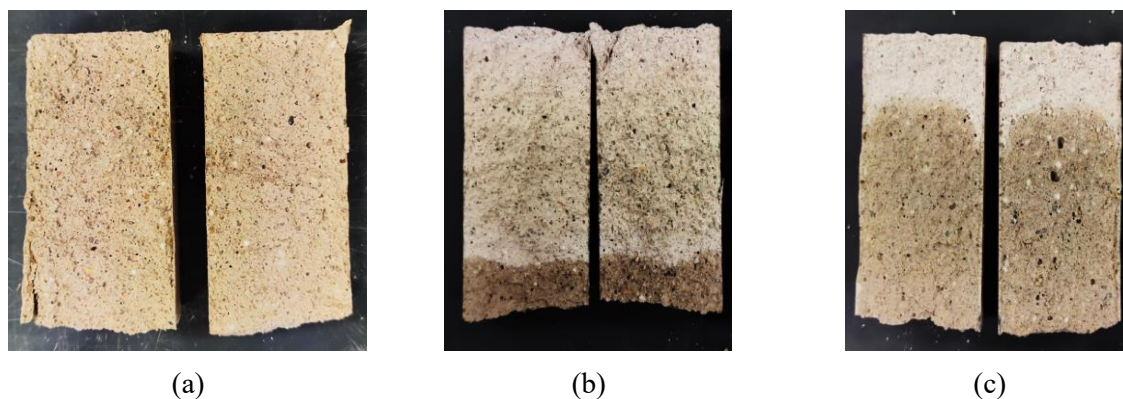

(a)   (b)   (c)

Figure 4.33. Capillary uptake in mortar halves after 90 minutes, following a 90-day curing period in a DC environment: (a) NHL 3.5-M; (b) AHL2-30-M; (c) AHL3-30-M

A simple linear regression analysis was employed to evaluate the capillary water absorption process after 28 and 90 days of curing in a DC environment. This assessment involved tracking the change in mass (kg/m^2) over specified time intervals. The investigation into the kinetics of capillary rise, as illustrated in Figure 4.34 and Figure 4.35, unveiled distinct initial and secondary uptake phases, with a transitional period occurring between the 1st and 5th minute of testing.

During the initial uptake phase within the first minute, there was a sharp increase in absorption, followed by a brief 5-minute transition period characterized by a reduced flow rate. Subsequently, a secondary flow phase exhibited another steep rise in absorption. Notably, AHL mortar mixtures displayed a more pronounced transition period, indicating a reduced absorption rate. This observation was reinforced by the shape of the capillary imbibition curves, whereas the control NHL 3.5-M mortar displays the steepest slope as well as the highest values of capillary absorption coefficient. In comparison to control mortar samples, the water flow did not reach the top of the AHL mortar samples. This difference can be attributed to the varying porosity and constraints inherent in each system.

The AHL2-30-M sample exhibits a gentle slope in its mass increase over time, which corresponds to its characteristic pore distribution. This behaviour can be associated to the higher pore volume within the range of medium capillary pores (0.01-0.05 μm) and a relatively substantial volume of pores within the large capillary range (2-10 μm). The coexistence of large pores with low capillary suction, along with the presence of fine pores exhibiting slower capillary absorption, results in an overall capillary absorption pattern that does not follow a simple t$^{1/2}$ kinetics, as acknowledged by [164]. Moreover, the pores with a radius smaller than 0.05 μm are termed 'sorption pores' and are typically not considered to actively participate in water transfer reactions [78].
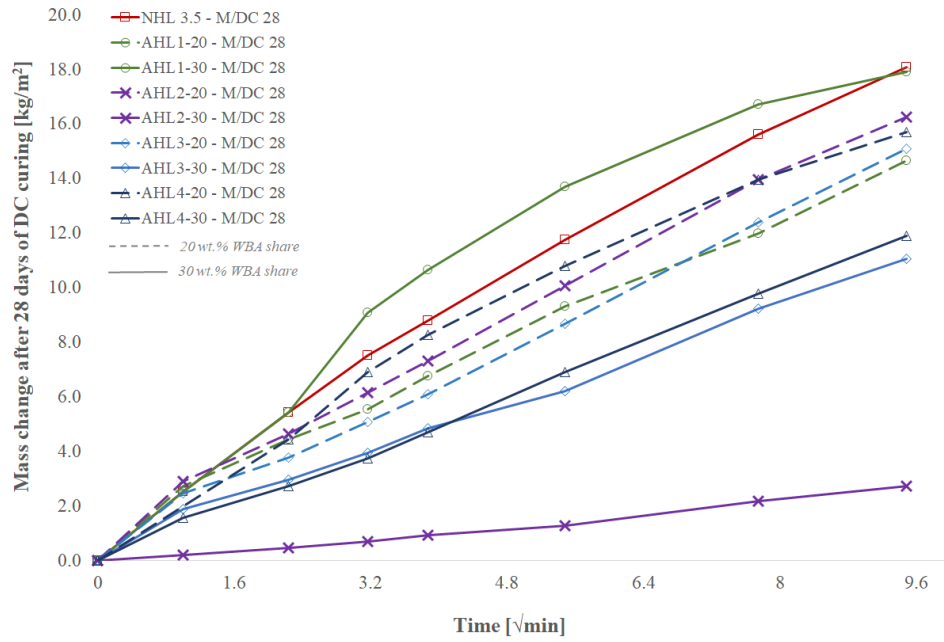
Figure 4.34. Time-dependent capillary water absorption of NHL 3.5 and AHL mortars containing 20 & 30 wt.% WBA, following a 28-day curing period in a DC environment
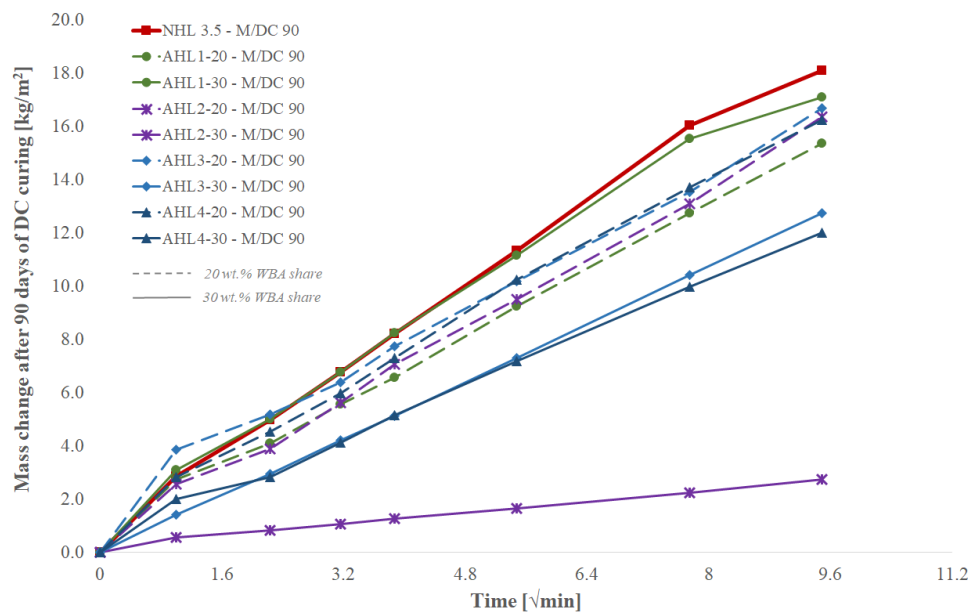

Figure 4.35. Time-dependent capillary water absorption of NHL 3.5 and AHL mortars containing 20 & 30 wt.% WBA, following a 90-day curing period in a DC environment

Examining capillary water absorption in NHL 5-M and AHL mortars with NHL 5 as the primary binder over time reveals a consistent trend. The capillary water absorption coefficient shows a steady decrease between the 28 and 90-day marks. When analysing the data over this specific time period, the decrease is most pronounced for the control mortar NHL 5-M. Despite a slight decrease in the absorption coefficient over time, AHL 5-40-M mortar stands out with a significant reduction of capillary absorption coefficient values compared to the control mortar as well as the AHL mortar with mixed ash. The disparity between AHL4-40-M is somewhat smaller, yet AHL mortar mixes demonstrate a decreasing trend in capillary water absorption compared to the NHL 5-M control mix. It is important to emphasize that the curing process had no significant influence on these results. Figure 4.36 illustrates the visible difference in capillary water absorption between the mortar halves observed at 90 minutes after a 90-day curing period in an HC environment. It is worth noting that none of the samples reached complete saturation and that there is a noticeable contrast between the mortars containing fly ash and the mixed ash. In the case of AHL 4-40-M, water uptake reached about 5 cm, while in the case of AHL 5-40-M, it is reduced to around one-third of the mortar half, i.e., about 3 cm.

Table 4.22. Hygro-thermal properties of NHL 5 & AHL mortars with 40 wt.% WBA cured in DC and/or HC environment

Mix ID	CE	capillary water absorption coefficient, C			water vapor permeance, Λ		water vapor diffusion resistance factor, μ		thermal conductivity, λ	
		kg/m²√min			kg/m²·s·Pa · 10^{10}		-		W/m·K	
		28 days	90 days	Trend	90 days	Trend	90 days	Trend	90 days	Trend
NHL 5 - M	HC	0.81	0.61	▼	2.42	-	40.26	-	0.94	-
	DC	0.74	0.50	▼			n/a			
AHL 4-40 - M	HC	0.61	0.51	▼	6.41	▲	15.72	▼	0.82	▼
	DC	0.62	0.45	▼			n/a			
AHL 5-40 - M	HC	0.36	0.31	▼	2.38	►	40.81	►	0.94	►
	DC	0.39	0.34	▼			n/a			

Trend legend: ► constant; ▲ increase; ▼ decrease
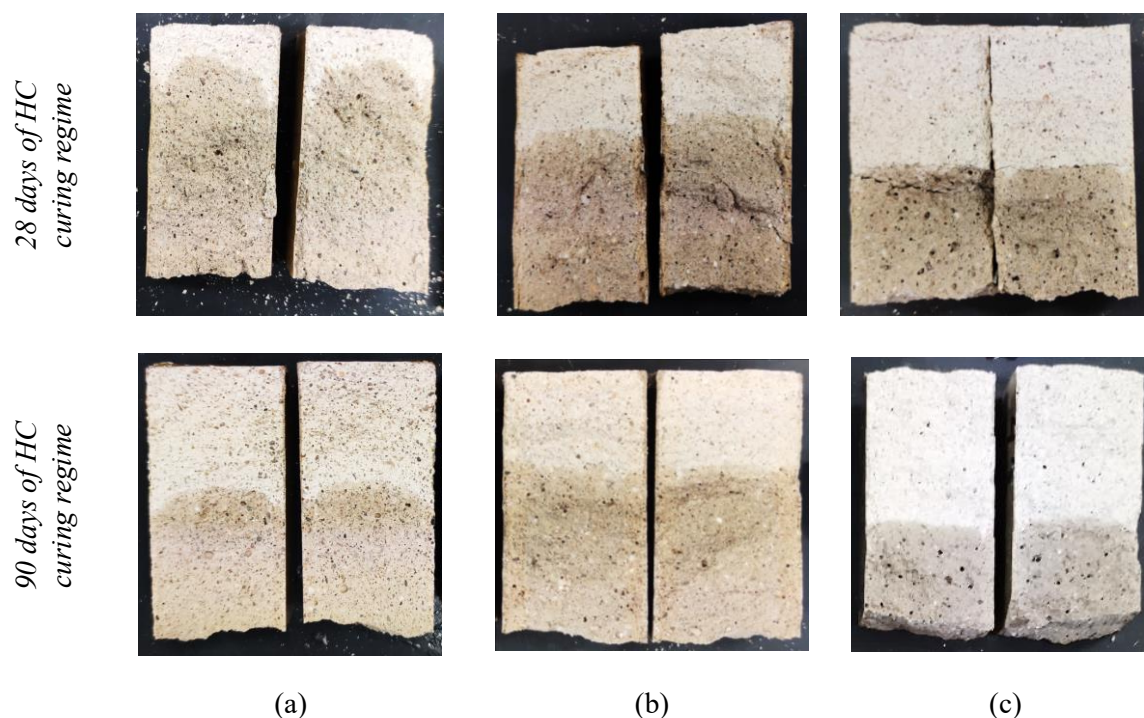
| Cured in DC | Cured in HC |

Figure 4.36. Capillary uptake in mortar halves after 90 minutes, following a 28 & 90-day curing period in a HC environment: (a) NHL 5-M; (b) AHL4-40-M; (c) AHL5-40-M

The study of capillary rise kinetics in mortars, with NHL 5 as the primary binder, after 28 and 90 days of curing in a DC environment, as depicted in Figure 4.37 and Figure 4.38, revealed behaviour similar to the mixes containing NHL 3.5. This behaviour includes distinct initial and secondary uptake phases, with a transitional period occurring between the 1st and 5th minute of testing. Interestingly, the curves of NHL 5-M, in relation to HC curing, displayed a steeper slope compared to the DC curing regime, indicating an increased absorption rate. In contrast, the AHL4-40-M sample exhibited a gentler slope in its mass increase over time, which is not consistent with its elevated porosity. In the case of NHL5-40-M, the steepest slope is observed, indicating quite different capillary kinetics compared to NHL 5-M and AHL 4-40-M, where a relatively comparable behaviour trend can be established. Again, the permeable porosity values are inversely proportional to the capillary uptake, which is more evident in the HC environment, while AHL 5-40-M has a permeable porosity of 27.32% and the control mortar of 23.79%. This behaviour can be attributed to the higher volume of pores with a diameter less than 0.1 µm, particularly in the range of 0.05-0.1 µm, and a relatively substantial volume of pores within the large capillary range (2-10 µm). To clarify, porosity ranging from 0.1 to 100 µm is typically associated with capillary pores and contributes to capillary water transfer, while porosity smaller than 0.1 µm is linked to the presence of sorption pores. In sorption pores, water is retained on the surface without being transported as moisture. Sorption pores are primarily due

to the presence of hydrated hydraulic phases such as CSH (calcium silicate hydrate) in mortars [165]. This is even more emphasised in the DC environment, where the aforementioned pore ranges significantly surpass the control mix.
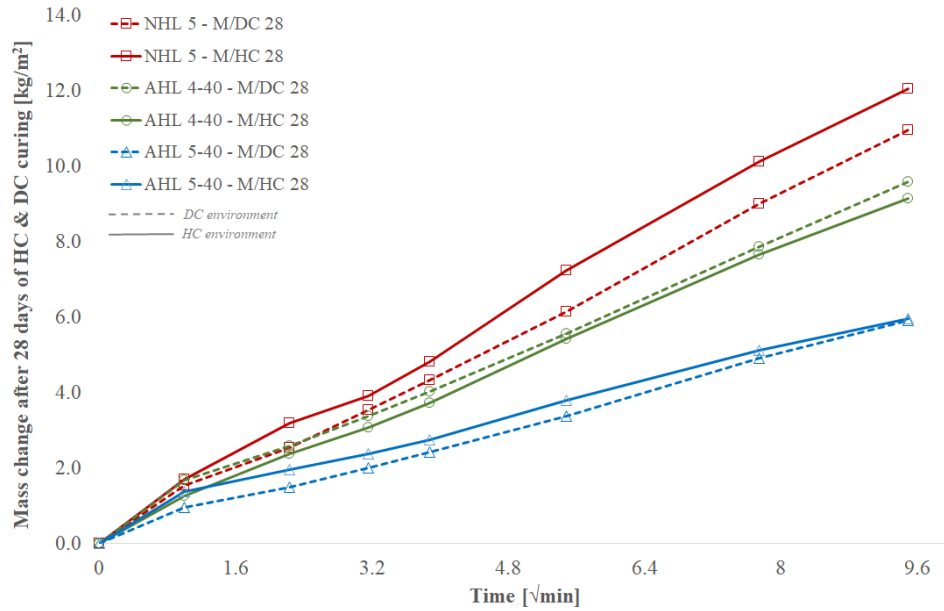

Figure 4.37. Time-dependent capillary water absorption of NHL 5 and AHL mortars containing 40 wt.% WBA, following a 28-day curing period in HC & DC environment
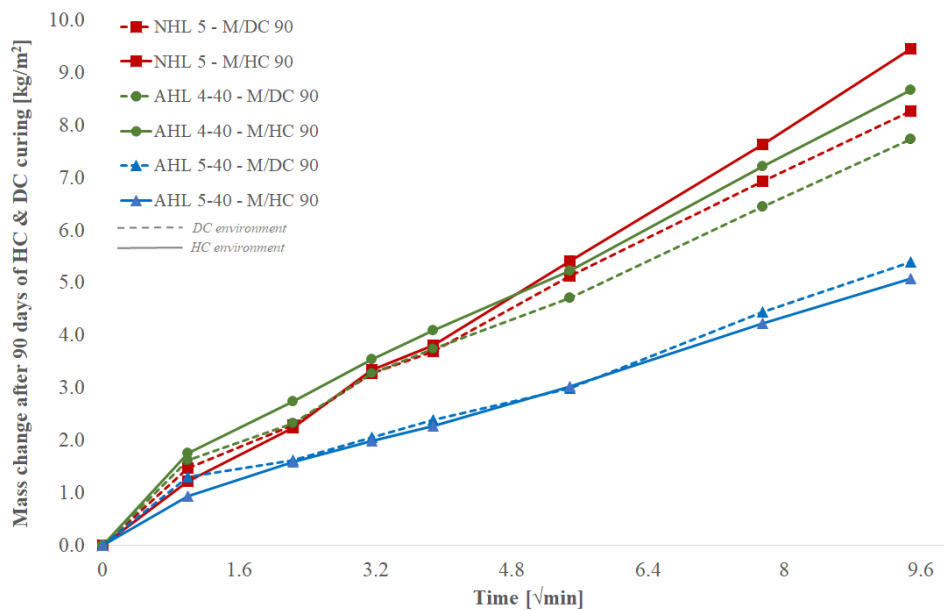

Figure 4.38. Time-dependent capillary water absorption of NHL 5 and AHL mortars containing 40 wt.% WBA, following a 90-day curing period in HC & DC environment

Furthermore, Table 4.21 presents data on the average water vapor permeance (Λ) and the corresponding water vapor diffusion resistance factor (μ) for NHL 3.5-M and AHL mortars containing 30 wt.% WBA. It also encompasses an observed behavioural trend of NHL-WBA systems in relation to the control NHL points. In this context, AHL mortars exhibited higher water vapor permeance values, resulting in inversely decreased μ values as opposed to the control mortar. This suggests that AHL mortars display higher permeability, with a discreet impact from the increased WBA hybridization ratio leading to increased resistance. Notably, the AHL 3-30-M mixture closely matched the values of NHL 3.5-M in both hybridization ratios, differing by only ±10%. Other mortars had approximately 40% lower permeability. Interestingly, the outlier AHL2-30-M did not follow the trend observed in capillary uptake. It is essential to mention that both the EN 998-1 standard [33] and the WTA directive 2-9-04/D (cited by Pavlíková et al. [166]) define a limit for water vapor permeability. This requirement stipulates a water vapor resistance factor μ <15 and <12, respectively, for renovation mortars intended for use on moist masonry walls containing water-soluble salts. Importantly, both NHL and AHL mortars met these criteria, favouring AHLs compatibility with permeable historical mortars. Based on the data obtained, AHL mortar systems can be considered highly permeable to water vapor, aiding in the drying of moist masonry and improving the hygrothermal condition of the repaired structure. Comparable high water vapor transmission rates have been reported by Ranesi et al. [65] and Banfill et al. [167]. In contrast, NHL 5-containing mortars with higher hydraulicity demonstrated significantly lower water vapor permeability (refer to Table 4.22). Both NHL 5-M and AHL 5-40-M had μ values of around 40, aligning more closely with cement mortars, which is presumed due to their high hydraulicity. On the contrary, AHL4-40-M demonstrated a μ value of 16, surpassing the upper limits prescribed for renovation mortars, yet experiencing a reduction of over fifty percent compared to the previous two cases. Although mortars containing NHL 5 as the primary binder displayed higher resistance to water vapor transport, limiting their use in highly moist masonry, they can still be considered vapor-permeable. They may find applications in new construction or in repairing cement-lime mortars when the risk of moisture-induced damage is low. The observed trend of increasing resistance as the critical pore size decreases is consistent with the permeability results, highlighting that pore structure, rather than the total porosity, is the primary factor to consider when assessing permeability.

The surface condition of mortar discs before and after the water vapor diffusion test (as indicated in Figure 4.39 and Figure 4.40) serves as an indicator of the differences in water vapor

permeance between the two binder groups. In this context, the specimens from the first group, which incorporate NHL 3.5 as the primary binder, exhibit the presence of a crystallized salt layer on their outer surface. This layer suggests higher permeability compared to the NHL 5 group, where no salt deposits were observed upon the completion of the testing. It can be inferred that an increase in the hydraulicity of the primary binder leads to higher resistance to water vapor diffusion.
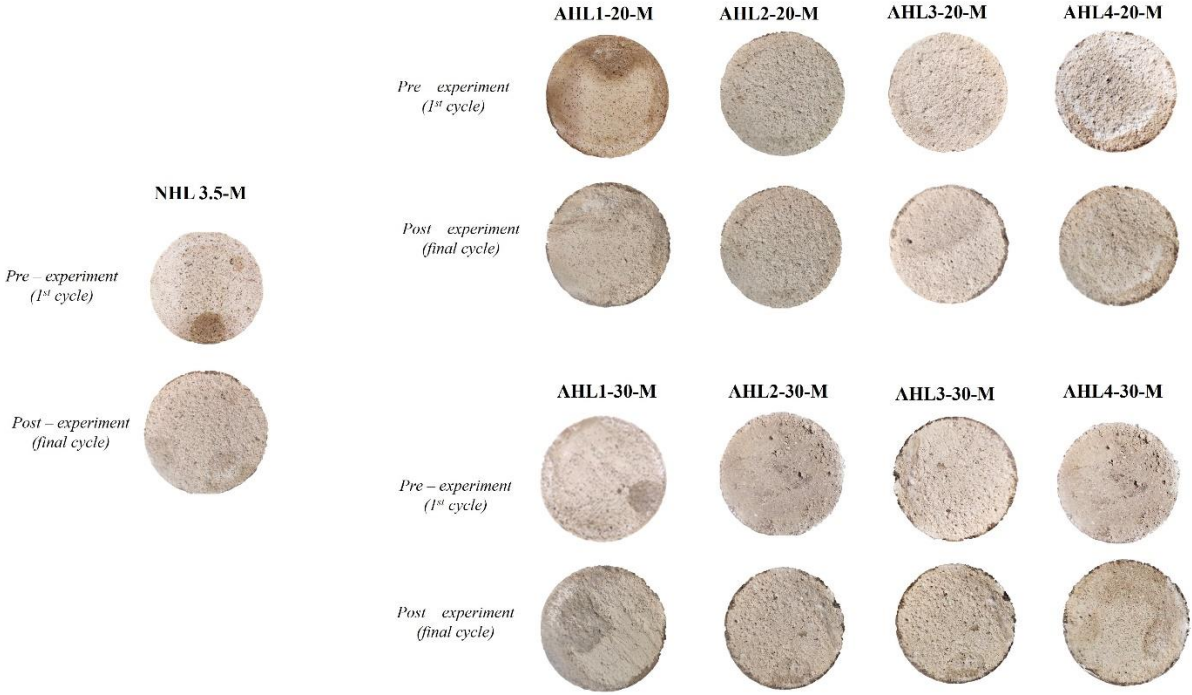

Figure 4.39. Surface condition of NHL 3.5 and AHL mortar with 20 & 30 wt.% discs before and after a water vapor diffusion test
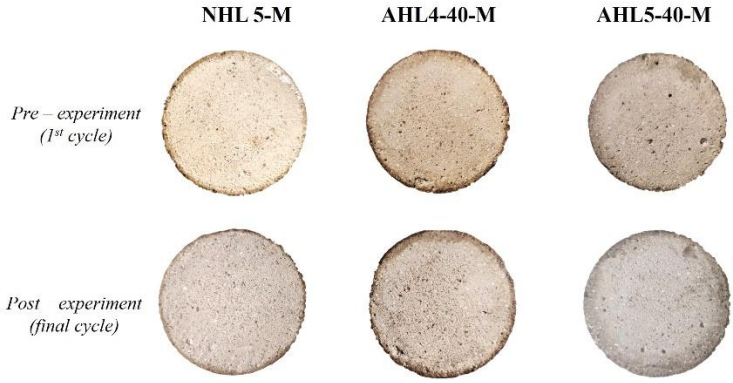

Figure 4.40. Surface condition of NHL 5 and AHL mortar with 40 wt.% discs before and after a water vapor diffusion test

Regarding thermal performance assessment, it can be stated that the λ values of AHL mortars remained largely unaffected with mixed ashes, and in the case of fly ash, they increased slightly. This minor increase, around 8%, indicates a marginal deterioration of thermal properties, suggesting that the higher WBA hybridization ratio did not significantly impact the thermal conductivity of NHL mortars. Mortars containing NHL 5 as the primary binder exhibited slightly higher λ values, approximately 0.9 W/m·K in NHL5-M and AHL5-40, and 0.8 in AHL4-40-M, indicating a positive effect of incorporating mixed ashes. This observation can be linked to the comparable permeable porosity values of the former (25%) and slightly higher porosity of the latter (30%).

4.3.7. Assessment of durability performance

Expanding upon the investigation into hygric properties closely linked to durability performance, additional durability properties of AHL mortars were studied through bond strength, resistance to freeze/thaw cycles, and susceptibility to sulphate attack.

4.3.7.1. Bond strength

Adhesive bond strength (pull-off) assessments were conducted after a 28-day period of curing in DC and HC environment, in accordance with the standards delineated in EN 1015-12:2000 [143]. The specimen with NHL 3.5 as the primary binder were exposed to DC and the specimen with NHL 5 as the primary binder were subjected do HC curing regime. Twelve different mortar slabs, i.e., 100 the pull-off tests were undertaken on plastered refractory brick substrate to assess the bond behaviour when AHL was applied directly on the brick surface (Figure 4.41).

Figure 4.41. Coating of brick substrate with AHL mortar for pull-off testing

As shown in Table 4.23, the highest average adhesive bond strength was observed in the case of control NHL mortars devoid of WBA, registering values of 0.40 MPa and 0.56 MPa for NHL 3.5 and NHL 5, respectively. Mortars featuring 20 wt.% WBA displayed the lowest values, aside from AHL1-20-M, which exhibited a value of 0.37 MPa, marginally lower than the corresponding control mix. The remaining 20% mixtures demonstrated adhesive bond strengths hovering around 0.1 MPa. This 75% decrease was accompanied by fractures at the interface between the mortar and the brick substrate, with select samples undergoing complete delamination during the testing process (Figure 4.43). This phenomenon is presumably attributable to the vibrational forces imparted by the drilling apparatus employed in the specimen preparation process.

Notably, mortar mixes containing 30 wt.% WBA, which also exhibited higher compressive strengths, displayed superior adhesive behaviour when compared to the lower WBA share. AHL 2-30-M surpassed the control value, while AHL3-30 presented adhesive strength matched

the control NHL3.5-M mix (Figure 4.42). It becomes evident that the testing methodology in its present form yielded less precise results for mortars containing lower WBA proportions, as evinced by the notably diminished adhesive values obtained. Mortar formulations featuring NHL 5 as the primary binder, coupled with a heightened 40 wt.% hybridization ratio, yielded adhesive performance akin to that of the first binder group incorporating 30 wt.% WBA. AHL 5-40-M showcased an adhesive strength equivalent to that of the control NHL5-M formulation (Figure 4.45). These outcomes underscore the necessity for a modified, more discerning testing protocol, possibly entailing the integration of moulds prior to the application of fresh lime-based mortar in pull-off tests, thereby mitigating the influence of stress introduced by the drilling apparatus. This particular matter is detailed in [34], where practical experiences in both positive and negative contexts (damage cases) are elaborated. Furthermore, it was noted that increased porosity may correlate with reduced bond strength in AHL mortars.

For the majority of the specimens, pull-off failures were observed either within the mortar itself (designated as failure mode B) or partially at the interface between the mortar and the substrate (termed as A/B). These failure modes clearly demonstrate that AHL mortars possess good adhesive bonding properties, especially in mixtures with increased strengths, where the negative effects of equipment-induced stress are minimized.

Table 4.23. Adhesive bond strength of NHL and AHL mortars after 28 days exposure to DC environment

Mix ID	$f_{u, av.}$ [MPa]	SD	Failure mode
refractory brick substrate	1.31	(±0.15)	B
NHL 3.5 - M	0.40	(±0.13)	A/B
NHL 5 - M	0.56	(±0.09)	B
AHL1-20 - M	0.37	(±0.19)	A/B
AHL2-20 - M	0.14	(±0.04)	A/B
AHL3-20 - M	0.08	(±0.03)	B
AHL4-20 - M	0.17	(±0.06)	B
AHL1-30 - M	0.21	(±0.08)	B
AHL2-30 - M	0.61	(±0.15)	A/B
AHL3-30 - M	0.42	(±0.13)	B
AHL4-30 - M	0.23	(±0.06)	B
AHL4-40 -M	0.29	(±0.09)	B
AHL5-40 - M	0.53	(±0.04)	A/B
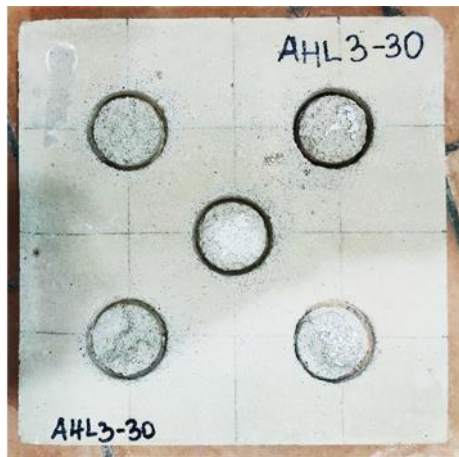
(a)   (b)

Figure 4.42. AHL 3-30-M mortar slab after pull-off test: (a) five test regions; (b) detail of failure mode (B)

Figure 4.43. Failure of AHL 2-20-M mortar slab after pull-off test (delamination)

(a)   (b)

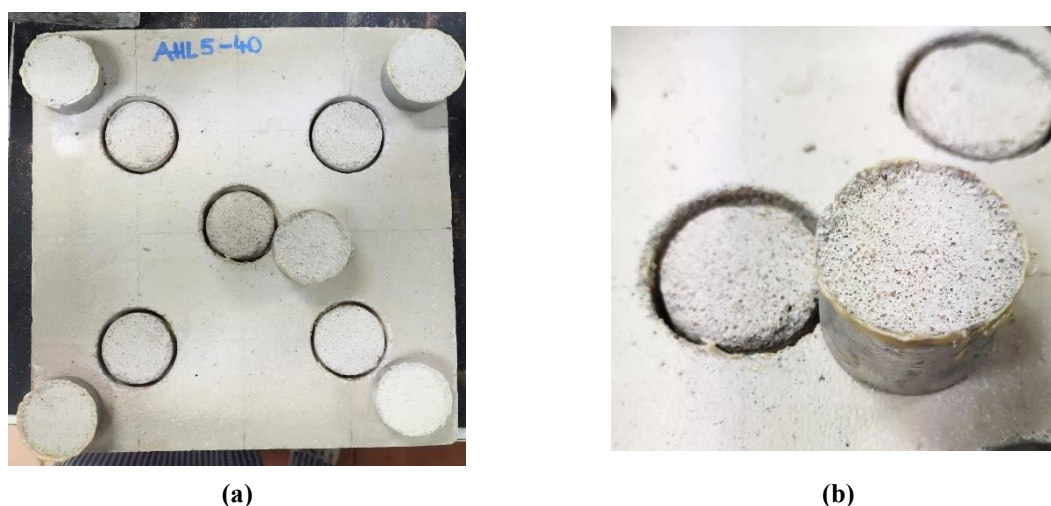**Figure 4.44.** AHL 2-30-M mortar slab after pull-off test: (a) five test regions; (b) detail of failure mode (A/B)

| (a) | (b) |

Figure 4.45. AHL 5-40-M mortar slab after pull-off test: (a) five test regions; (b) detail of failure mode (B)

4.3.7.2. *Resistance to freeze/thaw action and sulphate attack*

This research segment was dedicated to evaluating the durability of hardened mortar, specifically its resistance to freeze/thaw cycles and sulphate exposure as well as the combined effects of both, all in accordance with the guidelines established by RILEMs Technical Committee 127 [144].

The dominant approach in developing durability testing methods for masonry entails the use of composite models, incorporating both masonry units and mortar. This kind of comprehensive approach allows for the consideration of substrate properties and their effects on mortar durability, as highlighted in [168,169]. However, in the context of this research, the evaluation of the mortar was isolated. This choice aligns with the primary focus on investigating the impact of NHL-WBA mortar system constituents on weathering resistance.

The experimental protocol entailed the preparation of two mortar beds, positioned between sets of fully saturated brick units, as detailed in subchapter 3.2.2 Methods. These coupled units, alongside the corresponding cut-out mortar specimens (as illustrated in Figure 4.46 and Figure 4.50), underwent a curing process within a controlled HC environment, spanning over a period of more than three months.

| (a) | (b) |

Figure 4.46. Preparation of mortar beds: (a) set of brick units; (b) mortar and brick coupled units

Visual inspection assumed a central role in monitoring the condition of the mortar specimens following each cycle of sulphate addition and/or freezing-thawing. Upon the completion of 16 cycles, an all-encompassing assessment was carried out for each set of three specimens, corresponding to a specific deterioration mechanism. Subsequently, the quantified findings were averaged to provide a collective representation. These assessments involved assigning a Visual Assessment Rating (VAR) based on the extent of area loss, which ranged from 1 (indicating a 50% loss in area) to 10 (indicating an unaffected state). The VAR system facilitated an evaluation of the Overall Performance (OP) of the samples, with ratings ranging from excellent, very good, good, to marginal or poor. Moreover, it entailed the identification of patterns related to the Nature of Failure (NF), classified as per the categories outlined in Table 4.24.

Table 4.24. Assessment of the VAR and OP of mortar based on the extent of area loss

Area loss (%)	VAR	OP
50	1	poor
40	2	poor
30	3	marginal
20	4	marginal
15	5	marginal
10	6	good
5	7	good
2	8	very good
1	9	very good
unaffected	10	excellent

While the assessment protocol did involve the use of templates (as portrayed in Figure 4.47, Figure 4.48 and Figure 4.49) provided by [144], it was not exclusively reliant on them. This approach was adopted due to the diverse failure patterns observed, which could not be comprehensively evaluated using templates alone. Nevertheless, Figure 4.47 displays the templates employed for assessing the VAR of the mortar specimens, including (a) for the 0-10% range and (b) for the 10-50% range.
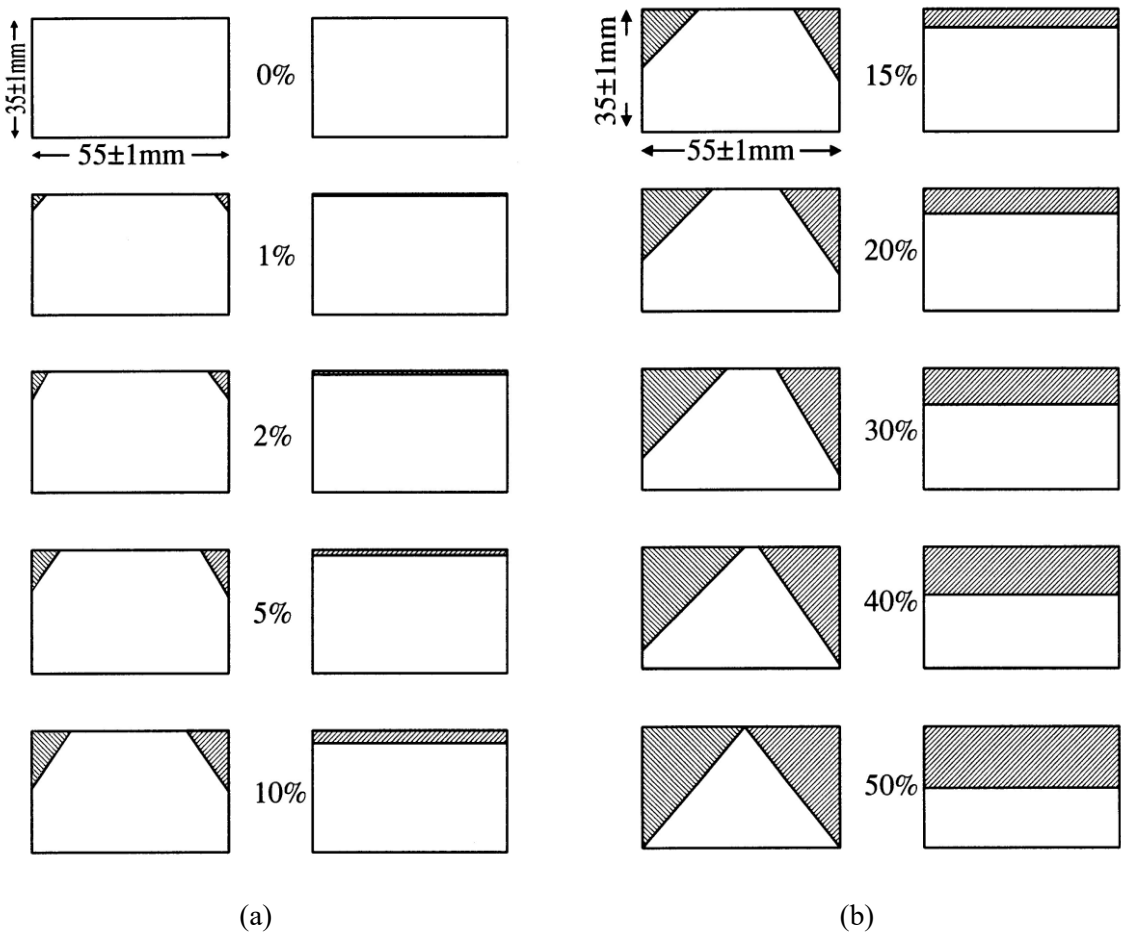

(a)   (b)

Figure 4.47. Templates for judging the VAR: (a) 0-10%; (b) 10-50% [144]
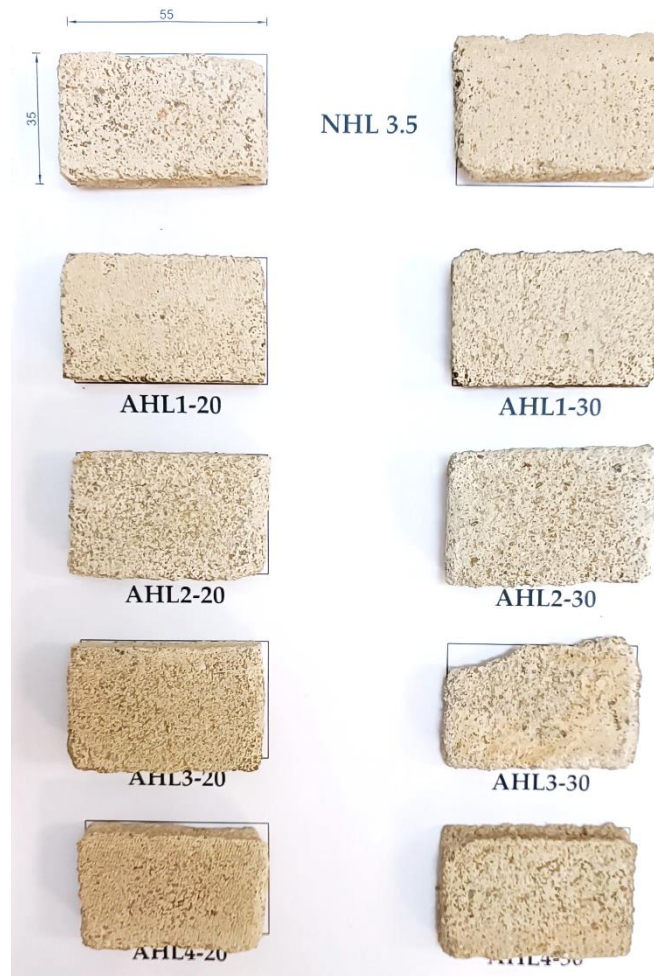
Figure 4.48. Cut-out specimens of NHL 3.5 and AHL mortars with 30 wt.% WBA before freeze-thaw and sulphate exposure testing
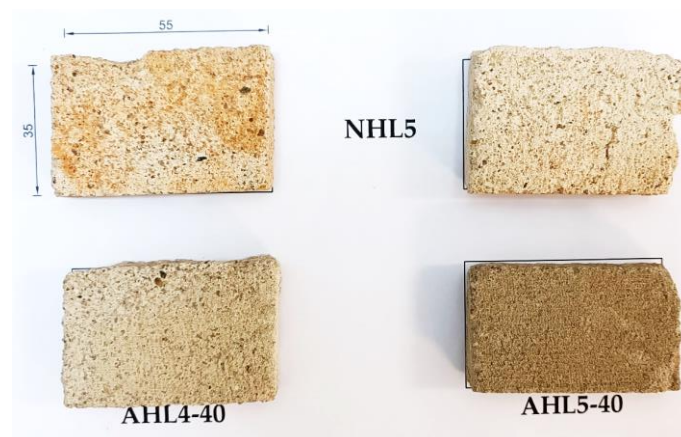
Figure 4.49. Cut-out specimens of NHL 5 and AHL mortars with 40 wt.% WBA before freeze-thaw and sulphate exposure testing

To categorize the exposed specimen into three distinct groups, each representing various deterioration mechanisms, a total of 9 specimens were required, with 3 specimens designated for each mechanism. The distribution of specimens among the groups is as follows:

–   Group 1 (Specimen S1): Exposed solely to potassium sulphate attack;

–   Group 2 (Specimen S2): Subjected to the combined effects of sulphate and frost attack;

–   Group 3 (Specimen S3): Exposed solely to frost attack.

Figure 4.50 illustrates a set of mortar specimens prepared to emulate diverse deterioration conditions. Within this collection, the following scenarios are depicted:

(a) AHL 4-40-M specimen 'S1-c,' tailored for simulating sulphate attack;

(b) AHL 4-40-M specimen 'S2-c,' designed to endure both freeze-thaw and sulphate attack;

(c) AHL 4-40-M specimen 'S3-c,' configured to undergo freeze-thaw conditions.

(d) 'Group 3' comprising a trio of specimens representing a unique test set.

This classification facilitated a comprehensive evaluation of the mortar's performance when subjected to a range of deterioration conditions with multiple specimen ensuring reliability and validity of the results.
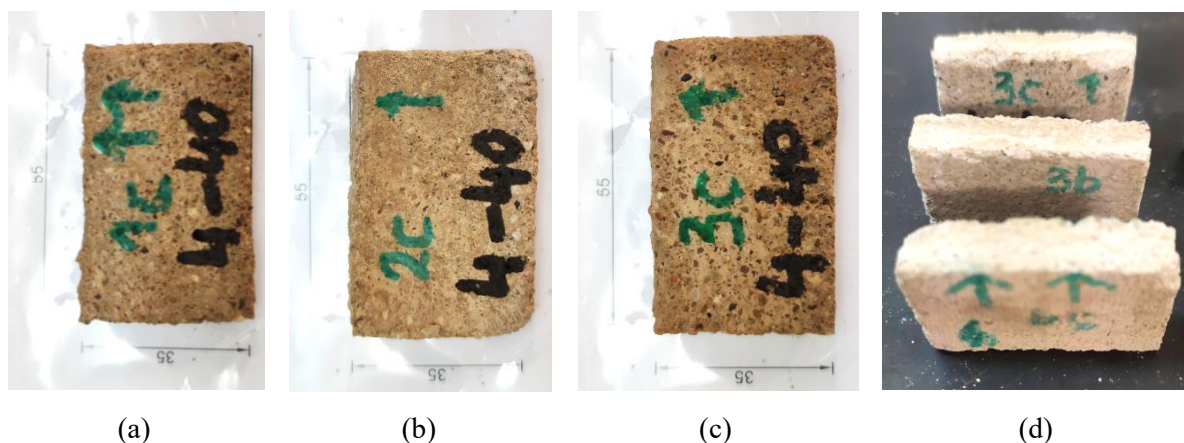

(a)   (b)   (c)   (d)

Figure 4.50. Example of set of specimens prepared for different deterioration conditions: (a) AHL 4-40-M specimen 'S1-c' set for sulphate attack; (b) AHL 4-40-M specimen 'S2-c' set for freeze-thaw and sulphate attack; (c) AHL 4-40-M specimen 'S3-c' set for freeze-thaw attack; (d) Group 3 consisting of three specimen

After each cycle was completed, each set of specimens (S1, S2, S3) was carefully packed in plastic cases and enveloped with insulation material, leaving only the tooled face exposed, as illustrated in Figure 4.51, following the cyclic testing protocol.
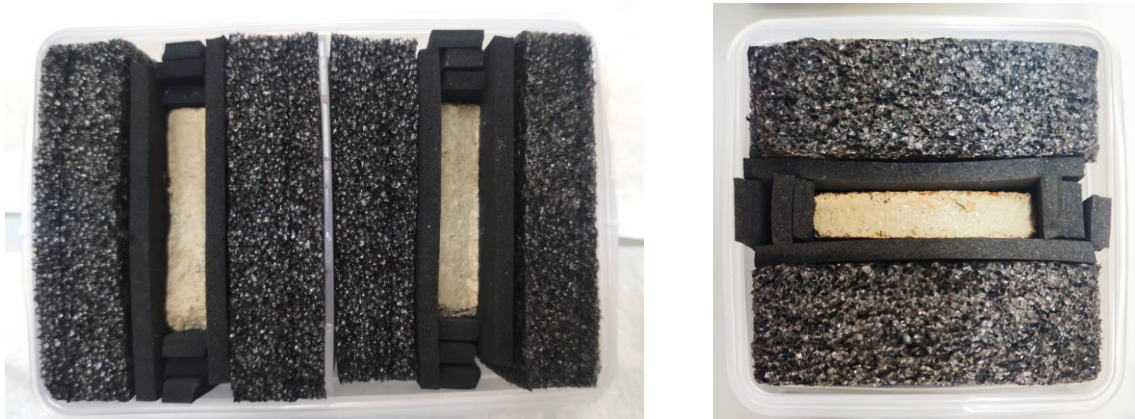
(a)   (b)

Figure 4.51. Cut-out mortar specimens packed in plastic cases, surrounded by insulation material, leaving only the tooled face exposed: (a) S2 & S3 specimen in double cases; (b) S1 specimen in single case

The initial signs of deterioration became evident after the 10th cycle among the deterioration groups of mortar where NHL 3.5 served as the primary binder. Yet, the control mix and both AHL mixes containing 30 wt.% WBA exhibited similar behaviour. Performance that aligned with this was observed in a way that specimens from the S1 group, subjected to sulphate attack, showed an average area loss of 1% (NHL 3.5-M and AHL 2-30-M) and 2% (AHL 3-30-M). For specimens in the S3 group, subjected to freeze-thaw attack, they displayed an average area loss of 2% (NHL 3.5-M and AHL 2-30-M) and 4% (AHL3-30-M), indicating modest variations compared to the control mix. However, specimens in the S2 group, which underwent sulphate attack in combination with freeze-thaw exposure, showed a more extensive average area loss, approximately 20% for NHL 3.5-M and 10% for AHL mixes. It's worth noting that the control mix's 20% average doesn't clearly reveal that one of the specimens (S2-b) exhibited significant deterioration, with an estimated 40% area loss. Following the 11th cycle, the referenced specimen from the NHL 3.5-M set, exhibited pronounced degradation (as shown in Figure 4.52) and was subsequently removed from further exposure to cycles.

Figure 4.52. The NHL 3.5-M 'S2-b' specimen, displaying prominent degradation after enduring 11 cycles

The attack mechanism of the S2 deterioration group involves the dissolution of salt in water, followed by the absorption of the saline solution through capillary action. Over time, as the samples undergo weathering cycles, the sulphate undergoes a series of precipitation (at higher temperatures) and dissolution (at lower temperatures) processes within the samples [170]. This led to visible decay, which became evident after the aforementioned 11 cycles. Aggelakopoulou et al. [171] affirmed that mortars used in conservation should exhibit resistance to the effects of soluble salts, ideally enduring at least 10 salt cycles during the aging test. Furthermore, they should not be a potential origin of soluble salts.

Upon completion of the final 16th cycle of testing, AHL mortars AHL 2-30-M and AHL 3-30-M demonstrated an overall performance comparable to the control mix. Specifically, they exhibited good overall performance in the S1 and S3 groups, with a marginal performance noted in the S2 group. The primary failure modes observed included corner loss, crumbling, delamination, and minor flaking on the lower section of the specimen. Additionally, some small salt deposits were observed on the upper, tooled surface (Table 4.26 and Table 4.27).

While assessing previously stated characteristics, including a compressive strength exceeding that of AHL 3-30-M by over 50%, AHL 2-30-M exhibited comparable performance across all three degradation categories. The behaviour observed in AHL5-40-M mortar, conversely, suggests that the heightened concentration of SO_4^- may exert a more pronounced influence on both internal and external sulphate attack, especially in conjunction with lower porosity. This assumption, however, has been refuted, which aligns with the capillary absorption pattern. An increased pore volume within the range of medium capillary pores (0.01-0.05 μm) is associated with reduced capillary uptake, responsible for absorbing both the saline solution and water.

Throughout the analysis of mortar deterioration groups employing NHL 5 as the primary binder, a resembling pattern emerged. Specifically, within the AHL 5-40-M specimens subjected to sulphate attack in combination with freeze-thaw exposure, significant indications of deterioration manifested after the 10th cycle, resulting in an approximate 10% loss in surface area. Afterward, by the 14th exposure cycle, one specimen from the AHL 5-40-M set, denoted as 'S2-c,' experienced complete structural degradation and was excluded from further exposure to cyclic conditions (as illustrated in Figure 4.53).

Figure 4.53. The AHL 5-40-M 'S2-c' specimen, displaying prominent degradation after enduring 14 cycles

At the conclusion of the 14th exposure cycle, the specimen from the AHL 4-40-M mix, which had been subjected to both sulphate attack and freeze-thaw conditions, displayed an average area loss of 10%, corresponding to the results of the AHL 5-40-M mix observed four cycles earlier. In contrast, the control mix remained resilient throughout the whole testing period, with an average area loss of only 3% in the S2 group, while S1 and S2 showed minimal indications of degradation. Thus, it is affirmed that the synergistic interplay between frost-thaw action and sulphates indeed results in an accelerated and intensified form of failure, in accordance with the premise proposed by [144] and [169]. Nonetheless, the control mix NHL 5-M exhibited very good overall performance across all three exposure groups (refer to Table 4.28). Notably, a recurring pattern of failure was observed, characterized by corner loss at the lower section of the specimen and visible cracks on the upper, tooled surface as well as throughout the specimen's structure. These cracks were more pronounced and expansive in specimens subjected to S2 deterioration group, although they were also present in S1. Given their absence in specimens from the S3 group, which were exposed solely to freeze-thaw conditions, it strongly suggests that they are a result of sulphate attack, leading to volume expansion due to salt crystallization.

In comparison, the AHL 4-40-M mortar, featuring a substantial WBA content of 40 wt.%, exhibited corresponding, very good overall performance within the S1 and S3 deterioration groups. In the notably aggressive S2 group, characterized as the most challenging environment, the mortar displayed a good overall performance rating. The predominant failure modes were identified as corner loss, crumbling, and delamination. The delaminated layers exhibited minimal thickness, mirroring the area loss observed within the S2 deterioration group, as detailed in Table 4.29.

The AHL 5-40-M mortar has demonstrated very good overall performance specifically in the case of isolated sulphate attack (S1). For freeze-thaw attack, it exhibited a good overall performance, whereas in the S2 deterioration group, characterized as the most challenging environment, a marginal overall performance was observed. Despite its notable attributes, including a compressive strength over 50% higher than that of AHL 4-40-M and a more than 30% increase compared to the control NHL 5-M mix, it displayed inferior performance in both the S2 and S3 deterioration groups. This discrepancy may be attributed to the elevated SO_4^- content, which exceeded triple that of NHL 5-M and doubled that of AHL 4-40-M, contributing to both internal and external sulphate attack. The observed downgrade in the S3 deterioration group likely derived from to the constrained availability of capillary pores for pressure equalization during freezing in larger pores. This can lead to an excess of water forming ice crystals, both of which contribute to rapid structural damage, as confirmed in [169]. The prevailing failure modes encompassed corner loss, crumbling, mortar delamination, and the presence of small cracks distributed across the specimen, mirroring the patterns observed in the other mortars within the same binder group (Table 4.30).

Within the scope of this research, it is deducible that AHL mortars are likely to attain a level of durability comparable to that of the NHL control mixes. Crucial parameters, gleaned from porosity metrics and alterations in the pore structure, coupled with internal salt loading resulting from the chemical composition of the WBAs, further facilitate the comprehension of experimental data and the assessment of result reliability. While there was a marginal decrease in durability performance observed in the AHL mortars containing 30% and 40% WBA, they still exhibited good to very good overall performance when subjected to sulphate attack or exposure to freeze-thaw cycles independently. However, it's worth noting that the most challenging conditions, which involve both factors simultaneously, in addition to the additional alkali and sulphates load present in WBA, can compromise durability of AHL mortars. This implies that AHL mortars could be well-suited for external environments with low to moderate

sulphate levels or for indoor applications. Furthermore, when determining mortar properties and testing protocols, it's crucial to consider the unique attributes of the historical substrate where the mortar will be applied. This includes special considerations like potential salt contamination and the prevailing climatic conditions.

Table 4.25. Assessment of NHL 3.5-M durability across various deterioration mechanisms after 16 cycles

	S1	S2	S3
NHL 3.5-M			
VAR	8	5	8
OP	good	Marginal*	good
NF	corner loss	lower edge disintegration delamination crumbling	corner loss

* three specimens were evaluated, but the final OP was based on the performance of two, as the third specimen disintegrated during the test.

Table 4.26. Assessment of AHL 2-30-M durability across various deterioration mechanisms after 16 cycles

	S1	S2	S3
AHL 2-30-M			
VAR	8	4	7
OP	good	marginal	good
NF	corner loss crumbling salt efflorescence	lower edge disintegration, delamination crumbling	corner loss

Table 4.27. Assessment of AHL 3-30-M durability across various deterioration mechanisms after 16 cycles

	S1	S2	S3
AHL 3-30-M			
VAR	7	3	7
OP	good	marginal	good
NF	corner loss	lower edge disintegration delamination	corner loss

Table 4.28. Assessment of NHL 5-M durability across various deterioration mechanisms after 15 cycles

	S1	S2	S3
NHL 5-M			
VAR	9	8	9
OP	very good	very good	very good
NF	lower corner loss cracks visible on the upper, tooled surface	lower corner loss notable cracks visible on the upper, tooled surface and across the samples	lower corner loss

Table 4.29. Assessment of NHL 4-40-M durability across various deterioration mechanisms after 15 cycles
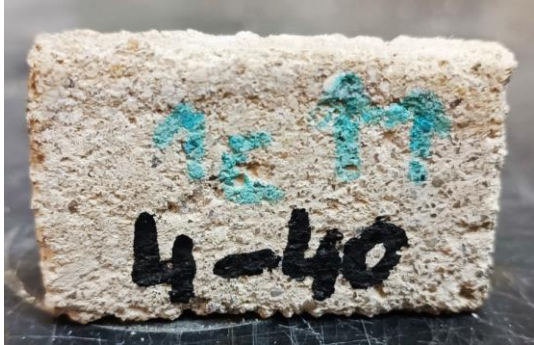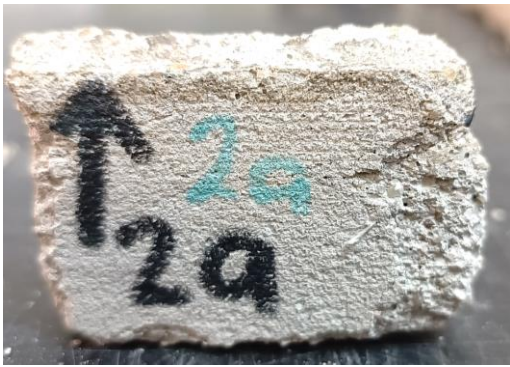
	S1	S2	S3
NHL 4-40-M			
VAR	9	6	8
OP	very good	good	very good
NF	lower corner loss	lower edge and side disintegration, delamination	lower edge disintegration, delamination

Table 4.30. Assessment of NHL 5-40-M durability across various deterioration mechanisms after 15 cycles

	S1	S2	S3
NHL 5-40-M			
VAR	9	4*	7
OP	very good	marginal	good
NF	lower corner loss, small cracks across the specimen	lower edge and side disintegration, delamination	lower edge disintegration, delamination

three specimens were evaluated, but the final OP was based on the performance of two, as the third specimen disintegrated during the test.

4.4. Conclusions and final remarks

The research segment presented herein was anticipated to yield the following *scientific contributions*:

− Determination of prospects for the use of WBA in artificial hydraulic lime based on the key factors governing the engineering behaviour and durability of a new composite;

− Development of an environmentally friendly lime mortar with WBA suitable for the rehabilitation and maintenance of historical buildings.

To identify the key factors governing the engineering behavior and long-term durability of AHL mortars, an extensive assessment encompassed various technical properties. These encompassed mechanical properties (such as compressive and flexural strength), deformability (quantified by the modulus of elasticity), hygro-thermal behavior (including capillary water absorption, water vapor permeability, and thermal conductivity), and durability performance (assessing adhesive bond strength, freeze-thaw resistance, and sulphate resistance). The findings illuminated promising avenues for the integration of WBA into lime mortars for conservation purposes.

In addition to the technical properties, compatibility stands as a fundamental cornerstone in the field of conservation practice. Consequently, when considering restoration mortars, it plays a crucial role in ensuring the long-term durability of the intervention while preventing any harm, either direct or indirect, to the original materials. This necessitates that the composition and microstructure of repair mortars ensure both favourable mechanical properties (albeit repair mortar being softer than the original material) and the capacity to accommodate masonry movements elastically. Furthermore, these mortars must offer effective weather protection and closely match the final aesthetic appearance of the original materials. It is imperative to note that the relative importance of each technical requirement varies depending on the specific application context, intervention goals, and prevailing environmental exposure conditions [39,146]. The determination of a suitable repair mortar, in terms of technical compatibility, involves assessing and comparing the properties of the new mortar with those of the original material. As such, defining the functional role of AHL mortar, related to the properties of a particular WBA and the mortar's functional requirements, within the NHL-WBA mortar system presents a multifaceted challenge. Each binder exhibits a spectrum of properties, which, when combined with varying grain sizes, grain size distributions, and additives, offer a diverse array of possibilities for mortar type classification.

As delineated in [137], the classification of mortar types concerning their decisive technical requirements are resulting from specific criteria inherent to each mortar type. In this context, repointing mortars and renders/plaster pose notable challenges, given their higher prioritization of the aforementioned technical parameters. Consequently, the assessment of AHL mortars with WBA encompassed these classifications, as others exhibit comparatively less stringent criteria. A summary of key findings on the properties of the AHL mortars under investigation in historical context is presented in Table 4.31.

These outcomes enable the highlighting of materials, such as AHL mortars with WBA, which not only align with the requisite technical requirements but also conform to compatibility constraints essential for the preservation of historic masonry. Therefore, the validation of the H3 hypothesis, which was originally proposed at the beginning of this chapter, is justified: 'Artificial lime with hydraulic properties containg WBA can be used to produce eco-friendly, cement-free mortar for restoration and/or rehabilitation of historical buildings.'

In the first experimental phase, prompted by the AHL binder and paste analysis, further validation of the H2 hypothesis was deemed necessary. This hypothesis proposes a direct relationship between the chemical and mineralogical composition of WBAs and their suitability in hydraulic binders, which is then mirrored in the context of mortar hardening.

During this research phase, the influence of SO_3-rich WBA5.F on the setting and hardening processes of hydraulic mortar was investigated, despite non-conformity with EN 459 criteria in the previous binder and paste level (AHL5-40-B exceeding both the chemical and final set restraints). The findings indicate that, although the paste exhibited extended setting times, it had no detrimental effect on the hardening process of the AHL5-40-M mortar. While mechanical properties showed improvement, there was a trade-off with durability due to the chemical composition.

Table 4.31. The influence of integrating WBA as a secondary binder into the NHL mortar system

Property	Major observation
Fresh state	Within an overall relationship with a constant water/binder ratio, workability depends in a complex way on the physical properties of the binder, while no significant segregation or bleeding noted after the testing.
	In AHL mortars, the addition of SP maintained a uniform w/b ratio, albeit with an increasing need for SP in proportion to the WBA content.
	The suitability of the selected additives may warrant further examination.
Mechanical properties	While the increase in compressive strength occurs gradually, in accordance with the hydraulic nature of the primary binder, the SAI values suggest the presence of potential pozzolanic activity due to WBA incorporation.
	The curing environment's influence (RH and CO_2) is notable, with a preference for a moderate to high humidity curing regime, particularly in the long term.
	Overall positive impact of WBA on the mechanical properties is observed with higher hybridization ratios. It's worth noting that the increase in strength doesn't necessarily imply reduced porosity, underscoring AHL mortars' potential for durability while remaining permeable.
	AHL mortars exhibit elastic behaviour, aligning with the properties commonly found in historic mortars.
Pore structure	Pores play a central role in shaping a wide spectrum of hardened mortar properties.
	AHL mortar exhibits a notable escalation in the prevalence of small and medium capillary pores, while, overall, maintaining porosity levels that closely approximate those observed in pure NHL formulations.
	The pore structure highly influenced by the curing environment, with a general trend of increasing porosity with the addition of WBA.
Hygro-thermal properties	The inclusion of WBA has resulted in enhancements in hygro-thermal performance, as indicated by a decrease in capillary absorption, increased permeability, and thermal conductivity in a similar range.
	These enhancements are intricately linked to the pore structure. Such advancements are deemed highly advantageous for the protection and longevity of masonry units exposed to wind-driven rain and moisture.

Property	Major observation
Durability performance	The salt content in the AHL mortars was notably elevated, particularly in mortars containing fly ash, falling short of one of the essential compatibility criteria.
	Even at a higher hybridization ratio of 30 wt.%, the durability performance remains strong, within the control NHL range in cases of isolated degradation.
	However, challenging conditions, which encompass both factors simultaneously and include the additional internal alkali and sulphate load from WBA, may compromise the durability of AHL mortars in harsh environments.

It is imperative to emphasize that within the extensive spectrum of significant properties, the progress of compressive strength in AHL lime mortars hybridized with commercially available NHLs of varying hydraulicity played a pivotal role in evaluating the performance of hardened AHL mortars. However, it was not regarded as the sole or definitive indicator in the development of an environmentally sustainable lime mortar suitable for conservation purposes. In addition to comparing data on renovation mortars available in the state-of-the-art literature, the assessment of AHL mortars complies with the standards governing building limes (EN 459) and mortar for masonry (EN 998 series). Employing the framework outlined in these aforementioned standards led to the discovery of the results presented in Table 4.32.

According to the findings presented, it can be asserted that integrating WBA into the NHL system across a moderate to high range of hybridization ratios (NHL:WBA of 80:20, 70:30, and 60:40) presents encouraging opportunities for utilizing WBA as a secondary binder in NHL-WBA mortar systems. Consequently, the substitution of NHL with WBA, especially in higher proportions, holds significant potential for advancing the sustainability of the hydraulic production sector while maintaining the authenticity of repair mortars.

Table 4.32. AHL mortar categorisation according to EN 459-1 and EN 998 series of standards

Hybridisation system	WBA – NHL 3.5	WBA – NHL 5
WBA share (wt.%)	20 & 30	40
EN 459-1:2016 Building limes	In the case of mixes featuring NHL 3.5 as the primary binder within the lower hydraulicity group, the HC curing environment demonstrated its favourability by surpassing the designated 3.5 MPa minimum threshold after 90 days, allowing FL 3.5 designation. However, it is noteworthy that the upper threshold of 10 MPa was not exceeded.	The minimum compressive strength requirement, set at 2.5 and 5 MPa, was achieved after 7 and 28 days in both curing environments, encompassing natural carbonation, thereby allowing for FL 5 designation. Notably, the maximum threshold of 15 MPa was not surpassed.
EN 998-1:2016 Rendering and plastering mortar	After 90 days, AHL mortars were categorized as either C II, C III, or C IV, denoting compressive strengths ranging up to 5, 7.5, and over 6 MPa, respectively. In nearly all cases, AHL mortars could be designated as 'renovation' mortars (R), with C II being the corresponding category.	AHL mortars displayed compressive strengths exceeding 6 MPa after 90 days. This categorization classifies them as CS IV, thereby permitting their designation as general-purpose (G) mortar.
EN 998-2:2016 Masonry mortar	All AHL mortars meet the criteria to be classified as general-purpose masonry mortars (G) under the M5 mortar classification, which requires a minimum compressive strength of 5 MPa.	All AHL mortars could be declared as general-purpose masonry mortars (G) within the M5 or M10 mortar classification and a minimum compressive strength of 5 MPa

5. CONCLUSIONS, CONTRIBUTIONS, AND OUTLOOKS

This chapter offers an overall summary of the research carried out as part of this doctoral thesis, emphasizing the main findings and highlighting the scientific and engineering contributions of the research. In conclusion, recommendations are provided concerning the practical utilization of WBA to advance the development of environmentally friendly lime mortars suitable for conservation purposes.

5.1. Conclusions

The findings of this research are summarized as follows, detailed upon the two main experimental phases that encompass binder and paste level, followed by the mortar level:

Paste level:

Classifying AHL produced with WBA within one of the subcategories of artificial hydraulic lime is in accordance with the criteria established for FL and HL in EN 459 standard. These criteria are rooted in chemical and physical parameters at the binder level. On the paste level, the emphasis is placed on setting time and soundness.

As WBAs are marked by high SO_3 content and the presence of expansive components like free MgO and CaO, with a minor persence of available lime in the form of $Ca(OH)_2$, the challenges that arisse necessitate pre-treatments to enhance fineness and reactivity. These challenges, in turn, lead to significantly prolonged setting times and increased expansibility of AHL paste.

However, the concerns mentioned may be overarched as the results of the subsequent phase of our study indicate that the mechanical properties of AHL mortars can be notably improved by the addition of WBA in moderate to moderately-high ratios..

According to EN 459-1 standard, the available lime content in FL spans from 15 to 80 wt.%, allowing for a diverse range of natural and artificial components to be blended into FL formulations. While classifying AHL with NHL and WBA as primary constituents under the FL category enables the tailored design of mortars and plasters, it does not account for their potential interaction with historical substrates.

In contrast to the HL designation solely in accordance with its compressive strength class, aligning AHL with WBA under the FL classification ensures a more straightforward

composition, thereby minimizing the risk of unforeseen damage within the historical framework.

Mortar level:

Following the completion of the first experimental phase, which involved selecting the favourable type and proportion of WBA suitable for AHL mortar, the subsequent phase of investigation was dedicated to the comprehensive evaluation of both fresh and hardened mortars. This investigation focused solely on the WBAs chosen during the preliminary screening, aiming to unveil their true potential for enhancing AHL mortar performance.

According to the findings presented, it can be asserted that integrating WBA into the NHL system across a moderate to morately high range of hybridization ratios (NHL:WBA of 80:20, 70:30, and 60:40) presents encouraging opportunities for utilizing WBA as a secondary binder in NHL-WBA mortar systems. Consequently, the substitution of NHL with WBA, especially in higher proportions, holds significant potential for advancing the sustainability of the hydraulic production sector while maintaining the authenticity of repair mortars.

The properties of fresh mortar were controlled through the use of additives, including superplasticizer and air-entraining agents. This approach was taken to mitigate the reduced workability resulting from the incorporation of WBA and prevent the anticipated instability of air content. However, it was imperative to conduct further assessments regarding the compatibility of these additives with AHL mortar constituents. Additionally, comprehensive studies are required to appraise their impact on the overall durability of the mortar.

Subsequently, the all-encompassing assessment reveals an overall positive impact of WBA on the mechanical properties and hygro-thermal behaviour, even at higher hybridization ratios. Notably, the environmental conditions during curing, including relative humidity (RH) and carbon dioxide concentration (CO_2), exert a significant influence. In the long term, a preference for a moderate to high humidity curing regimen becomes evident.

One of the key aspects influencing the mechanical properties, hygro-thermal behaviour, and durability of AHL composites is the alteration in the pore structure of the primary NHL binder induced by the presence of WBA. Moreover, challenging durability conditions, including the internal alkali and sulphate load introduced by WBAs, may pose challenges to the durability of AHL mortars in harsh environments. Particularly, the elevated salt content in AHL mortars,

especially those containing fly ash, raises concerns related to compatibility criteria. Internal salt attack may slightly favour mixed ashes over fly ash, primarily due to the lower initial salt load.

To assess the functional role of mortar within the NHL-WBA system, the EN 459 and EN 998 series of standards were employed. Consequently, categorization as FL (C) 3.5 and FL (C) 5 is consistent with EN 459-1. Simultaneously, the EN 988-1 standard for masonry rendering and plastering mortar suggests that AHL mortars with lower hybridization ratios (20 wt.%) could be classified as 'renovation mortars,' with category CII and a compressive strength range at 28 days from 1.5 MPa to 5.0 MPa. It is noteworthy that these categorizations are primarily based on compressive strength values, particularly at 28 days, which have been demonstrated to significantly underestimate the final strength of AHL mortars. In this context, at 90 days, the compressive strength values doubled in comparison to the 28-day values.

In light of the specified conclusions, the validation of the three formulated hypotheses is verified:

H I.   Building lime with hydraulic properties, i.e., an artificial hydraulic lime can be prepared with wood biomass ash;

H II.   The chemico-mineralogical composition of WBA, in addition to evaluating various WBA with different degrees of pozzolanity and hydraulicity, has a direct impact on its applicability in a hydraulic binder and the possibility of hardening of hydraulic lime mortar systems;

The H II hypothesis was partially validated, as it was confirmed that chemico-mineralogical restraints of WBA, governing the prospects of its applicability in a hydraulic binder, had no detrimental effect on the hardening process on the mortar level.

H III. Artificial lime with hydraulic properties containing WBA can be used to produce eco-friendly cement-free mortar for restoration and/or rehabilitation of historical buildings.

5.2. Contributions of this research to science and engineering

The scientific contributions of this research and its implications for the utilization of WBA in the development of building lime with hydraulic properties can be summarised as follows:

SC1. Determination of prospects for the use of WBA in artificial hydraulic lime based on the key factors governing the engineering behaviour and durability of a new composite.

The research methodology involved a comprehensive and interconnected series of analytical steps, encompassing everything from the analysis of binders to the preparation of pastes and mortars. The properties evaluated at each phase are recognised as key factors that influence the NHL-WBA binder system and, by extension, shape the mechanical properties and durability of AHL mortar.

Initiating the first experimental phase of the research, an analysis of the physical and chemico-mineralogical properties of WBAs was conducted at the binder and paste levels. Subsequently, the second experimental phase included mechanical testing, encompassing evaluations of compressive and flexural strength. The assessment also included the measurement of deformability, as indicated by the modulus of elasticity. Beyond the mechanical properties, the examination extended into the domain of hygro-thermal behaviour, covering factors such as capillary water absorption, water vapor permeability, and thermal conductivity.

SC2. Development of an environmentally friendly lime mortar with WBA suitable for the rehabilitation and maintenance of historical buildings.

The presented findings of the experimental phases suggest that integrating WBA into the NHL system, within moderate to high hybridization ratios (NHL:WBA at 80:20, 70:30, and 60:40), offers promising prospects for employing WBA as a secondary binder in NHL-WBA mortar systems. These results not only accentuate the suitability of materials like AHL mortars with WBA, meeting both technical requisites and compatibility constraints of the NHL system - utilized as the benchmark material for the restoration and conservation of historical masonry - but also signify a noteworthy advancement in the sustainable practices of the hydraulic production sector. This substitution of NHL with WBA, especially in higher proportions, stands as a key avenue for bolstering the sustainability of the hydraulic production sector while preserving the integrity and authenticity of repair mortars.

5.3. Outlooks

The aforementioned levels of assessment are recognized as cornerstones underpinig the development of repair mortars conservation purposes. Subsequently, recommendations and outlooks for further research are provided.

a. Industrial-scale pre-treatments of WBA

The pre-treatments of WBA, in its broader context, should not be interpreted as a disadvantageous factor, as it is already an integral aspect of the raw material production process. Mechanical treatments, specifically centered on sieving and grinding, were presumed mirroring those employed in the industrial production of hydraulic binders, whereas its environmental and energy impact is low. As a result, the idea of expanding the pre-treatment methods for WBA from the laboratory setting to an industrial scale deserves detailed inspection. The upscaling would offer the potential to retain the WBAs hydraulic properties. This strategic shift toward an industrial-scale approach is crucial for addressing the inherent compositional variations in the ashes and optimizing particle size distribution. The future research should focus on finding practical methods to enhance quality, with a special emphasis on preventing internal salt attack. It's important to recognize that these efforts often require the use of chemical treatments, which should be approached carefully and systematically.

b. Incorporation and suitability of additives

Decisions regarding the incorporation of additives in lime mortars should be made after a comprehensive evaluation of their appropriateness for the particular project, considering both preservation and performance objectives. When chosen and applied correctly, additives have the potential to improve lime mortar properties, thus ensuring the long-term conservation of historic and heritage structures. Nevertheless, it is crucial to conduct additional assessments to determine the compatibility of these additives within the AHL mortar system. Moreover, in-depth studies are necessary to assess their influence on the overall durability of the mortar.

c. Adjustments and optimisation of the mix design

Tailoring mortar mix design is the practice of creating a mortar mix that is precisely adjusted for a specific project's requirements. It takes into consideration various factors, including the type of masonry units, environmental conditions, desired strength levels, and compatibility with historical materials. This process involves the careful selection of the appropriate types of

binder, aggregates, additives to achieve the desired mortar properties. For instance, it would require choosing between various types of hydraulic lime and aggregates, taking into account factors like sand type and gradation to meet the project's specific needs. Therefore, further adjustments and optimisation of the mix design of AHL mortars is essential for optimising workability, strength, and durability. Fine-tuning the water-binder ratio, aggregate-to-binder ratio, and incorporating specific additives deserves special attention in the future.

d. In-depth investigation of complex masonry-mortar systems

In the context of this research, the evaluation of the AHL mortar was isolated. This choice aligns with the primary focus on investigating the impact of WBA on the primary binder in the NHL-WBA mortar system. The recommended approach in further research should entail the use of composite models, incorporating both masonry units and mortar. This kind of comprehensive approach would allow for the consideration of substrate properties and their effects on mortar durability.

e. Life Cycle Assessment

Embedded within this dissertation is the pioneering introduction of the socio-environmental dimension within the historical framework, underpinned by the principles of circular design. This integration represents a transformative paradigm shift, deemed essential for fostering long-term, life-cycle thinking within the industrial ecosystem. Within this context, the application of Life Cycle Assessment (LCA) emerges as a valuable tool in the ex-ante phase, offering insights that enable more informed "micro" level design decisions, including the choice of materials. LCA facilitates a delicate balance between the conservation of historical buildings and the imperative for sustainable and environmentally responsible practices.

One notable aspect where LCA shines is in its ability to quantify the environmental benefits associated with the use of alternative materials such WBA and consequently the AHL mortars. Whether these alternatives are used alongside conventional raw materials or entirely replace them in mortar production, this quantification would not only foster collaboration between conservators and engineers but also shed light on the tangible environmental advantages that can be harnessed through these material choices.

References

1. Directive 2008/98/EC of the European Parliament and of the Council of 19 November 2008 on waste and repealing certain Directives. *Off. J. Eur. Union* 2018, 22.11.2008., 3–30.

2. European Commission, *Communication from the Commission to the European Parliament, the Council, the European Economic and Social Committee and the Committee of the Regions—New European Bauhaus. Beautiful, Sustainable, Together.*; Brussels, Belgium, 2021; Available online: https://eur-lex.europa.eu/legal-content/EN/TXT/HTML/?uri=CELEX:52021DC0573 (accessed on 3 April 2023).

3. The European Green Deal; European Commission, Brussels, Belgium, 2019, Volume 58.

4. European Comission Cement and Lime Available online: https://ec.europa.eu/growth/sectors/raw-materials/related-industries/non-metallic-products-and-industries/cement-and-lime_en (accessed on April 1, 2023).

5. EuLA - The European Lime Association *A Competitive and Efficient Lime Industry - Cornerstone for a Sustainable Europe*; 2014;

6. Directive (EU) 2018/2001 of the European Parliament and of the Council of 11 December 2018 on the promotion of the use of energy from renewable sources (recast). *Off. J. Eur. Union* 2018, *Volume 61*, L 328/82-209.

7. Carević, I.; Baričević, A.; Štirmer, N.; Šantek Bajto, J. Correlation between physical and chemical properties of wood biomass ash and cement composites performances. *Constr. Build. Mater.* **2020**, *256*, 14, doi:10.1016/j.conbuildmat.2020.119450.

8. European Commission, European Green Deal: Commission proposes transformation of EU economy and society to meet climate ambitions. *Eur. Comm. - Press release* 2021.

9. Scarlat Nicolae; Dallemand Jean-Francois; Taylor Nigel; Banja Manjola *Brief on biomass for energy in the European Union*; Javier, S.L., Marios, A., Eds.; Publications Office of the European Union, 2016;

10. IEA Bioenergy Technology Roadmap Delivering Sustainable Bioenergy. *IEA Publ.* 2017, 89.

11. Independent Group of Scientists appointed by the Secretary-General *Global Sustainable Development Report 2019: The Future is Now – Science for Achieving Sustainable Development*; United Nations, New York, 2019;

12. Agrela, F.; Cabrera, M.; Morales, M.M.; Zamorano, M.; Alshaaer, M. Biomass fly ash and biomass bottom ash. In *New Trends in Eco-efficient and Recycled Concrete*; 2019; pp. 23–58 ISBN 9780081024805.

13. ETIP Bioenergy. Bioenergy in Europe; ETIP Bioenergy: Brussels, Belgium, 2020.

14. Bioenegy Europe: Bioenergy: A renewable energy champion 2021, 1–7.

15. Milovanović, B.; Štirmer, N.; Carević, I.; Baričević, A. Wood biomass ash as a raw material in concrete industry. *Građevinar* 2019, *71*, 505–514, doi:10.14256/JCE.2546.2018.

16. Udoeyo, F.F.; Inyang, H.; Young, D.T.; Oparadu, E.E. Potential of wood waste ash as an additive in concrete. *J. Mater. Civ. Eng.* 2006, *18*, 605–611, doi:10.1061/(ASCE)0899-1561(2006)18:4(605).

17. Alonso, M.M.; Gascób, C.; Morales, M.M.; Suárez-Navarro, J.A.; Zamorano, M.; Puertas, F. Olive biomass ash as an alternative activator in geopolymer formation: A study of strength, radiology and leaching behaviour. *Cem. Concr. Compos.* 2019, *104*, doi:10.1016/j.cemconcomp.2019.103384.

18. Freire, M.; Lopes, H.; Tarelho, L.A.C. Critical aspects of biomass ashes utilization in soils: Composition, leachability, PAH and PCDD/F. *Waste Manag.* 2015, *46*, 304–315, doi:10.1016/j.wasman.2015.08.036.

19. Pesonen, J.; Kuokkanen, T.; Rautio, P.; Lassi, U. Bioavailability of nutrients and harmful elements in ash fertilizers: Effect of granulation. *Biomass and Bioenergy* 2017, *100*, 92–97, doi:10.1016/j.biombioe.2017.03.019.

20. Directive (EU) 2018/851 of the European Parliament and of the Council of 30 May 2018 amending Directive 2008/98/EC on waste. *Off. J. Eur. Union* 2018, 109–140, doi:10.1023/A:1009932427938.

21. Directive 2018/850 of the European Parliament and of the Council of 30 May 2018 amending Directive 1999/31/EC on the landfill of waste. *Off. J. Eur. Union* 2018, *2018*, 100–108.

22. Pavlíková, M.; Zemanová, L.; Pokorný, J.; Záleská, M.; Jankovský, O.; Lojka, M.; Zbyšek Pavlík Influence of Wood-Based Biomass Ash Admixing on the Structural , Mechanical, Hygric, and Thermal Properties of Air Lime Mortars. *Materials (Basel).* 2019, *12*, 22, doi:10.3390/ma12142227.

23. Almeida, N.G. De; Faria, P. Lime mortars with rice husk ash for ancient masonry. In Proceedings of the HMC08 - Historical Mortars Conference: Characterization, Diagnosis, Conservation, Repair and Compatibility; Lisbon, 2008.

24. Fořt, J.; Čáchová, M.; Vejmelková, E.; Černý, R. Mechanical and hygric properties of lime plasters modified by biomass fly ash. *IOP Conf. Ser. Mater. Sci. Eng.* 2018, *365*, 032059, doi:10.1088/1757-899X/365/3/032059.

25. Fusade, L.; Viles, H.; Wood, C.; Burns, C. The effect of wood ash on the properties and durability of lime mortar for repointing damp historic buildings. *Constr. Build. Mater.* 2019, *212*, 500–513, doi:10.1016/j.conbuildmat.2019.03.326.

26. Baričević, A.; Carević, I.; Bajto, J.Š.; Štirmer, N.; Bezinović, M.; Kristović, K. Potential of using wood biomass ash in low-strength composites. *Materials (Basel).* 2021, *14*, 1–24, doi:10.3390/ma14051250.

27. Arizzi, A.; Cultrone, G. Mortars and plasters—how to characterise hydraulic mortars. *Archaeol. Anthropol. Sci.* 2021, *13*, doi:10.1007/s12520-021-01404-2.

28. EN 459-1:2015 Building lime -- Part 1: Definitions; specifications and conformity criteria 2015, 52.

29. The Building Limes Forum edited by Ian Brocklebank *Building limes in conservation*; Brocklebank, I., Ed.; 1st ed.; Routledge, 2012; ISBN 978-1-873394-95-3.

30. English Heritage Building Materials. *Conserv. Bull.* 2012, 53, doi:10.1071/aj14071.

31. Figueiredo, C.; Lawrence, M.; Ball, R.J. Chemical and physical characterisation of three NHL 2 binders and the relationship with the mortar properties. In Proceedings of the Rehabend 2016;

Burgos, Spain; Vol. 2016-May, pp. 1293–1300.

32. Forster, A.M. How hydraulic lime binders work - hydraulicity for beginners and the hydraulic lime family 2018.

33. EN 998-1:2016-Specification for mortar for masonry -- Part 1: Rendering and plastering mortar.

34. Groot, C.; Veiga, R.; Papayianni, I.; Van Hees, R.; Secco, M.; Alvarez, J.I.; Faria, P.; Stefanidou, M. RILEM TC 277-LHS report: lime-based mortars for restoration–a review on long-term durability aspects and experience from practice. *Mater. Struct. Constr.* **2022**, *55:245*, 33, doi:10.1617/s11527-022-02052-1.

35. Elsen, J.; Van Balen, K.; Mertens, G. Hydraulicity in historic lime mortars: A review. *RILEM Bookseries* **2013**, *7*, 125–139, doi:10.1007/978-94-007-4635-0_10.

36. Figueiredo, C., Lawrence, M., and Ball, R.J. Mechanical properties of standard and commonly formulated NHL mortars used for retrofitting. In Proceedings of the Proceedings of the Integrated Design Conference ID@50: Building our Future.; Emmitt, S., Adeyeye, K., Eds.; University of Bath: Bath, United Kingdom, 2016; p. 13.

37. Kang, S.H.; Lee, S.O.; Hong, S.G.; Kwon, Y.H. Historical and scientific investigations into the use of hydraulic lime in Korea and preventive conservation of historic masonry structures. *Sustain.* **2019**, *11*, doi:10.3390/su11195169.

38. Alvarez, J.I.; Veiga, R.; Martínez-Ramírez, S.; Secco, M.; Faria, P.; Maravelaki, P.N.; Ramesh, M.; Papayianni, I.; Válek, J. RILEM TC 277-LHS report: a review on the mechanisms of setting and hardening of lime-based binding systems. *Mater. Struct. Constr.* **2021**, *54*, doi:10.1617/s11527-021-01648-3.

39. Gulotta, D.; Goidanich, S.; Tedeschi, C.; Nijland, T.G.; Toniolo, L. Commercial NHL-containing mortars for the preservation of historical architecture. Part 1: Compositional and mechanical characterisation. *Constr. Build. Mater.* **2013**, *38*, 31–42, doi:10.1016/j.conbuildmat.2012.08.029.

40. M.J. VarasT, M. Alvarez de Buergo, R.F.; Institute Natural cement as the precursor of Portland cement: Methodology for its identification M.J. *Cem. Concr. Res.* **2005**, *35*, 2055 – 2065, doi:10.1016/j.cemconres.2004.10.045.

41. El-Turki, A.; Ball, R.J.; Allen, G.C. The influence of relative humidity on structural and chemical changes during carbonation of hydraulic lime. *Cem. Concr. Res.* **2007**, *37*, 1233–1240, doi:10.1016/j.cemconres.2007.05.002.

42. Lanas, J.; Sirera, R.; Alvarez, J.I. Compositional changes in lime-based mortars exposed to different environments. *Thermochim. Acta* **2005**, *429*, 219–226, doi:10.1016/j.tca.2005.03.015.

43. Cizer, Ö.; Rodriguez-Navarro, C.; Ruiz-Agudo, E.; Elsen, J.; Van Gemert, D.; Van Balen, K. Phase and morphology evolution of calcium carbonate precipitated by carbonation of hydrated lime. *J. Mater. Sci.* **2012**, *47*, 6151–6165, doi:10.1007/s10853-012-6535-7.

44. Cultrone, G.; Sebastián, E.; Huertas, M.O. Forced and natural carbonation of lime-based mortars with and without additives: Mineralogical and textural changes. *Cem. Concr. Res.* **2005**, *35*, 2278–2289, doi:10.1016/j.cemconres.2004.12.012.

45.   EN 1015-11:2019 Methods of test for mortar for masonry -- Part 11: Determination of flexural and compressive strength of hardened mortar 2019.

46.   Cizer, Ö.; Van Balen, K.; Van Gemert, D. Competition between hydration and carbonation in hydraulic lime and lime-pozzolana mortars. *Adv. Mater. Res.* 2010, *133–134*, 241–246, doi:10.4028/www.scientific.net/AMR.133-134.241.

47.   Grilo, J.; Faria, P.; Veiga, R.; Santos Silva, A.; Silva, V.; Velosa, A. New natural hydraulic lime mortars - Physical and microstructural properties in different curing conditions. *Constr. Build. Mater.* 2014, *54*, 378–384, doi:10.1016/j.conbuildmat.2013.12.078.

48.   Carević, I.; Štirmer, N.; Banjad Pečur, I.; Milovanović, B.; Rukavina Jelčić, M. Potential of use wood biomass ash in the cement composites. *Proccedings 1st Int. Conf. Constr. Mater. Sustain. Futur. Zadar, Croat. 19 - 21 April 2017* 2017, 109–114.

49.   Banja, M.; Sikkema, R.; Jégard, M.; Motola, V.; Dallemand, J.F. Biomass for energy in the EU – The support framework. *Energy Policy* 2019, *131*, 215–228, doi:10.1016/j.enpol.2019.04.038.

50.   Berra, M.; Mangialardi, T.; Paolini, A.E. Reuse of woody biomass fly ash in cement-based materials. *Constr. Build. Mater.* 2015, *76*, 286–296, doi:10.1016/j.conbuildmat.2014.11.052.

51.   Rajamma, R.; Ball, R.J.; Tarelho, L.A.C.; Allen, G.C.; Labrincha, J.A.; Ferreira, V.M. Characterisation and use of biomass fly ash in cement-based materials. *J. Hazard. Mater.* 2009, *172*, 1049–1060, doi:10.1016/j.jhazmat.2009.07.109.

52.   Carević, I.; Štirmer, N.; Trkmić, M.; Jurić, K.K. Leaching characteristics of wood biomass fly ash cement composites. *Appl. Sci.* 2020, *10*, 1–17, doi:10.3390/app10238704.

53.   Vassilev, S. V.; Baxter, D.; Andersen, L.K.; Vassileva, C.G. An overview of the composition and application of biomass ash.: Part 2. Potential utilisation, technological and ecological advantages and challenges. *Fuel* 2013, *105*, 19–39, doi:10.1016/j.fuel.2012.10.001.

54.   Odzijewicz, J.I.; Wołejko, E.; Wydro, U.; Wasil, M.; Jabłońska-Trypuć, A. Utilization of Ashes from Biomass Combustion. *Energies* 2022, *15*, doi:10.3390/en15249653.

55.   Carevic, I.; Štirmer, N.; Serdar, M.; Ukrainczyk, N. Effect of wood biomass ash storage on the properties of cement composites. *Materials (Basel).* 2021, *14*, doi:10.3390/ma14071632.

56.   Fort, J.; Šál, J.; Ševcík, R.; Dolezelová, M.; Keppert, M.; Jerman, M.; Záleská, M.; Stehel, V.; Cerny, R. Biomass fly ash as an alternative to coal fly ash in blended cements: Functional aspects. *Constr. Build. Mater.* 2021, *271*, doi:https://doi.org/10.1016/j.conbuildmat.2020.121544.

57.   Desire Ndahirwa Valorization of different biomass ashes and sunflower particles in bio-based building materials : relation composition-structure- properties, Normandie Université, 2023.

58.   Fusade, L.; Viles, H.; Chris Wood; Burns, C. The effect of wood ash on the properties and durability of lime mortar for repointing damp historic buildings. *Constr. Build. Mater.* 2019, *212*, 500–513, doi:10.1016/j.conbuildmat.2019.03.326 CITATIONS.

59.   Pavlíková, M.; Zemanová, L.; Záleská, M.; Pokorný, J.; Lojka, M.; Jankovský, O.; Pavlík, Z. Ternary Blended Binder for Production of a Novel Type of Lightweight Repair Mortar. *Materials (Basel).* 2019, *12*, doi:10.3390/ma12060996.

60.   Almeida, N.G.; Faria, P.; Pinto, A.P. Lime mortars with rice husk ash for ancient masonry BLA. In Proceedings of the HMC08 - Historical Mortars Conference; Lisbon, 2008.

61.   Government of the Republic of Croatia *Croatia earthquake - Rapid Damage Assessment and Needs 2020*; 2020;

62.   Regulation (EU) No 305/2011 of the European Parliament and of the Council of 9 March 2011 laying down harmonised conditions for the marketing of construction products and repealing Council Directive 89/106/EEC, consolidated text. 2021.

63.   Monaco, M.; Aurilio, M.; Tafuro, A.; Guadagnuolo, M. Sustainable Mortars for Application in the Cultural Heritage Field. *Materials (Basel)*. 2021, *14*, 1–16, doi:https://doi.org/10.3390/ma14030598.

64.   Zhang, S.; Sun, M.; Guo, Q.; Zhao, L.; Li, Z. Study on the Mechanical Properties and Durability of Hydraulic Lime Mortars Based on Limestone and Potassium Feldspar. *Appl. Sci.* 2023, *13*, 1–14, doi:10.3390/app13042412.

65.   Ranesi, A.; Faria, P.; Veiga, M.D.R. Traditional and modern plasters for built heritage: Suitability and contribution for passive relative humidity regulation. *Heritage* 2021, *4*, 2337–2355, doi:10.3390/heritage4030132.

66.   Zhang, D.; Zhao, J.; Wang, D.; Wang, Y.; Ma, X. Influence of pozzolanic materials on the properties of natural hydraulic lime based mortars. *Constr. Build. Mater.* 2020, *244*, doi:10.1016/j.conbuildmat.2020.118360.

67.   Branco, F.G.; Belgas, M. de L.; Mendes, C.; Pereira, L.; Ortega, J.M. Mechanical performance of lime mortar coatings for rehabilitation of masonry elements in old and historical buildings. *Sustain.* 2021, *13*, doi:10.3390/su13063281.

68.   Ergenç, D.; Gómez-villalba, L.S.; Fort, R. Materials Characterization Crystal development during carbonation of lime-based mortars in di ff erent environmental conditions. *Mater. Charact.* 2018, *142*, 276–288, doi:10.1016/j.matchar.2018.05.043.

69.   European Commission *The Green Deal Industrial Plan: putting Europe's net-zero industry in the lead*; Brussels, 2023;

70.   Bing, L.; Ma, M.; Liu, L.; Wang, J.; Niu, L.; Xi, F. An investigation of the global uptake of CO2 by lime from 1963 to 2020. *Earth Syst. Sci. Data* 2022, *7112485*, 1–21, doi:doi.org/10.5194/essd-2022-327.

71.   European Green Deal: EU agrees stronger legislation to accelerate the rollout of renewable energy Available online: https://ec.europa.eu/commission/presscorner/detail/en/IP_23_2061.

72.   Mühlenhoff, J.; Bonadio, J. *Building a Paris Agreement Compatible (PAC) energy scenario*; 2020;

73.   Bioeconomy, T.E.C.K.C. for *Brief on biomass for energy in the European Union*; 2019;

74.   Cowie, A.L.; Berndes, G.; Bentsen, N.S.; Brandão, M.; Cherubini, F.; Egnell, G.; George, B.; Gustavsson, L.; Hanewinkel, M.; Harris, Z.M.; et al. Applying a science-based systems perspective to dispel misconceptions about climate effects of forest bioenergy. *GCB Bioenergy* 2021, *13*, 1210–1231, doi:10.1111/gcbb.12844.

75.   Fořt, J.; Čáchová, M.; Vejmelková, E.; Černý, R. Mechanical and hygric properties of lime plasters modified by biomass fly ash. *IOP Conf. Ser. Mater. Sci. Eng.* 2018, *365*, doi:10.1088/1757-899X/365/3/032059.

76. García-González, J.; Faria, P.; Pereira, A.S.; Lemos, P.C.; Juan-Valdés, A. A sustainable production of natural hydraulic lime mortars through bio-amendment. *Constr. Build. Mater.* 2022, *340*, doi:10.1016/j.conbuildmat.2022.127812.

77. RILEM Technical Committee TC 203-RHM *State of the Art Report of RILEM Technical Committee TC 203-RHM: 'Repair Mortars for Historic Masonry';* Maurenbrecher, P., Groot, C., Eds.; 2016; ISBN 978-2-35158-163-6.

78. Apostolopoulou, M.; Bakolas, A.; Kotsainas, M. Mechanical and physical performance of natural hydraulic lime mortars. *Constr. Build. Mater.* 2021, *290*, 123272, doi:10.1016/j.conbuildmat.2021.123272.

79. Silva, B.A.; Ferreira Pinto, A.P.; Gomes, A. Natural hydraulic lime versus cement for blended lime mortars for restoration works. *Constr. Build. Mater.* 2015, *94*, 346–360, doi:10.1016/j.conbuildmat.2015.06.058.

80. Government of the Republic of Croatia *National Plan for Recovery and Resilience 2021. - 2026.*; 2021;

81. Kostanić Jurić, K.; Razvoj metodologije za primjenu pepela drvne biomase u betonu, University of Zagreb, 2021.

82. ASTM C 188-17 - Standard Test Method for Density of Hydraulic Cement, 1995.

83. EN ISO 10523:2012 Water quality -- Determination of pH, 2012.

84. ASTM D7348-13 Standard Test Methods For Loss On Ignition (LOI) Of Solid Combustion Residues, 2021.

85. EN ISO 16967:2015 - Solid biofuels -- Determination of major elements (Al, Ca, Fe, Mg, P, K, Si, Na and Ti), 2015.

86. EN 196-2:2013 Methods of testing cement -- Part 2: Chemical analysis of cement, 2013.

87. EN ISO 16968:2015 Solid biofuels - Determination of minor elements.

88. ASTM D 6722-19 Standard Test Method for Total Mercury in Coal and Coal Combustion Residues by Direct Combustion Analysis.

89. The European Committee for Standardization EN 196-11:2019 Methods of testing cement -- Part 11: Heat of hydration -- Isothermal Conduction Calorimetry method. 2019.

90. Chowdhury, S.; Mishra, M.; Suganya, O. The incorporation of wood waste ash as a partial cement replacement material for making structural grade concrete: An overview. *Ain Shams Eng. J.* 2015, *6*, 429–437, doi:10.1016/j.asej.2014.11.005.

91. Hrnčířová, M.; Pospíšil, J.; Michalšpiláček, M.M. Size Analysis of Solid Particles Using Laser Diffraction and Sieve Analysis. *Eng. Mech.* 2013, *20*, 309–318.

92. Bagchi, S.S.; Ghule, S. V.; Jadhav, R.T. Fly ash fineness - Comparing residue on 45 micron sieve with Blaine's surface area. *Indian Concr. J.* 2012, *86*, 39–42.

93. Vassilev, S. V.; Vassileva, C.G.; Petrova, N.L. Mineral Carbonation of Biomass Ashes in Relation to Their CO2 Capture and Storage Potential. *ACS Omega* 2021, *6*, 14598–14611, doi:10.1021/acsomega.1c01730.

94. Wang, Q.; Wang, D.; Zhuang, S. The soundness of steel slag with different free CaO and MgO contents. *Constr. Build. Mater.* 2017, *151*, 138–146, doi:10.1016/j.conbuildmat.2017.06.077.

95. Liyanage, J.B.; Gamage, R.P. The hydration and volume expansion mechanisms of modified expansive cements for sustainable in-situ rock fragmentation: A review. *Energies* 2021, *14*, doi:10.3390/en14185965.

96. Zhou, M.; Cheng, X.; Chen, X. Studies on the volumetric stability and mechanical properties of cement-fly-ash-stabilized steel slag. *Materials (Basel).* 2021, *14*, 1–16, doi:10.3390/ma14030495.

97. Ukrainczyk, N.; Vrbos, N.; Koenders, E.A.B. Reuse of Woody Biomass Ash Waste in Cementitious Materials. *Chem. Biochem. Eng. Q.* 2016, doi:10.15255/CABEQ.2015.2231.

98. EN 450-1:2013 Fly ash for concrete - Part 1:Definition, specifications an conformity criteria, 2013.

99. Snellings, R.; Mertens, G.; Elsen, J. Supplementary cementitious materials. *Rev. Mineral. Geochemistry* 2012, *74*, 211–278, doi:10.2138/rmg.2012.74.6.

100. Ottosen, L.M.; Hansen, E.Ø.; Jensen, P.E.; Kirkelund, G.M.; Golterman, P. Wood ash used as partly sand and/or cement replacement in mortar. *Int. J. Sustain. Dev. Plan.* 2016, *11*, 781–791, doi:10.2495/SDP-V11-N5-781-791.

101. Dabrio, C.J.; Santisteban, J.I.; Mediavilla, R.; Lo, E.; Castan, S.; Zapata, M.B.R.; Jose, M. Loss on ignition: a qualitative or quantitative method for organic matter and carbonate mineral content in sediments? ′. *J. Paleolimnol.* 2004, *32*, 287–299.

102. Gualtieri, A.F.; Viani, A.; Montanari, C. Quantitative phase analysis of hydraulic limes using the Rietveld method. *Cem. Concr. Res.* 2006, *36*, 401–406, doi:10.1016/j.cemconres.2005.02.001.

103. Kang, S.H.; Lee, S.O.; Hong, S.G.; Kwon, Y.H. Historical and scientific investigations into the use of hydraulic lime in Korea and preventive conservation of historic masonry structures. *Sustain.* 2019, *11*, 1–16, doi:10.3390/su11195169.

104. Edwin Eckel *Cements, Limes and Plasters Their Materials, Manufacture and Properties*; 1st Editio.; Routledge, 2005; ISBN 9781873394731.

105. Thirumalini, S.; Ravi, R.; Rajesh, M. Experimental investigation on physical and mechanical properties of lime mortar: Effect of organic addition. *J. Cult. Herit.* 2018, *31*, 97–104, doi:10.1016/j.culher.2017.10.009.

106. Figueiredo, C.P.; Lawrence, M.; Ball, R.J. Mechanical properties of standard and commonly formulated nhl mortars used for retrofitting. In Proceedings of the International Conference on Integrated Design; Bath, United Kingdom, 2016.

107. Saint-Astier; Hydraulicity & Properties. Available online: https://limes.us/technical-info/hydraulicity-properties (accessed on April 24 2023).

108. Grubor, M.; Serdar, M.; Grubor, M.; Grubor, M.; Serdar, M. Shrinkage of mortar with the addition of wood biomass ash and recycled tyre polymer fibres. *Građevinar* 2023, *75*, 367–378, doi:doi.org/10.14256/JCE.3642.2022.

109. Callebaut, K.; Elsen, J.; Van Balen, K.; Viaene, W. Nineteenth century hydraulic restoration mortars in the Saint Michael's Church (Leuven, Belgium): Natural hydraulic lime or cement?

Cem. Concr. Res. 2001, *31*, 397–403, doi:10.1016/S0008-8846(00)00499-3.

110.   Psycharis, V.; Chatzigeorgiou, M.; Koumpouri, D.; Beazi-katsioti, M.; Katsiotis, M. Structure–Superstructure Inter-Relations in Ca2SiO4 Belite Phase. *Crystals* 2022, *12*, doi:10.3390/cryst12121692.

111.   Hedayati, A.; Lindgren, R.; Skoglund, N.; Boman, C.; Kienzl, N.; Öhman, M. Ash Transformation during Single-Pellet Combustion of Agricultural Biomass with a Focus on Potassium and Phosphorus. *Energy and Fuels* 2021, *35*, 1449–1464, doi:10.1021/acs.energyfuels.0c03324.

112.   Hedayati, A.; Sefidari, H.; Boman, C.; Skoglund, N.; Kienzl, N.; Öhman, M. Ash transformation during single-pellet gasification of agricultural biomass with focus on potassium and phosphorus. *Fuel Process. Technol.* 2021, *217*, doi:10.1016/j.fuproc.2021.106805.

113.   Milinovic, J.; Dias, Á.A.; Janeiro, A.I.; Pereira, M.F.C.; Martins, S.; Petersen, S.; Barriga, F.J.A.S. XRD identification of ore minerals during cruises: Refinement of extraction procedure with sodium acetate buffer. *Minerals* 2020, *10*, doi:10.3390/min10020160.

114.   Grilo, J.; Santos Silva, A.; Faria, P.; Gameiro, A.; Veiga, R.; Velosa, A. Mechanical and mineralogical properties of natural hydraulic lime-metakaolin mortars in different curing conditions. *Constr. Build. Mater.* 2014, *51*, 287–294, doi:10.1016/j.conbuildmat.2013.10.045.

115.   Scrivener, K.; Snellings, R.; Lothenbach, B. *A Practical Guide to Microstructural Analysis of Cementitious Materials*; 1st Editio.; CRC Press, 2017; ISBN 9781138747234 - CAT# K32538.

116.   Sigvardsen, N.M.; Geiker, M.R.; Ottosen, L.M. Reaction mechanisms of wood ash for use as a partial cement replacement. *Constr. Build. Mater.* 2021, *286*, 122889, doi:10.1016/j.conbuildmat.2021.122889.

117.   Navarrete, I.; Vargas, F.; Martinez, P.; Paul, A.; Lopez, M. Flue gas desulfurization (FGD) fly ash as a sustainable, safe alternative for cement-based materials. *J. Clean. Prod.* 2021, *283*, 124646, doi:10.1016/j.jclepro.2020.124646.

118.   The European Committee for Standardization EN 459-2:2021 Building lime -- Part 2: Test methods 2021.

119.   Fapohunda, C.; Akinbile, B.; Oyelade, A. A Review of the properties, structural characteristics and application potentials of concrete containing wood waste as partial replacement of one of its constituent material. 2008, *6*, 1–12, doi:10.1016/j.jassh.2005.02.001.

120.   Cheah, C.B.; Ramli, M. The implementation of wood waste ash as a partial cement replacement material in the production of structural grade concrete and mortar: An overview. *Resour. Conserv. Recycl.* 2011, *55*, 669–685, doi:10.1016/j.resconrec.2011.02.002.

121.   Adhitya, L.W.; Januarti, J.E.; Triwulan Factors influencing strength and setting time of fly ash based-geopolymer paste. *MATEC Web Conf.* 2017, *138*, doi:10.1051/matecconf/201713801010.

122.   Nuaklong, P.; Wongsa, A.; Sata, V.; Boonserm, K.; Sanjayan, J.; Chindaprasirt, P. Properties of high-calcium and low-calcium fly ash combination geopolymer mortar containing recycled aggregate. *Heliyon* 2019, *5*, e02513, doi:10.1016/j.heliyon.2019.e02513.

123.   Zunino, F.; Bentz, D.P.; Castro, J. Reducing setting time of blended cement paste containing high-SO3 fly ash (HSFA) using chemical/physical accelerators and by fly ash pre-washing. *Cem.*

Concr. Compos. 2018, *90*, 14–26, doi:10.1016/j.cemconcomp.2018.03.018.

124. Martínez-García, R.; Jagadesh, P.; Zaid, O.; Șerbănoiu, A.A.; Fraile-Fernández, F.J.; de Prado-Gil, J.; Qaidi, S.M.A.; Grădinaru, C.M. The Present State of the Use of Waste Wood Ash as an Eco-Efficient Construction Material: A Review. *Materials (Basel).* 2022, *15*, doi:10.3390/ma15155349.

125. Weeks, C.; Hand, R.J.; Sharp, J.H. Retardation of cement hydration caused by heavy metals present in ISF slag used as aggregate. *Cem. Concr. Compos.* 2008, *30*, 970–978, doi:10.1016/j.cemconcomp.2008.07.005.

126. Teker Ercan, E.E.; Andreas, L.; Cwirzen, A.; Habermehl-Cwirzen, K. Wood Ash as Sustainable Alternative Raw Material for the Production of Concrete — A Review. *Materials (Basel).* 2023, *16*, 2557, doi:https://doi.org/10.3390/ma16072557.

127. Yang, Z.; Huddleston, J.; Brown, H. Effects of Wood Ash on Properties of Concrete and Flowable Fill. *J. Mater. Sci. Chem. Eng.* 2016, *4*, 101–114, doi:10.4236/msce.2016.47013.

128. Chatterji, S. Mechanism of expansion of concrete due to the presence of dead-burnt CaO and MgO. *Cem. Concr. Res.* 1995, *25*, 51–56, doi:10.1016/0008-8846(94)00111-B.

129. Santos, T.A.; Neto, J.S.A.; Cilla, M.S.; Ribeiro, D. V. Influence of the Content of Alkalis (Na2O and K2O), MgO, and SO3 Present in the Granite Rock Fine in the Production of Portland Clinker. *J. Mater. Civ. Eng.* 2022, *34*, doi:10.1061/(asce)mt.1943-5533.0004201.

130. Banfill, P.F.G.; Forster, A.M.; Mackenzie, S.; Sanz, M.P.; Szadurski, E.M. Natural hydraulic limes for masonry repair : hydration and workability. In Proceedings of the 34th Annual Cement and Concrete Science Conference and Workshop on Waste Cementation; University of Shefield: Sheffiled, 2014.

131. Tkaczewska, E.; Małolepszy, J. Hydration of coal-biomass fly ash cement. *Constr. Build. Mater.* 2009, *23*, 2694–2700, doi:10.1016/j.conbuildmat.2008.12.018.

132. Jaafri, R.; Aboulayt, A.; Alam, S.Y.; Roziere, E.; Loukili, A. Natural hydraulic lime for blended cement mortars: Behavior from fresh to hardened states. *Cem. Concr. Res.* 2019, *120*, 52–65, doi:10.1016/j.cemconres.2019.03.003.

133. Šantek Bajto, J.; Štirmer, N.; Baričević, A. Sustainable Hybrid Lime Mortars for Historic Building Conservation: Incorporating Wood Biomass Ash as a Low-Carbon Secondary Binder. *Heritage* 2023, *6*, 5242–5269, doi:10.3390/heritage6070278.

134. Forster, A.M.; Valek, J.; Hughes, J.J. Lime binders for the repair of historic buildings: Considerations for CO2 abatement. *J. Clean. Prod.* 2020, *252*, doi:10.1016/j.jclepro.2019.119802.

135. The European Committee for Standardization EN 1015-6:2000 Methods of test for mortar for masonry -- Part 6: Determination of bulk density of fresh mortar.

136. EN 12350-1:2019 - Testing fresh concrete -- Part 1: Sampling and common apparatus, 2019.

137. RILEM TC 203-RHM *Repair mortars for historic masonry*; 2012; Vol. 45; ISBN 9782351581636.

138. ASTM ASTM C 618 -01 Standard Specification for Coal Fly Ash and Raw or Calcined Natural Pozzolan for Use as a Mineral Admixture in Concrete. *Annu. B. ASTM Stand.* 2010, 3–6.

139. EN 12504-4:2021 - Testing concrete in structures -- Part 4: Determination of ultrasonic pulse velocity, 2021.

140. EN 1015-18:2002 -Methods of test for mortar for masonry -- Part 18: Determination of water absorption coefficient due to capillary action of hardened mortar, 2002.

141. EN 1015-19:2000 - Methods of test for mortar for masonry -- Part 19: Determination of water vapour permeability of hardened rendering and plastering mortars, 2000.

142. EN 12664:2002 - Thermal performance of building materials and products -- Determination of thermal resistance by means of guarded hot plate and heat flow meter methods -- Dry and moist products of medium and low thermal resistance, 2002.

143. EN 1015-12:2016 - Methods of test for mortar for masonry -- Part 12: Determination of adhesive strength of hardened rendering and plastering mortars on substrates, 2016.

144. Bekker, P.; Borchelt, G.; Bright, N.; Emrich, F.; Forde, M.; Gallegos, H.; Groot, C.; Hedstrom, E.; Lawrence, S.; Maurenbrecher, P.; et al. RILEM TECHNICAL COMMITTEES MS-A . 1 Determination of the resistance of wallettes against sulphates and chlorides. 1998, *31*, 2–19.

145. EN 1015-17:2000/A1:2004 - Methods or test for mortar for masonry -- Part 17: Determination of water-soluble chloride content of fresh mortars, 2000.

146. RILEM Technical Committee TC 203-RHM Repair Mortars for Historic Masonry - State of the Art Report of RILEM Technical Committee TC 203-RHM 2016, 178.

147. Branco, F.G.; Belgas, M. de L.; Mendes, C.; Pereira, L.; Ortega, J.M. Characterization of fresh and durability properties of different lime mortars for being used as masonry coatings in the restoration of ancient constructions. *Sustain.* 2021, *13*, doi:10.3390/su13094909.

148. Lanas, J.; Sirerab, R.; Alvarez, J.I. Study of the mechanical behavior of masonry repair lime-based mortars cured and exposed under different conditions. *Cem. Concr. Res.* 2006, *36*, 961–970, doi:doi.org/10.1016/j.cemconres.2005.12.003.

149. Wang, S.; Miller, A.; Llamazos, E.; Fonseca, F.; Baxter, L. Biomass fly ash in concrete: Mixture proportioning and mechanical properties. *Fuel* 2008, *87*, 365–371, doi:10.1016/j.fuel.2007.05.026.

150. Łaźniewska-Piekarczyk, B.; Miera, P.; Szwabowski, J. Plasticizer and Superplasticizer Compatibility with Cement with Synthetic and Natural Air-Entraining Admixtures. In Proceedings of the IOP Conference Series: Materials Science and Engineering; 2017; Vol. 245.

151. EN 998-2:2016 Specification for mortar for masonry -- Part 2: Masonry mortar. 2012.

152. Siedel, H. Salt efflorescence as indicator for sources of damaging salts on historic buildings and monuments: a statistical approach. *Environ. Earth Sci.* 2018, *77*, 1–20, doi:10.1007/s12665-018-7752-4.

153. Silva, B.A.; Ferreira Pinto, A.P.; Gomes, A. Influence of natural hydraulic lime content on the properties of aerial lime-based mortars. *Constr. Build. Mater.* 2014, *72*, 208–218, doi:10.1016/j.conbuildmat.2014.09.010.

154. Arizzi, A.; Martinez-Huerga, G.; Sebastián-Pardo, E.; Cultrone, G. Mineralogical, textural and physical-mechanical study of hydraulic lime mortars cured under different moisture conditions. *Mater. Constr.* 2015, *65*, doi:10.3989/mc.2015.03514.

155. Marwa Aly; Sara Pavia Mechanical and hygric properties of natural hydraulic lime (NHL) mortars with pozzolans. *SMAR 2015 - Third Conf. Smart Monit. Assess. Rehabil. Civ. Struct.* 2015, 1–13.

156. Moropoulou, A.; Bakolas, A.; Moundoulas, P.; Aggelakopoulou, E.; Anagnostopoulou, S. Strength development and lime reaction in mortars for repairing historic masonries. *Cem. Concr. Compos.* 2005, *27*, 289–294, doi:10.1016/j.cemconcomp.2004.02.017.

157. Olaniyan, S.A. Pore Structure as a Determinant of Flexibility in Sustainable Lime-Cement Mortar Composites. *Eur. J. Eng. Technol. Res.* 2021, *6*, 113–122, doi:10.24018/ejeng.2021.6.6.2598.

158. Silva, B.A.; Ferreira Pinto, A.P.; Gomes, A.; Candeias, A. Effects of natural and accelerated carbonation on the properties of lime-based materials. *J. CO2 Util.* 2021, *49*, 101552, doi:10.1016/j.jcou.2021.101552.

159. Forster, A. An assessment of the relationship between the water vapour permeability and hydraulicity of lime based mortars with particular reference to building conservation material science An assessment of the relationship between the water vapour permeability and. 2015.

160. Editors:; Elsen, J.; Groot, C. Chapter 2.5 Characterisation: Porosity of mortars. In *Characterisation of Old Mortars with Respect to their Repair*; RILEM publications SARL, 2007.

161. Karagiannis, N.; Karoglou, M.; Bakolas, A.; Moropoulou, A. Building Materials Capillary Rise Coefficient: Concepts, Determination and Parameters Involved. 2016, 27–44, doi:10.1007/978-981-10-0648-7_2.

162. Nogueira, R.; Paula, A.; Pinto, F.; Gomes, A. AC SC. *Cem. Concr. Compos.* 2018, doi:10.1016/j.cemconcomp.2018.03.005.

163. Fusade, L.; Orr, S.A.; Wood, C.; O'Dowd, M.; Viles, H. Drying response of lime-mortar joints in granite masonry after an intense rainfall and after repointing. *Herit. Sci.* 2019, *7*, 1–20, doi:10.1186/s40494-019-0277-7.

164. Ioannou, I.; Andreou, A.; Tsikouras, B.; Hatzipanagiotou, K. Application of the Sharp Front Model to capillary absorption in a vuggy limestone. *Eng. Geol.* 2009, *105*, 20–23, doi:10.1016/j.enggeo.2008.12.008.

165. Brunello, V.; Canevali, C.; Corti, C.; De Kock, T.; Rampazzi, L.; Recchia, S.; Sansonetti, A.; Tedeschi, C.; Cnudde, V. Understanding the microstructure of mortars for cultural heritage using X-ray CT and MIP. *Materials (Basel).* 2021, *14*, 7–21, doi:10.3390/ma14205939.

166. Pavlíková, M.; Kapicová, A.; Pivák, A.; Záleská, M.; Lojka, M.; Jankovský, O.; Pavlík, Z. Zeolite lightweight repair renders: Effect of binder type on properties and salt crystallization resistance. *Materials (Basel).* 2021, *14*, doi:10.3390/ma14133760.

167. Banfill, P.F.G. Hygrothermal properties of NHL mortars. *Energy Effic. Hist. Build.* 2018, *5*, 71–79.

168. Papayianni, I.; Hughes, J. Testing properties governing the durability of lime-based repair mortars. *RILEM Tech. Lett.* 2018, *3*, 135–139, doi:10.21809/rilemtechlett.2018.81.

169. Ruegenberg, F.; Schidlowski, M.; Bader, T.; Diekamp, A. NHL-based mortars in restoration: Frost-thaw and salt resistance testing methods towards a field related application. *Case Stud.*

Constr. Mater. 2021, *14*, e00531, doi:10.1016/j.cscm.2021.e00531.

170.   Arizzi, A.; Viles, H.; Cultrone, G. Experimental testing of the durability of lime-based mortars used for rendering historic buildings. *Constr. Build. Mater.* 2012, *28*, 807–818, doi:10.1016/j.conbuildmat.2011.10.059.

171.   Eleni Aggelakopoulou, Evangelia Ksinopoulou, V.E. Evaluation of mortar mix designs for the conservation of the Acropolis monuments. *J. Cult. Heritage,* 2022, *Volume 55*, 300–308, doi:https://doi.org/10.1016/j.culher.2022.04.004.

Biography

Jelena Šantek Bajto was born on July 3rd, 1986, in the city of Zagreb. In October 2012, she graduated from the Faculty of Civil Engineering at the University of Zagreb, specializing in "Construction materials" and completed her master's thesis on "Energy certification of public buildings".

Post-graduation, she gained valuable experience as an energy efficiency and acoustics designer with a company focused on energy-efficient building design and noise protection. During this period, spanning from 2013 to 2017, she oversaw the execution of specialized construction works in energy renovations, conducted energy audits employing infrared thermography for thermal assessments, and played a significant role in planning and managing efficient energy consumption in buildings. Her expertise also extends to material selection and technologies for renovation of protected cultural heritage buildings. She actively contributed to the formerly obligatory revisions of projects related to energy savings, thermal protection, and the development of low-energy building designs. From 2013 to 2015, she was an engaged member of the Technical Committee of Croatian Bureau of Standards HZN/TO 163 - "Thermal insulation."

Subsequently, she transitioned into the role of a project manager at the Central Finance and Contracting Agency (CFCA) within the Directorate for implementation of Infrastructural Projects, Infrastructural and Construction Works Service from 2017 to 2018. In this role, she oversaw the implementation of construction and spatial planning contracts funded by CFCA programs, conducted on-site checks, and verified project costs. She also completed a specialist training program in the field of public procurement. She has been a member of the Croatian Chamber of Civil Engineers since 2015, having successfully passed the professional exam in Spatial Planning and Construction.

Since 2018, she is employed as an assistant at the Department of Materials in the Faculty of Civil Engineering in Zagreb and is enrolled in Postgraduate Doctoral Studies at the Faculty of Civil Engineering, University of Zagreb, with the aim of achieving the academic title of Doctor of Science in the field of technical sciences. This pursuit has been made possible through financial support from the Croatian Science Foundation and the European Social Fund under the project entitled "Young Researchers' Career Development Project – Training New Doctoral Students" (ESF DOK-01-2018).

List of published papers

Papers in journals

Šantek Bajto, J.; Štirmer, N.; Baričević, A.; *Sustainable Hybrid Lime Mortars for Historic Building Conservation: Incorporating Wood Biomass Ash as a Low-Carbon Secondary Binder*. Heritage, 2023, 6, 5242–5269. DOI: 10.3390/heritage6070278

Šantek Bajto, J.; Štirmer, N.; Cerković, S.; Carević, I.; Kostanić Jurić, K.; *Pilot Scale Production of Precast Concrete Elements with Wood Biomass Ash*. Materials, 2021, 14 (21), 6578. DOI: 10.3390/ma14216578

Baričević, A.; Carević, I.; Šantek Bajto, J.; Štirmer, N.; Bezinović, M.; Kristović, K.; *Potential of Using Wood Biomass Ash in Low-Strength Composites*. Materials, 2021, 14 (5), 1250. DOI: 10.3390/ma14051250; https://www.bib.irb.hr/1114260

Carević, I.; Baričević, A.; Štirmer, N.; Šantek Bajto, J.; *Correlation between physical and chemical properties of wood biomass ash and cement composites performances*. Construction and Building Materials, 2020, 256, 119450. DOI: 10.1016/j.conbuildmat.2020.119450, https://www.bib.irb.hr/1062784

Book chapters

Šantek Bajto, J.; Štirmer, N.; Baričević, A.; *Restoring Historical Buildings Amid Climate Crisis: Hydraulic, Waste-Based Lime*. In book: Conservation and Restoration of Historic Mortars and Masonry Structures, RILEM Bookseries, volume 42, June 2023. DOI: 10.1007/978-3-031-31472-8_28.

Štirmer, N.; Banjad Pečur, I.; Bjegović, D.; Gabrijel, I.; Baričević, A.; Jelčić Rukavina, M.; Milovanović, B.; Serdar, M.; Carević, I.; Grubor, M.; Kostanić Jurić, K.; Šantek Bajto, J.; Cerković, S.; *Predgotovljeni betonski rubnjaci i kanalice s pepelom drvne biomase*. Inovacije Sveučilišta u Zagrebu / Pap, K.; Šimpraga, M.o (Ed.)., Zagreb, 2021. str. 134-136.

Conference contributions: Published papers and abstracts:

Šantek Bajto, J.; Štirmer, N.; Baričević, A.; *Assessing the Performance of Wood Biomass Ash in Hybrid Lime Binders for Mortar Systems under Varying Curing Conditions*; The 1st International Online Conference on Buildings: Advances in Building Planning, Design, Construction, and Operation; IOCBD 2023 Book of abstracts, October 2023.

Šantek Bajto, J.; Štirmer, N.; Baričević, A.; *Restoring historical buildings amid climate crisis: hydraulic, waste-based lime*; 6th Historic Mortars Conference, September 2022, Ljubljana, Slovenia, Conference Proceedings, edited by Violeta Bokan Bosiljkov et al., Faculty of Civil and Geodetic Engineering Ljubljana*, 2022, ISBN 978-961-6884-77-8, COBISS.SI-ID 121348355,* https://www.bib.irb.hr/1256171.

Cerković, Sonja; Štirmer, Nina; Carević, Ivana; Šantek Bajto, Jelena: *Use of Wood Biomass Ash in Prefabricated Concrete Elements*; 5th International Conference on Technologies & Business Models for Circular Economy: Book of Abstracts, Maribor: University of Maribor, University Press, 2022. str. 57-59,

doi:10.18690/um.fkkt.6.2022, https://press.um.si/index.php/ump/catalog/book/714

Šantek Bajto, Jelena; Štirmer, Nina; Cerković, Sonja: Održiva rješenja s pepelom drvne biomase za sanaciju povijesnih zgrada u jeku klimatske i energetske krize, Zbornik sažetaka predavanja – 16. Dani Hrvatske komore inženjera građevinarstva, Opatija: Hrvatska komora inženjera građevinarstva, 2022. str. 90-90, https://www.bib.irb.hr/1222609

Šantek Bajto, J.; Štirmer, N.; Baričević, A.: *Razvoj bescementnih hidrauličnih veziva s otpadnim pepelom drvne biomase*, Graditeljstvo i klimatske promjene, Vodice: Hrvatski savez građevinskih inženjera, 2021. str. 55-64, doi:10.14256/8SHG.2021.167, https://www.bib.irb.hr/1153903

Štirmer, N., Šantek Bajto, J.; Carević, I.; Hržan, I.; *Mechanical properties of concrete containing wood biomass ash*. Proceedings of the 2nd International Conference on Construction Materials for Sustainable Future, COMS 2020/21, Volume 1, 295-302 / Šajna, A.; Legat, A.; Jordan, S.; Horvat, P.; Kemperle, E.; Dolenec, S.; Ljubešek, M.; Michelizza, M.; Slovenian National Building and Civil Engineering Institute, Ljubljana, 2020. https://www.bib.irb.hr/1113361

Šantek Bajto, J.; Štirmer, N.; Ereš, I.; *Oštećenje mikrostrukture betona s pepelom drvne biomase pri djelovanju smrzavanja i odmrzavanja*; Zajednički temelji - Sedmi skup mladih istraživača iz područja građevinarstva i srodnih tehničkih znanosti; Zbornik radova ISBN 978-953-6953-51-6, str. 31-36; Rijeka, 2019. https://www.bib.irb.hr/1028695

Šantek Bajto, J.; Štirmer, N.; *Mogućnosti primjene pepela drvne biomase u proizvodnji opeke*; 5. Simpozij Doktorskog studija Građevinarstva (Zbornik radova), str. 81-93, Zagreb, 2019; Nina Štirmer (Ed.). https://doi.org/10.5592/CO/PhDSym.2019.07
https://www.bib.irb.hr/1021147

Štirmer N.; Carević, I.; Šantek Bajto, J.; Kostanić Jurić, K.; *Physical Properties of Cement Pastes with Different Wood Biomass Ash Contents*; Proceedings of the 1st International Conference on Innovation in Low-Carbon Cement & Concrete Technology, Bai, Y.; Ghazizadeh, S.; Mangabhai, R.; Shi S.; Zhou, J. (ur.), University College London; London 2019. https://www.bib.irb.hr/1008870

Šantek Bajto, J.; Štirmer, N.; Carević; I., Cerković, S.: *Impact of wood biomass fly ash on the setting time of cement pastes*, Proceedings of the International Conference on Sustainable Materials, Systems and Structures (SMSS2019), PhD Symposium, Carević, I.; Lakušić, S.; Schlicke, D. (Ed.), RILEM Publications S.A.R.L., str. 55-56; 2019.
https://www.bib.irb.hr/1024404

Šantek Bajto, J.; Štirmer, N.; *Pepeo drvne biomase: od otpada do sirovine*; 10. Zagrebački energetski tjedan 2019. - Stručni skup studenata "Mi imamo rješenja – vizije novih generacija za održivi, zeleni razvoj"; Zagreb 2019.
https://www.bib.irb.hr/1028700

Bezinović, M.; Kristović, K.; Šantek Bajto, J.; *Ekološki mortovi za sanaciju povijesnih građevina*; 10. Zagrebački energetski tjedan 2019. - Stručni skup studenata "Mi imamo rješenja – vizije novih generacija za održivi, zeleni razvoj"; Zagreb, 2019.
https://www.bib.irb.hr/1125647